NetrinA and Frazzled in regulation of wing disc epithelia

Sofya Golenkina

A thesis submitted in total fulfilment of the requirements of the degree of Doctor of Philosophy

School of Biosciences, Faculty of Science,
University of Melbourne

October 2017

Abstract

The chemotropic factor Netrin and its receptors play a critical role during axon outgrowth, organogenesis and cancer progression. In this work I show that *Drosophila* NetrinA and its receptor Frazzled also control an epithelial-mesenchymal transition (EMT) event during the eversion of wing imaginal discs. EMTs are a key process of embryogenesis, regeneration and tumor metastasis whereby epithelial cells lose apico-basal polarity and cell-cell adhesions, invade through the basement membrane and become migratory. Wing disc eversion provides a tractable genetic model for EMT in which cells of the squamous peripodial epithelium lose their zonula adherens cell-cell contacts, break through the basement membrane, and develop F-Actin-rich protrusions that help them migrate as an epithelial sheet in the process of thorax closure.

Previously our lab has shown that loss of *netrinA* or overexpression of *frazzled* can inhibit eversion leading to disrupted wings and missing thoracic tissue. Here, I demonstrate that both loss of *netrinA* and elevation of *frazzled* expression in the wing imaginal disc peripodial epithelium suppress zonula adherens dissociation and promote extensive F-actin-rich stress-fibre like structures. Basement membrane degradation is not significantly affected suggesting that this process is regulated independently of zonula adherens dissociation and cytoskeletal modifications.

Previous results suggest that NetrinA and Frazzled play opposing roles in eversion, and that the NetrinA contribution to the EMT is realised by downregulation of Frazzled. Therefore, another aim of this work was to uncover the functional role of Frazzled in epithelia. Two pieces of evidence were obtained, confirming a

positive role for Frazzled in supporting the integrity of the peripodial epithelium. Firstly, I found that RNAi knockdown of *frazzled* accelerates zonula adherens dissociation in the peripodial epithelium. Secondly, *netA.IR* eversion phenotypes were substantially suppressed by heterozygosity for the deficiency Df(2R)BSC880 which removes one copy of *frazzled*. Surprisingly, unlike reports from other labs, no phenotypes were observed in *frazzled* loss-of-function clones. Over-expression analysis of *frazzled* in the disc proper epithelium showed that Frazzled controls basolateral localisation of junctional proteins (E-Cadherin and β-catenin) and phospho-Moesin. In addition, overexpression of the receptor resulted in enhanced F-actin protrusions and cell shape changes (apical constriction and basal expansion) typical of tissue invagination events.

A key question arising from these studies is whether the Frazzled signaling pathways that regulate cell motility are distinct from those that control epithelial phenotypes. To address this I conducted a structure function analysis to determine which of the three conserved intracellular P-domains of Frazzled are required for inhibiting wing eversion, and which are required for regulating E-Cadherin, F-Actin and cell shape changes. I show that P1 and P3 motifs are required for eversion disruption, that the P1 motif is most important for the cell shape changes and that the formation of F-actin protrusions is most dependent upon the P3 motif. The loss of E-Cadherin from basolateral regions was dependent on each P-motif of Frazzled. The differential requirement of P-motifs for these phenotypes provide evidence that multiple molecular pathways are acting downstream of Frazzled in epithelial cells.

A final aim of this study was to identify factors acting downstream of NetrinA and Frazzled and see if different molecular components are required for each cellular function of the receptor. I therefore performed a modifier RNAi screen to identify genes that could suppress or enhance *netA.IR* and *frazzled* overexpression eversion defects. The key finding from this work was that the apical polarity protein Par6 is required for inhibiting eversion and is partly required for E-Cadherin delocalization.

Based on these results a model is proposed in which high levels of Frazzled lead to activation of Rac1 in basal regions of the cell, and increased Rho1 and Par6

activity in apical regions of the cell, and this in turn leads to basal protrusions, apico-basal shape changes, and disruptions to E-Cadherin trafficking and adherens junction stability.

The results establish a new role for Netrin signaling in a developmental EMT and highlight the complexity of NetrinA/Frazzled pathway regulation of epithelial cells.

Declaration

The work presented in this thesis entitled "NetrinA and Frazzled in regulation of wing disc epithelia" is based on the original work done by me under the guidance of Dr. Michael J. Murray, School of BioSciences, the Faculty of Science, The University of Melbourne, and has not been included in any other thesis submitted previously for the award of any degree. The thesis contains no material previously published or written by another author, except where due reference is made in the text of the thesis. To the best of my knowledge, the thesis is fewer than the maximum word limit in length (i.e. 80,000 words), exclusive of tables and bibliographies.

Acknowledgements

I am grateful for a number of people in encouraging me to start the PhD research, persevere with it and eventually to get a great, accomplished story.

I owe a personal debt to Dr. Michael J. Murray for exceptional supervision and constant support, for helping me to develop ideas and solve all the research puzzles. He was always available for timely meetings, open for new ideas and patient for my mistakes and insane suggestions.

I also want to express my sincere gratitude to Prof Robert Saint, who gave me an opportunity to start PhD in Melbourne University, and then, despite of his busy schedule, was always ready to talk and provide important feedback, which made this project more comprehensive.

It is a great pleasure to thank Dr. Rose Manhire-Heath for her kind help and support during first year of my research and letting me contribute to her manuscript.

I wish to thank my committee members, A/Prof Gary Hime and Prof Alex Andrianopoulos, for useful discussion and valuable comments, which drove this work in the right direction.

I thank all my friends and family for their love, helping me survive all the stress of the PhD and not letting to give up. First of all, I am indebted to my husband Yuri for his invaluable support and assistance. Without him this work would not be completed. I am also grateful to my parents, sister, nephews for being worry for me, for always listening and giving me encouraging words. Finally, I am happy to thank my beloved friends, who made this time enjoyable even when life seemed tough and unfair.

List of Abbreviations

aa	amino acid
aPKC	atypical Protein Kinase C
AJ	adherens junction
APF	after puparium formation
ATP	Adenosine Triphosphate
BM	basement membrane
BMP	Bone Morphogenetic Protein
CI	confidence interval
CNS	central nervous system
DCC	Deleted in Colorectal Cancer
DE-Cad	*Drosophila* E-cadherin
DP	disc proper
Dpp	Decapentapledgic
ECM	extracellular matrix
EMT	epithelial-to-mesenchymal transition
ERK	Extracellular signal-Regulated Kinase
ERM	Ezrin, Radixin and Moesin proteins
GAP	GTPase-activating protein
GEF	Guanine nucleotide exchange factor
GFP	Green Fluorescent Protein
EGF	Epidermal Growth Factor
F-actin	Filamentous actin

FAK	Focal Adhesion Kinase
FCS	fetal calf serum
FGF	Fibroblast Growth Factor
FL	full-length
FLP	Flipase
FRT	FLP recombination target
IR	inverted repeat
Jak/STAT	Janus kinase/Signal Transducers and Activators of Transcription
JNK	c-Jun N-terminal Kinase
MAP	Mitogen-Activated Protein
MAPK	Mitogen-Activated Protein Kinase
MARCM	mosaic analysis with a repressible cell marker
MDCK	Madin-Darby canine kidney
MET	mesenchymal-epithelial transition
MLCK	Myosin Light-Chain Kinase
pMLC	phosphorylated Myosin Light-Chain
MMP	Matrix Metalloproteinase
Par	Partitioning-defective proteins
PBS	phosphate-buffered saline
PBS-T	phosphate-buffered saline with Triton X-100
PE	peripodial epithelium
PDGF	Platelet-Derived Growth Factor
pMLC	phosphorylated Myosin Light Chain
RFP	Red Fluorescent Protein
ROCK	Rho-associated protein Kinase
RTKs	receptors tyrosine kinases
S.E.M.	standard error of the mean
SMAD	Mothers Against Decapentaplegic
TGF	Transforming Growth Factor
TJ	tight junction

TIMP	Tissue Inhibitor of Metalloproteinase
VEGF	Vascular Endothelial Growth Factor
WASp	WiskottAldrich Syndrome protein
WT	wild type
ZA	zonula adherens

Table of Contents

List of Figures

List of Tables

CHAPTER 1

Introduction

1.1 Epithelia and epithelial-mesenchymal transition

1.1.1 The epithelial tissue

Epithelial tissues consist of cells organized densely into sheets covering the body surface and the majority of body structures. The main features defining the epithelial type of cell include immobility, apico-basal polarity, attachment to the basement membrane and the presence of a variety of intercellular junctions (i.e. tight junctions/septate junctions, adherens junctions, desmosomes and gap junctions) (Figure 1.1).

The membrane of epithelial cells is divided into two distinct surfaces, one facing the environment or the lumen (apical domain) and the other contacting the extracellular matrix (ECM) and neighbouring cells (basolateral domain) (Simons and Fuller, 1985 [1]). Formation of both domains is controlled by antagonistic functions of three protein complexes (reviewed in Tepass, 2012 [2]):

i) the apical Par (partition defective) complex, comprising Par6, Bazooka/Par3,

atypical protein kinase C (aPKC) and Cdc42 proteins;

ii) the apical Crumbs (Crb) complex, comprising Crumbs, Stardust (Sdt) and Pals1-associated tight junctions (Patj) proteins; and

iii) the basolateral Scribble (Scrib) complex, comprising Scribble, Discs large (Dlg) and Lethal giant larvae (Lgl) proteins (reviewed in Goldstein and Macara, 2007 [3]; Assèmat *et al.*, 2008 [4]; Tepass, 2012 [2]).

The major regulator of apical polarity is considered to be the Par complex (Goldstein and Macara, 2007 [3]). In *Drosophila*, after cellularization, the Rho GTPase Cdc42 binds Par6 in a Baz-dependent manner, and this interaction recruits Par6 to the apical cortex. In turn, Par6 promotes the apical position and kinase activity of aPKC (Hutterer *et al.*, 2004 [5]; Atwood *et al.*, 2007 [6]). Once accumulated under the apical membrane, the Par complex recruits other apical polarity proteins, such as Crb and Patj. Then, the apical domain of a cell is considered completed (Hutterer *et al.*, 2004 [5]). Being apically located, the Par complex initializes the formation of adherens junctions (hereafter AJ; Harris and Peifer, 2004 [7]). The main component of AJs is the homophilic cell adhesion molecule E-Cadherin, which connects to F-Actin filaments via interactions between its cytoplasmic domain, β-catenin and α-catenin. Baz/Par3 acts as a landmark for AJ assembly, and its localization coincides with cadherin-catenins clusters. At the same time, Par6 and aPKC segregate from Baz and localize above the AJ assembly spot, where they are thought to control dynein- and microtubule-dependent transport of Baz and AJ components (Harris and Peifer, 2005 [8]; McGill *et al.*, 2009 [9]).

Crb is a transmembrane protein localized apically to the AJ (Tepass, 2012 [2]). Crb plays a key role in specifying apical domain promoting proper localization of apical components (Wodarz *et al.*, 1995 [10]). Loss of *crb* results in failed assembly of AJs, which results in severe polarity defects and disintegration of epithelia (Tepass *et al.*, 1990 [11]). In contrast, overexpression of *crb* leads to enormous expansion

of the apical membrane domain and reduction of the basolateral domain (Wodarz *et al.*, 1995 [10]). The Crb complex is maintained by two binding partners of Crb, Std and Patj. Std appears to be more essential, and mutations of *std* phenocopy *crb* mutations (Tepass and Knust, 1993 [12]).

The Scrib complex is distributed along the basolateral membrane with a stronger accumulation at intercellular junctions (AJs and tight/septate junctions; Bilder and Perrimon, 2000 [13]). The main role of this complex is to restrict the distribution of apical markers (e.g. the Par complex, the Crb complex, AJ and tight junctions proteins) to the apical domain (Assèmat *et al.*, 2008 [4]). Lgl competes for Par3 in binding to Par6 and aPKC antagonising formation of the Par complex (Yamanaka *et al.*, 2003 [14]). In turn, aPKC phosphorylates and inactivates Lgl restricting its activity to the basolateral domain (Hutterer *et al.*, 2004 [5]). In addition to regulation of apico-basal polarity, the Scrib complex participates in establishing planar cell polarity (Montcouquiol *et al.*, 2003 [15]; Courbard *et al.*, 2009 [16]).

In *Drosophila* as well as in the other species, polarity complexes are tightly integrated with the intercellular junctions (Tepass, 2012 [2]). The latter have three main functions in epithelial tissue (Green, 1984 [17]):

i) anchoring, i.e. physical attachment of one cell to another in a firm sheet;

ii) occluding, i.e. preventing ions and small molecules from leaking though the epithelial sheet;

iii) communicating, i.e. transport and exchange of ions and small molecules between neighbouring cells.

The major structures carrying the first function are AJs (Green, 1984 [17]). AJs (including zonula adherens and spot AJs) are based on homophilic contacts between E-Cadherin clusters on the outer surface of adjacent cells (Baum and Georgiou, 2011 [18]). E-Cadherin (Shotgun in *Drosophila*) is a transmembrane protein, whose

cytoplasmic tail forms a complex with β-Catenin (Armadillo in *Drosophila*), which in turn binds to α-Catenin. AJs are morphologically associated with the F-actin cytoskeleton presumably via actin-binding proteins such as Vinculin, formins and an α-Catenin coupling protein EPLIN (Watabe-Uchida *et al.*, 1998 [19], Kobielak *et al.*, 2004 [20]; Abe and Takeichi, 2008 [21]). These binding partners allow E-Cadherin to modulate organization of the underlying F-actin network (Baum and Perrimon, 2001 [22]).

Vertebrate tight junctions (hereafter TJ) and invertebrate septate junctions play important roles in restricting paracellular diffusion and also in apico-basal polarization of the epithelia (Behr *et al.*, 2003 [23]). *Drosophila* septate junctions are assembled later than AJs, and are found at the lateral cell surface, basally to the zonula adherens (Tepass, 2003 [24]). Septate junctions consist of at least 12 components, including three Claudin homologues (Sinuous, Megatrachea and Kune-kune), the Na^+/K^+-ATPase, Neuroglian, Neurexin-IV, Contactin, Lachesin, Gliotactin and two intracellular components, Coracle and Varicose, which interact with the transmembrane proteins of the septate complex (reviewed by Oshima and Fehon, 2011 [25]). An important feature of the septate complexes is their ability to maintain basolateral polarity in epithelial cell during organogenesis (Laprise *et al.*, 2009 [26]).

Epithelial monolayers are separated from the underlying tissues by the basement membrane, a specialized type of ECM (Gumbiner, 1996 [27]). The *Drosophila* BM consists of four major types of glycoproteins, Collagen IV, Laminins, Nidogen and Perlecan, and some other minor components (LeBleu *et al.*, 2007 [28]). All the components form a durable scaffold protecting overlying cells from mechanical stresses, and also gathering signaling molecules to regulate various vital functions of the epithelium. The communication and signal trafficking between the cells and BM is implemented by the cellular receptor molecules, among which the integrins are principal in animal cells (Hynes, 2002 [29]). Integrins are transmembrane molecules consisting of two glycoprotein subunits, α and β, which link the actin cytoskeleton and the ECM (Hynes, 1992 [30]). Besides the function of anchoring epithelial cells to the ECM, integrins are also involved in the control of basal laminin assembly, es-

tablishing and maintaining apico-basal polarity, and also promoting cell invasiveness and migration (reviewed in Manninen, 2015 [31]).

1.1.2 Epithelial-mesenchymal transition

During the epithelial-mesenchymal transition (EMT) static epithelial cells lose their characteristics and transition into motile mesenchymal cells. EMTs result in significant alterations to epithelial characteristics: the cell-cell and cell-basement membrane adhesions are disrupted, the cytoskeletal structures reorganize, cells lose their apical-basal polarity and acquire migratory activity, invasiveness and elevated resistance to apoptosis (Figure 1.2). It should be noted that cells can cycle between epithelial and mesenchymal states via EMT and the reverse process, mesenchymal-epithelial transition (MET) (reviewed by Lim and Thiery, 2012 [32]; Kalluri and Weinberg, 2009 [33]). The ability of cells to move back and forth along this axis of epithelial and mesenchymal phenotypes is termed epithelial plasticity.

The EMT is an extremely conserved cellular program that occurs in many different organisms and underlies various vital processes. EMTs can be divided into three types based on the biological context (reviewed by Kalluri and Weinberg, 2009 [33]):

i) EMTs that are involved in development, which give rise to diverse mesenchymal cell types, such as mesenchymal stem cells. Examples of developmental processes involving EMT include endoderm and mesoderm formation during gastrulation, neural crest delamination, and the formation of many organs such as the heart and lung;

ii) EMTs that are involved in wound healing, tissue regeneration and fibrosis. These EMTs occur following trauma or inflammatory injury and involve creation of cells associated with repair such as fibroblasts;

iii) EMTs that are associated with neoplastic growth. At the stage of tumour dissemination, the EMT program is switched on in cancerous cells to impart mobility

and invasiveness for individual or collective migration to distant body areas via the circulatory system.

As the genetic control of different types of EMTs have much in common, understanding the genetic pathways and molecular interactions that regulate developmental EMTs can shed light on general EMT mechanisms and thereby aid in the development of more effective therapies for pathologies such as cancer.

1.1.3 Genetic regulation of the EMTs

As with any fundamental process, the EMT is regulated by a variety of genetic and epigenetic factors, which can control the process at transcriptional, post-transcriptional, translational and post-translational levels (Figure 1.2). A common mechanism by which EMT signaling pathways are induced is by different growth factors binding and activating their cell surface receptors. Among the best characterised EMT inducers are members of the TGF-β (transforming growth factor) superfamily (reviewed in Moustakas and Heldin, 2007 [34]; Katsuno *et al.*, 2013 [35]; Gonzalez and Medici, 2014 [36]; Moustakas and Heldin, 2016 [37]). Intracellular signaling of secreted TGF-β-related factors occurs through binding to receptors with both serine/threonine and tyrosine kinases activity (Lawler *et al.*, 1997 [38]). There are seven type I receptors and five type II receptors currently known in mammals (Derynck and Feng, 1997 [39], Heldin and Moustakas, 2016 [40]). Binding of a TGF-β family protein induces assembly of a specific heterotetrameric receptor complex composed of two type I and two type II receptors (Heldin and Moustakas, 2016 [40]). Upon ligand-mediated complex formation, the type II receptor transphosphorylates the type I receptor in its juxtamembrane region (GS domain), inducing its kinase activity (Derynck and Feng, 1997 [39], Shi and Massagué, 2003 [41]). In turn, the type I receptors transmit their signal through a number of pathways, which can be split into SMAD-dependent and SMAD-independent pathways (Gonzalez and Medici, 2014 [36]). In the canonical SMAD-dependent pathways, activation of the receptor leads to phosphorylation of the SMAD (MAD = mothers against

decapentaplegic) transcription factors which can then directly control transcription of EMT-associated genes (Vincent *et al.*, 2009 [42]). SMAD-independent signaling involves well-known kinase pathways such as PI3K-Akt, Src, JNK (c-Jun N-terminal kinase), ERK (extracellular signal-regulated kinase) and p38 (reviewed in Moustakas and Heldin, 2005 [43]). The TGF-β receptor can also phosphorylate, and thereby activate, the polarity protein Par6, which then, through interaction with the E3 ubiquitin ligase Smurf1 can promote EMT via degradation of the RhoA GTPase (Ozdamar *et al.*, 2005 [44]; Hutchison *et al.*, 2009 [45]).

In addition to TGF-β signaling, the EMT can be induced in response to several growth factors such as EGF (epidermal growth factor), FGF (fibroblast growth factor) and PDGF (platelet-derived growth factor). After binding the cell membrane receptor, these factors act through the RTK (receptor tyrosine kinase) pathway activating SMAD-independent signaling cascades (e.g. TGF-β-activated kinase 1 (TAK), Ras, PI3K/Akt, focal adhesion kinase (FAK) and Src kinase; Moustakas and Heldin, 2005 [43], Gonzalez and Medici, 2014 [36], Lamouille *et al.*, 2014 [46]). The other well-characterized EMT-inducing pathways include Wnt, Notch and Hedgehog (Barker, 2008 [47]; Bolos *et al.*, 2009 [48]; Taipale and Beachy, 2001 [49]).

Independently of, or in conjunction with, the canonical molecular pathways, the initiation of EMTs can also be caused by environmental or tissue-specific signals, such as hypoxia, mechanical stress, inflammation or extracellular matrix-generated signals (Finger and Giaccia, 2010 [50]; Heise *et al.*, 2011 [51]; Nisticò *et al.*, 2012 [52]).

The key downstream effectors of many EMT-initiating pathways are transcription factors such as Twist, Snail, ZEB1/2 and Srp/GATA factors, which regulate genes responsible for intercellular contacts. Among these, the members of the Snail family appear to play a central role in EMT. Snail family transcription factors are able to bind the promoter of the gene encoding E-Cadherin (the main component of ZA), repressing its transcription (Cano *et al.*, 2000 [53]). Also, Snail inhibits the transcription of genes encoding the polarity protein Crumbs, resulting in dissociation of polarity complexes (Whiteman *et al.*, 2008 [54]). Twist is another major activator

of EMT. This helix-loop-helix (bHLH) transcription factor was originally discovered as a master regulator of the *Drosophila* mesoderm (Leptin and Grunewald, 1990 [55]) and has more recently been identified as a positive regulator of metastatic growth of mammary carcinoma cells (Yang *et al.*, 2004 [56]). The activation of Snail can occur due to Twist binding the *snail* promoter (Yang *et al.*, 2004 [56]; Casas *et al.*, 2011 [57]). However, Twist can also repress E-Cadherin and activate N-Cadherin during the cadherin switching, independently of Snail (Yang *et al.*, 2010 [58]; Yang *et al.*, 2012 [59]). In addition to E-cadherin repression, Twist is involved in modulation of the cytoskeleton presumably via regulation of the Rho GTPase RhoC (Clark *et al.*, 2000 [60]). E-Cadherin can also be repressed by transcription factors from ZEB and LEF families either independently or as a result of Twist/Snail activation (Peinado *et al.*, 2007 [61]). For example, ZEB1 and ZEB2 recruit numerous transcription factors and cofactors (e.g. SMADs, p300/pCAF acetyltransferases, the Mi-2/NuRD complex, ATPase BRG1 and CtBPs) to either upregulate TGF-β signaling targets (e.g. E-Cadherin, Crumbs, PATJ, Claudin, miR-200 family) or repress some of them (e.g. Vimentin, Fibronectin, MMP1, MMP2, MMP14; reviewed in Sànchez-Tillò *et al.*, 2012 [62]). LEF-1 can repress *CDH1* (the E-cadherin coding gene in mammals) transcription and induce EMT acting in a complex with β-catenin which relocalizes to the nucleus under Wnt signaling (Kim *et al.*, 2002 [63], Jamora *et al.*, 2003 [64]).

Apart from elimination of epithelial cell-cell adhesion, EMT-signaling also affects cell polarity, cytoskeletal characteristics, and integrity of underlying ECM components of the BM. The loss of apico-basal polarity and increased ability for directional movement mostly rely on activation of Rho GTPase family members (Nobes and Hall, 1999 [65]). The concerted function of the three main GTPases, RhoA, Rac1 and Cdc42, promotes the dissociation of polarity complexes, formation of actin-based membrane extensions (lamellipodia and filopodia) and subsequent retraction-protrusion cycles during migration (Yilmaz and Christofori, 2009 [66]). Rho GTPases cycle between an inactive GDP-bound form and an active GTP-bound form, and coordination of this cycle relies on positive regulators, the guanine nucleotide

exchange factors (GEFs), and negative regulators, the GTPase-activating proteins (GAPs), which in turn are regulated by EMT signaling (Cherfils and Zeghouf, 2013 [67]). Besides GEFs and GAPs, activity of Rho GTPases can be also modulated directly through ubiquitylation, phosphorylation, ADP-ribosylation, adenylation, glycosylation and other post-translational modifications (Visvikis *et al.*, 2010 [68]). Finally, EMT signals induce matrix metalloproteinases (MMPs), which cause degradation of the ECM underlying the epithelium (i.e. the basement membrane) allowing migrating cells to leave the original epithelial layer (McNiven, 2013 [69]). Integrity of the basement membrane was also found to depend on Rho GTPases: repression of basal RhoA activity destabilizes the basal microtubule network supporting ECM resulting in basement membrane disassembly (Nakaya *et al.*, 2008 [70]).

1.1.4 *Drosophila melanogaster* as a genetic model for study of the EMT

Nowadays, *Drosophila melanogaster* is often used as a model organism for EMT studies, which can address both natural developmental EMT events and genetically induced EMTs (e.g. metastatic overgrowth and wound healing) (Murray, 2015 [71]). During development, flies undergo a number of EMT and EMT-like processes. As in all other animals, the first EMT event occurs during *Drosophila* gastrulation with the formation of the mesoderm. The mesodermal layer originates from a ventral band of ectoderm cells which form a furrow and invaginate (Leptin and Grunewald, 1990 [55]; Sweeton *et al.*, 1991 [72]). After furrow formation, the future mesodermal cells lose their epithelial morphology due to elevated Twist and Snail expression, and are able to disseminate along the inner surface of the ectodermal layer (Stathopoulos and Levine, 2002 [73]). Then, the cells undergo an MET and form an epithelial monolayer (McMahon *et al.*, 2010 [74]). Next, both EMT and MET events are involved in the formation of the *Drosophila* midgut/endoderm (Reuter, 1994 [75]). The midgut structure is formed by two ectodermal primordia, located at both anterior and posterior poles of the embryo, which invaginate, undergo an EMT and

then migrate towards each other. Cells migrate along the visceral mesoderm, which serves as a cellular substrate and also expresses expresses integrins, laminins and Netrins (Tepass and Hartenstein, 1994 [76]; Devenport and Brown, 2004 [77]; Pert *et al.*, 2015 [78]). As the two primordia are migrating they are also undergoing an MET and forming the gut epithelium (Reuter, 1994 [75], Tepass and Hartenstein, 1994 [76]).

At pupal stages, the eversion of wing discs and other imaginal discs require EMTs. As the goal of this project is the investigation of genetic pathways controlling the wing disc eversion, we will discuss this process in more detail below. An EMT also occurs in the *Drosophila* ovary. Within an ovary each ovariole consists of a chain of developing egg-chambers, each consisting of 16 germline cells surrounding by a follicular epithelium (Montell *et al.*, 2012 [79]). At stage 8 of egg-chamber development, two follicle cells at the anterior tip become specified as the polar cells. These secrete the cytokine Unpaired, activating the Jak/STAT pathway in neighbouring follicle cells (border cells), which in turn round up and encapsulate the polar cells. After that, the resulting cluster detaches from the follicular epithelium and migrates towards the oocyte. Migration requires protrusion formation and contractility of the border cells, and also adhesion to the nurse cells, which serve as a substrate. Eventually, the cluster contributes to the formation of the micropyle, a structure needed for sperm entry (Van De Bor *et al.*, 2011 [80]).

1.2 Wing disc eversion

1.2.1 Wing disc eversion requires a partial EMT

Wing disc eversion is the process, during metamorphosis, when the wing imaginal discs undergo dramatic morphogenetic changes that give rise to the wing and thorax of the adult. Wing imaginal discs are the larval sac-like structures consisting of a single, continuous epithelial layer that comprises two distinct classes of epithelia, a large population of columnar cells forming the disc proper epithelium (hereafter DP)

and a smaller population of large, overlying squamous cells of peripodial epithelium (hereafter PE) (Wehman, 1969 [81]). By the end of wing disc eversion, the DP cells will have given rise to the majority of the wings and thorax. The PE has a reduced contribution to adult tissues, but plays a crucial role in the eversion process (Pastor-Pareja *et al.*, 2004 [82]) (Figure 1.3). During larval stages, right up until metamorphosis, discs are attached to the larval epidermis by a stalk region, which is also composed of squamous PE cells.

At the late third instar larval stage, pulses of steroid hormone 20-hydroxyecdysone trigger further eversion, expansion and fusion of the imaginal discs to accomplish the dramatic developmental transformation of the larva into the imago (Richards, 1981 [83]). In particular, the wing disc eversion commences in the first hours after puparium formation, when a subset of PE cells starts to invade the larval epidermis and replace larval cells on the pupal surface. The progressive loss of adhesion and polarity of PE cells leads to the formation of a hole in the PE, through which the DP is extruded, widened and eventually acquires the adult wing shape. Once the PE cells have invaded the larval epidermal cells, they then assemble at the front of the everted disc and form a leading edge. This leading edge guides the migration of the two thoracic halves towards each other in the direction of the midline during the process known as thorax closure (Figure 1.4) (Pastor-Pareja *et al.*, 2004 [82]). Although the precise details of PE cell behaviour and their fate during wing disc eversion remains enigmatic, it is clear that transitions between epithelial and mesenchymal cell types take place and play a key role in the entire process. To begin with, the perforation of the PE is facilitated by dramatic changes in epithelial morphology, highly reminiscent of an EMT, in a subgroup of PE cells (Pastor-Pareja *et al.*, 2004 [82]). Pastor-Pareja and co-authors refer to this as a pseudo-EMT but we will refer to it in this thesis as a partial EMT. The results provided in Chapter 3 provide further confirmation that eversion involves an EMT event by clarifying the cellular and molecular events during this stage. After the invasion and migration typical of mesenchymal cell behaviour, PE cells at the leading edge are believed to undergo an MET event to facilitate the formation of the final

thoracic epithelial sheet. The subsequent fate of PE cells is not clear. Cell lineage tracking shows that most will not contribute to the final adult tissue (Pastor-Pareja *et al.*, 2004 [82]), suggesting that they are eliminated by apoptosis. Apoptosis of PE cells does indeed occur during eversion of *in vitro* cultured discs (Aldaz *et al.*, 2010 [84]), but this has not been shown *in vivo*, and expression of the apoptosis inhibitor *p35* does not block eversion (Pastor-Pareja *et al.*, 2004 [82]).

1.2.2 Genetic control of wing disc eversion

The epithelial transitions of the PE during eversion make wing discs a useful model for the investigation of EMT mechanisms and their genetic regulation, particularly the processes of tumor invasion and metastasis. In comparison with embryonic EMT events, wing eversion has some important advantage as a model system for EMTs. Firstly, since wing eversion occurs late in development, it is possible to get effective RNAi knockdown of genes, making it possible to utilise the large UAS-RNAi libraries of stocks. Secondly, since eversion failure leads to adult phenotypes that are easy to score, it opens the possibility of carrying out more comprehensive genetic screening *in vivo*. Despite these experimental advantages, our understanding of the genetic control of eversion as well as the mechanics of wing epithelial cell behaviour during eversion are limited.

1.2.2.1 JNK pathway

At the present time, the best characterised pathway known to be required for wing disc eversion is the c-Jun N-terminal kinase (JNK) signaling pathway (Martín-Blanco *et al.*, 1998 [85], Zeitlinger and Bohmann, 1999 [86], Agnès *et al.*, 1999 [87], Tateno *et al.*, 2000 [88], Pastor-Pareja *et al.*, 2004 [82]). JNK belongs to a conserved subfamily of mitogen-activated protein (MAP) kinases. The JNK pathway implements the transmission of signals in a range of pivotal cellular processes such as cell proliferation, differentiation, and apoptosis. In *Drosophila*, JNK signaling mediates epithelial morphogenesis during dorsal closure and wound healing. The core of the *Drosophila*

JNK signaling pathway is constituted by two stress-activated kinases JNKK and JNK encoded by the genes *hemipterous* (*hep*) and *basket* (*bsk*) respectively. The activity of Bsk is modulated by the downstream dual-specificity phosphatase *puckered* (*puc*), which is able to inactivate Basket in a negative feed-back loop (Martín-Blanco *et al.*, 1998 [85]). The loss of Bsk activity or overexpression of Puc in the peripodial cells produces defects in the disc eversion process and thorax formation suggesting a key role for this pathway in this process (Zeitlinger and Bohmann, 1999 [86]; Agnès *et al.*, 1999 [89]; Pastor-Pareja *et al.*, 2004 [82]). JNK pathway activation is required at multiple stages of disc eversion and is maintained in the PE throughout the whole process. At the beginning of eversion, JNK is necessary for the apposition of the PE and larval epidermis. Then, it regulates the adhesion of peripodial cells to the epidermis and promotes their further invasiveness and migration (Pastor-Pareja *et al.*, 2004 [82]). JNK also induces expression of the matrix metalloproteinases, MMP1 and MMP2, which control degradation of the basement membrane (Srivastava *et al.*, 2007 [90]). Finally, JNK signaling is involved in imaginal disc spreading and fusion, and is necessary for the integrity of the larval tissue (Martín-Blanco *et al.*, 2000 [91]).

1.2.2.2 Dpp pathway

In addition to the JNK pathway, the gene *decapentaplegic* (*dpp*), another key developmental regulator, is also involved in wing disc eversion. Dpp is the *Drosophila* homolog of the secreted vertebrate bone morphogenetic proteins BMP2/4 (BMPs) and is a member of the TGF-β protein family. As a principal morphogen, Dpp guides many major aspects of fly development, from the egg and imaginal discs patterning to the regeneration of the adult gastrointestinal tract (reviewed by Hamaratoglu *et al.*, 2014 [92]). For example, the most famous studies are dedicated to the patterning and growth control of the wing discs. Through its ability to control gene transcription, Dpp can play a positive or negative role in cell proliferation and migration, tissue scaling and growth (Hamaratoglu *et al.*, 2014 [92]). To actuate signaling, Dpp binds to a heterodimeric receptor consisting of a type I receptor, Thickveins (Tkv)

or Saxophone (Sax), and the type II receptor Punt (Put). Activated Tkv (Sax) then mediates the association of the Smad protein, Mothers-against-Dpp (Mad) with the co-Smad Medea (Med) and their further accumulation in the nucleus and transcriptional activation of target genes (Pyrowolakis *et al.*, 2004 [93]).

Developing wing discs of *Drosophila* larvae express *dpp* in a curved longitudinal stripe, which partially overlaps with the *puc* expression pattern in the stalk and in a subset of cells of the PE (Zeitlinger and Bohmann, 1999 [86]). During eversion, *dpp* expression is found in leading edge peripodial cells suggesting a role in thorax closure (Spencer *et al.*, 1982 [94]). Indeed, a hypomorphic mutation in *dpp* results in defective thorax closure. Strong cleft phenotypes are also produced by loss of *dpp*-associated genes, *tkv*, *put* and *med* (Martín-Blanco *et al.*, 2000 [91]). Loss of Dpp signaling blocks the filopodial extensions in the leading edge peripodial cells disrupting the migration of the disc during thorax closure (Martín-Blanco *et al.*, 2000 [91]).

1.2.2.3 Upstream regulators of the JNK pathway

The central importance of the JNK pathway in eversion is highlighted by the fact that several other genes, whose mutation are known to cause eversion failures, act as upstream regulators of the JNK pathway.

For example, mutations in *src42A* (and to a lesser degree *src64* and *Tec29*) cause defects in embryonic dorsal closure and thorax closure, and these phenotypes appear to be due to failure of JNK pathway activation (Tateno *et al.*, 2000 [88]). *src42A* mutants fail to activate *puc-lacZ* expression in both the embryos and wing discs, and expression of an active form of Src42 can increase Bsk phosphorylation levels. Furthermore, *src42A* phenotypes are enhanced by loss of one copy of *hep* or *bsk* and suppressed by reducing dosage of the negative regulator *puc* (Tateno *et al.*, 2000 [88]).

The Homeodomain Interacting Protein kinase (HipK) can also activate JNK signaling (Huang *et al.*, 2011 [95]). HipK nuclear localisation is promoted by sumoylation, but when that is disrupted, for example by mutation of the SUMO gene *smt3*,

Hipk is found in the cytoplasm where it can activate the JNK pathway and cause eversion failure.

Another regulator of the JNK pathway is Pvr. RNAi knockdown of *Pvr* causes split thoraxes or thoraxes with a midline lacking bristles. *Pvr* encodes the *Drosophila* PDGF and VEGF receptor related (one of the *Drosophila* RTKs, and homolog of the mammalian PDGF and VEGF receptors), and is implicated in a range of cellular functions, including migration, proliferation and survival. In response to localised expression of its ligands (PVF1, PVF2 and PVF3), Pvr directs migration of the hemocytes, midline glia, salivary glands and ovarian border cells (reviewed by Sopko and Perrimon, 2013 [96]). Pvr stimulates the activation of Rac1 GTPase, via interaction with the Crk/Mbc/ELMO complex (where Mbc (Myoblast city) is a homolog of the mammalian GEF DOCK1), and also the Cdc42 GTPase via an unknown mechanism. Both GTPases contribute to the activation of JNK and subsequently promote thorax closure (Ishimaru *et al.*, 2004 [97]).

Finally, a member of the dedicator of cytokinesis family proteins (DOCK), Sponge (Spg; a homolog of mammalian DOCK3 and DOCK4), has been reported to induce JNK signaling to regulate thorax development. Similar to *mbc*, *spg* encodes a GEF protein activating Rac1 GTPase suggesting a role in regulation of actin cytoskeletal rearrangement. It is also known to be involved in embryonic CNS development and in photoreceptor differentiation during eye development (Eguchi *et al.*, 2013 [98]). In wing discs, RNAi knockdown of *spg* results in reduced *puc* expression and in a split thorax phenotype (Morishita *et al.*, 2014 [99]).

1.2.2.4 Centralspindlin, a novel regulator of wing and thorax development

Recently the centralspindlin complex, best known as an essential factor of central spindle assembly during cytokinesis, has been identified as a novel regulator of thorax closure (Sfregola, 2014 [100]). Centralspindlin is a heterotetramer containing two proteins in equal proportions: Tumbleweed (Tum) and Pavarotti (Pav) (Mishima *et al.*, 2002 [101], Zavortink *et al.*, 2005 [102]). Tum functions as a scaffolding

protein but also has Rac1 GAP activity (Goldstein *et al.*, 2005 [103]), while Pav is a kinesin-like protein responsible for proper organization of microtubule bundles (Adams *et al.*, 1998 [104], Tao *et al.*, 2016 [105]). Downregulation of Tum in wing disc results in thoracic clefts and reduction of sensory bristles (Sfregola, 2014 [100]). Interestingly, the overexpression of Tum alone also produced light eversion phenotypes. Furthermore, the overexpression of the whole centralspindlin complex results in loss of epithelial integrity and formation of filopodial protrusions, which presumably affect the normal eversion process and cause the severe thoracic cleft phenotype. The nuclear position of the centralspindlin complex also appears to be important as the mislocalization of it to the cell periphery leads again to the cleft phenotype. Whether these genetic manipulations affect the JNK or Dpp pathway activation remains to be determined.

1.3 Genetic screening for new regulators of wing disc eversion

In recent years our laboratory has conducted a large-scale genetic RNAi screen (≈1700 genes) for novel regulators of the PE cell EMT. The screen utilised the GAL4/UAS system (Brand and Perrimon, 1993 [106]) and the large publicly available UAS-inverted repeat RNAi constructs (hereafter UAS-IR) libraries (the Vienna *Drosophila* Research Centre (VDRC), the Bloomington *Drosophila* Stock Centre's TRiP collection or the National Institute of Genetics (NIG-FLY)). To knockdown the genes specifically in the cells critical for the peripodial EMT, five different drivers were tested: *grunge-GAL4*, *puckered-GAL4*, *Ultrabithorax-GAL4*, *pannier-GAL4* and *MZ980-GAL4*. The widest spectrum of phenotypes (including full eversion failure with internalised wings and missing thoracic tissue) was obtained with the *Ultrabithorax-GAL4* driver (hereafter *Ubx-GAL4*; Pallavi and Shashidhara, 2003 [107]).

The eversion defects in adult flies can be divided into four main categories:

i) late pupal lethality with normal wing and thorax structures;

ii) a crumpled wing phenotype (thorax normal);

iii) thoracic defects, which may include also uneverted/internalised wings, thoracic clefts, complete loss of thoracic and wing tissue;

iv) larval or early pupal lethality.

Ultimately, the screen identified a set of approximately 170 genes that, when knocked down, produced wing eversion defects (Manhire-Heath R., Thompson J., Saint R. and Murray M. J., unpublished results). Among them, the knockdown of *Drosophila* NetrinA caused the strongest effect on wing disc eversion. In the following sections, I describe Netrin family proteins and the subsequent analysis of the netrin phenotype uncovered in the screen.

1.3.1 *Drosophila* NetrinA is required for wing disc eversion

1.3.1.1 Netrin family proteins

Drosophila NetrinA belongs to the family of Netrin proteins, well-known as secreted chemotropic guidance cues for both axons and migrating cells. They also regulate epithelial morphogenesis during the formation of a variety of organs such as the vasculature, lung, pancreas and mammary glands (reviewed in Lai Wing Sun *et al.*, 2011 [108]). Importantly, the cellular processes regulated by netrins, such as migration and adhesion, are directly relevant to EMT/MET-associated events. Both *netrinA* and its only *Drosophila* paralog *netrinB* are located in tandem on the X chromosome and show 41% amino acid sequence identity (Harris *et al.*, 1996 [109]). Being highly conserved, *Drosophila* Netrins share the same domain organization with the Netrins from other organisms: an N-terminal signal peptide, followed by

the domains VI and V that are homologous to laminins, one of the principal components of basement membrane. Domain V comprises three EGF-like repeats (Harris *et al.*, 1996 [109]; Mitchell *et al.*, 1996 [110]). The C-terminal domain diverges from the laminin structure, and, interestingly, contains the netrin module (NTR), which is also found in tissue inhibitor of metalloproteinases (TIMP) (Bányai and Patthy, 1999 [111]; Figure 1.5).

Netrins were first shown to act during axon guidance, migration and oligodendroglial branching (reviewed in Lai Wing Sun *et al.*, 2011 [108]). In all the model organisms tested, including *Drosophila*, netrins are responsible for the formation of commissures connecting the two halves of the developing CNS (Kennedy *et al.*, 1994 [112]; Serafini *et al.*, 1994 [113]; Harris *et al.*, 1996 [109]; Mitchell *et al.*, 1996 [110]; Newquist *et al.*, 2013 [114]). Secreted by the midline cells, netrins can act either as chemoattractants or chemorepellents to guide the migration of extending axons (Colamarino and Tessier-Lavigne, 1995 [115]). Whether the netrin signal becomes attractive or repulsive depends mostly on which netrin receptors are involved (see details below): during axon pathfinding, the association of netrin with the UNC-5 type of receptor stimulates a repulsive response of the growth cones, whereas the association with DCC/Frazzled causes axon attraction (Hong *et al.*, 1999 [116]). Besides the axons, attraction/repulsion signaling of netrins and their receptors can control other cell types in *Drosophila* embryos such as glial cells (Von Hilchen *et al.*, 2010 [117]) and midgut cells (see below). Also, netrins control development of distal structures of the nervous system. As an example, during fetal stages of vertebrate development, the migration of neural crest derived precursors of submucosal and pancreatic ganglia to the final location is regulated by netrins that are secreted by the enteric or pancreatic mesenchyme and attract the DCC-expressing cells (Jiang *et al.*, 2003 [118]; Ratcliffe *et al.*, 2006 [119]).

Netrins are also involved in the development of structures outside the CNS. *In vitro* cell culture studies suggest that during pancreas development, Netrin-1 interacts with $\alpha 6\beta 4$ and $\alpha 3\beta 1$ integrins to mediate adhesion to the substrate and migration of putative pancreatic progenitor cells (Yebra *et al.*, 2003 [120]). In the

developing mammary gland, Netrin-1 acts through its receptor Neogenin to support adhesion between cap and prelumenal cell layers. The defects in this adhesion resulting from elimination of Netrin-1 or Neogenin result in an abnormal structure of the terminal end buds, including an exaggerated subcapsular space containing many isolated cells, together with the breaks in the basal lamina (Srinivasan *et al.*, 2003 [121]). During *Drosophila* midgut development, both NetrinA and NetrinB are expressed by the visceral mesoderm, where they are required for normal migration and MET of the primary midgut epithelial cells, which themselves express Frazzled. Loss of either Netrins or Frazzled, also disrupts βPS and αPS1 integrin localization at the interface between the visceral mesoderm and the midgut suggesting some interactions between these signaling pathways (Pert *et al.*, 2015 [78]). The control of migration by netrins is also likely to involve the activation of Rho GTPases. *In vitro* experiments using embryonic commissural neurons and neuroblastoma cells overexpressing DCC showed that Netrin-1 could induce Rac1 and Cdc42 activation, which resulted in increased filopodial numbers and a larger cell surface area (Shekarabi and Kennedy, 2002 [122]).

Netrins are also able to regulate branching morphogenesis. During mammalian lung development, the distal ends of endothelial tubules form the primordial buds which eventually give rise to the respiratory tree. Netrin-1 and Netrin-4 expression at the proximal epithelium prevents inappropriate budding and subsequent branching apparently by inhibiting FGF-mediated activation of MAPK and ERK pathways (Liu *et al.*, 2004 [123]). Netrin-1 is also involved in angiogenesis (Castets and Mehlen, 2010 [124]), which is known to involve a partial endothelial-mesenchymal transition (a variant of the EMT). Endothelial cells express EMT-associated genes and break the basement membrane, but do not lose cell-cell adhesion and instead migrate as a train of interconnected cells (Welch-Reardon *et al.*, 2015 [125]).

In nematodes, the Netrin ortholog UNC-6 is found to be a key regulator of anchor cell invasion (Ziel *et al.*, 2009 [126]). This process, when a single cell of the somatic gonad (anchor cell) breaks the basement membrane separating the uterine and vulval epithelia and makes a contact between these two tissues, is used as a simple model

for studying invasion (Sherwood and Sternberg, 2003 [127]). Local secretion of UNC-6 polarizes its receptor UNC-40 promoting membrane protrusions through the activation of F-actin and phosphatidylinositol 4,5-bisphosphate (Ziel *et al.*, 2009 [126]).

Furthermore, human Netrin-1 acts as an oncogene and its overexpression is associated with a large number of metastatic cancers, e.g. ovarian, breast, pancreatic and prostate (Papanastasiou *et al.*, 2011 [128], Fitamant *et al.*, 2008 [129], Huang *et al.*, 2014 [130], Kong *et al.*, 2013 [131], Ramesh *et al.*, 2011 [132]).

1.3.1.2 Loss of *Drosophila* Netrins disrupts wing disc eversion

The identification of NetrinA in our genetic screen for wing disc eversion defects described above was followed up by further studies published in 2013 in *Nature Communications* (Manhire-Heath *et al.*, 2013 [133]). This paper reported the results of collaborative research between Dr Manhire-Heath and myself (my contribution to this study was the cellular analysis of wing discs (Manhire-Heath *et al.*, 2013 [133], Fig. 3) and constitutes the majority of Chapter 3 of this thesis). In this section I will briefly review the work reported in that paper and in R. Manhire-Heath's PhD thesis.

NetrinA and NetrinB are enriched in peripodial cells of the third instar wing discs, where they localize to cytoplasmic puncta. *Ubx-GAL4*-driven RNAi knockdown of *netrinA* (*Ubx>netA.IR*; the genotype caused by downregulation of NetrinA is referred to as *netA.IR* hereafter) resulted in eversion phenotypes in 31.2% of the live progeny, ranging from shrivelled wings and twisted thorax to severe thoracic clefts and complete single or double uneverted wings. In addition to adult phenotypes, 15% of progeny were pupal lethal. *Ubx-GAL4*-mediated expression of *netrinB.IR* lines also produced thoracic clefting and single uneverted wings though only with a 1.3% to 2% penetrance, respectively, suggesting that NetrinB contributes to the disc eversion process but is not the major factor. Supporting this, co-expression of *UAS-IR* constructs for both netrins increased the eversion failure penetrance to 32.9% and pupal lethality to 44.8%. Moreover, the other striking illustration of

redundancy between the two Netrins is the fact, that co-expression of *UAS-netB* almost completely rescued the *netA.IR* phenotype (Figure 1.6).

To confirm the RNAi knockdown results, pupae hemizygous for the classical loss-of-function small deficiency $netAB^{\Delta}$ (Brankatschk and Dickson, 2006 [134]) were examined. Although the deletion of both *Drosophila* Netrins caused 95.8% lethality during pupal stages, dissection and staining with a nuclear marker, Hoechst 33258, of dead pupae showed that 35% of progeny had eversion defects (Figure 1.6, f). To confirm that adult defects were a result of failed wing disc eversion, live imaging experiments were performed. The movements of pupal discs were recorded *in vivo* from the onset of pupariation, when the discs appose larval epidermis, till their fusion at the midline (Figure 1.6, h-k). The disc eversion disruptions correlated with the adult phenotypes: either the disc eversion was significantly delayed or a single or both discs failed to evert. The imaging results indicated that the *netA.IR* adult phenotypes were caused by malfunction of the intrinsic properties or behaviour of the wing discs at the early stages of morphogenesis.

Finally, the study demonstrated that NetrinA is likely involved in two distinct stages of the wing disc eversion process. Firstly, NetrinA is required for the PE EMT. This result, which is described in Chapter 3, comes from the *in vitro* disc culturing (Aldaz *et al.*, 2010 [84]), which has shown that 32% of *Ubx>netA.IR* failed to evert when cultured in media containing the molting hormone, 20-Hydroxyecdysone. Secondly, the analysis of the *Ubx>netA.IR* pupae revealed that RNAi knockdown of *netrinA* resulted in a reduced number of leading edge peripodial cells and reduced filopodial protrusions during thorax closure suggesting a role for NetrinA during the epithelial sheet migration stage of eversion (R. Manhire-Heath, PhD thesis). Thus, several lines of evidence indicate the importance of Netrins as wing disc eversion regulators.

1.3.1.3 Molecules acting downstream of NetrinA

One of the most interesting questions is what proteins act downstream and upstream of NetrinA during the wing disc eversion. The first obvious candidate that might be

affected by RNAi knockdown of *netrinA* is JNK, a central EMT regulator of wing eversion. However, an expression analysis of the JNK pathway reporters, such as *misshapen*, *puckered* and *matrix metalloproteinase 1*, indicated that JNK pathway activation was normal in *netA.IR* discs (Manhire-Heath *et al.*, 2013 [133]). This important finding suggests that either Netrins act downstream of JNK signaling or function in a parallel pathway.

The other natural targets of NetrinA as a secreted protein are its receptors. Four types of Netrins receptors are described in the literature: members of the DCC family which includes Deleted in Colorectal Cancer (DCC) and Neogenin in vertebrates, Frazzled in flies and UNC-40 in *C. elegans*; the Unc-5 family; Down syndrome cell adhesion molecule (DSCAM) and Integrins (reviewed in Lai Wing Sun *et al.*, 2011 [108]). All *Drosophila* orthologs of these receptors were tested in an RNAi screen (R. Manhire-Heath, PhD thesis). Surprisingly, only RNAi knockdown of $\alpha PS3$ (gene *scab*), encoding a *Drosophila* α integrin subunit, produced thoracic defects in 34.5% of progeny. Knockdown of the other integrins subunits as well as other NetrinA receptors did not affect wing and thorax development. However, further investigations revealed Frazzled as a regulator of wing disc eversion (R. Manhire-Heath, PhD thesis and Manhire-Heath *et al.*, 2013 [133]).

1.3.2 The receptor of NetrinA, Frazzled, is involved in wing disc eversion

1.3.2.1 Frazzled, the *Drosophila* DCC ortholog

Drosophila Frazzled (Kolodziej *et al.*, 1996 [135]) is a member of the DCC family of proteins (DCC, Neo1, Frazzled and UNC-40) which are characterised by functional extracellular and intracellular regions (Figure 1.5). The extracellular part consists of four immunoglobulin C2 structural domains (IG) and six fibronectin type III domains (FNIII), which are essential for netrin binding (Geisbrecht *et al.*, 2003 [136]; Kruger *et al.*, 2004 [137]). Intracellularly, the receptor has no catalytic domains but contains three highly conserved sequences termed the P1, P2 and P3 motifs,

among which the P3 was shown to be critical in axon guidance. The P domains also mediate association with the cytoplasmic domains of other receptors. The P1 domain mediates association with the Unc5 receptor (Hong *et al.*, 1999 [116]), while the P3 domain mediates association with the Robo receptor (Stein *et al.*, 2001 [138]). The P3 domain is also responsible for self-association in mammals (Stein *et al.*, 2001 [138]) though not in *Drosophila* (Garbe *et al.*, 2007 [139]). A detailed description of the function of these intracellular domains is provided in Chapter 5.

DCC/Frazzled/UNC-40 are expressed on commissural axons and growth cones and mediate netrin-dependent axon guidance across the midline (Keino-Masu *et al.*, 1996 [140]; Kolodziej *et al.*, 1996 [135]; Chan *et al.*, 1996 [141]; Hiramoto *et al.*, 2000 [142]). Although DCC receptors by themselves mediate attractive netrin signaling, the interaction with other receptors converts this response to repulsion. For example, in *Xenopus* spinal explants, the Netrin-1/DCC attraction signal can be silenced by direct interaction between Roundabout (Robo) and DCC cytoplasmic domains (Stein and Tessier-Lavigne, 2001 [143]). In *Drosophila*, heterodimerization of Frazzled with the Unc-5 receptor (normally responsible for short-range repulsion) promotes cell-autonomous long-range repulsion (Keleman and Dickson, 2001 [144]).

Currently, the DCC receptors are also actively being investigated in cancer progression (reviewed by Duman-Scheel, 2012 [145]). Human DCC is known as a tumor suppressor, and roughly 70% of colorectal cancers are characterized by loss of heterozygosity of chromosome 18q, a region which includes the DCC locus (Fearon *et al.*, 1990 [146]; Mehlen and Fearon, 2004 [147]). DCC inactivation has also been documented in oral cavity squamous cell carcinomas and myeloid leukemia (Gotley *et al.*, 1996 [148], Arantes *et al.*, 2015 [149], Qu *et al.*, 2015 [150]). Interestingly, even in *Drosophila* loss of Frazzled has been reported to produce metastatic growth of epithelial tissue (see Chapter 4 for details; VanZomeren-Dohm *et al.*, 2011 [151]). Several studies suggest that the ability of DCC to inhibit tumor metastasis is due to its dependence receptor activity, which causes apoptosis induction in tumor cells when the Netrin ligand is unavailable (Mehlen *et al.*, 1998 [152], Castets *et al.*,

2011 [153]). On the other hand, the dependence effect plays an essential role during CNS development, when the presence of Netrin-1 ensures the survival of neurons expressing DCC (Llambi *et al.*, 2001 [154]; Furne *et al.*, 2006 [155]).

Similar to Notch receptors, intracellular domains (ICDs) of DCC family receptors can be released from the membrane via γ-secretase cleavage, and then move to the nucleus where they can activate transcription (Taniguchi *et al.*, 2002 [156]; Goldschneider *et al.*, 2008 [157]; Neuhaus-Follini and Bashaw, 2015 [158]). The biological importance of this has been recently demonstrated whereby the Fra ICD activated expression of another axon guidance factor, Commissureless (Neuhaus-Follini and Bashaw, 2015).

Another remarkable aspect of netrin-DCC relationships is that the receptor can be downregulated by ubiquitin-proteasome-mediated degradation upon binding its ligand (Hu *et al.*, 1997 [159], Kim *et al.*, 2005 [160]). This effect underlies the mechanism of the growth cone's desensitization to netrin guidance cues, which is presumably designed to fine-tune axonal outgrowth. For example, in one study DCC levels were shown to be the highest in the distal axonal projections, but as axons elongated towards their target, which had intense expression of Netrin-1, the levels were reduced (Shu *et al.*, 2000 [161]).

1.3.2.2 NetrinA downregulates Frazzled from the peripodial cell membrane to promote wing disc eversion

Both wing disc epithelia express *frazzled*. However, DP cells carry higher levels of Frazzled and it is enriched around the cell perimeter, whereas PE expression levels of *frazzled* are reduced in comparison with DP and the receptor is more widely distributed throughout the cytoplasm. The ratio of mean Frazzled levels in PE cells to mean levels of an adjacent region of DP cells is increased in *Ubx>netA.IR,GFP* discs in comparison with *w1118;Ubx>GFP* control discs, suggesting a role for NetrinA as a negative regulator of its receptor (Figure 1.7; Manhire-Heath *et al.*, 2013 [133]). Furthermore, the cytoplasmic localization of Frazzled in the PE is shown to be associated with an early endosome marker Rab5, suggesting NetrinA dependent

regulation of Frazzled involves endocytosis. Thus, increased Frazzled in *netA.IR* discs might be the reason for eversion failure. Indeed, ectopic *Ubx-GAL4*-driven expression of a *UAS-frazzled* construct causes eversion failure similar to *Ubx>netA.IR* phenotypes (Figure 1.7, a, b, g). The idea that up-regulated Frazzled in *netA.IR* discs could account for the eversion failure is also supported by the fact that reduction of *frazzled* levels either by RNAi (Manhire-Heath *et al.*, 2013 [133])) or loss of one copy (this work), significantly rescued the *netA.IR* phenotype (Figure 1.7, h). Taken together, these observations suggest that NetrinA binding of Frazzled promotes its trafficking through the endocytic degradative pathway, thereby facilitating wing disc eversion.

1.3.3 An ERM protein, Moesin, is a potential downstream component of the NetrinA/Frazzled pathway

Since loss of NetrinA increased Frazzled levels, and loss of *frazzled* could rescue *netA.IR* phenotypes, we hypothesized that Frazzled might inhibit the peripodial cell's EMTs. The idea that Frazzled maintains the epithelial state is also supported by recent findings whereby the loss of *frazzled* made eye-antennal disc epithelial cells metastasize and form distant tumors in adult *Drosophila* (VanZomeren-Dohm *et al.*, 2011 [151]). Further research of downstream effectors of Frazzled would shed light on the possible mechanisms of NetrinA/Frazzled dependent wing disc eversion. Among the many epithelial factors known to interact with Frazzled or DCC, Moesin is known to have a role in maintaining epithelial stability in *Drosophila*. *Drosophila* Moesin (Dmoe) is the only identified member of the conserved ERM protein family, which is composed of three proteins, Ezrin, Radixin and Moesin (Edwards *et al.*, 1994 [162]; McCartney and Fehon, 1996 [163]). In mammals, these three paralogs are widely expressed in the organism, however each protein has its tissue specificity. In the cell, ERM proteins are localized under the cell cortex complex in the filamentous actin-rich zone, where, when activated, they play an important role in crosslinking the phospholipids and transmembrane proteins to

the cytoskeleton. ERM proteins are involved in essential cellular processes such as changes in cell shape, protrusion formation, cell motility, membrane trafficking and also signaling pathways via interaction with regulators of Rho GTPase proteins (reviewed by Louvet-Vallèe, 2000 [164]; Bretscher *et al.*, 2002 [165]; Fehon *et al.*, 2010 [166]). The juxtamembrane region of mammalian DCC contains an ERM binding domain (Martin *et al.*, 2006 [167]) through which the receptor binds Ezrin in respond to a Netrin-1 signal, and initiates further Ezrin phosphorylation (Antoine-Bertrand *et al.*, 2011 [168]).

Similar to mammalian ERM proteins, Dmoe connects plasma membrane structures with actin filaments and controls cell shape changes, polarity, cell migration and adhesion (Edwards *et al.*, 1997 [169]; Bloor and Kiehart, 2002 [170]; Polesello *et al.*, 2002 [171]). Although Frazzled contains a region that is reasonably conserved with the DCC-ERM-binding domain, there is no evidence that Frazzled is able to bind Moesin directly. Speck and co-authors demonstrated in *Drosophila* imaginal disc epithelia that $Dmoe^{-/-}$ cells lose epithelial characteristics, such as apical-basal polarity, cell-cell junctions and basement membrane adhesion, and delaminate from the epithelium (Speck *et al.*, 2003 [172]). Analogous basal extrusion of wing columnar cells occurs in cells lacking the *Drosophila sterile-20 kinase* (*slik*), a kinase known to phosphorylate Moesin (Hipfner *et al.*, 2004 [173]). Increased cell motility and invasion are associated with depletion of apical F-actin and overactivated Rho1 signaling. In wing DP epithelia, Dmoe was shown to recruit the RhoGTPase GAP factor, Conundrum (Conu), which in turn reduces Rho1 activity (Neisch *et al.*, 2013 [174]). Furthermore, activated Rho1 in $Dmoe^{-/-}$ null mutant cells causes an elevated caspase level associated with JNK-dependent apoptosis suggesting Moesin as well as Rho1, regulates cell survival (Neisch *et al.*, 2010 [175]).

In our model, the PE cells of *netA.IR* and *frazzled* overexpressing peripodial cells have moderately increased phosphorylated Dmoe (hereafter pMoe) levels compared to control *w1118;Ubx>GFP* discs (Figure 1.7). This result suggests the ability of Frazzled to up-regulate the level of activated pMoe, which might contribute to EMT failure due to fortified epithelial integrity. Consistent with this, co-expression

of *UAS-moe.IR* in *netA.IR* discs successfully suppresses eversion defects. However, contrary to expectations, ectopic *Ubx-GAL4*-driven expression of the constantly activated phosphomimetic form, Moe^{T559D}, did not affect flies. Thus, although Moesin is likely involved in NetrinA/Frazzled pathway, its role in the PE during eversion still remains obscure.

1.4 Outstanding questions and aims of this study

These data identified a new genetic pathway controlling *Drosophila* wing disc eversion. However, it was still unclear whether peripodial cells undergo a true EMT at the beginning of eversion, and what the role of netrin signaling might be in that process. It was also unclear what the cellular role of Frazzled is in epithelial cells. In particular, whether the role of Frazzled in motile cells and epithelial cells is molecularly separable in terms of the protein domains involved and/or the downstream molecular components it interacts with.

Therefore, the aims of this study were:

i) to understand whether the *netA.IR* and *frazzled* overexpression eversion phenotypes are due to failure of the EMT-associated cellular events in the peripodial epithelium;

ii) to understand roles of Frazzled in a stable epithelium and during the EMT;

iii) to understand whether Frazzled controls two separate signaling pathways that either support epithelial integrity or promote motility;

iv) to investigate potential components acting upstream and downstream of NetrinA and Frazzled.

In the first experimental chapter, I establish an approach separating the EMT

stage from subsequent invasion and migration of wing disc eversion, and then characterize molecular and cellular events (i.e. zonula adherens breakdown, cytoskeletal modifications, basement membrane degradation) in *netA.IR* and *frazzled* overexpressing PE during the EMT. The second experimental chapter describes the effects of *frazzled* loss-of-function and *frazzled* gain-of-function on epithelial cell phenotypes. The last two experimental chapters focus on understanding the molecular mechanisms acting downstream of Frazzled and whether its roles in motility and epithelial function are separable. Two approaches were taken: i) a structure-function analysis to determine which cytoplasmic region of the receptor is responsible for different cellular processes; and ii) a small RNAi modifier screen to identify downstream components of NetrinA/Frazzled pathway. Altogether, the results obtained in the last chapters suggest a possible mechanism of formation of *netA.IR* and *frazzled* overexpression phenotypes.

Figure 1.1: ***Drosophila* epithelial cell.** Idealised schematic of typical *Drosophila* epithelial cell. The main domains of the plasma membrane are indicated to the right. The main cell-cell and cell-ECM junctions and main regulatory complexes are shown. Abbreviations: Crb (Crumbs), Std (Stardust), Patj (PALS1-associated tight junction protein), Baz (Bazooka), aPKC (atypical Protein Kinase C), Scrib (Scribbles), Dlg (Discs large), Lgl (Lethal giant larvae). See section 1.1.1 for details.

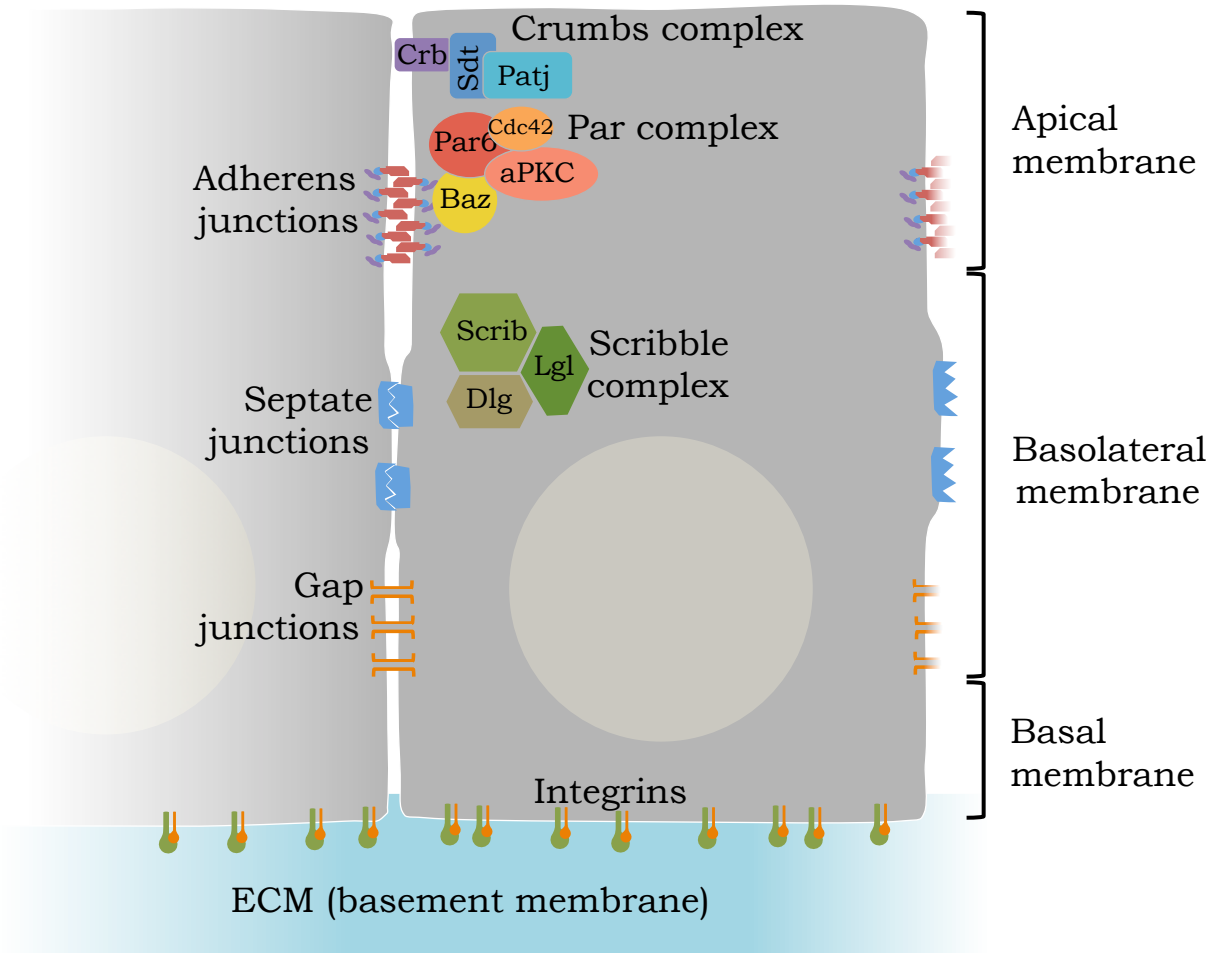
Crumbs complex
Crb
Sdt
Patj
Par complex
Par6
Cdc42
aPKC
Baz
Adherens junctions
Scribble complex
Scrib
Lgl
Dlg
Septate junctions
Gap junctions
Integrins
ECM (basement membrane)
Apical membrane
Basolateral membrane
Basal membrane

Figure 1.2: **Genetic pathways controlling EMTs.** A schematic of a vertebrate epithelium undergoing EMT. Cells lose apico-basal polarity, become motile, and break through the underlying basement membrane. Mesenchymal cells can also transition back to an epithelial cell type (MET). A variety of extracellular signals and environmental factors can trigger EMT. Changes in adhesion and motility are effected by key transcription factors (Snail/Twist/ZEB/LEF), and signaling molecules such as Rho GTPases. See section 1.1.3 for details.

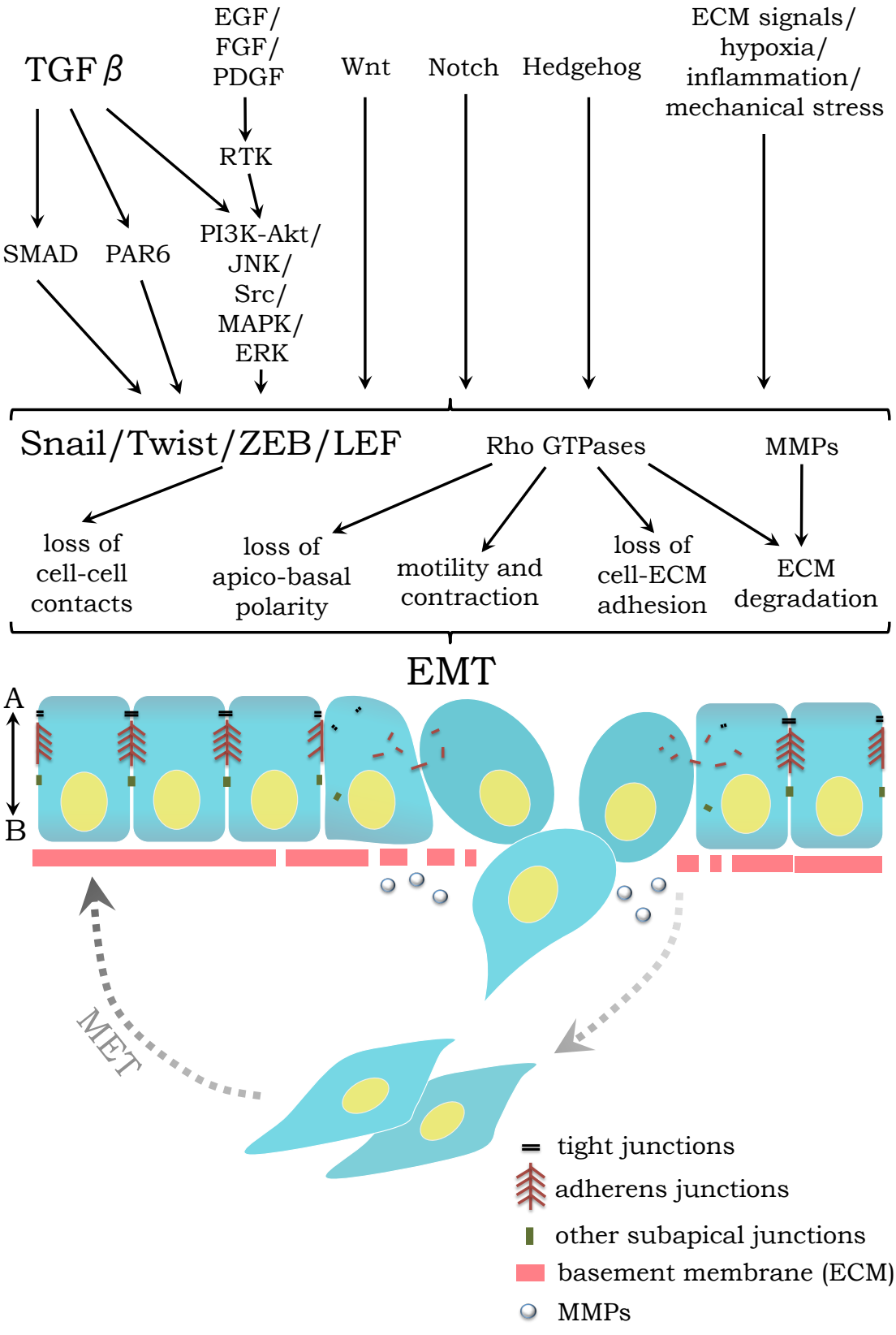
TGF β
EGF/
FGF/
PDGF
Wnt
Notch
Hedgehog
ECM signals/
hypoxia/
inflammation/
mechanical stress
RTK
SMAD
PAR6
PI3K-Akt/
JNK/
Src/
MAPK/
ERK
Snail/Twist/ZEB/LEF
Rho GTPases
MMPs
loss of
cell-cell
contacts
loss of
apico-basal
polarity
motility and
contraction
loss of
cell-ECM
adhesion
ECM
degradation
EMT
A
B
MET
tight junctions
adherens junctions
other subapical junctions
basement membrane (ECM)
MMPs

Figure 1.3: ***Drosophila* wing disc.** A schematic of the *Drosophila* wing imaginal disc shown in cross-section. The disc is an epithelial sac, which attaches to the larval epidermis, and is surrounded by a basement membrane (light green). The disc is comprised of two distinct types of epithelium: the thin, squamous peripodial epithelium (dark green) and the columnar disc proper (DP) epithelium (pink).

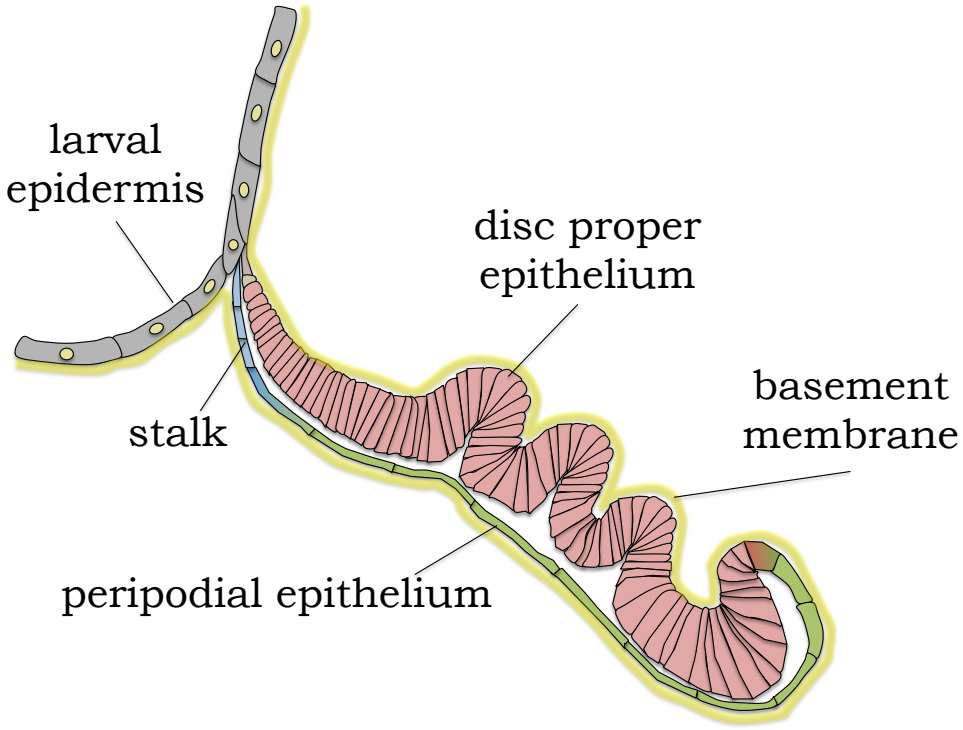
larval
epidermis
disc proper
epithelium
basement
membrane
stalk
peripodial epithelium

Figure 1.4: ***Drosophila* wing disc eversion.** The process of wing disc eversion. At the beginning of pupariation, the wing imaginal disc becomes closely apposed to the overlying larval epidermis. The peripodial epithelium then undergoes a partial EMT while the basement membranes lying between the disc and epidermal cells breaks down. The perforations in the peripodial epithelium grow while the disc epithelium begins an epithelial sheet migration across the top of the larval epidermis. Migrating sheets from either side eventually meet at the thoracic midline where they fuse to form the thorax epithelium. Abbreviations: BM - basement membrane; PE - peripodial epithelium; DP - disc proper epithelium; EMT - epithelial-mesenchymal transition; MET - mesenchymal-epithelial transition. See section 1.2.1 for details.

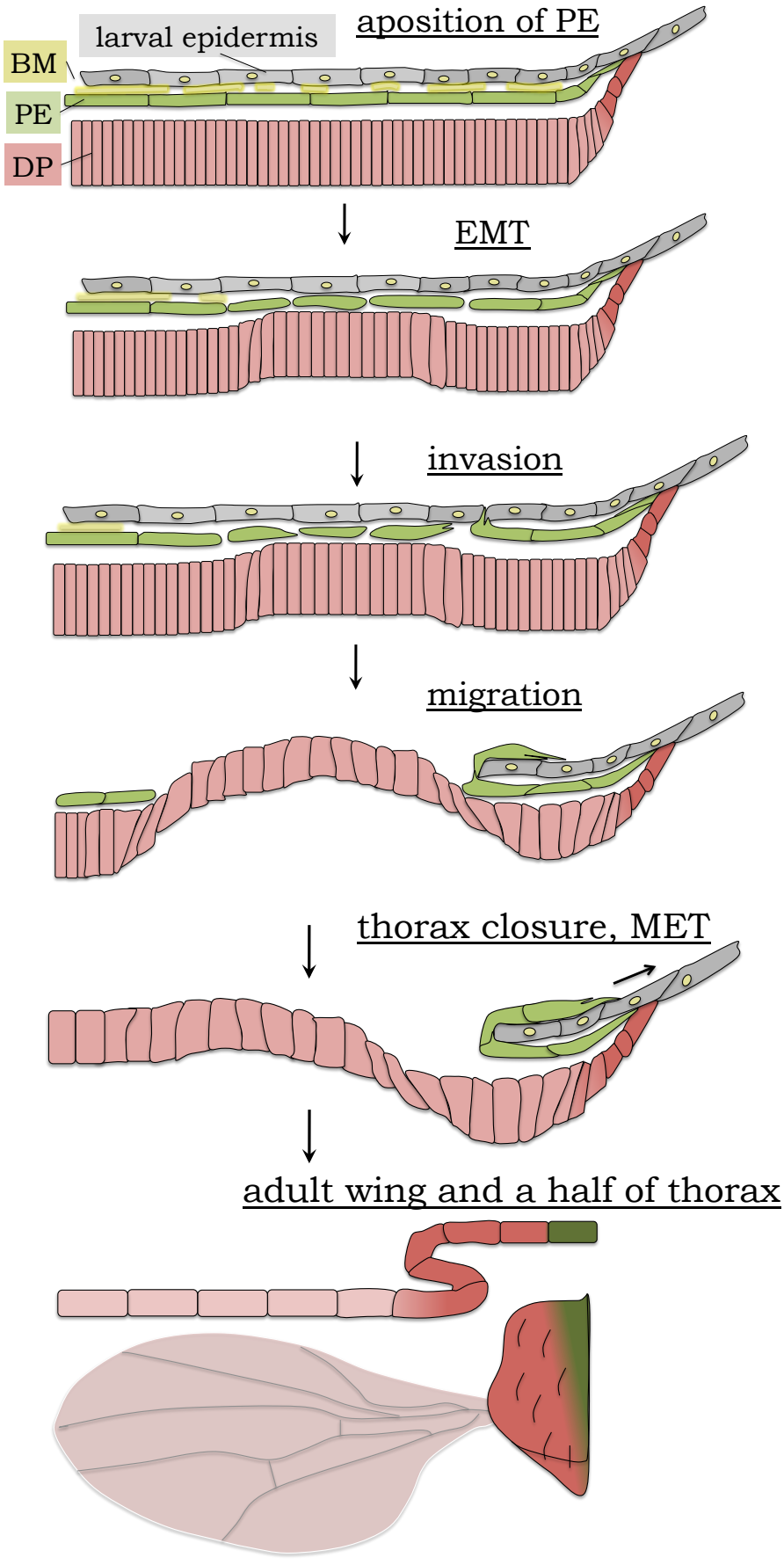
larval epidermis
aposition of PE
BM
PE
DP
EMT
invasion
migration
thorax closure, MET
adult wing and a half of thorax

Figure 1.5: **Protein structures of *Drosophila* Netrins and Frazzled.** The structure of the two *Drosophila* netrins, NetrinA and NetrinB, and the Frazzled protein is depicted. The Netrins consists of N-terminal domain, which shares homology with the VI and V domains of Laminins, followed by a positively charged C-terminal domain, also known as the Netrin module (NTR). The V domain is comprised of 3 EGF-like repeats. The two paralogs share 41% amino-acid sequence identity.

The Frazzled protein consists of a signal peptide, an extra-cellular domain (consisting of 4 Ig repeats and 6 FNIII repeats), a transmembrane domain, and three highly conserved intracellular domains, termed the P1, P2 and P3 domains. Abbreviations: SP (Signal Peptide), Ig (Immunoglobulin), FN (Fibronectin), TM (transmembrane). See sections 1.3.1.1 and 1.3.2.1 for details.

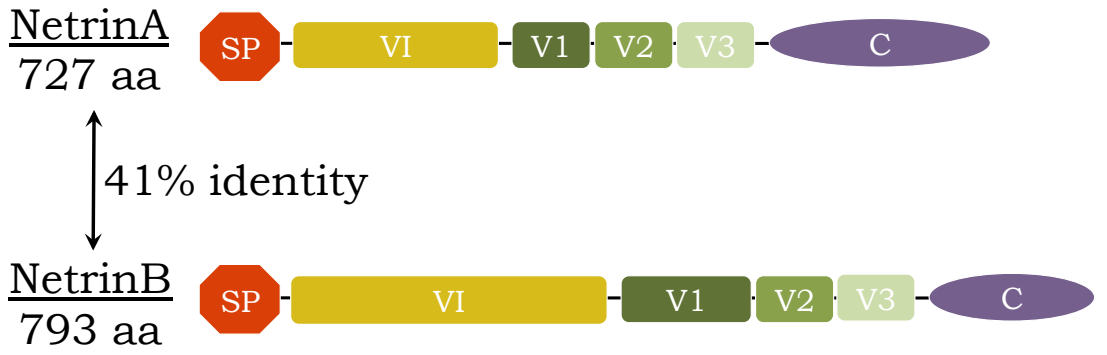

SP	signal peptide
VI	Laminin homology regions
V1, V2, V3	EGF repeat structures
C	NTR containing domain
IG	Immunoglobulin repeats
FNIII	Fibronectin III repeats
TM	transmembrane domain
P1, P2, P3	P-motifs

Figure 1.6: **Netrin is required for *Drosophila* wing disc eversion** (Images courtesy of R. Manhire-Heath and M.J. Murray; Manhire-Heath *et al.*, 2013 [133]). (a) *Ubx-GAL4/+* control fly. (b-e) *Ubx>netA.IR* fly phenotypes including twisted thorax and crumpled wing tissue (b), thoracic cleft (c), single sided eversion failure with internalized adult wing visible and loss of associated thoracic tissue (d), and double eversion failure with both wings internalized and no external thoracic tissue (e). (f) Dissected $NetAB^{\Delta}$ pupae, approximately 4 hours after puparium formation (APF). A single disc has everted while the second disc remains internalized (arrowhead). Nuclei are marked using Hoechst 33258. (g) Penetrance of defects generated by altered *netA* and *netB* expression. The three categories are: "No defect" - which includes both eclosed and pharate adults with normal wings and thorax, "Eversion defect" - which includes defects shown in (b-e). "Pupal lethality" - where pupae died before adult eversion phenotypes could be assayed. For each genotype n>50 progeny were scored. Error bars show 95% confidence intervals (CI). (h-k) Live imaging of control *Ubx-GAL4/+* (h) and *Ubx>netA.IR* (i-k) pupae expressing the nuclear marker *His2Av-EGFP*. (h) Control sequence in which wing imaginal discs move laterally (1:00 hrs), break through the epidermis (2:00 hrs), migrate together (2:30 hrs) and meet at the midline. (i) A *Ubx>netA.IR* pupa in which both discs evert, but the thorax closure process is abnormal. (j) A *Ubx>netA.IR* pupa in which a single disc fails to evert (red arrowhead). (k) A *Ubx>netA.IR* pupa where both discs fail to evert. Note that haltere discs (red asterisks) always everted. Scale bars 100μm.

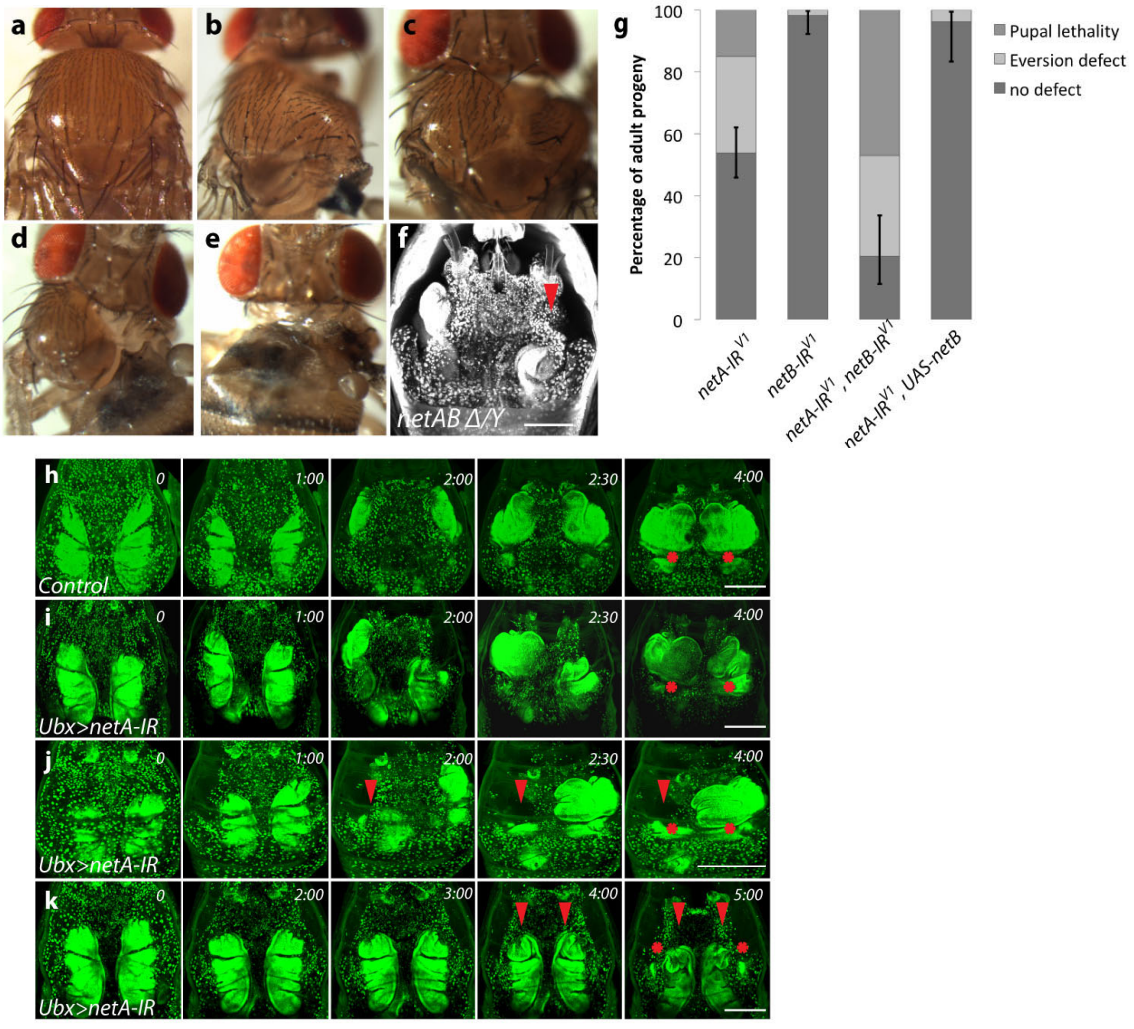
a
b
c
d
e
f
netAB Δ/Y
g
Percentage of adult progeny
100
80
60
40
20
0
Pupal lethality
Eversion defect
no defect
netA-IR V1
netB-IR V1
netA-IR V1 , netB-IR V1
netA-IR V1 , UAS-netB
h
Control
i
Ubx>netA-IR
j
Ubx>netA-IR
k
Ubx>netA-IR
0
1:00
2:00
2:30
3:00
4:00
5:00

Figure 1.7: **Frazzled antagonizes wing disc eversion** (Images courtesy of R. Manhire-Heath and M.J. Murray; Manhire-Heath *et al.*, 2013 [133]). (a, b) *Ubx>fra* adults displayed thoracic clefting (a) and eversion failures (b). (c-f) Anti-Fra immunostaining (red) of early and late third instar wing discs. Peripodial cells (marked with *Ubx>GFP* - green) are to the right and DP cells to the left. (c-d) *frazzled* expression in control, *w1118;Ubx>GFP* third instar wing discs. (c) In early third instar wing discs Fra, both in DP and PE cells, was primarily localised around the cell perimeter. (d) In peripodial cells of late third instar discs Fra became localised to cytoplasmic puncta and appeared reduced in levels. Localisation in DP cells appeared unchanged. (e) *Ubx>GFP,fra.IR* late third instar disc showing that, as expected, expression of the RNAi construct in the Ubx pattern reduced levels of peripodial Fra but did not affect expression in the DP. (f) In *Ubx>GFP,fra* third instar discs the level of peripodial Fra was greatly increased. Some cellular protrusions are evident (arrows). (Note: exposure levels in panel f are reduced with respect to panels c-e). (g) Penetrance of defects generated by *frazzled* overexpression at various temperatures. For each genotype n>40 progeny were scored. (h) *netA.IR* defects are rescued by co-expression of *UAS-fra.IR*, and *UAS-moe.IR*. (k) Mean intensity levels for Fra in late third instar peripodial cells relative to adjacent DP cells. RNAi knockdown of *netrinA* and expression of *YFP-rab5DN* result in increased Fra levels, relative to the DP. The elevated Fra levels in *netA.IR* discs were rescued by co-expression of *fra.IR* , but not *moe.IR*. (l-n) pMoe staining is punctate and reduced in peripodial cells of *w1118;Ubx>GFP* control discs (l) but increased in *netA.IR* discs (m), and when *frazzled* is overexpressed (n). (o) Mean intensity levels for pMoe in late third instar peripodial cells relative to adjacent DP cells. RNAi knockdown of *netrinA* and overexpression of *frazzled* result in increased pMoe levels, relative to the DP. The elevated pMoe levels in *netA.IR* discs were rescued by co-expression of *fra.IR* . Error bars = 95% CI (g, h) and S.E.M (k, o). Scale bars: 10μm.

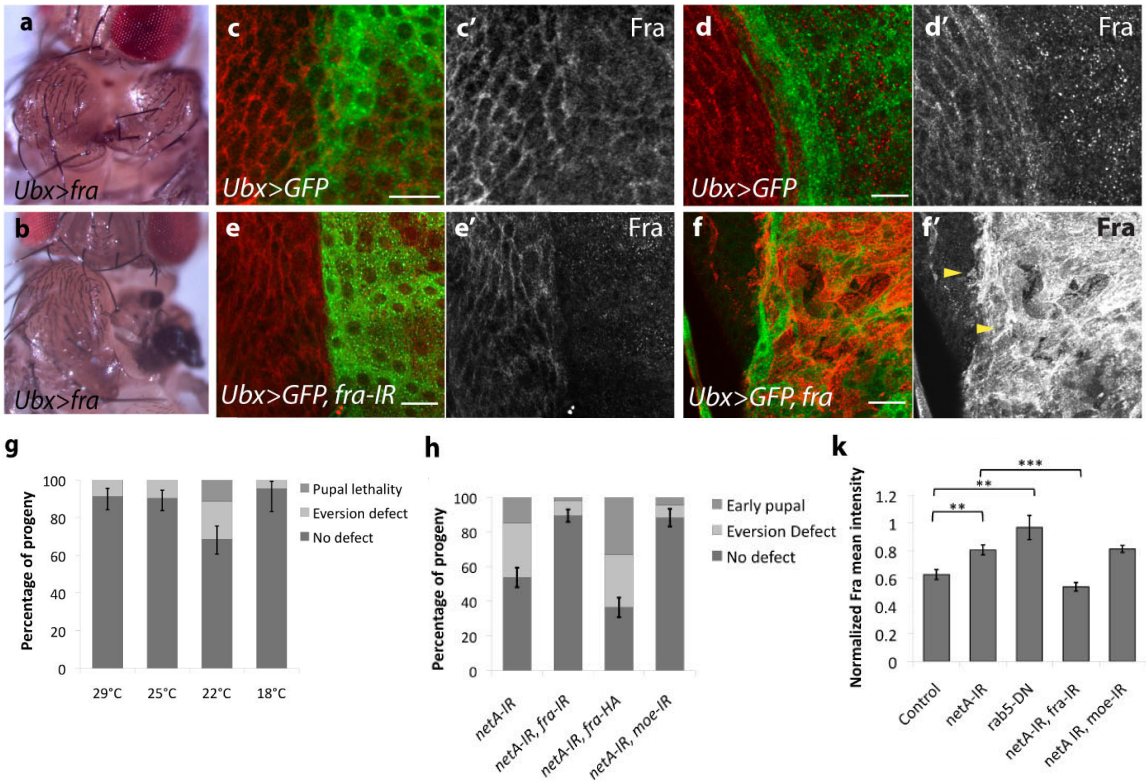
a
Ubx>fra
c
Ubx>GFP
c′
Fra
d
Ubx>GFP
d′
Fra
b
Ubx>fra
e
Ubx>GFP, fra-IR
e′
Fra
f
Ubx>GFP, fra
f′
Fra
g
Percentage of progeny
100
80
60
40
20
0
29°C
25°C
22°C
18°C
Pupal lethality
Eversion defect
No defect
h
Percentage of progeny
100
80
60
40
20
0
netA-IR
netA-IR, fra-IR
netA-IR, fra-HA
netA-IR, moe-IR
Early pupal
Eversion Defect
No defect
k
Normalized Fra mean intensity
1.2
1
0.8
0.6
0.4
0.2
0
**
**
***
Control
netA-IR
rab5-DN
netA-IR, fra-IR
netA IR, moe-IR

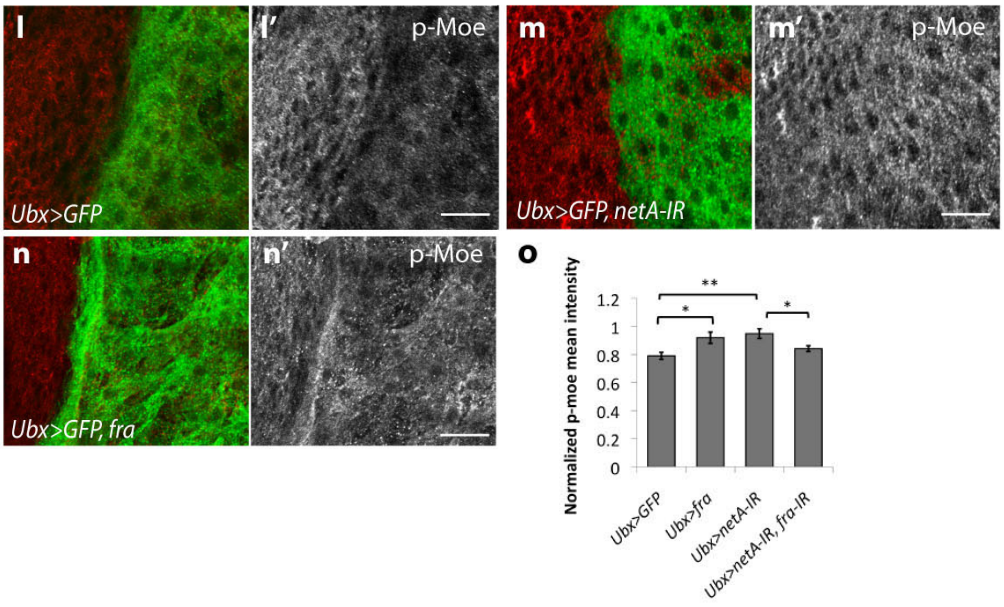
l
Ubx>GFP
l′
p-Moe
m
Ubx>GFP, netA-IR
m′
p-Moe
n
Ubx>GFP, fra
n′
p-Moe
o
Normalized p-moe mean intensity
1.2
1
0.8
0.6
0.4
0.2
0
**
*
*
Ubx>GFP
Ubx>fra
Ubx>netA-IR
Ubx>netA-IR, fra-IR

CHAPTER 2

Materials and methods

2.1 Materials

2.1.1 Chemicals

All reagents were of analytical grade, or the highest grade obtainable:

Formaldehyde 37% (Sigma)

Triton X-100 (American Biosciences)

Glycerol (VWR Chemicals)

FCS (fetal calf serum) (Sigma)

20-Hydroxyecdysone (Sigma)

2.1.2 Antibiotics

Penicillin-Streptomycin (Invitrogen)

2.1.3 Antibodies

2.1.3.1 Primary antibodies

The following antibodies were used:

DCAD2 (DE-Cad): Developmental Studies Hybridoma Bank; rat; used at 1/200 dilution

Mab N27A1anti-Armadillo (Arm): Developmental Studies Hybridoma Bank; mouse; used at 1/200 dilution

anti-Frazzled (Fra): a kind gift from Florence Maschat (Kolodziej *et al.*, 1996 [135]); rabbit; used at 1/1000 dilution

Phospho-Ezrin (Thr567)/Radixin (Thr564)/Moesin (Thr558) (41A3), i.e. anti-phosphoMoesin (pMoe): Cell Signaling Technology; rabbit; used at 1/100 dilution

anti-phosphoMLC (pMLC): Cell Signaling Technology; rabbit; used at 1/100 dilution

anti-Conundrum (Conu): guinea pig; a kind gift from Richard G. Fehon (Neisch *et al.*, 2013 [174]); used at 1/100

anti-GFP: Life Technologies; rabbit; used at 1/500.

2.1.3.2 Secondary antibodies

All secondary antibodies used were "highly cross-absorbed":

Goat anti-Rat Dy649: Jackson Immunoresearch Laboratories, used at 1/200 dilution

Goat anti-Rabbit Alexa 568: Invitrogen, used at 1/200 dilution

Goat anti-Mouse Alexa 568: Invitrogen, used at 1/200 dilution

Goat anti-Guinea pig Cy5: Jackson Immunoresearch Laboratories, used at 1/200 dilution

2.1.4 F-Actin stains

To label F-actin, tissues were incubated with 50 μM Rhodamine-conjugated phalloidin (or alternately Alexa-488 Phalloidin or Alexa-555 Phalloidin; Invitrogen) in PBS-T for 3 hours at 25°C or overnight at 4°C.

2.1.5 Buffers and solutions

The following buffers and solutions were used:

PBS (10×), pH 7.4: 13.7 mM NaCl, 2.7 mM KCl, 10 mM Na_2HPO_4, 1.76 mM KH_2PO_4

PBS-T: 1×PBS, 0.1% Triton X-100

Fixative solution: 10% of 37 % formaldehyde in 1×PBS

Culture medium: Shields and Sang M3 insect medium, 2% FCS, 0.5% penicillin-streptomycin, 0.2 μg/mL 20-Hydroxyecdysone

Tegosept solution (fungal inhibitor): 100 g methyl-4-hydrobenzoate powder, 950 mL 100% ethanol, 50 mL water

Acid mix: 412 mL propionic acid, 42 mL orthophosphoric acid, 546 mL water

2.1.6 *Drosophila* media

Molasses fly food:

450 g fresh baker yeast, 700 g molasses, 30 g agar and 80 g glucose were dissolved together in 4 L of hot tap water and boiled. The mixture of 630 g semolina and 3 L cold tap water were added to the boiling mixture, and boiled again, and then removed from the heat. 69 mL tegosept and 131 mL acid mix were added to the mixture and stirred. The mixture was then dispensed into bottles or vials. A few grains of active yeast were sprinkled on the fly food before use.

2.1.7 *Drosophila melanogaster* strains

2.1.7.1 Wild-type stock

The wild-type control for phenotypic analysis used was the w^{1118} strain (Bloomington).

2.1.7.2 *GAL4/UAS*-stocks

For the eversion study, *frazzled* loss-of-function and *frazzled* overexpression analysis, structure function assay and screening the following strains were used:

Ultrabithorax-GAL4 (*Ubx-GAL4*) was a kind gift from L. S. Shashidhara (Pallavi and Shashidhara, 2003 [107]).

UAS-FraMYC; *UAS-FraΔP1MYC*; *UAS-FraΔP2MYC*; *UAS-FraΔP1P2MYC*, *UAS-FraΔP3MYC* and *UAS-FraΔP3.5MYC* were kind gift from G. J. Bashaw (Garbe *et al.*, 2007 [139]).

patched-GAL4 (*ptc-GAL4*); *UAS-mCD8-GFP*; *UAS-frazzled*; *UAS-dicer2*; *UAS-GAL4*; *Df(2R)BSC880* and *UAS-p35* were obtained from the Bloomington *Drosophila* Stock Centre.

Ubx-GAL4,UAS-mCD8-GFP; *Ubx-GAL4,GAL80^{ts}*; *Viking-GFP;Ubx-GAL4* recombinants were made previously by other members of the lab.

UAS-FraMYC;Ubx-GAL4,GAL80^{ts}/TM6B was made in this study.

2.1.7.3 *MARCM*-stocks

For MARCM analysis the following stocks were used:

hs70-FLP,UAS-GFP; FRT42D,tub-GAL80/FRT42D; tub-GAL4 and *w^{1118};FRT42D* were a kind gift from Carole Poon.

FRT42D, fra^{3} recombinants were made in this study.

2.1.7.4 *FLP/FRT*-stocks

For flip-out *fra.IR* and *frazzled* overexpression assay the following stocks were used:

hsFLP; *Act5C-FRT-CD2-FRT-GAL4, UAS-GFP* and *hsFLP; Act5C-FRT-CD2-FRT-GAL4, UAS-RFP* which were a kind gift from Tony Brumby.

2.1.7.5 *UAS-RNAi*-stocks

All *UAS-RNAi*-stocks that were used for wing disc eversion assay or in epistasis test were obtained from either the Vienna *Drosophila* Resource Centre (VDRC) or Bloomington *Drosophila* Stock Centre.

2.1.7.6 *frazzled* alleles stocks

FRT13D, fra^{3} and *FRT13D, fra*^{4} were obtained from the Bloomington *Drosophila* Stock Centre.

2.2 Methods

2.2.1 *Drosophila* cultures

Flies were raised at 18°C, 25°C or 29°C on Molasses fly food.

2.2.2 Culturing of imaginal discs

In vitro disc culture was performed as described in Aldaz *et al*., 2010 [84]. Wandering third instar larvae were washed in 1×PBS (hereafter PBS). Then, the larvae were dissected for wing imaginal discs in PBS. To do this, a larvae was torn apart in two halves, and a front part was turned inside out. Then fat bodies and gut were removed. A wing disc was set apart from the mass of the body wall, but a small piece of the body epithelium was still left attached to the stalk. The dissected wing discs were then transferred into glass cavity block with culture medium using a 1000 mL pipette (tip cut off). Discs were cultured for 7 or 8 hours at 25°C in at humidified chamber. Discs were dissected out of multiple larvae within 20-30 minutes such that accuracy of the timed culturing periods were ±15 minutes. To stain the discs with antibodies or Rhodamine phalloidin after culture, they were washed three times in PBS, and then fixed in 3.7% formaldehyde in PBS for 15 minutes. Then, the standard staining procedure was applied.

2.2.3 Immunostaining of imaginal discs

Wing imaginal discs were dissected out of wandering third instar larvae in PBS, and fixed in 3.7% formaldehyde in PBS for 15 minutes. The discs were then washed three times in PBS-T, each wash for 15 minutes. Primary antibodies diluted in PBS-T were incubated with the discs for 3 hours at 25°C or overnight at 4°C. The incubation with the primary antibodies could be combined with Rhodamine phalloidin. Then, discs were washed three times in PBS-T quickly and then four more times, each for 15 minutes. After that, the discs were incubated with secondary antibodies in PBS-T for 2 hours at 25°C or overnight at 4°C. Following this the discs were washed again in PBS-T three times quickly and then four more times, each for 15 minutes. Then, the discs were cleared in 70% glycerol in PBS and mounted for imaging. The mounted discs were then imaged using confocal microscopy.

2.2.4 Mosaic wing discs and heat-shocking

To create clones in mosaic MARCM or flip-out wing discs, flies were raised in vials at 25°C for 72±11 hours after setting up the cross, at which point larvae were roughly first instar stage. Then, the adults were removed, and the vial was placed in a water bath incubator at 37°C for 15 minutes. Wandering third instar larvae were dissected in PBS and mosaic wing imaginal discs used for further *in vitro* culture or immunostaining.

2.2.5 MARCM as a method for *frazzled* loss-of-function analysis

To investigate cellular phenotypes of clones homozygous for the null allele fra^3 null-allele the MARCM technique was used. This technique allows one to generate homozygous mutant cells labelled by a fluorescent marker in wild-type heterozygous environment (Lee and Luo, 2001 [176]). MARCM is based on FLP/FRT-mediated recombination in cells undergoing mitosis. In this study, one parent contained heat-

shock inducible *hsFLP*, *GAL4* driven by a strong *tubulin1*-promoter (*tub*), UAS-GFP, and an *FRT42D* site located distal to a *tub*-driven *GAL80* on the same chromosome. The second parent had an *FRT42D* site located distal to fra^3 mutation. In order to get clones of 10 or more cells in the PE and DP, the optimal age for the heat-shocking was found to be 72±11 hours after egg deposition (McClure and Schubiger, 2005 [177]). FLP/FRT mitotic recombination produced two types of cells, one of which carried a *tub-GAL80* insertion, and the other did not have *GAL80* but was homozygous for fra^3. Thus, clones with wild-type *frazzled* had repressed *GFP*-expression, whereas fra^3 mutant clones were marked by *GFP* (Figure 2.1).

2.2.6 Microscopy

Light microscopy was performed on a Leica M165 FC stereomicroscope and images of flies were collected digitally with a Leica IC80 HD camera. Fluorescence microscopy was performed on an Olympus FV1000 confocal microscope. All images acquired were at 1024×1024 pixel resolution.

2.2.7 Analysis of confocal images

To enable visualization of a maximum intensity projection of the squamous PE cells without interference from the underlying DP epithelium, the images were processed as follows. For each slice in which there was a clear gap between the PE and DP layer a polygonal region capturing the DP cells was digitised, and then this region was subtracted from the original image (Figure 2.2).

The images of the DP epithelium shown in Chapters 4 and 5 were presented as single z-slices from a stack (width of 1 μm).

2.2.8 Lethality assay

The number of escapers with the desired genotype counted in the assay (chapter 4, section 4.2.3) was compared to the expected total number of progeny with the same

genotype that should emerge as adults according to Mendelian inheritance ratios. Adult genotypes were determined using *CyO* marker (a balancer chromosome II).

2.2.9 Quantification analysis

To quantify the levels of DE-Cad or pMoe immunostaining for a disc I calculated the ratio of mean intensity (arbitrary units) between a *ptc*-expression region and an adjacent non-*ptc* region of the DP epithelium (Figure 2.4, a-a", b-b"). To quantify the degree of basal expansion, I calculated the ratio between basal and apical sides of epithelial cells within the *ptc*-expression region in the DP epithelium (Figure 2.4, c-c'). For all quantification assays, the measurements were performed on the cross-sectional slices in a particular area of the hinge region (Figure 2.3) of the *ptc*-expression stripe (Figure 2.4, d). A single value for each disc (see scatter dot plots shown in Chapter 4 and 5) was obtained by taking the average of 4-7 measurements.

To quantify the length of protrusions, I measured the length of the DP protrusions (the hinge region; Figure 2.3) in the *ptc*-area of wing discs expressing *MYC*-tagged *frazzled* transgenes (Figure 2.5). For each disc at least 10 protrusions (all, which were detectable) were measured, and a single average value obtained per disc.

2.2.10 Software

The following software and online resources were used:

ImageJ was used for all image preparation.

GraphPad Prism was used for charting DE-Cad and pMoe mean intensity, length of protrusions and basal-apical ratio data.

Wilson score interval calculation: http://epitools.ausvet.com.au/

Fisher's exact test: http://graphpad.com/

Student's t-test: http://www.graphpad.com/

Figure 2.1: **Generation of MARCM *fra*^{3} mutant clones in wing discs.** Schematic representation of MARCM technique.

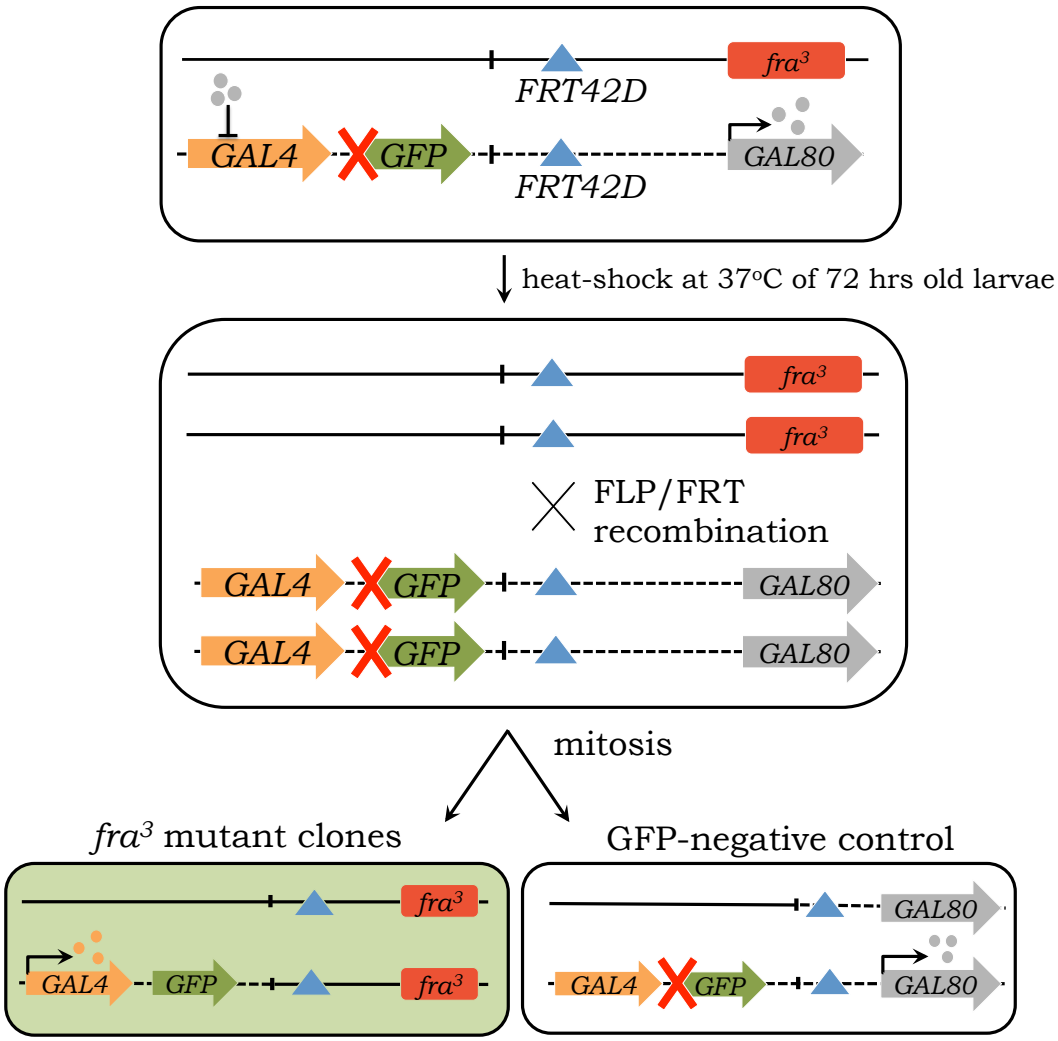
fra3
FRT42D
GAL4
GFP
FRT42D
GAL80
heat-shock at 37°C of 72 hrs old larvae
fra3
fra3
FLP/FRT
recombination
GAL4
GFP
GAL80
GAL4
GFP
GAL80
mitosis
fra3 mutant clones
GFP-negative control
fra3
GAL4
GFP
fra3
GAL80
GAL4
GFP
GAL80

Figure 2.2: **Visualisation of the PE in confocal images.** Z-stack of a *Ubx>GFP* third instar disc stained for DE-Cad (grayscale). GFP-positive PE marked in green. (a) A single slice with DP cells outlined. (b) A single slice with DP cells removed. (c) Maximum projections with intact DP. (d) Final maximum projections with DP removed. For details see Manhire-Heath *et al.*, 2013 [133].

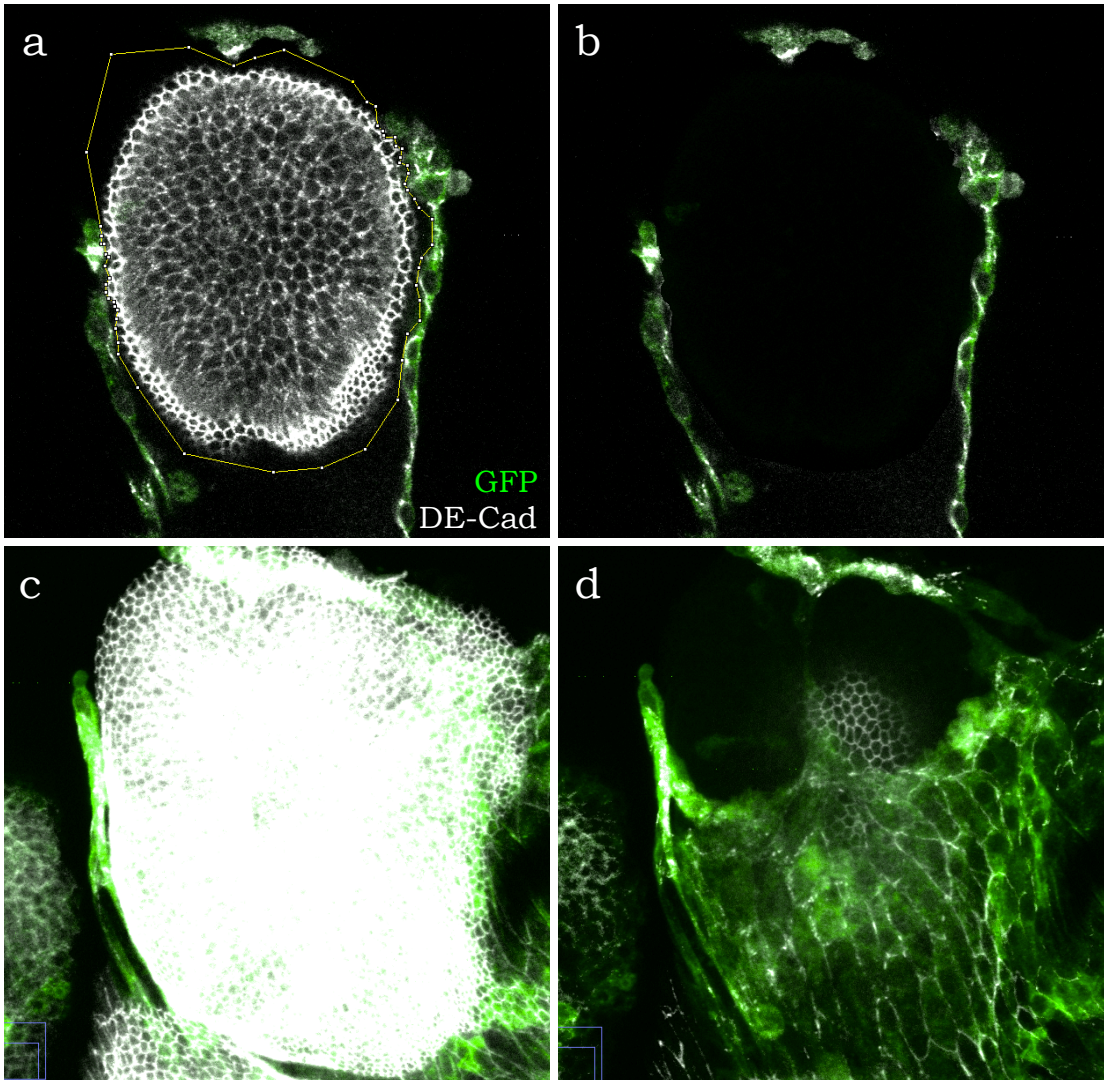
a
GFP
DE-Cad
b
c
d

Figure 2.3: **A wing disc map.** A map was used to standardise phenotypic and quantitative analysis. Abbreviations: PE - peripodial epithelium. DP - disc proper. A - apical side of the DP. B - basal side of the DP. I-IV - folds of the DP.

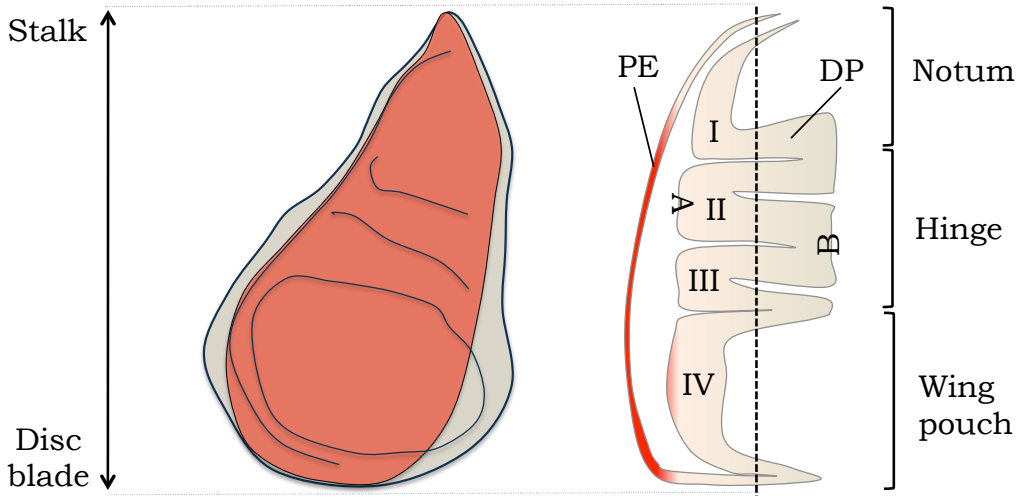
Stalk
Disc
blade
PE
DP
I
II
III
IV
A
B
Notum
Hinge
Wing
pouch

Figure 2.4: **Quantification of DE-Cad and pMoe mean intensities and apico-basal ratio.** (a-a") A *ptc>GFP* wing disc immunostained for DE-Cad (grayscale). (b-b") A *ptc>GFP* wing disc immunostained for pMoe (grayscale). To quantify levels of DE-Cad and pMoe in basolateral regions of DP cells, the ratio between mean protein intensity of the zone X and mean protein intensity of the zone Y was taken. Dashed lines indicate *ptc*-expression areas. (c-c') A *ptc>GFP* wing disc immunostained for DE-Cad (grayscale). The "Apico-basal ratio" was defined as the ratio between a length of apical side (X) and a length of basal side (Y) was taken. (d) Measurements were taken at successive positions in the proximal-distal axis of the second fold of the DP (red box; Figure 2.3). Scale bars 10 μm.

a) DE-Cad intensity = $X_{mean\ int}/Y_{mean\ int}$

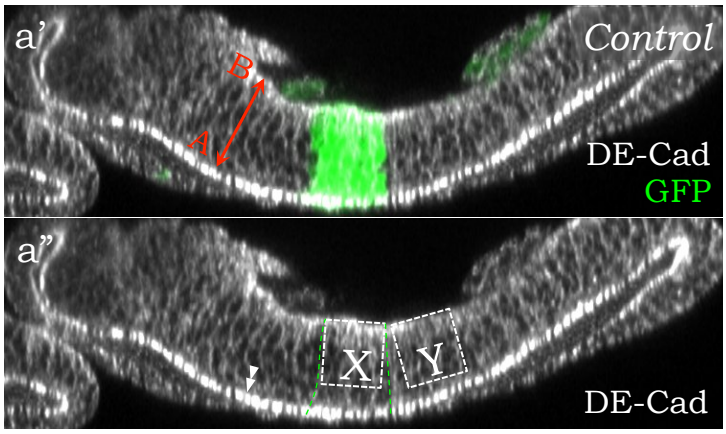

b) pMoe intensity = $X_{mean\ int}/Y_{mean\ int}$

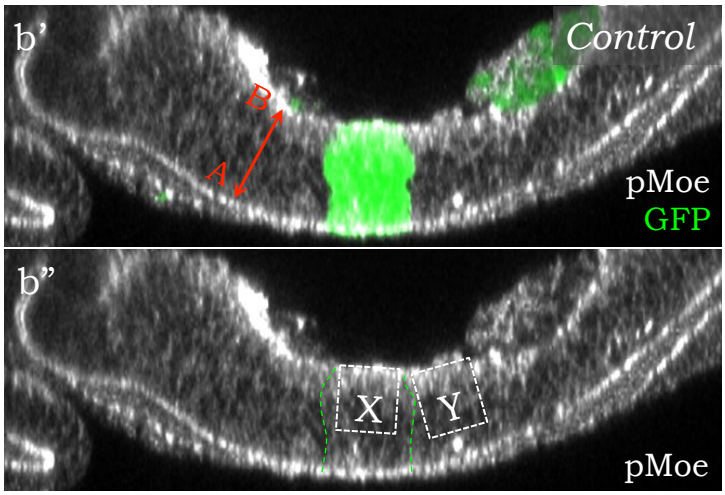

c) Apical-basal ratio = X/Y

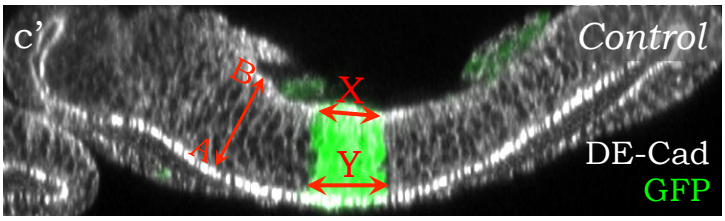

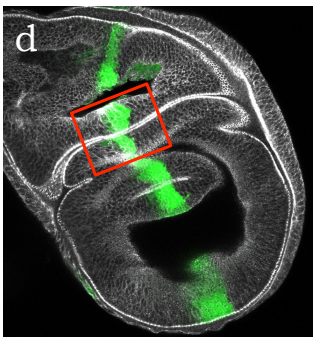

Figure 2.5: **Quantification of length of protrusions.** (a-b) A *ptc>fraMYC; GFP* wing disc immunostained for MYC (red (a) or grayscale (b, c)) and DE-Cad (blue). Measurements of all visible protrusions were taken from the basal side of the DP in the hinge region (dashed box; Figure 2.3). (c) Magnified area of the dashed box (b) with an example of measurement. Scale bars 10 μm.

Length of protrusions

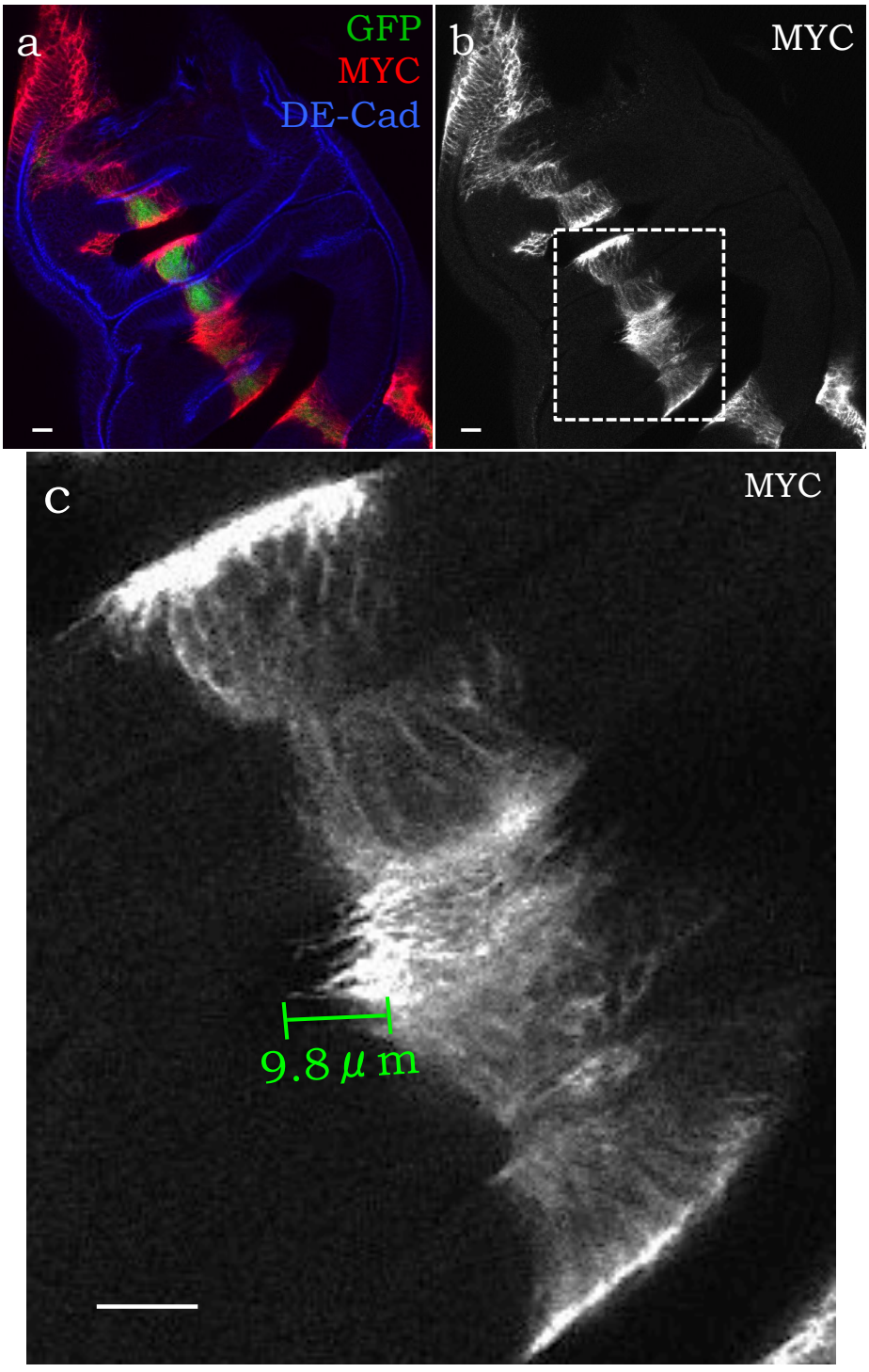

CHAPTER 3

Characterization of molecular and cellular events during the partial EMT of the peripodial epithelium

3.1 Introduction

3.1.1 Difficulties of analysing peripodial cells *in vivo* during wing disc eversion

Chapter 1 described limitations in our understanding of the cellular events that underlie NetA-associated wing disc eversion phenotypes. Although our knowledge of how PE cells drive the eversion process is fragmentary, one can define three main stages of the eversion process in which the PE cells almost certainly play a role:

i) the EMT or partial EMT process;

ii) invasion and migration;

iii) thorax closure and MET.

In addition, there is the possibility that the PE might have an influence on the DP morphogenesis by controlling its constriction, invaginations and changing cell morphology. To elucidate what stages of wing disc eversion are affected by the lack of NetrinA or overexpression of Frazzled, I have to investigate these stages separately from each other. However, there are several difficulties associated with the investigation of cellular events in the PE.

The first main problem is that it is not practical to conduct detailed cellular analysis *in vivo* because of the difficulties in visualising with confocal microscopy the thin squamous PE cells through the dense pupal case, the overlying larval epidermis and surrounding tissues, such as fat bodies, gut and other structures. To study the early stages of eversion, therefore, the wing discs must be isolated from the pupal case. Another challenge is that, despite their large size, the thin and squamous nature of PE cells makes them extremely vulnerable to damage during the preparation and imaging. Furthermore, due to the close apposition of the PE layer with the underlying DP epithelium, it is difficult to image PE cells without also imaging the underlying DP cells. Finally imaging of cultured discs, particularly live imaging, is confounded by the large three-dimensional movements that developing discs undergo, such as expansion, folding and of course the breakdown of the PE layer itself. These effects could be reduced by attaching the disc to the substrate, but this then risks damage to the delicate PE and potentially introduces artificial physical constraints on the movements of the epithelium that could introduce artefacts.

3.1.2 *In vitro* wing disc eversion investigation

An important step forward in the characterization of the eversion process has been the development of an *in vitro* wing disc culture method. It has long been known that dissected imaginal discs can develop into recognizable adult structures when incubated in media containing steroid hormone 20-Hydroxyecdysone (hereafter ecdysone), the natural moulting hormone of Arthropods (Guillermet and Mandaron, 1980 [178]).

Aldaz and colleagues substantially developed this methodology allowing them to image, live, the eversion process, and show that the PE cells break apart, lose their epithelial morphology and retract over the DP (Aldaz *et al.*, 2010 [84]). Using this method it becomes possible to separate early stages of eversion, which might involve EMT of PE cells, from the invasion and subsequent migration in the later stages. In this chapter I describe the adaptation of the *in vitro* wing disc culture method for our purposes and the analysis of the PE cell's behaviour in the beginning of eversion.

3.1.3 Characterization of the EMT

As it was still unclear whether the PE undergoes a real EMT, it was important to determine whether PE cells display the major EMT hallmarks, such as the loss of cell-cell contacts and apico-basal polarity, cytoskeletal rearrangements, increased cell contractility and basement membrane degradation. The loss of intercellular contacts in invertebrates might be characterised by the downregulation of proteins forming epithelial cell-cell adhesions (AJ) or a trans-epithelial barrier (septate junctions). The paramount marker of EMT is the breakdown of the apico-lateral continuous belt of adherens junctions known as zonula adherens (hereafter ZA). ZA breakdown is usually brought about by transcriptional repression of E-Cadherin. The large size of the PE cells and availability of the antibodies (anti-DE-Cad or anti-Arm) allows me to clearly visualize the changes in the ZA during eversion.

The dissolution of septate junctions can be also used as a good marker of EMT. For example, downregulation of the proteins composing analogous TJ in vertebrates is known to correlate with the loss of epithelial characteristics and appearance of the migratory phenotype (Ikenouchi *et al.*, 2003 [179], Martin and Jiang, 2009 [180]). The process of assembly/disassembly of the *Drosophila* septate junctions during epithelial remodelling remains largely uncharacterised.

Loss of epithelial state is also necessarily associated with the loss of apico-basal polarity. The establishment and loss of apico-basal polarity are strictly dependent on

maturation and dissociation of cell-cell contacts respectively. Once EMT is initiated, the expression of polarity proteins (i.e. Par6, Baz, aPKC, Crb, Std, Patj, Scrib, Dlg and Lgl) is transcriptionally repressed, which further destabilizes polarity (Aranda *et al.*, 2008 [181], Royer and Lu, 2011 [182], Martin-Belmonte and Perez-Moreno, 2012 [183]). Although the depolarization is a valid characteristic of EMT, the squamous shape of PE cells makes it very difficult to visualize this process, especially in regards to the analysis of protein localization relative to the cell membrane.

The transition to a mesenchymal phenotype entails reconstruction of the cytoskeleton to develop the motility machinery. The cytoskeleton is a dynamic intracellular structure consisting of actin microfilaments and microtubules. EMT triggers polymerisation of cortical actin followed by the formation of stress fibers and actin-rich membrane projections (lamellipodia and filopodia) (reviewed by Lamouille *et al.*, 2014 [46]). Cell motility is often accompanied with contractility, which is promoted by the function of non-muscle myosin (Narumiya *et al.*, 2009 [184]).

Finally, EMT can be characterised by the degradation of the basement membrane (hereafter BM). One of the major functions of the BM is to maintain epithelial stability by blocking cell invasiveness and motility. Due to this, in tumor cells, inappropriate BM breakdown is strongly associated with increased cell invasion and metastasis. During EMT, the links between the ECM components (i.e. glycoproteins, Collagen IV, Laminins, Nidogen and Perlecan) undergo proteolytic cleavage. In *Drosophila*, the degradation of Collagen IV is promoted by two MMPs, one secreted (DmMmp1) and one membrane anchored (DmMmp2) (Llano *et al.*, 2000 [185], Llano *et al.*, 2002 [186]). The BM evenly covers the outside surface of the epithelial sac of a wing disc and is readily available for observation. To track the BM degradation during EMT I used a protein-trap line *Viking-GFP*, where the *GFP* coding sequence is inserted inside the locus of the *Drosophila Collagen IV* (Morin *et al.*, 2001 [187]).

3.1.4 This chapter

Previous results have uncovered a novel genetic pathway regulating wing disc eversion. Further investigation may potentially yield a significant contribution to our rather limited knowledge of genetic mechanisms regulating *Drosophila* EMTs. Also, given the high degree of evolutionary conservation of Netrins and Frazzled/DCC receptors, the results will help our understanding of important EMT-based processes, such as cancer metastasis and tissue regeneration. This chapter describes the establishment of a more refined method for the cellular analysis of peripodial cells at the beginning of the eversion process. Using this method, I show that peripodial cells undergo the characteristic EMT-associated events of ZA breakdown, cytoskeletal rearrangements and BM degradation. The method also enabled me to determine whether loss of NetrinA or elevated levels of Frazzled have a direct influence on the EMT hallmarks, dissociation of E-Cadherin (hereafter DE-Cad) from the ZA, actin filaments modification and breakdown of Collagen IV network.

3.2 Results

3.2.1 EMT initiation occurs after 8 hrs culturing in a characteristic area of the wing disc

To explore whether loss of *netrinA* or overexpression of *frazzled* in the PE can cause disruptions during the EMT stage of eversion, the wing discs were dissected from late third instar larva and cultured at 25°C in media with 0.2 μg/mL of ecdysone (see Materials and Methods). Under these conditions, complete disc eversion occurs *in vitro* after approximately 11-12 hrs of culturing (Aldaz *et al.*, 2010 [84]). To monitor the fate of PE cells during the early stages of eversion, I isolated discs from wandering third instar larva, and cultured them until the PE cells began to undergo the EMT - as characterised by BM breakdown, ZA dissociation and reorganization of actin cytoskeleton (Thiery *et al.*, 2009 [188]) and formation of one or more holes

in the PE (Pastor-Pareja *et al.*, 2004 [82]).

After testing different time-periods I determined that the average time sufficient for control *w1118;Ubx>GFP* (hereafter *Ubx>GFP*) wing discs to reach the stage of EMT initiation was approximately 8 hrs, though there was significant variation in the degree to which the EMT had progressed (Figure 3.1). A proportion of the cultured wing discs progressed far into the eversion process, with the PE already having broken apart and greatly retracted over the DP (Figure 3.1, d). Other discs either did not have visible holes or had incipient holes in the PE (small holes; Figure 3.1, b), while others had a distinct hole in the PE through which the DP was seen protruded (big holes; Figure 3.1, c). Overall, 90% of *Ubx>GFP* discs (n=40) displayed typical EMT characteristics.

Having established the time and place for EMT initiation in cultured wing discs, three *Drosophila* genotypes, *Ubx>netA.IR, GFP* (hereafter, *Ubx>netA.IR*), *Ubx>fra, GFP* (hereafter *Ubx>fra*) and control *Ubx>GFP*, were analysed for the ability of PE cells to undergo EMT *in vitro*. As noted earlier, the shape of PE cells allows me to assess three major EMT hallmarks: ZA breakdown, cytoskeletal rearrangements and BM degradation.

To standardise our data analysis, I established landmarks based on the pattern of GFP expression and the folds of the underlying DP in the wing disc, which allowed me to define a characteristic region in which the EMT was most often initiated. Along the anterior side of the PE dense accumulation of longitudinally stretched cells (known as medial edge cells (Tripura *et al.*, 2011 [189]) forms a sharp edge of GFP expression pattern. On the posterior side, GFP expression levels drop gradually. Also, I used three clear folds of the DP surface as additional landmarks. With these landmarks I found that the most common area for EMT initialization is positioned between the stalk and the lower fold of the disc, adjacent to the sharp edge of GFP-expression pattern. I named this area the "initiation region" (Figure 3.2).

3.2.2 Downregulation of *netrinA* as well as overexpression of *frazzled* inhibit zonula adherens breakdown

In the research described here, the degree of ZA integrity was assessed by analysis of DE-Cad immunostaining. At the start of the culturing period, PE and DP cells had well-defined ZAs with DE-Cad stains encircling the cell (Figure 3.3, b). When cultured for 8 hrs with ecdysone, 90% of control *Ubx>GFP* discs (n=40) exhibited a distinct graded DE-Cad distribution in the PE (Figure 3.3, e, arrows). Among these, 62.5% of the discs had a perforated PE (i.e., big and small holes), with regions of complete ZA degradation. 27.5% of the discs had partially dissociated and fragmented DE-Cad staining along the ZA lines in the initiation region. The remaining 10% of the discs had an intact ZA throughout the whole surface of the PE (Figure 3.6; Table 3.1).

In *Ubx>netA.IR* and *Ubx>fra* wing discs, ZA breakdown was significantly reduced compared to control discs (Figure 3.6; Table 3.1). 47% of the cultured *Ubx>netA.IR* discs (n=47) had an intact ZA in the PE (Figure 3.4, e), five times more than the same rate in control discs (p=0.0003, this and all other p-values in this chapter are based on a two-tailed Fischer's exact test). 23% of the *Ubx>netA.IR* discs had small or big perforations in the PE and 30% of the discs had delocalization of DE-Cad from the ZA (Figure 3.5, asterisk in e). In *Ubx>fra* discs, ZA breakdown completely failed in 35% of cases (n=20, p=0.0315; Figure 3.4, h). 35% of discs had small or big perforations in the PE and 30% of the discs had delocalization of DE-cad from ZA (Figure 3.5, asterisk in h). Whether the significantly decreased proportion of the everting discs in mutant genotypes, is indicative of complete failure of ZA breakdown or merely a delay is not known, but in either case the results show that NetrinA regulates normal DE-Cad dissociation from the ZA, and strongly suggests that this occurs via its receptor, Frazzled.

Similar effects on ZA breakdown were observed in the experiments aimed at studying BM degradation. In this case *netA.IR* and *frazzled* were expressed using the *Viking-GFP; Ubx-GAL4/TM6B* line (detailed explanation below). Although

the focus of these experiments was the BM breakdown, ZA breakdown was also examined. Among the control *w1118; Viking-GFP; Ubx-GAL4* discs, the ratio of discs with normally dissociating ZA to discs with intact ZA was almost the same as before, 89% and 11% respectively (Figure 3.6; Table 3.1; n=27). Also, when *netrinA* was downregulated (n=29) or *frazzled* overexpressed (n=28), the proportion of discs with failed DE-Cad delocalization was significantly increased with respect to control discs to 59% and 35.5% respectively (p=0.0003 and p=0.0322 respectively). These results were not significantly different from those obtained without the Viking-GFP (p=0.35 and p=1 respectively).

3.2.3 Downregulation of *netrinA* or overexpression of *frazzled* do not prevent F-actin accumulations near the initiation region, but induce formation of "stress-fibre"-like structures.

Cytoskeletal changes were assessed on the basis of F-actin localization using Rhodamine-labelled phalloidin. In non-cultured wing discs, F-actin filaments presented as thin aligned fibers surrounding epithelial cells and seemed partially colocalized with the DE-Cad distribution (Figure 3.3, c, c'). When cultured for 8 hrs, F-actin filaments in the *Ubx>GFP* PE were strongly enriched in the initiation region (Figure 3.3, f). Thin cortical F-actin bundles were remodelled to thick filaments densely distributed in the PE cytoplasm (Figure 3.3, i). Moreover, there was a prominent gradation of F-actin morphology depending on proximity to the PE holes. Distant cells, at the start of ZA breakdown, maintained the primary cytoskeletal morphology, whereby thin F-actin strands encircled cells along the perimeter (Figure 3.3, g). As the degree of DE-Cad degradation increased, F-actin filaments became more concentrated into dense clusters distributed within the initiation zone cells. Approaching the hole, clusters increased in number and size. Finally, on the boundary of perforations, F-actin clusters were strictly accumulated to the rim of a hole (Figure 3.3, f, arrowheads). In addition, the cross-sectional views of the disc eversion area revealed

noticeable changes in the shape of the PE cells at the edge, from squamous and hexagonal to a more spherical morphology, giving them a more mesenchymal-like phenotype (Figure 3.3, asterisk in d'-f', arrow in i).

In many respects the same modifications occurred in normally everting *Ubx>netA.IR* discs. In cells with partially fragmented ZAs, parallel filaments of F-actin were thicker and enriched in cells on the edge of the hole, and F-actin was agglomerated in rounded clusters oriented to the rim of the hole (Figure 3.5, f, f', arrowheads). However, along with the concentrated peripheral strands and dense rounded clusters, F-actin filaments were also found to form straight thick bundles reminiscent RhoA-induced stress fibre (Figure 3.5, double arrowheads in f; Ridley and Hall, 1992 [190]). Typically, these structures were located on the basal side of the PE (Figure 3.5, k') and presented as thick spikes with seemingly random orientation. Although the structures were mostly specific for the cells with partially dissociated DE-Cad, they could also be found in PE cells with a solid ZA (Figure 3.4, double arrowheads in l). Interestingly, in the EMT initiation region of *Ubx>netA.IR* discs that lacked ZA breakdown, F-actin was also present as enriched circumferential strands, round clusters and spiky elements (Figure 3.4, f, arrowheads). These findings suggest that the EMT associated cytoskeleton rearrangements are not dependent on ZA breakdown having progressed to the full extent. Moreover, apparently loss of NetrinA, and overexpression of *frazzled*, do not prevent F-actin accumulations, and can actually induce its reorganization into "stress-fiber"-like structures.

The successfully everting *Ubx>fra* discs also have noticeably elevated F-actin in the EMT initiation region, especially on the edge of a PE hole, where F-actin is considerably enriched and accumulated at the rim (Figure 3.5, j, j', arrowheads). Similar to *Ubx>netA.IR* discs, overexpression of *frazzled* promoted "stress-fiber"-like structures in cells with integral or partially degraded DE-Cad (Figure 3.5, double arrowheads in j, and also see Figure 3.4, double arrowheads in m). However, the number and density of spiky structures appeared to be more striking than in *netA.IR* discs. In *Ubx>fra* discs, the individual fibers had equal length and thickness, and were often assembled in a fan-like arrangement. Notably, these stress fibers were

generated only under ecdysone stimulus. Non-cultured *Ubx>netA.IR* and *Ubx>fra* wing discs had circumferential F-actin similar to control discs (data not shown). Taking into consideration that overexpression of *frazzled* produced higher amounts of the receptor than in the *netA.IR* background, I propose that ectopic levels of Frazzled is the primary cause of these structures, and suggest that Frazzled activates a Rho1 pathway. Further evidence that Frazzled is involved in regulation of cytoskeletal morphology via Rho GTPases signaling is presented in the following chapters.

3.2.4 Downregulation of *netrinA* or overexpression of *frazzled* has modest effect on the basement membrane degradation

To track the BM degradation during EMT I used the *VikingGFP; Ubx-GAL4/TM6B* line, where *VikingGFP* is a GFP exon trap inside the locus of the *Drosophila* Collagen IV. When discs were everting *in vitro*, the BM degradation proceeded at two locations within the PE: the stalk and the blade regions. The nature of the BM degradation appeared to occur in two different ways (Figure 3.7). In many cases, particularly near the stalk, areas of reduced/degraded Collagen IV had "soft" edges, which could be a result of degradation by gradually distributed extracellular proteolytic enzymes, i.e. MMPs (Figure 3.7, b). In other cases the Collagen IV layer had quite abrupt edges, suggesting the BM structure was under mechanical tension and had ruptured under the pressure of a widened and curved DP tissue. This was often observed in the blade region (Figure 3.7, c). Whether or not this mechanical rupture also occurs *in vivo*, where disc movements would be limited by the surrounding tissues, is not known. Thus, two processes appear to contribute to BM removal.

At the start of culturing, the basal surfaces of the whole wing disc were closely surrounded by evenly spread Collagen IV fibres (Figure 3.7, a). When cultured for 8 hrs, 89% of control *w1118; VikingGFP; Ubx-GAL4* discs began losing the Collagen

IV adjacent to the PE side (n=27; Figure 3.9, a; Table 3.2). Interestingly, after 8 hrs of culture the degradation of the BM reached different phases (Figure 3.7), and the degree of BM loss was strongly correlated with the degree of ZA fragmentation. For example, 89% of successfully everting wing discs having a distinctly fragmented ZA and perforations in the PE, had lost a substantial part of the BM envelope. Moreover, perforations in the PE were generally observed in those places where the BM had already been greatly retracted. However, some areas of PE cells with a fragmented ZA still had an intact layer of Collagen IV fibers (Figure 3.8, d-f). However, in these cases, the attachment of the BM to the PE cells seemed less solid suggesting the contacts between epithelial cells and the ECM (e.g. integrins) were being downregulated. 11% of the cultured discs with an intact BM also had a completely intact ZA (Figure 3.8, a-c). Altogether, these observations suggest that the degradation of the BM and the ZA breakdown are interconnected, and likely the removal of the BM is a primary event of wing disc eversion.

When cultured for 8 hrs, *VikingGFP; Ubx>netA.IR* discs showed no significant change in BM breakdown efficiency (83% degraded, n=29; p>0.1; Figure 3.9, a; Table 3.2) suggesting that NetrinA does not play a role in BM degradation. Consistent with previous results, most of the discs with an intact BM (14% out of 17%) and almost a half of the discs with normally degrading BM (45% out of 83%) had kept a completely intact ZA in PE cells confirming that NetrinA does play a role in regulation of ZA breakdown (Figure 3.9, b; Table 3.3). Cultured *VikingGFP; Ubx>fra* discs also showed no significant change in BM degradation compared to control discs (75% degraded, n=28; p=0.29 compared to control, and p=0.84 compared to *netA.IR* discs; Figure 3.9; Table 3.2). The proportion of discs with an intact ZA in *VikingGFP; Ubx>fra* was not significantly different to the *VikingGFP; Ubx>netA.IR* genotype: approximately half of the discs with an intact BM (14% out of 25%) and one third of the discs with normally degrading BM (21% out of 75%) had an intact ZA in the PE (p>0.2; Figure 3.9, b; Table 3.3).

ZA breakdown and BM degradation therefore are tightly correlated and most likely connected processes during the EMT. NetrinA and Frazzled were found to

inhibit ZA breakdown but not BM degradation suggesting that these two processes are regulated by independent genetic pathways.

3.3 Discussion

The first aim of the current research was to understand the origin of wing eversion failure when the PE is deficient for *netrinA* or is overexpressing *frazzled*. Since it was known that during eversion PE cells undergo typical EMT events (e.g. DE-Cad delocalization and BM degradation; Pastor-Pareja *et al.*, 2004 [82]; Srivastava *et al.*, 2007 [90]), I was interested in determining whether NetrinA and Frazzled were involved in those processes. To address this question, I established a new approach that allowed me to separate the EMT-stage from the latter events of wing disc eversion, adapting to my purposes the published method for *ex vivo* culturing of imaginal discs (Aldaz *et al.*, 2010 [84]). I found that 90% of the wild type discs were passing through or had already gone through the EMT stage 8 hrs after the culturing had begun. By this time, a range of different degrees of ZA breakdown could be clearly observed together with extensive F-actin modifications and areas of degraded BM at the basal surface of peripodial layer. At the same time, the DP tissue undergoes substantial extension and folding in preparation for the following process of disc evagination. I found that the process of delocalization of DE-Cad gets under way in a characteristic region of the PE surface, which was termed the "initiation region".

These results have shown for the first time that loss of *netrinA* or overexpression of *frazzled* inhibits DE-Cad dissociation in PE cells and disturbs F-actin filament organization, suggesting the interaction between NetrinA and Frazzled plays a substantial role in regulation of ZA breakdown and cytoskeletal rearrangements during EMT. The BM degradation was not significantly affected in *netA.IR* and *frazzled* overexpressing discs. Thus, I speculate that disruption to ZA breakdown and F-actin organization are the major contributing factors to the adult eversion defects associated with *netrinA* knockdown and *frazzled* overexpression.

3.3.1 NetrinA and Frazzled control zonula adherens stability

Given that deregulation of the NetrinA pathways disrupts ZA disassembly, an important future aim will be to understand the molecular mechanism that connects the two. To achieve ZA disassembly, epithelial cells can employ several mechanisms: i) inhibiting *e-cadherin* expression transcriptionally, ii) inhibiting transport of newly synthesized and recycled E-Cadherin to the membrane, and/or iii) removal of E-Cadherin from the cellular junctions followed by its lysosomal degradation (Cano *et al.*, 2000 [53], Baum and Georgiou, 2011 [18]). Could *netA.IR* or *frazzled* overexpression disrupt transcriptional repression of *DE-cadherin/shotgun*? One way that NetrinA might achieve this is by activating expression of one of the transcription factors that can inhibit *shotgun* expression, such as Snail or Twist (Oda *et al.*, 1998 [191]). Arguing against this, neither *snail* nor *twist* RNAi causes eversion failure (M. J. Murray, unpublished observations).

Another possibility is that downregulation of *netrinA* or overexpression of *frazzled* affects the delivery of newly synthesized or recycled DE-Cad to the cell membrane. DE-Cad can be transported in Rab11-positive vesicles from the Golgi directly to the ZA, where it is exocytosed by a function of the exocyst complex which contains Sec5, Sec6, and Sec15 (Langevin *et al.*, 2005 [192], Woichansky *et al.*, 2016 [193]). The increased Frazzled in *netA.IR* and *frazzled* overexpressing cells could also influence the processes of modification and sorting of junctional components in the endoplasmic reticulum and Golgi. For example, the induction of apoptosis in human epithelial and carcinoma cell lines results in increased *O*-glycosylation of newly synthesized E-cadherin and β-catenin, which blocks their transport to the membrane and downregulates intercellular adhesion (Zhu *et al.*, 2001 [194]).

In the *Drosophila* dorsal thorax, DE-Cad recycling is positively regulated by Cdc42 and the polarity proteins Par6 and aPKC (Georgiou *et al.*, 2008 [195]). Depleting each of three proteins caused fragmentation of AJs, abnormal DE-Cad-rich extensions and DE-Cad puncta associated with the cell surface. Further investiga-

tion showed that this phenotype was due to defects in the endocytic internalization of junctional components. The maintenance of epithelial integrity via Cdc42 induced endocytic pathways has been also reported for the *Drosophila* neuroectoderm (Harris and Tepass, 2008 [196]). Another study of a mammalian cell line indicated that Cdc42 is highly expressed in the Golgi, where it promotes vesicle formation and their polarized trafficking to adherens and tight junctions (Kroschewski *et al.*, 1999 [197]). The activation of Cdc42 GTPase might well be associated with the binding of NetrinA to Frazzled, as this is known to occur during mammalian neurite outgrowth in response of Netrin-1/DCC signaling (Li *et al.*, 2002 [198]).

Finally, NetrinA and Frazzled might be involved in the process of DE-Cad degradation. This process becomes intensified during the EMT in order to sustain *E-cadherin* repression and efficient ZA breakdown (Janda *et al.*, 2006 [199]). For example, a very recent study of migratory behaviour of mesenchymal stem cells showed that the mammalian ortholog, Netrin-1, increases MMP-12-mediated degradation of E-cadherin leading to increased cell dissociation and motility (Lee *et al.*, 2014 [200]). In *Drosophila*, MMP1 is also reported to preferentially cleave DE-Cad associated with AJs to promote fat body cell dissociation (Jia *et al.*, 2014 [201]). Thus, one can envisage a model whereby NetrinA induces MMP1 to contribute to ZA breakdown during wing disc eversion. Arguing against this, MMP1 expression appears normal in Ubx>netA-IR discs (Manhire-Heath *et al.*, 2013 [133]). DE-Cad degradation might also be inhibited through disruptions to Src kinase pathways, which are also known to function downstream of netrins (Li *et al.*, 2004 [202]). One study using a human breast cancer cell line demonstrated that activated Cdc42 induces Src-dependent phosphorylation of E-Cadherin which is required for its ubiquitination and degradation, and this subsequently increased the rate of cell migration (Shen *et al.*, 2008 [203]).

The main question arising from the above results is how NetrinA and Frazzled regulate ZA remodelling, i.e. whether NetrinA acts via binding Frazzled or whether they function independently via individual signaling pathways. Results from our lab show an atypical up-regulation of Frazzled in the cytoplasmic regions of PE cells

in both cases, when *netrinA* is downregulated and when *frazzled* is overexpressed (Manhire-Heath *et al.*, 2013 [133]). Thus, hypothetically, in order to promote EMT, NetrinA might be necessary for reduction of Frazzled in the PE membrane, influencing the epithelial state of cells. Taking all this information into consideration, it is likely that Frazzled maintains epithelia by supporting ZA integrity and blocking EMT signaling.

3.3.2 Cytoskeletal reorganization is partially independent of zonula adherens breakdown

Loss of DE-Cad was accompanied by a consolidation of F-actin filaments and their assembly into dense round clusters accumulated preferentially on the edge of PE perforations. These observations agree with the clear links in other systems between downregulation of junctional genes during EMT and increased expression of genes promoting cell motility (reviewed by Lamouille *et al.*, 2014 [46]). The cytoskeletal changes and DE-Cad dissociation from ZA was seen in all three genotypes, again suggesting that these two processes are interdependent. A likely reason for this is that several signaling factors - such as small Rho GTPases, Rho1, Rac1, and Cdc42, and their regulators, GEFs and GAPs - regulate both ZA breakdown and cytoskeletal reorganization. For instance, at the onset of EMT Rho1 is activated for initial stress fiber formation (Yilmaz and Christofori, 2009 [66]). As the EMT progresses and there is continued dissociation of the ZA, Rho1 is progressively repressed by cytoplasmic p120 catenin liberated from the junctions (Anastasiadis *et al.*, 2000 [204]). This process leads to the loss of cellular contacts, consistent for a role for Rho1 in general ZA maintenance. At the same time, p120 stimulates activation of Rac1 and Cdc42 to promote membrane protrusions and cell motility (Lamouille *et al.*, 2014 [46]).

On the other hand, the F-actin enrichment in *netA.IR* and *frazzled* overexpressing discs with solid ZAs suggests that the initial actin filament polymerization does not require ZA breakdown. The idea that polymerization is not affected in *netA.IR* and

frazzled overexpressing discs is supported by a previous finding that loss of *netrinA* does not affect JNK expression (Manhire-Heath *et al.*, 2013 [133]). Absence of JNK activity impairs wound healing due to failed formation of actin-rich cables and filopodial protrusions (Bosch *et al.*, 2005 [205]). In wing discs, JNK also determines motility of the leading edge cells (Pastor-Pareja *et al.*, 2004 [82]). JNK is reported to up-regulate a gene *chickadee* (*chic*) coding a Profilin family protein, which is involved in F-actin polymerization and complements Cdc42 function (Cooley *et al.*, 1992 [206], Yang *et al.*, 2000 [207]). Loss of *chic* in embryos results in dorsal closure defects (Jasper *et al.*, 2001 [208]).

3.3.3 High levels of Frazzled cause the formation of structures reminiscent of stress fibers

In both *netA.IR* and *frazzled* overexpressing discs, F-actin was often organized into thick straight bundles, which appear to be more prominent in *Ubx>fra* PE cells. Although the stick-like shape and basal position of the observed structures highly resemble stress fibers, their identification as this kind of actin structure must be confirmed. Firstly, the molecular composition of the structures must be further investigated. Genuine stress fibers have a core consisting of continuous bundles of actin filaments, which are tightly connected to periodically distributed filaments of non-muscle myosin II. Additionally, there are other proteins always found along stress fibers that are important for their assembly and function: filamin, myosin light chain kinase (MLCK), caldesmon, tropomyosin, α-actinin and palladin. Filamin displays a continuous distribution similar to actin, while the other proteins are distributed periodically either co-localizing or alternating with myosin (reviewed by Pellegrin and Mellor, 2007 [209]; Naumanen *et al.*, 2008 [210]; Tojkander *et al.*, 2012 [211]).

Secondly, it is important to establish the precise localization with, and attachment to, the focal adhesion complexes as this information tells us about the type and the possible physiological role of stress fibers. In a recent review, four classes of

stress-fibres were described: dorsal stress fibres, ventral stress fibres, transverse arcs, and perinuclear actin caps (for details see Tojkander *et al.*, 2012 [211]). The straight actin bundles lying along the base of *Ubx>netA.IR* and *Ubx>fra* PE cells could be ventral stress fibers. This type of stress fibers are the most commonly observed structures, which are positioned along the ventral side of the cell and are connected to the integrin-rich focal adhesions at both ends. They are believed to play a significant role in cell adhesion to the ECM and contraction (Burridge, 1981 [212]; Chen, 1981 [213]). If it is the case, it suggests another possible reason for delayed eversion might be an inhibition of cell rounding and motility due to increased adhesion of PE cells to the BM. Indeed, some authors propose that stress fibers contribute mostly to cell adhesion and inhibit cell migration (Tojkander *et al.*, 2012 [211]).

An investigation into the nature of these actin structures might also aid identification of the downstream effectors of NetrinA and Frazzled since a major factor promoting the assembly of thick and stable stress fibers is the RhoA GTPase via its effectors Rho-associated kinase (ROCK) and the diaphanous-related formin mDia1 (Ridley and Hall, 1992 [190]; Hill *et al.*, 1995 [214]; Hotulainen and Lappalainen, 2006 [215]). ROCK inhibits actin filament disassembly, while mDia1 induces the polymerization of long parallel actin filaments (Maekawa *et al.*, 1999 [216]). Besides RhoA, the other GTPases, Rac1 and Cdc42, also influence stress fiber formation indirectly by activating actin polymerization complexes (Nobes and Hall, 1995 [217]; Pollard, 2007 [218]). In particular, the deletion of *rac1* abolishes stress fiber formation due to a disturbance in the association of the focal adhesion components to integrins. Interestingly, the overexpression of RhoA and ROCK are not able to rescue Rac-null phenotype suggesting that Rac1 regulates stress fibers assembly downstream or in parallel way of RhoA and ROCK (Guo *et al.*, 2006 [219]). Thus, the fact that the actin structures seem more prominent when *frazzled* is overexpressed suggests the higher levels of the receptor are causing an up-regulation of Rho GTPases stimulating the formation of stress fibers. Alternatively, given the earlier hypothesis that Frazzled might inhibit Rho1 activity by increasing phospho-

rylation levels of Moe (Speck *et al.*, 2003 [172]), it may be that elevated Frazzled creates stress-fibres by inducing Rac1 activity or by upregulating mDia1 or ROCK independently of Rho1 signaling.

3.3.4 Possible mechanisms of basement membrane degradation during wing disc eversion

Degradation of the BM is a critical step for developmental or tumor EMTs. It allows motile cells to invade into surrounding cell layers and migrate towards other locations. It has been previously demonstrated *in vivo* that BM degradation is indispensable for cells from imaginal wing discs to be able to break through the overlying larval epidermis during eversion (Srivastava *et al.*, 2007 [90]). Here, I used an *in vitro* culture technique to monitor BM remodelling during the early stages of eversion. I found that the first regions of the degrading BM appear over the PE near the stalk area and at the tip of the disc blade. The results suggest that the loss of the BM normally precedes the complete delocalization of DE-Cad from the ZA of PE cells. In both *Viking-GFP; Ubx>netA.IR* and *Viking-GFP; Ubx>fra* cultured wing discs, no significant effect on the BM degradation was observed. Both genotypes displayed a misregulation of the normal course of events where BM degradation precedes ZA breakdown.

It cannot be ruled out that *in vitro* culturing of explanted wing discs might affect the natural progression of BM degradation. In the whole larva, wing discs are tightly supported by adjacent imaginal discs, the intestinal tube, fat bodies, larval epidermis *etc.* All these tissues impede superfluous extension and movements of the everting discs, and support the BM and underlying delicate PE from mechanical breakup. To observe eversion *in vitro*, I used discs which were dissected free from surrounding tissues and most of the larval epidermis was removed. Further work is required to confirm that the breakups of the BM at the tip of the disc blades occur *in vivo*.

Although the complete degradation of the BM mostly precedes the disintegration

of the ZA, I observed several patches of Collagen IV over the PE cells that already had a fragmented ZA. Interestingly, the close attachment of the BM to these PE cells appeared to be lost, suggesting that eversion may involve a gradual elimination of cell adhesion to the ECM. Most of the interactions between the BM and the wing disc epithelia are promoted by Integrins. Due to the ability of integrins to make contact simultaneously with the ECM and with intracellular actin filaments, epithelial cells can strongly adhere to a rigid substrate (Hynes, 2002 [29]). There are multiple roles for Integrins during *Drosophila* epithelial morphogenesis. For instance, during wing disc eversion, βPS1 (Myospheroid, or Mys) and αPS2 (Inflated, or If) integrins are necessary for the formation of an adult wing blade as they maintain proper adhesion between the ventral and dorsal surfaces of the evaginating DP (Brower and Jaffe, 1989 [220]). Moreover, integrins are involved in maintenance of the columnar shape of DP cells, and this function is presumably based on the correct assembly of integrins and contact with matrix molecules (Dominguez-Gimenez *et al.*, 2007 [221]). The expression of dominant-negative β-integrin subunits causes a precocious transition from a columnar to a cuboidal cell shape together with the disorganization of Laminin. A similar effect of early cell flattening and evagination was observed after overexpression of *Mmp2* (Dominguez-Gimenez *et al.*, 2007 [221]). Also, integrins control the polymerization and morphology of actin filaments. For example, during embryonic dorsal closure, JNK signaling induces *mys* and *scab* (encoding the αPS3 subunit) to promote polymerization of actin filaments into a cable in the leading edge cells and form the "supracellular purse string" structure (Homsy *et al.*, 2006 [222]). During oocyte maturation, the switch between two integrins, Mew (Multiple edematous wings, αPS1) and If (Inflated, αPS2), is required for flattening of the follicular epithelium as much as for increase of basal F-actin levels and stress fibers elongation and adhesion (Delon and Brown, 2009 [223]). In culture experiments, the breakdown of the ZA in PE cells follows the increase in F-actin levels and changes in cell morphology. Thus, it is possible to consider a model where the integrins maintain a certain level of PE adhesion to the BM, and that this function is required for maintenance of ZA integrity, and downregulation

of this adhesion is required for the normal transition of PE cells to a mesenchymal phenotype during eversion.

Knockdown of *netrinA* and the overexpression of *frazzled* in the PE do not inhibit BM degradation. However, I cannot exclude the possibility that either NetrinA or Frazzled are still involved in BM breakdown. To generate a hypothesis of how these molecules might contribute to BM degradation, I have to consider pathways potentially regulating the degradation of the BM.

There are known only a few molecules involved in the degradation of the BM in *Drosophila*. First of all, the matrix metalloproteinases, MMPs, are well known to cleave BM components in both, flies and mammals (Mott *et al.*, 2004 [224]). The reduction of *Drosophila* MMP1 and MMP2 function as well as the overexpression of the only MMP inhibitor, *dtimp* (encoding the Tissue Inhibitor of Metalloproteases), results in a lack of BM degradation during wing disc eversion causing thoracic clefts or uneverted wings in adult progeny (Srivastava *et al.*, 2007 [90]). The best characterised regulator of MMPs in *Drosophila* is the JNK signaling pathway, the major regulator of wing disc eversion. During wing disc eversion and also during the re-epithelialization process during wound healing, JNK activation is sufficient only for MMP1 expression (Srivastava *et al.*, 2007 [90], Stevens and Page-McCaw, 2012 [225]). Neoplastic growth due to chromosomal instability in *Drosophila* epithelia also leads to up-regulation of *puc* together with the increased MMP1-mediated BM degradation (Dekanty *et al.*, 2012 [226]). Thus, there is a possibility that ectopic levels of Frazzled inhibit JNK signaling leading to reduced levels of MMPs though I was unable to detect this.

Besides the MMPs and JNK, there are other components that potentially have a role in BM degradation. For example, to initiate outer border cells migration during *Drosophila* oogenesis, the pre-invasive polar cells undergo rapid degradation of BM proteins, accumulated asymmetrically over anterior polar cells, and this process is initiated by the Jak/STAT pathway, a signaling cascade regulating a wide variety of cellular responses including cell proliferation, differentiation, survival, and apoptosis (Levy and Darnell, 2002 [227]). The expression of dominant-negative forms

of Domeless (Dome), the receptor for the Jak/STAT pathway, blocks the removal of the BM cap and the outer polar cells are not able to migrate. Interestingly, the MMPs do not seem to be involved in this process (Medioni and Noselli, 2005 [228]). Finally, the study of *Drosophila* air sac development from the air sac primordium revealed that Cathepsin-L (encoded by the *Drosophila* gene *cp1*) may regulate the degradation of the BM and promote the precursor cells to migrate and invade into the wing disc to form a tubular epithelial structure (Dong *et al.*, 2015 [229]). Together with the MMPs, Cathepsin-L represents another class of proteases that are associated with human cancers. Although it is unknown whether *Drosophila* netrins or the netrin receptors interact with the Jak/STAT signaling or Cathepsin-L, some oncology studies show that human Netrin-4 could induce Jak/STAT, PI3K/Akt, and ERK/MAPK oncogenic pathways (Lv *et al.*, 2015 [230]). Moreover, Netrin-1 stimulates glioblastoma invasiveness via the activation of RhoA and the recruitment of Cathepsin-B to a cell's surface. However, while RhoA is well-known to promote stress fiber formation and cell motility, the function of Cathepsin-B, cysteine protease, remains unclear (Shimizu *et al.*, 2013 [231]).

Table 3.1: **DE-Cad degradation in cultured wing discs.**

Disc culturing performed at 25°C. Total n-value indicates number of wing discs.

Culturing time (hrs)	Genotype	DE-Cad intact (%)	DE-Cad fragmented (%)	Holes (%)	Total (n)
8	*+;+;Ubx-GAL4,UAS-GFP/+*	10	27.5	62.5	40
	+;UAS-netA.IR/+;Ubx-GAL4,UAS-GFP/+*	47	30	23	47
	*+;+;UAS-fra**/Ubx-GAL4,UAS-GFP*	35	30	35	20
	+;Vkg-GFP/+;Ubx-GAL4/+	11	37	52	27
	+;Vkg-GFP/UAS-netA.IR;Ubx-GAL4/+	59	28	14	29
	+;Vkg-GFP/+;UAS-fra/Ubx-GAL4	35.5	29	35.5	28
7	*+;+;Ubx-GAL4,UAS-GFP/+*	61.1	33.3	5.6	18
	*+;+;UAS-fra.IR***/Ubx-GAL4,UAS-GFP*	21.8	65.2	13	23

Fly stocks used for culturing experiments:

* *v108577*

** *BL8814*

*** *BL31469*

Table 3.2: **BM degradation in cultured wing discs.**

Disc culturing performed at 25°C. Total n-value indicates number of wing discs.

Culturing time (hrs)	Genotype	BM intact (%)	BM degraded (%)	Total (n)
8	*+;Vkg-GFP/+;Ubx-GAL4/+*	11	89	27
	+;Vkg-GFP/UAS-netA.IR;Ubx-GAL4/+	17	83	29
	+;Vkg-GFP/+;UAS-fra/Ubx-GAL4	25	75	28

Table 3.3: **Correlation of the BM degradation and ZA breakdown in cultured discs.**

Disc cultured for 8 hrs at 25°C. Total n-value indicates number of wing discs.

Genotype	BM intact/ DE-Cad intact (%)	BM breakdown/ DE-Cad intact (%)	BM breakdown/ DE-Cad breakdown (%)	BM intact/ DE-Cad breakdown (%)	Total (n)
+;Vkg-GFP/+;Ubx-GAL4/+	11	0	89	0	27
+;Vkg-GFP/UAS-netA.IR;Ubx-GAL4/+	14	45	38	3	29
+;Vkg-GFP/+;UAS-fra/Ubx-GAL4	14	21	54	11	28

Figure 3.1: **Perforation of the PE after 8 hrs culture.** Third instar wing discs cultured and then fixed and stained for DE-Cad (red) and expressing Viking-GFP (Green). (a) A third instar wing disc cultured for 0 hrs. The PE is intact. (b-d) Wing discs cultured for 8 hrs. The PE displays perforations of different size, from the small (b, arrow) and medium holes (c, arrow) to major retraction (d, arrowheads). Discs are shown as 3-dimensional renderings.

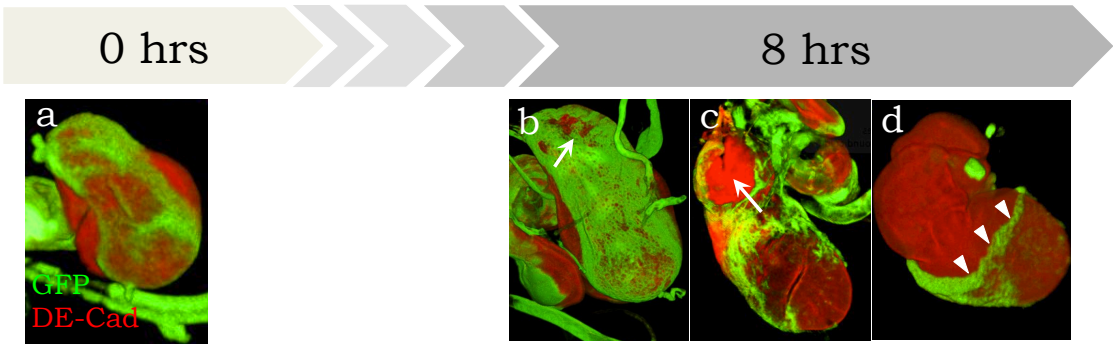
0 hrs
8 hrs
a
GFP
DE-Cad
b
c
d

Figure 3.2: **The initiation region.** (a) A third instar wing disc with GFP expression (green) driven by *Ubx-GAL4*, and stained for DE-Cad (red). (b) Schematic representation of the initiation region. All the discs below are presented as maximum projections (see Materials and Methods) with a stalk region above and disc blade below, and anterior (A) side is to the right and posterior (P) side is to the left.

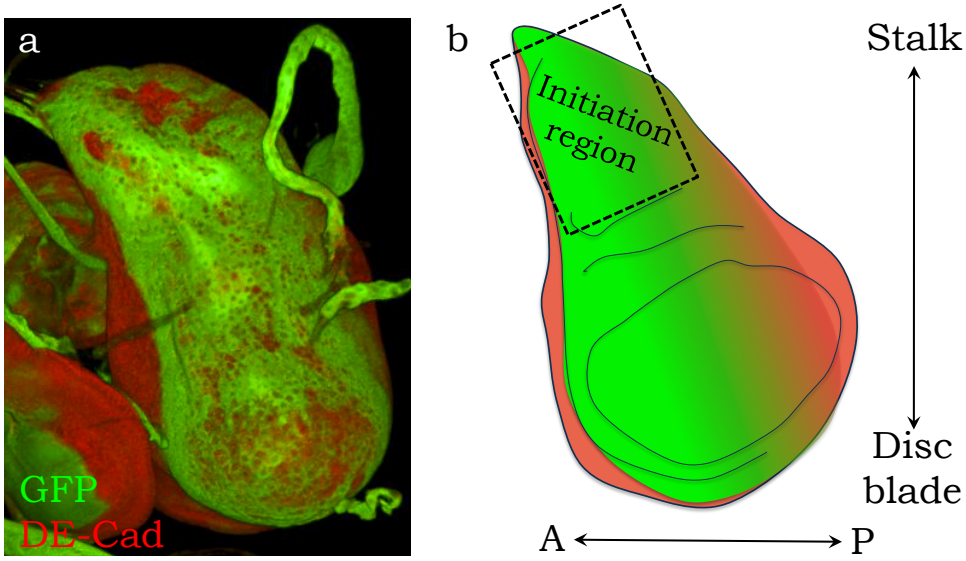
a
GFP
DE-Cad
b
Initiation region
Stalk
Disc blade
A
P

Figure 3.3: **Control wing discs display EMT hallmarks after 8 hrs culturing.** Third instar *Ubx>GFP* wing discs cultured with ecdysone for 0 hrs (a-c) or for 8 hrs (d-f). The discs were fixed and stained for DE-Cad (blue (a, a', d, d') or grayscale (b, b', e, e', h)) and for Rhodamine phalloidin (a marker for F-actin; red). (a, a', d, d') Merged images of the PE positive for GFP (green). Dashed lines (a, d) indicate areas for the cross-sections in a'-f'. The dashed arrows in a' indicate the position of the PE and DP epithelium of the disc. (b, b') DE-Cad (grayscale) stays intact after 0 hrs culture. The ZA keeps its integrity, PE cells have squamous morphology (b'). (e, e', h) After 8 hrs culture DE-Cad is dissociated from ZA (e, arrows). PE cells acquire spherical morphology (e', h). The asterisk (d'-f') indicates the spherical morphology of the cell undergoing the EMT. (c, c') F-actin (red) has cortical and cytoplasmic distribution after 0 hrs of culture. Its distribution around the cell perimeter largely coincides with the distribution of DE-Cad. (f, f', i) After 8 hrs culture F-actin is accumulated in round clusters around the areas with broken ZA (f, arrowheads). (g) The co-localization (arrows) of DE-Cad and F-actin in regions with an intact ZA (shown in the magnified area from the dashed box in f). (h, i) Magnified images of the dashed boxes in e' and f' respectively. Arrow (i) indicates a round cell undergoing the EMT. Arrowheads (i) indicate the clusters of F-actin accumulated at the rim of cells undergoing the EMT. Discs are presented as maximum projections. Scale bars 10 μm.

Ubx>GFP, 0 hrs culture

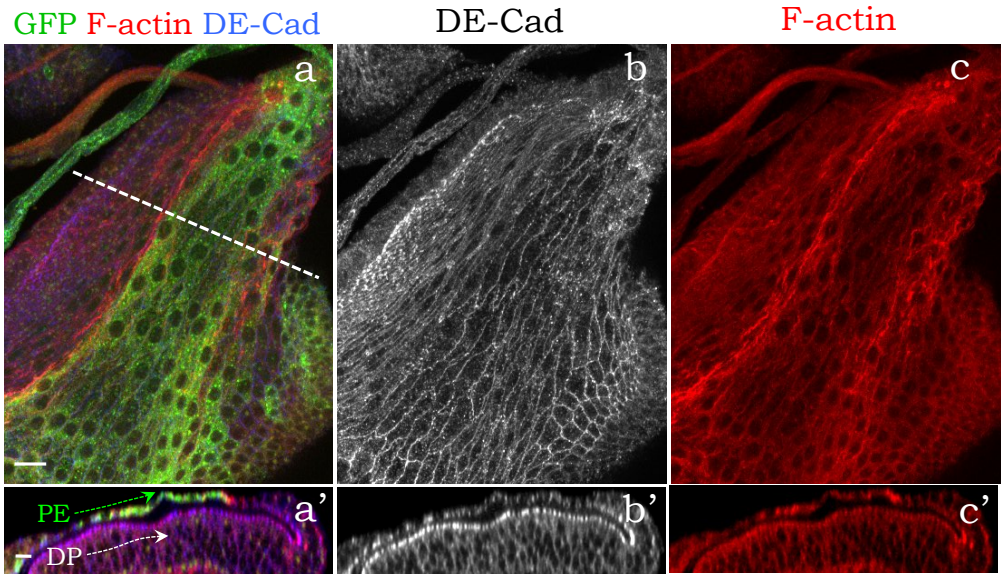

8 hrs culture

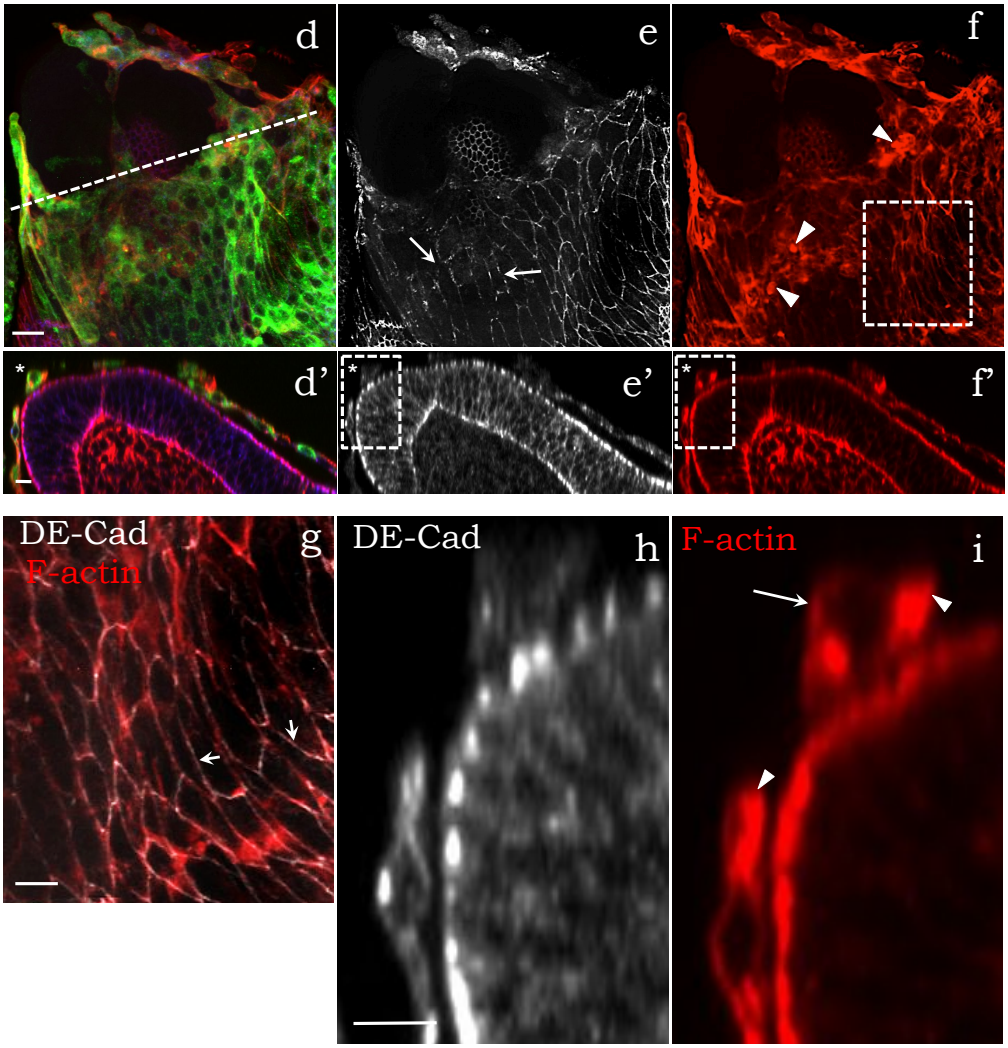

Figure 3.4: **Loss of NetrinA or overexpression of Frazzled inhibits ZA breakdown during the wing disc eversion EMT.** Third instar *Ubx>GFP* (a-c), *Ubx>netA.IR* (d-f) and *Ubx>fra* (g-j) wing discs cultured with ecdysone for 8 hrs. The *Ubx>netA.IR* and *Ubx>fra* discs with the inhibited EMT are depicted. The discs were fixed and stained for DE-Cad (blue or grayscale) and for Rhodamine phalloidin (F-actin; red). (a, d, g) Merged images of the PE positive for GFP (green). Dashed lines (a, d, g) indicate areas for the cross-sections in a'-j'. (b, b') DE-Cad is dissociated from ZA after 8 hrs culturing in *Ubx>GFP*. (arrows, e, e', h, h') DE-Cad remains intact in ZA after 8 hrs culturing in *Ubx>netA.IR* and *Ubx>fra*. PE keeps squamous morphology. (c, c') After 8 hrs culture F-actin is accumulated in round clusters around the areas with broken ZA in *Ubx>GFP* (c, arrowheads). (f, f', j, j') F-actin filaments are clustered (arrowheads in f, j) and form "stress fibers"-like structures (double arrowheads in f, j, l, m) after 8 hrs culturing in *Ubx>netA.IR* and *Ubx>fra*. (k) Magnified image (dashed box in c) of the F-actin outlining the PE cells in *Ubx>GFP*. (l, m) Magnified images (dashed boxes in f and j) of the "stress fibers"-like structures (double arrowheads) in *Ubx>netA.IR* (l) and *Ubx>fra* (m) respectively. *Ubx>GFP* control data is reproduced from Figure 3.3. Discs are presented as maximum projections. Scale bars 10 μm.

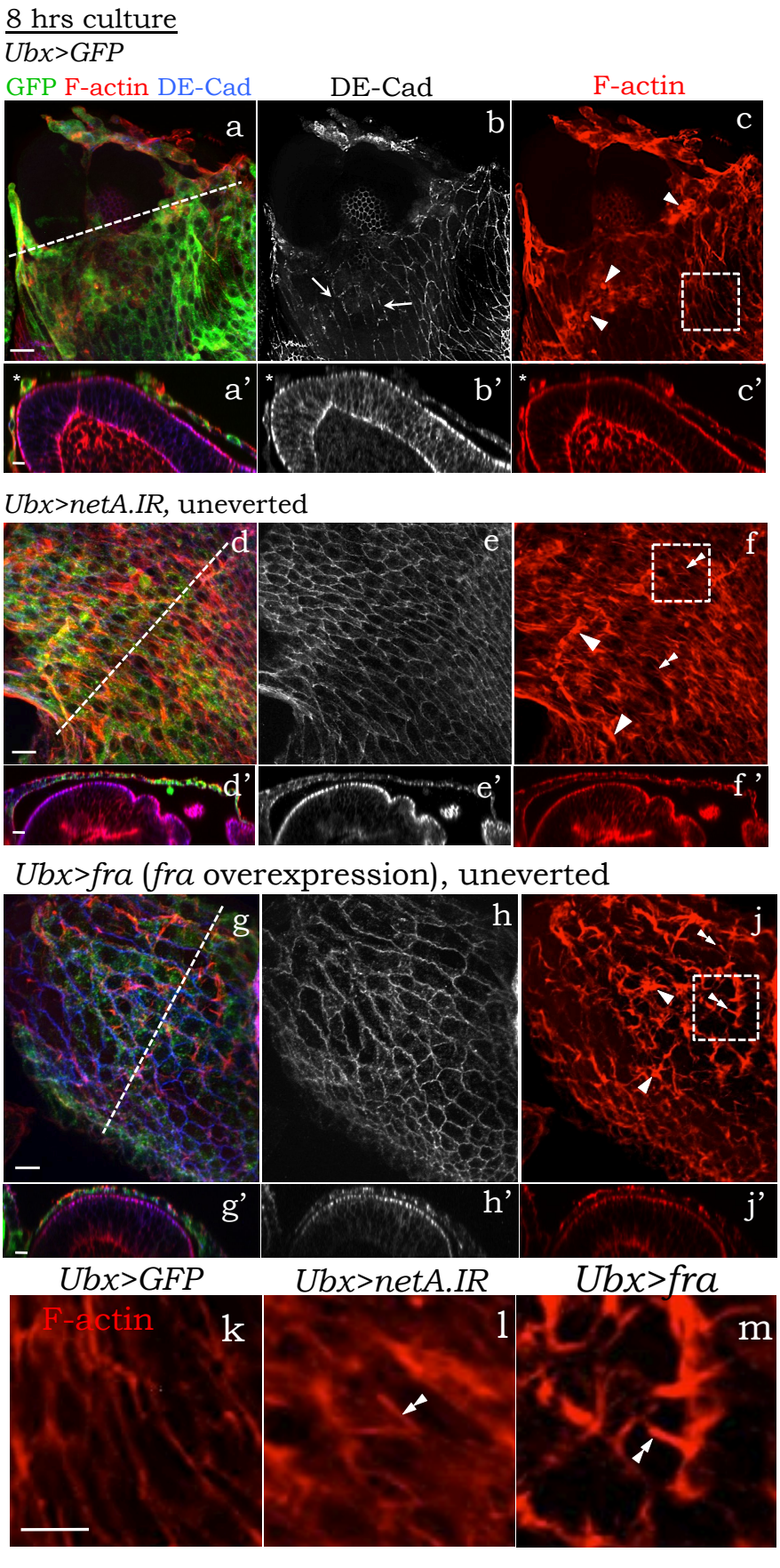
8 hrs culture
Ubx>GFP
GFP F-actin DE-Cad
DE-Cad
F-actin
a
b
c
a'
b'
c'
Ubx>netA.IR, uneverted
d
e
f
d'
e'
f'
Ubx>fra (fra overexpression), uneverted
g
h
j
g'
h'
j'
Ubx>GFP
Ubx>netA.IR
Ubx>fra
F-actin
k
l
m

Figure 3.5: **Loss of NetrinA or overexpression of Frazzled induces formation of "stress fiber"-like structures.** Third instar *Ubx>GFP* (a-c), *Ubx>netA.IR* (d-f) and *Ubx>fra* (g-j) wing discs cultured with ecdysone for 8 hrs. The discs undergoing EMT are depicted. The discs were stained for DE-Cad (blue or grayscale) and for Rhodamine phalloidin (F-actin; red). (a, a', d, d', g, g') Merged images of the PE positive for GFP (green). Dashed lines (a, d, g) indicate areas for the cross-sections in a'-j' and k-l. (b, b', e, e', h, h') DE-Cad is dissociated from ZAs after 8 hrs culturing (asterisk). PE cells lose their squamous morphology (asterisk). (c, c', f, f', j, j') F-actin filaments are clustered around the regions with dissociated DE-Cad (arrowheads in c, c', f, f', j, j'). F-actin can also be formed into "stress fiber"-like structures in *Ubx>netA.IR* and *Ubx>fra* (double arrowheads in f and j). (k, l) Cross-sections of the *Ubx>netA.IR* (k, k') and *Ubx>fra* (l, l') wing discs. (k', l') Magnified images of the dashed boxes in k and l respectively. The "stress fiber"-like structures (double arrowheads) are localized preferably on the basal side. Apical-basal axis of the PE (k', l') is marked by the double-headed arrows. *Ubx>GFP* control data is reproduced from Figure 3.3. Discs are presented as maximum projections. Scale bars 10 μm.

8 hrs culture

Ubx>GFP

GFP F-actin DE-Cad DE-Cad F-actin

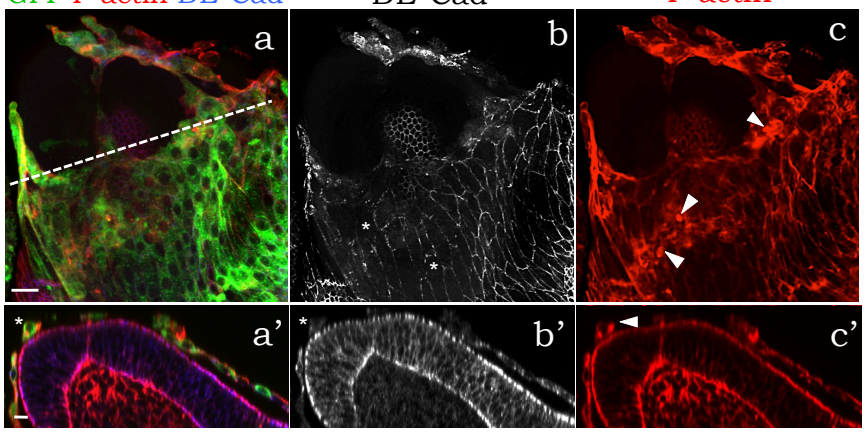

Ubx>netA.IR, everted

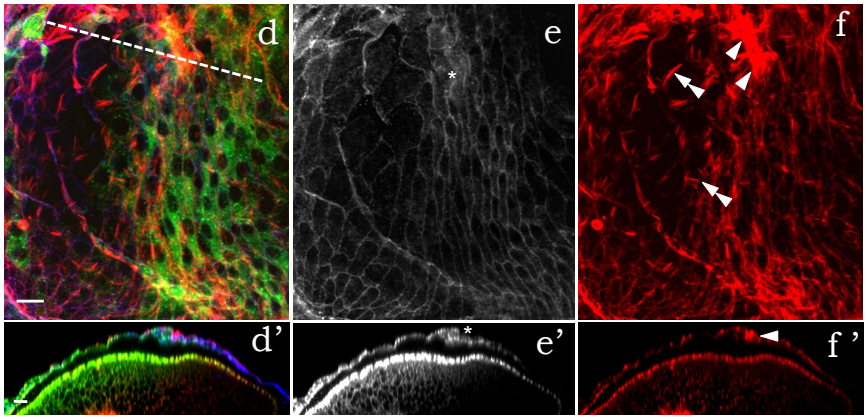

Ubx>fra (*fra* overexpression), everted

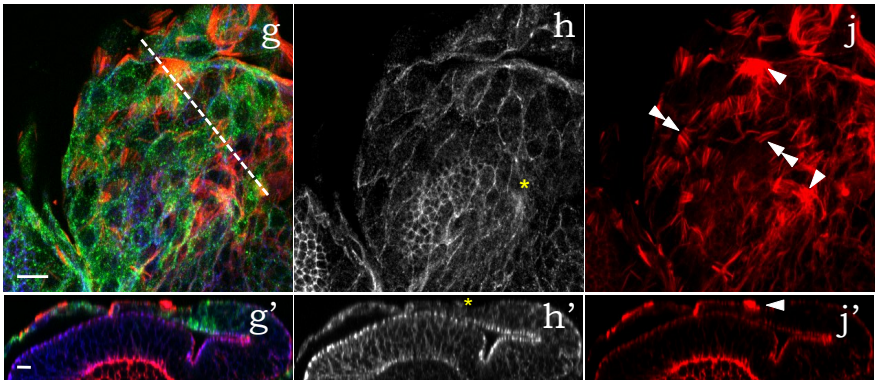

Ubx>netA.IR *Ubx>fra*

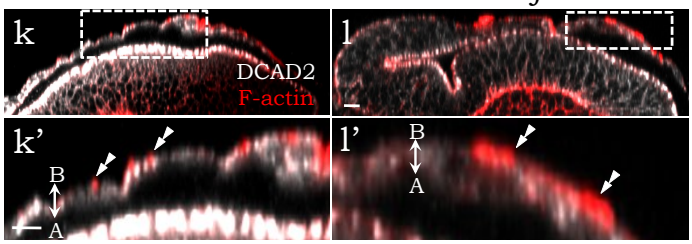

Figure 3.6: **Loss of *netrinA* or overexpression of *frazzled* in the PE inhibits ZA breakdown.** Quantification of eversion outcomes for two groups of wing discs after culturing for 8 hrs in ecdysone. The first group: *Ubx>GFP* (*Control*, n=40), *Ubx>netA.IR* (*netA.IR*, n=47) and *Ubx>fra* (*fra*, n=20) wing discs. The second group: *w1118;VikingGFP;Ubx-GAL4* (*Control*, n=27), *VikingGFP;Ubx>netA.IR* (*netA.IR*, n=29) and *VikingGFP;Ubx>frazzled* (*fra*, n=28) wing discs. In the first group, the percentage of the discs with intact DE-Cad in control discs is significantly less than in *netA.IR* or *frazzled* discs (p=0.0002 and p=0.0315 respectively). In the second group, the percentage of the discs with intact DE-Cad in control discs is significantly less than in *netA.IR* or *frazzled* discs (p=0.0003 and p=0.0322 respectively). The difference between *netA.IR* and *frazzled* discs within both groups is not statistically significant (p=0.428 and p=0.114 respectively). The difference between the three genotypes from the first group and three genotypes from the second group is not statistically significant (p>0.35). Error bars show 95% CI for the proportion of discs with ZA intact (by Wilson Score method).

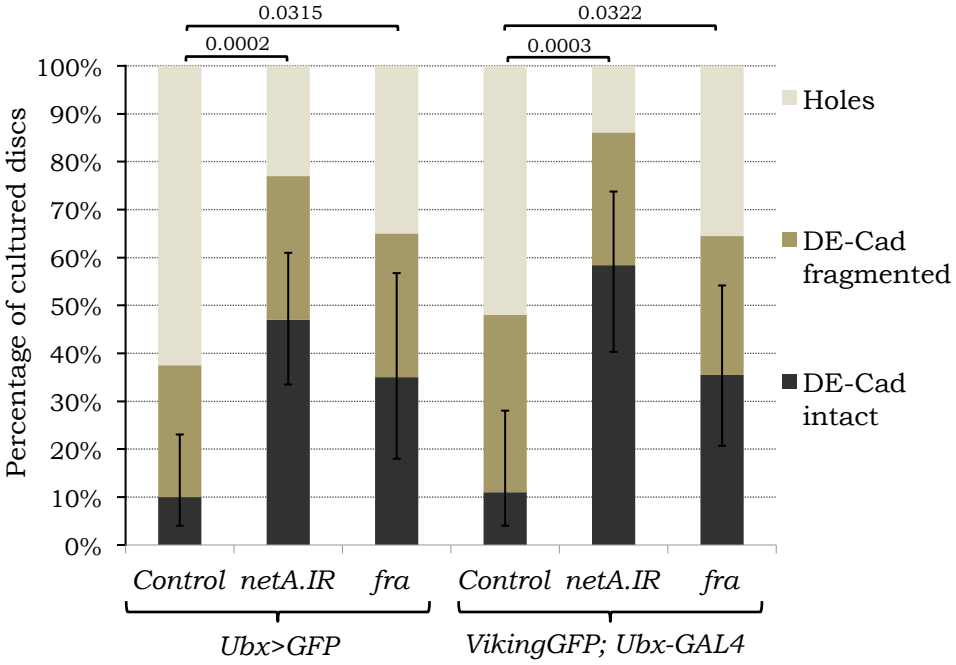
0.0315
0.0002
0.0322
0.0003
100%
90%
80%
70%
60%
50%
40%
30%
20%
10%
0%
Percentage of cultured discs
Holes
DE-Cad fragmented
DE-Cad intact
Control
netA.IR
fra
Control
netA.IR
fra
Ubx>GFP
VikingGFP; Ubx-GAL4

Figure 3.7: **BM degradation is initiated at the stalk and at the blade region.** (a-c) The progression of the BM (green) degradation after 8 hrs culturing. A non-cultured disc is evenly covered with the BM (a); after 8 hrs culture, the BM is degraded at the stalk (b, arrowheads) and at the tip of the blade (b, c, arrows). (d) Two processes contribute to the BM degradation. Dashed boxes indicate magnification images in e and f. (e) The gradual dissolution of the BM is probably mediated by the MMPs (arrowheads). (f) The BM is broken and pulled off the disc due to widening and bending of the DP (arrows). All the discs are stained for DE-Cad (red). Discs are shown as 3-dimensional renderings. Scale bars 10 μm.

w1118; Viking-GFP; Ubx-GAL4

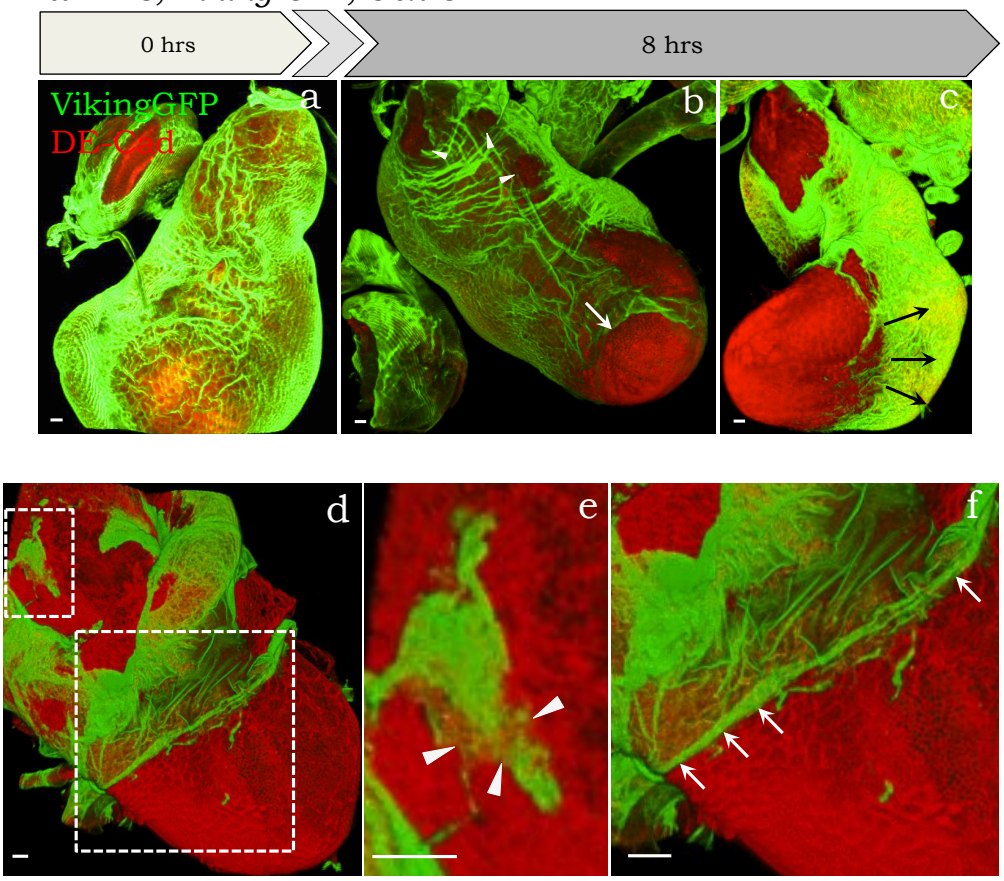

Figure 3.8: **BM degradation/retraction generally precedes ZA breakdown.** (a-c) A control *w1118;VikingGFP;Ubx-GAL4* disc which has failed to undergo the EMT after 8 hrs culture. The BM (green) remains intact (a) and is tightly apposed to the PE (c). DE-Cad (red) in the PE remained intact (b). (d-g) A control *w1118;VikingGFP;Ubx-GAL4* which has undergone the EMT after 8hrs culture. The BM is degrading over the PE (d). DE-Cad is fragmented in the PE (e, arrows). The holes (e, f, asterisk) were formed in regions where the BM has already been removed. The islets of BM remain over the PE with a fragmented ZA, but the apposition to the PE is not tight (arrowhead, f, g). Dashed lines (a, d) indicate areas for the cross-sections in c and f. Green dashed line (e) indicate borders of the BM in d. Dashed box (f) indicates magnification image in g. Discs are presented as maximum projections. Scale bars 10 μm.

Control, 8 hrs culture

EMT failed

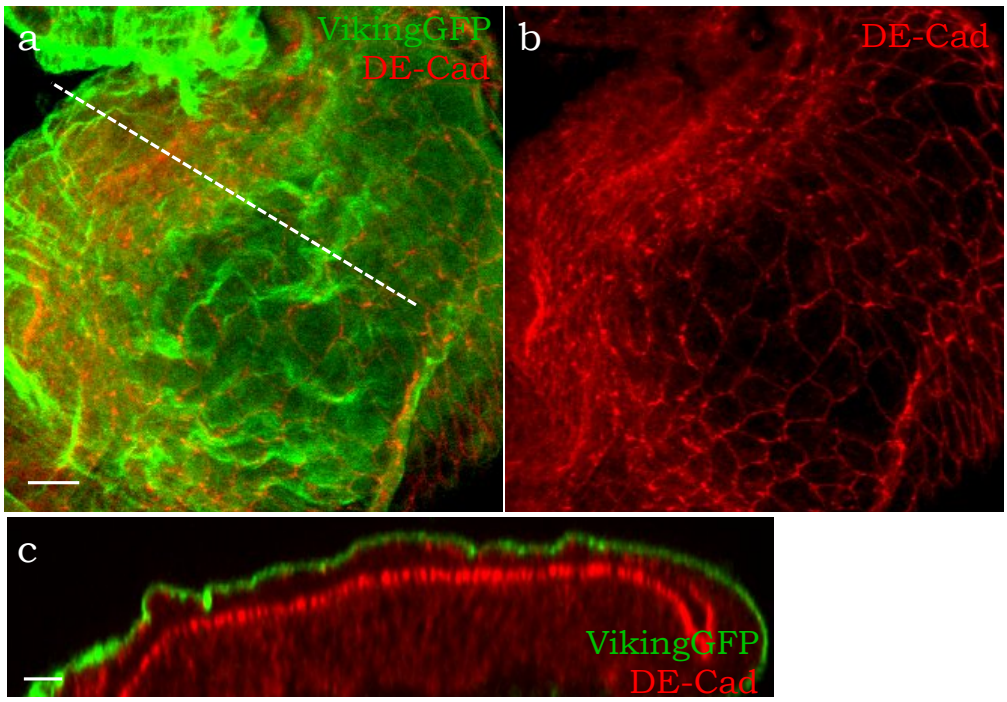

EMT

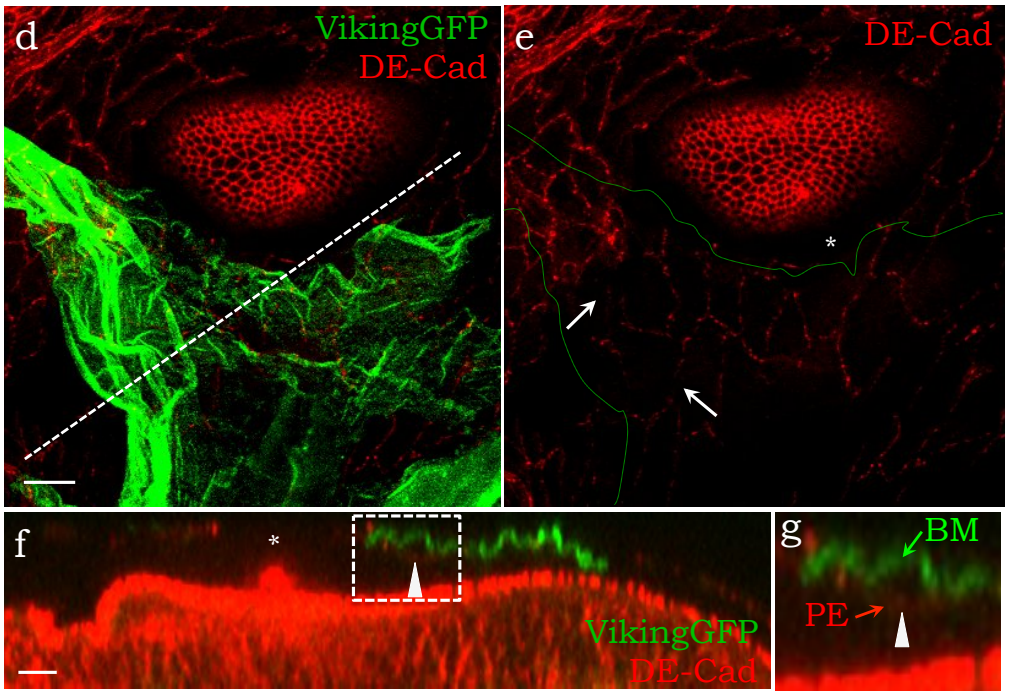

Figure 3.9: **Loss of *netrinA* or overexpression of *frazzled* in the PE does not significantly affect BM degradation.** Quantification of the eversion results for *w1118;VikingGFP;Ubx-GAL4* (*Control*, n=27), *VikingGFP;Ubx>netA.IR* (*netA.IR*, n=29) and *VikingGFP;Ubx>frazzled* (*fra*, n=28) wing discs after 8 hrs culture. (a) The percentage of the discs with a degraded BM in control discs is not significantly different from *netA.IR* and *frazzled* discs ($p>0.1$). (b) Correlation of the BM degradation and ZA breakdown in *Control*, *VikingGFP;Ubx>netA.IR* (*netA.IR*) and *VikingGFP;Ubx>frazzled* (*fra*) discs. In *netA.IR* discs, ZA breakdown is inhibited more than in *frazzled* discs. In *frazzled* discs, the BM degradation is inhibited more than in *netA.IR* discs. The percentages are indicated in the wedges. Error bars show 95% CI of the proportion of discs with BM degradation (by Wilson Score method).

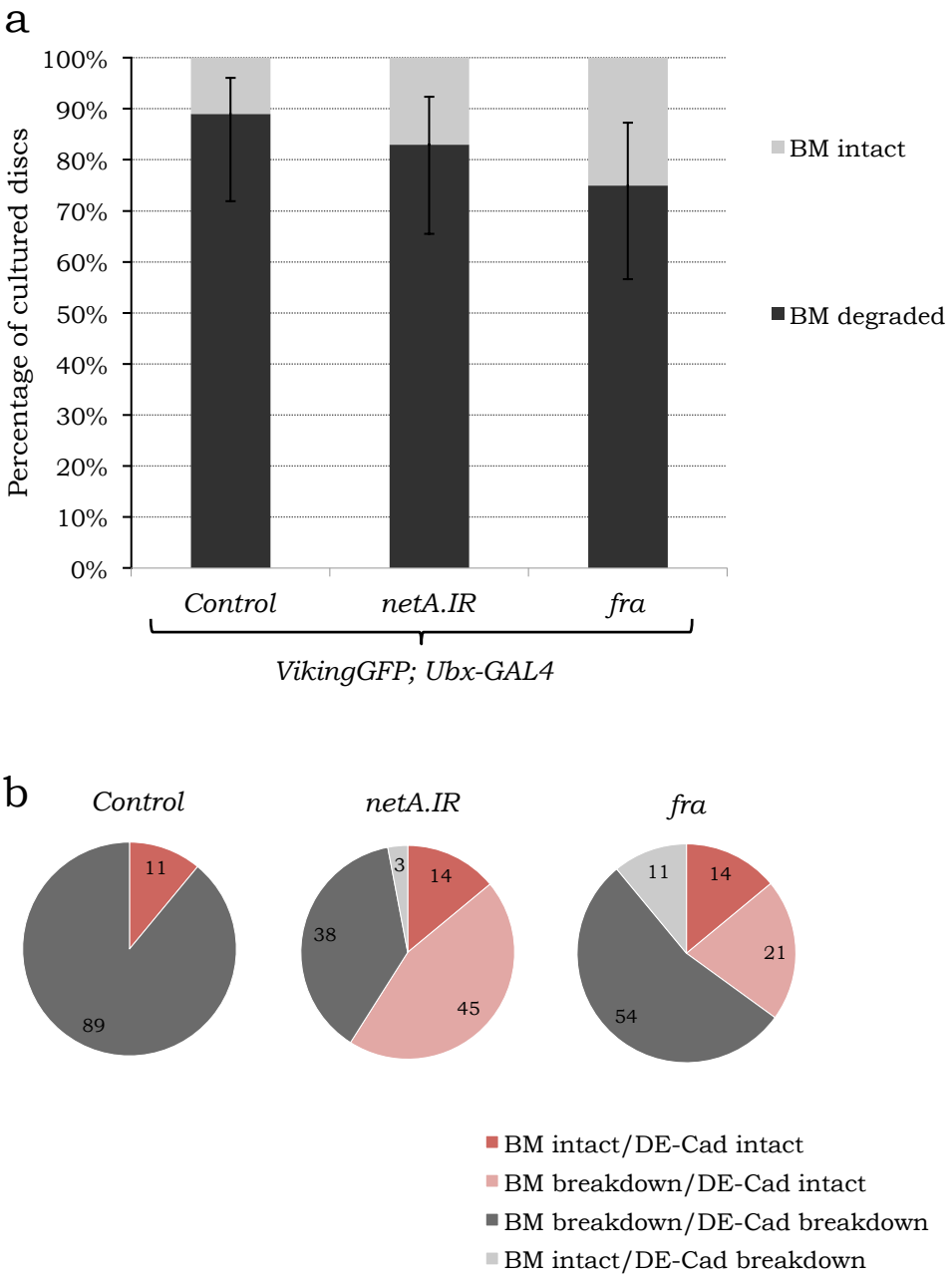
a
100%
90%
80%
70%
60%
50%
40%
30%
20%
10%
0%
Percentage of cultured discs
BM intact
BM degraded
Control
netA.IR
fra
VikingGFP; Ubx-GAL4
b
Control
netA.IR
fra
11
89
3
14
38
45
11
14
21
54
BM intact/DE-Cad intact
BM breakdown/DE-Cad intact
BM breakdown/DE-Cad breakdown
BM intact/DE-Cad breakdown

CHAPTER 4

Phenotypes associated with *frazzled* loss-of-function and overexpression in epithelial cells

4.1 Introduction

4.1.1 Frazzled function in epithelia

In Chapter 3, I showed that overexpression of Frazzled throughout the PE could inhibit eversion. At cellular level this involved an inhibition of ZA breakdown, and, to a lesser extent, inhibition of BM breakdown, as well as strong induction of F-actin stress-fiber-like structures. In this chapter the ability of Frazzled to regulate epithelial cell phenotypes was investigated in more depth using mosaic clones that were either homozygous for loss-of-function *frazzled* mutations, or were overexpressing *frazzled*.

The idea that Frazzled-family receptors might promote epithelial stability, and actually inhibit cell invasiveness and motility, is somewhat controversial. Since the DCC receptor was first identified, its role in cancer progression has been disputed (Duman-Scheel, 2012 [145]). Despite a large percentage of colorectal cancers having

reduced DCC expression (Mehlen and Fearon, 2004 [147]), there are only a limited number of reports confirming that genetic elimination of the receptor can stimulate metastasis. Only two mammalian studies have directly demonstrated an increased tumor aggressiveness in response to loss of DCC (Castets *et al.*, 2011 [153]; Krimpenfort *et al.*, 2012 [232]). There is also evidence that DCC and its orthologs are able to maintain ZAs. For example, DCC-transfected colonic epithelial cells are resistant to scattering upon treatment with TPA (12-*O*-Tetradecanoylphorbol-13-acetate). The authors found that the cytosolic pools of E-Cadherin were apparently redirected to the AJs, making them stronger (Martin *et al.*, 2006 [167]). A recent study of Caco-2 cells, a human intestinal cancer line, demonstrated that Neogenin supports junctional stability by regulating E-Cadherin endocytosis and controlling junctional tension (Lee *et al.*, 2016 [233]).

In 2011, VanZomeren-Dohm and colleagues also found that *Drosophila* Frazzled may play the role of an invasive tumor suppressor (VanZomeren-Dohm *et al.*, 2011 [151]). Using the Mosaic Analysis with a Repressible Cell Marker (MARCM) technique the authors generated *frazzled* loss-of-function clones in eye-antennal discs. In their experiments, they used either of two amorphic alleles, fra^3 or fra^4, both of which are known to cause early lethality in flies because of strong disruptions to axon guidance (Kolodziej *et al.*, 1996 [135]). Unfortunately, *frazzled* mutant clones were very small and showed elevated expression of apoptotic markers. Therefore, to obtain clones that could be analysed, the authors had to block apoptosis by ectopic expression of the baculovirus caspase inhibitor p35. Strikingly, these p35-rescued *frazzled* mutant clones were discovered in various distant sites of the fly (e.g. legs or wings), suggesting that the loss of Frazzled induces invasive behaviour typical of metastatic tumors. These cells exhibited several features of invasive tumor such as pJNK, MMP1 and pERK, delocalized DE-Cad, disrupted F-actin and Discs-large distribution, increased levels of the proliferation marker phospho-Histone H3, and degradation of the BM adjacent to the clones. Live imaging confirmed that *frazzled* mutant cells had the ability to invade the surrounding BM and move away from the epithelium. The authors suggested that *frazzled* loss-of-function phenotypes were

partially due to activated Rho1 pathway since expression of dominant negative-Rho1 could partially block the invasive behaviour.

A major caveat with this study is that p35 inhibits effector caspase activity, but not the upstream initiator caspase Dronc. Thus expression of p35 in apoptosing cells can place them in an "undead" state (Huh *et al.*, 2004 [234]; Ryoo *et al.*, 2004 [235]; Pèrez-Garijo *et al.*, 2005 [236]). Although the authors controlled for the p35 by creating clones overexpressing p35, a more appropriate control would have been to examine cells induced to undergo apoptosis, in a *fra*-independent way, but co-expressing p35. Recently Rudrapatna and colleagues (2013) performed just this experiment and showed that co-expression of the cell death gene *hid* together with *p35* led to activation of the JNK pathway, expression of MMP1 and migratory and invasive behaviour (Rudrapatna *et al.*, 2013 [237]). Thus the phenotypes reported in VanZomeren-Dohm *et al.*, 2011 [151] may not be due to loss of *frazzled*.

While the ability of DCC family receptors to stabilise epithelia is controversial, their role in motility is well documented. Overexpression of Frazzled as well as DCC can promote filopodia and lamellipodia in axons and non-neural cells (Li *et al.*, 2002 [198]; Shekarabi and Kennedy, 2002 [122]; Martin *et al.*, 2006 [167]; Lee *et al.*, 2014 [200]). For example, Frazzled signaling modulates reorganization of the actin cytoskeleton for the CNS growth cone to cross the midline. This regulation is mediated by Abelson cytoplasmic tyrosine kinase (Abl), Trio (Rac/Rho GEF) and the actin polymerization factor, Enabled (Ena; Forsthoefel *et al.*, 2005 [238], Dorsten *et al.*, 2010 [239], O'Donnell and Bashaw, 2013a [240]). DCC-expressing kidney or neuroblastoma cells cultured *in vitro* increase substrate adhesion and protrusions number in response to Netrin-1 (Shekarabi and Kennedy, 2002 [122]). Intracellular regions of DCC allow the receptor to interact with tubulin (Qu *et al.*, 2013 [241]) and potentially with focal adhesion kinase (FAK; Ren *et al.*, 2004 [242]). Also DCC indirectly regulates myosin II activity (Dorsten *et al.*, 2007 [243]).

Thus, one is faced with two apparently contradictory functions that Frazzled might have in epithelia: on the one hand Frazzled might support a stationary epithelial state, but, under certain conditions or signaling events, Frazzled might also

induce motile characteristics. Wing discs provide an excellent model system in which to examine these potential roles for Frazzled as they are comprised of both a very stable epithelial type, the DP epithelium, and one which is predisposed to undergo the EMT and adopt an invasive and migratory phenotype, the PE.

4.1.2 This chapter

The aim of this part of the study was to understand the Frazzled-mediated cellular and molecular changes that might potentially underlie the eversion phenotype. To elucidate the role of Frazzled in epithelial cells, I investigated the effects of loss or overexpression of *frazzled* in wing discs. This chapter describes a few different approaches to *frazzled* loss-of-function analysis, including MARCM (see Materials and Methods) and RNAi downregulation, performed in cultured and non-cultured wing discs, and also in adult flies. Based on advice that the *FRT G13* chromosome can itself have an effect on clone growth (Linda Parsons, personal communication), I first created a recombinant *FRT42D fra*^{3} chromosome. Surprisingly, in contrast to the results of VanZomeren-Dohm *et al.*, 2011 [151], I saw no evidence of apoptosis or other cellular phenotypes. Possible reasons for this are discussed later (Section 4.3.1). In contrast, the *frazzled* overexpression analysis revealed several potential signaling pathways that might be activated downstream of the receptor, which could contribute to eversion failure.

4.2 Results

4.2.1 Loss of one copy of *frazzled* rescues *Ubx>netA.IR* eversion phenotypes

As was mentioned earlier, *netA.IR* eversion defects appear to be largely due to excess Frazzled. Three lines of evidence have previously supported this idea: i) the PE of *netA.IR* discs displays higher level of the receptor; ii) RNAi knockdown of *frazzled* rescues the *netA.IR* phenotypes; and iii) overexpression of *frazzled* can

phenocopy loss of *netA* (Manhire-Heath *et al.*, 2013 [133]). In addition, further evidence was obtained here using a *frazzled* deficiency. Heterozygosity for the deficiency Df(2R)BSC880, which removes one copy of *frazzled*, was able to suppress the *netA.IR* eversion phenotypes, elevating the number of normal progeny from 54% up to 86.5% (p=0.0008, this and all other p-values in this chapter are based on a two-tailed Fischer's exact test; Figure 4.1).

4.2.2 EMT is accelerated in cultured *Ubx>fra.IR* discs

One possible explanation of why an increased amount of Frazzled in the PE might causes eversion defects is an ability of the receptor to maintain an epithelial state. To provide further evidence for this hypothesis, I tested whether reducing the amount of the receptor could facilitate the EMT process in the PE. Indeed, I found that RNAi knockdown of *frazzled* was able to accelerate the fragmentation of DE-Cad and formation of holes in the PE (Figure 4.2). For this comparison I shortened the disc culture time-slot to 7 hours, since after the standard 8 hrs the majority of the *fra.IR* discs had developed large holes, which are more difficult to analyse. After 7 hours culture, 65.2% of the cultured *Ubx>fra.IR* discs displayed degradation of DE-Cad at the ZA, and 13% of the discs had perforations in the PE, characteristic of later stages of the EMT (n=18). The proportions of control *Ubx>GFP* discs with the same characteristics was almost reduced by half to 33.3% and 5.5% respectively (n=23; p-value=0.0225; Figure 4.2; Table 3.1).

4.2.3 fra^3/fra^4 mutant flies display thoracic closure defects

Although *Ubx-GAL4*-mediated RNAi knockdown of *frazzled* in PE cells did not produce any eversion defects in adults, thorax deformations were seen in flies trans-heteroallelic for a null allele and a hypomorphic allele of *frazzled* . For a null allele I used fra^3 which has a stop-codon in the first exon and is a protein null (Kolodziej *et al.*, 1996 [135]; Pert *et al.*, 2015 [78]). fra^3 homozygotes exhibit strong disruptions of axon guidance and embryonic lethality (Kolodziej *et al.*, 1996 [135]).

For a hypomorphic allele I used *fra*^{4} obtained from Bloomington *Drosophila* Stock Centre. The molecular basis of this allele is unknown, but it has previously been described as a protein null (Kolodziej *et al.*, 1996 [135]; Dorsten *et al.*, 2007 [243]). In our hands, however, *fra*^{4} homozygotes still exhibit Frazzled immunostaining (using the Kolodziej antibody). Surprisingly, besides a high percentage of early lethality (approx. 90% of expected progeny; see Lethality assay in Material and Methods, and Figure 4.3), 10.5% of expected *fra*^{3}/*fra*^{4} progeny survived and approximately half of these (4.8% of total) had thoracic clefts ($p<0.0001$; Figure 4.3). This result suggests that in addition to playing an inhibitory role during the early, EMT, stages of eversion, Frazzled might also play a positive role during the later, epithelial sheet migration phase.

4.2.4 Clonal analysis of the wing disc epithelial cells lacking Frazzled

4.2.4.1 *fra*^{3}/*fra*^{3} clones in wing discs do not display any cellular abnormalities

In addition to understanding the role of Frazzled during the peripodial EMT, I was interested in whether the loss of the receptor could affect the functioning of a stable epithelium. I therefore created GFP-labeled clones of cells homozygous for *fra*^{3} in the DP epithelia of a third instar wing disc using a standard MARCM protocol (Wu and Luo, 2007 [244]). First, I used anti-Frazzled immunostaining to confirm that the *fra*^{3}/*fra*^{3} clones displayed an obvious reduction of the receptor compared to wild type clones (Figure 4.4). However, *fra*^{3}/*fra*^{3} clones were still slightly positive for anti-Frazzled antibodies (Figure 4.4, b', arrows), suggesting perdurance of *frazzled* transcripts and/or Frazzled protein in the cells created prior to the FLP-induced recombination. We do not believe this to be background staining since the subcellular localization was qualitatively similar to normal Frazzled (Figure 4.4, b').

Interestingly, in contrast to VanZomeren-Dohm *et al.*, (2011) [151], the *fra*^{3}/*fra*^{3} clones in different epithelia throughout the larvae (including other kinds of imaginal

discs) seem to survive successfully throughout the whole *Drosophila* metamorphosis. VanZomeren-Dohm *et al.*, 2011 found that fra^4 and fra^3 clones in third instar eye discs were usually very small, and revealed increased Caspase-3 activity, suggesting that the clones get eliminated due to apoptosis. In our mosaic system, the fra^3/fra^3 clones were easily produced (without expression of p35) and the number of cells could be as high as the number of cells in the whole PE.

No obvious morphological differences, such as size or shape, were observed in *frazzled*-null cells compared to the surrounding control cells. Also the clonal loss of *frazzled* had no effect on adult flies. Moreover, immunohistochemical analysis of mosaic wing discs did not reveal noticeable changes in mutant clones. In particular, the cellular distribution of DE-Cad, F-actin and pMoe appeared to be unaltered (Figures 4.5, 4.6 and 4.7), in contrast to the results described by VanZomeren-Dohm for the mosaic eye disc. Similarly, fra^3/fra^3 clones in eye-antennal imaginal discs appeared normal (data not shown).

Given that the EMT was accelerated in cultured *fra.IR* discs, I next tested whether PE cells homozygous for fra^3 would display a difference in E-Cadherin localisation, with respect to surrounding control cells. However, in wing disc cultured for 8 hrs with ecdysone, no differences were identified between the mutant and wild type clones, including the degree of degraded DE-Cad from ZA, changes F-actin levels and morphological modifications (data not shown).

4.2.4.2 *fra.IR* "flip-out" clones do not display any cellular abnormalities

Since I encountered no phenotypes in the MARCM analysis, I next carried out a mosaic expression of *fra.IR* using a *Act5C-FRT-CD2-FRT-GAL4* line (hereafter *Act5C:CD2:GAL4*). For this experiment, I used two different *UAS-fra.IR* fly lines: i) BL31469 which has been used previously (Figure 4.2) and ii) BL40826 which was recommended (personal communication, Dr. Molly Duman-Scheel). The flip-out clones were generated upon conditional expression of FLPase via a brief heat-shock period (15 min) at the larval age of 72±11 hours after eggs deposition. The *fra.IR* clones were marked by the expression of either GFP or RFP.

The immunohistochemical analysis of DE-Cad, F-actin and pMoe distribution was applied to *fra.IR* clones in third instar larval wing discs. Similar to the MARCM results, RNAi downregulation of *frazzled* (with either RNAi line) in wing disc epithelia did not cause any visible alterations in cell morphology, nor levels and distribution of DE-Cad, F-actin and pMoe (data not shown).

To enhance the efficiency of RNAi knockdown of *frazzled* in flip-out clones, three different approaches were undertaken: i) UAS-controlled co-expression of the endoribonuclease Dicer-2 (Dietzl *et al.*, 2007 [245]), an enzyme that facilitates RNA interference (Mikuma *et al.*, 2004 [246]; Kim *et al.*, 2005 [247]); ii) UAS-controlled co-expression of GAL4 to elevate the production of the GAL4 protein; iii) loss of one copy of *frazzled* by heterozygosity for the null-allele fra^3. Unfortunately, anti-Fra immunostaining revealed that the flip-out clones still had noticeable residual expression of *frazzled* (Figure 4.8). Further analysis did not revealed any changes in the cellular distribution of DE-Cad or F-actin in the *fra.IR* wing disc clones (data not shown) suggesting that the normal morphology of stable wing disc epithelia can be supported by very low levels of Frazzled.

4.2.4.3 *fra.IR* "flip-out" clones in the tracheal epithelium display delocalization of DE-Cad and F-actin

Although the epithelial cells of the wing discs appeared unaffected by reductions in Frazzled levels, an interesting effect was observed in the large cells of the tracheal tube (three mosaic tracheal tubes were observed). RNAi knockdown of *frazzled* (BL31469) caused a marked redistribution of DE-Cad puncta away from ZA area, with no detectable changes in ZA integrity (Figure 4.9, b). Secondly, the flip-out clones displayed a mild reduction of cytoplasmic F-actin and also disintegration of the junctionally associated F-actin line (Figure 4.9, c). Considering that tracheal epithelial cells are polyploid, I speculate that expression of the *UAS-fra.IR* transgene was stronger than in the diploid cells of the imaginal discs.

4.2.5 Clonal analysis of the wing disc epithelial cells overexpressing *frazzled*

In the previous chapter I found that the *Ubx*-mediated overexpression of *frazzled* in the PE causes delays in ZA breakdown as well as an excess of "stress fibers" formation during eversion. To better understand how ectopic Frazzled levels affect wing disc epithelia, I performed a clonal analysis of the third instar discs prior to epithelial dissociation. In a manner similar to that used in the *fra.IR* analysis, I generated flip-out clones overexpressing *frazzled* using a *Act5C:CD2:GAL4* cassette. As before, the clones were generated via a brief heat shock period (15 min) at the larval age of 72±11 hours after eggs deposition, and were positive for either GFP or RFP expression. The mosaic discs were examined for morphological and molecular changes.

4.2.5.1 Overexpression of *frazzled* produces extensive protrusions in both wing disc epithelia

The epithelial cells of wild type wing discs, particularly PE cells, are characterized by relatively low levels of Frazzled. Interestingly, the localization of Frazzled differs between the DP and PE: whereas in DP cells, Frazzled has a punctate/mottled appearance and is enriched along the cell perimeter, PE cells have nearly even cytoplasmic punctate distribution of the receptor (Manhire-Heath *et al.*, 2013 [133]).

In contrast, overexpressed Frazzled was mostly associated with the cell surface in both DP and PE cells. Moreover, *frazzled* overexpression clones displayed numerous protrusions in PE and DP cells (Figure 4.10, arrows in b' and d'). The protrusions spread extensively and did not display any preferred orientation. To more clearly see these protrusions a *MYC*-tagged *frazzled* was overexpressed and the expressing cells detected by anti-MYC staining (Figure 5.3). This clearly demonstrated protrusions in the PE and also on the basal side of the DP (see the Chapter 5). These results suggest that epithelial cells are competent to respond to Frazzled-induced activation of motility pathways. The basal location of these cellular protrusions suggests they

may be adhering to the surrounding BM.

Further investigation of mosaic discs stained with Rhodamine phalloidin confirmed that the massive protrusions of PE cells were enriched for F-actin. In contrast, PE cells from GFP-positive clones as well as from the GFP-negative cells of control mosaic discs (*w1118/FLP*; *Act5C:CD2:GAL4/UAS-GFP*) have mainly peripheral localization of F-actin (Figure 4.11 (a-a')).

Clonal overexpression of *frazzled* also produces extended bundles of F-actin filaments similar to the Frazzled-associated protrusions (Figure 4.11, b-b', arrows). Curiously, an altered F-Actin distribution was also seen in the non-GFP cells, where F-actin was not just organized in circumferential filaments but was also arranged in short, thin protrusions spreading along the cell cortex (Figure 4.11, b', arrowheads). Thus, *frazzled* overexpression appears to be able to have a non-autonomous effect on the cytoskeleton structure in PE cells.

4.2.5.2 Overexpression of *frazzled* reduces junctional proteins, DE-Cad and β-catenin, in the basolateral regions of disc proper cells

Given that changing Frazzled levels in the PE affected the breakdown of the ZA I next examined the distribution of AJ components in *frazzled* -expressing clones in the DP. In wild type cells of the DP epithelium DE-Cad puncta were densely accumulated in the basal region (Figure 4.12, b' and c', arrowheads). Staining intensity gradually reduces towards the middle of the lateral membrane (arrows). Then, at the ZAs the concentration of DE-Cad reaches its highest levels (double-arrowheads). In the flip-out clones, overexpression of *frazzled* greatly reduced levels of basally polarised DE-Cad and also slightly decreased lateral DE-Cad levels (Figures 4.13 and 4.15). In contrast, DE-Cad levels at the ZA did not obviously change (Figures 4.13 and 4.15, b' and c', arrowheads). However, we cannot rule out the possibility that DE-Cad levels were also reduced in the ZA within clones but this was undetectable due to the very strong intensity of antibody staining.

Whether or not overexpression of *frazzled* in PE cells had a similar effect on DE-Cad distribution could not be determined due to the squamous morphology of these

cells, which makes the lateral and basal pools of DE-Cad indistinguishable. Similar to DP clones, I could not detect any differences in ZA associated DE-Cad in flip-out clones generated in the PE (Figure 4.14).

The reduction of basal DE-Cad in DP cells of mosaic discs was confirmed by the *patched-GAL4*-driven expression of the *UAS-fra* (hereafter *ptc>fra,GFP*), where the pattern of expression is restricted to a narrow stripe between the anterior and posterior compartments in the DP. Similar to wild type clones in mosaic discs, the DP epithelium of control wing discs *w1118; ptc>GFP* (hereafter *ptc>GFP*) inside as well as outside of the GFP-positive stripe was characterised by a rich pool of DE-Cad at the ZA and also by the intense basal and lateral accumulation of the protein (Figure 4.12). As expected, the *patched-GAL4*-driven overexpression of *frazzled* caused a distinct loss of basolateral DE-Cad within the GFP-positive stripe (Figure 4.15).

Since the random clones in mosaic discs were quite heterogeneous in size, number and location, I used the *patched-GAL4*-driven expression to quantify cellular and molecular changes that were initially found in the clonal analysis. To quantify the degree of DE-Cad reduction from the basolateral sides of the epithelium, I used the cross-sectional views of the DP to calculate the ratio of DE-Cad antibody intensity of the basolateral parts of cells inside the *patched*-expression expression domain relative to cells outside the domain (see Materials and Methods, Figure 2.4, a). Overexpression of *frazzled* caused a significant loss of DE-Cad from basal and lateral sides of the DP with the ratio changing from 1.08±0.05 in control discs to 0.86±0.05 in *ptc>fra,GFP* (p=0.0003, by Student's t-test; Figure 5.15, a).

Similar to DE-Cad, the other junctional protein β-catenin (Armadillo) was distributed not only at the ZA (Figure 4.16, b' and c', double-arrowheads) but also along the whole cortex of DP cells (arrows). Similar to DE-Cad, there was a clearly defined gradient from the most basal regions towards the middle part of lateral membrane, and then the ZA exhibited the brightest intensity. In the flip-out clones, Armadillo immunostaining showed a clear decrease of the protein in the lateral and basal areas (Figure 4.16, arrows and arrowheads respectively) but levels in the ZA

appeared unaffected (double-arrowheads). Thus, overexpression of *frazzled* disrupts the lateral and basal pools of AJ proteins which might correlate with the delays in ZA breakdown during wing disc eversion.

4.2.5.3 Overexpression of *frazzled* causes basal expansion in disc proper cells

In this study, I found that cells overexpressing *frazzled* generated in mosaic DP epithelia were characterised by substantial tissue expansion on the basal side due to either basal relaxation or the apical constriction of the clonal cells (Figure 4.17). Often, in the sites of basally expanded cells, the DP tissue also formed apical folds (Figure 4.17, d, arrows). These changes in cell morphology are suggestive of an effect on cellular contractility, whereby overexpression of *frazzled* is causing either relaxation in the basal parts of the cell or constriction of the apical regions. However, I was not able to detect any increase in anti-pMLC (phosphorylated/activated Myosin regulatory light chain) in apical regions of the *frazzled* overexpressing clones arguing against active apical constriction (Figure 4.18).

Basal expansion of DP cells was also observed in the *ptc>fra,GFP* wing discs (Figure 4.19). To quantify this I calculated the ratio between basal and apical sides of epithelial cells within the *ptc*-expression stripe (see Materials and Methods, Figure 2.4, c). In control *ptc>GFP* wing discs, GFP-positive cells in cross-sectional views have either a rectangular shape or slightly constricted on the basal side (mean ratio=0.88±0.09). The *frazzled* overexpressing cells from *ptc>fra,GFP* wing discs were generally widened on the basal side (mean ratio=1.5±0.23) and had an apical furrow within the GFP-band (Figure 4.19, b, c, arrows). Thus, DP cells overexpressing *frazzled* undergo significant expansion of the basal side compared to control cells (p=0.0009, by Student's t-test; Figure 5.15, b).

4.2.5.4 Overexpression of *frazzled* slightly reduces pMoe in basolateral regions of disc proper cells

Next, the localization of pMoe was assessed in the *frazzled* overexpressing and wild type clones. Peripodial overexpression of *frazzled* has been previously shown to significantly increase pMoe levels (Manhire-Heath *et al.*, 2013 [133]). In the DP epithelium, pMoe puncta had a similar localization to the junctional proteins, in that the dots of pMoe were mostly accumulated in the basal regions (Figure 4.20, b', c', arrowheads) and near the ZA (double-arrowheads). Also, some amount of the protein was distributed along the lateral cell walls (arrows). Surprisingly, clonal and *patched-GAL4*-driven overexpression of *frazzled* reduced pMoe levels at the basolateral side of the DP cells similar to what was observed for DE-Cad and Arm (Figures 4.21 and 4.22 respectively). Quantification of the mean pMoe intensity using *ptc>fra,GFP* and control *ptc>GFP* discs (see Materials and Methods, Figure 2.4, b) revealed that the ratio between the *ptc*- and non-*ptc*-regions dropped from 1.07±0.04 in control discs (n=4) down to 0.93±0.02 in *ptc>fra,GFP* discs (n=5) (two-tailed p=0.0025, by Student's t-test; Figure 4.23). Changes in apical pMoe intensity were not detected.

Since activated Moesin is able to recruit RhoGAP Conundrum (Conu) to the apical cortex of epithelial cells (Neisch *et al.*, 2013 [174]), I also tested localisation of Conu in mosaic discs with frazzled overexpressing clones. However, this did not reveal any obvious changes in distribution or intensity in DP cells (Figure 4.24). This result suggest that the basally localized pMoe does not affect Conu expression. Presumably, the partial loss of basolateral pMoe is a consequence of downregulated junctional complexes.

4.3 Discussion

In this chapter, I used two basic approaches to investigate possible roles for Frazzled in epithelial cells. Firstly, I used a loss-of-function assay whereby clones of

homozygous mutant cells were created in the disc proper and other larval tissue. Unfortunately, this analysis did not reveal a requirement for Frazzled function in the disc proper epithelium despite previous reports that *frazzled* mutant clones display tumor-like phenotypes (VanZomeren-Dohm *et al.*, 2011 [151]). Presumably the small amount of Frazzled protein still present in mutant clones is sufficient for its function in this epithelial type. Reduction of Frazzled levels in the PE did however show a phenotype in that it was able to rescue the *netA.IR* eversion phenotype, and accelerate eversion of cultured wing discs.

The second approach to understand Frazzled function was to use overexpression. This approach can create cellular phenotypes that reveal the ability of Frazzled to activate signaling pathways in epithelial tissue. Overexpression of Frazzled resulted in three distinct cellular phenotypes, which together might explain the eversion phenotypes. Firstly, the PE and DP cells produced extensive membrane protrusions, resembling filopodial structures, which were rich in F-actin filaments and strong for Frazzled immunoreactivity. Secondly, there was a loss of DE-Cad, Arm and pMoe from the basolateral membrane of columnar cells of the DP. Finally, there was an expansion of the basal surface and contraction of the apical surface in the DP cells. Taken together, these findings help me to speculate how Frazzled might impede the wing disc eversion process, and also shed light on potential molecular functions of the receptor in a stable epithelium.

4.3.1 Frazzled suppresses peripodial epithelial dissociation during wing disc eversion

Unlike *netrinA*, RNAi knockdown of *frazzled* in the PE did not cause eversion phenotypes, whereas overexpression of *frazzled* did (Manhire-Heath *et al.*, 2013 [133]). These results led us to hypothesise that Frazzled acts in the opposite way to NetrinA during eversion, just as DCC and Netrin-1 have opposing effects on tumour growth and metastasis (Rodrigues *et al.*, 2007 [248]). The first confirmation of this hypothesis was that co-expression of *fra.IR* with *netA.IR* almost completely rescued

the *netA.IR* phenotype (Manhire-Heath *et al.*, 2013 [133]). Additional evidence was obtained (in this work) by showing that loss of one copy of *frazzled* could also rescue the *netA.IR* eversion phenotypes, and that downregulation of the receptor could accelerate DE-Cad dissociation from ZAs in cultured discs. These data are consistent with the finding described in Chapter 3 that overexpression of *frazzled* could maintain the integrity of the ZA. Assuming Frazzled has a negative effect on epithelial dissociation, one would expect that the receptor would normally need to be inactivated or removed to allow eversion to proceed. This idea is supported by observations that Frazzled protein levels decrease in PE cells as wing discs mature from early to late third instar larvae, and this decrease appears to be netrin dependent since Frazzled levels are elevated in $netAB^{\Delta}$ or *netA.IR* wing discs (Manhire-Heath *et al.*, 2013 [133]). A similar ligand-dependent elimination of the receptor from the cell surface has been shown for Netrin-1 and DCC, where this mechanism is required to impair the Netrin-1-sensitivity of axons to DCC in order to prevent overgrowth (Kim *et al.*, 2005 [160]). Thus, the additional repression of Frazzled activity by RNAi might actually facilitate the natural EMT progression and hence show no phenotype *in vivo*.

The mechanism by which Frazzled levels are lowered is yet to be studied. The proteosome appears to be involved since its inhibition increases Frazzled levels (Manhire-Heath *et al.*, 2013 [133]). But given that Frazzled is found in endosomes, and co-localises with the late endosomal marker Rab7 in the embryonic midgut (Pert *et al.*, 2015 [78]), it might also be subject to lysosomal degradation.

Surprisingly, fra^3/fra^3 clones displayed no obvious phenotypes in either the DP or PE, even after 7 hrs culturing. Based on the results with *Ubx>fra.IR* cultured discs I expected *frazzled* clones would exhibit more advanced ZA-dissociation. One possible explanation for the lack of phenotypes is that *frazzled* has non cell-autonomous effects in epithelial sheets, so that cells in mutant clones are somehow rescued by the surrounding cells that still express Frazzled. Although this might seem unlikely, some evidence for non-autonomy was seen in discs with mosaic overexpression of Frazzled, where the increased F-Actin stress-fibre-like structures were seen in both

overexpressing cells, and in neighbouring wild type cells.

The results are in disagreement with the published study by VanZomeren-Dohm *et al.*, 2011 [151] where the authors reported apoptosis and changes in epithelial characteristics, such as DE-Cad and F-actin delocalization and loss of BM integrity in fra^3/fra^3 and fra^3/fra^4 clones of eye imaginal discs. One possible explanation is that VanZomeren-Dohm and colleagues may have achieved a stronger reduction in Frazzled levels, but unfortunately Frazzled levels were not assessed. The discrepancy might also be explained by the different genetic backgrounds. VanZomeren-Dohm and colleagues used a chromosome with *FRT G13* sites, which can cause artifactual cell growth phenotypes (Linda Parsons, personal communication). In addition it has recently been shown that expression of *p35* in apoptosing cells can activate the JNK pathway, and create the sorts of invasive phenotypes reported (Rudrapatna *et al.*, 2013 [237]). Additional investigation will be required to clarify these matters.

4.3.2 Frazzled is required for thorax closure

In this study, I unintentionally found, that 10% of the fra^3/fra^4 expected progeny were able to develop to adult stages, and approximately half of these flies exhibited mild to severe thoracic closure defects. Similar results have been previously reported by Dorsten and VanBerkum, 2008 ([249]), though the authors did not focus on these thoracic defects.

The fact that fra^3/fra^4 transheterozygotes are semi-viable when fra^3 or fra^4 homozygotes are embryonic lethal is likely due to the fact that fra^4 is only a hypomorphic allele, but could also be due to second site mutations that enhance phenotypes when homozygous. Given that fra^3/fra^4 mutant embryos exhibit multiple axonal pathfinding errors (Hiramoto *et al.*, 2000 [142], Dorsten and VanBerkum, 2008 [249], Mauss *et al.*, 2009 [250], Morikawa *et al.*, 2011 [251], Evans *et al.*, 2015 [252]) I speculate that during thorax closure, Frazzled drives the formation of F-actin-associated protrusions in the leading edge of migrating PE cells. The *frazzled* overexpression phenotypes described in this work show that Frazzled can strongly induce F-actin

polymerization in epithelial cells as well neural cells (discussed in details below). Thus, I speculate that although Frazzled initially inhibits the partial EMT of the PE, it later plays a positive role during thorax closure. In support of this idea, in *netA.IR* pupae in which thorax closure is in progress, leading edge cells show a marked lack of protrusions (Rose Manhire-Heath and Michael Murray, unpublished data).

4.3.3 In the tracheal epithelium, knockdown of Frazzled induces DE-Cad and F-actin delocalization

In contrast with wing epithelia, a *frazzled* loss-of-function phenotype was detected in the trachea. The walls of *Drosophila* tracheal tubes consist of a monolayer of large and squamous epithelial cells, which are tightly interconnected with each other by DE-Cad-based ZAs (Tepass *et al.*, 1994 [76]). RNAi knockdown of *frazzled* results in a redistribution of DE-Cad puncta away from the ZA area, without any visible changes in ZA integrity. Due to the squamous morphology of the tracheal epithelium, it is not clear whether the DE-Cad puncta accumulate on the cells surface or in the cytoplasm. At the same time, together with a general decrease in F-actin intensity, the filaments associated with the ZA line lose their continuity in *fra.IR* expressing clones. Taking into consideration that most tracheal cells have a polyploid nucleus during larval stages (Whitten, 1957 [253]), it is possible that having multiple copies of the *frazzled* RNAi constructs might increase gene silencing, enabling me to see the effects of *frazzled* knockdown in this epithelium. However, the phenotypes might also indicate that Frazzled has some particular role in tracheal epithelium development which does not occur in the wing disc.

The appearance of DE-Cad puncta away from the ZA in *frazzled* knockdown cells suggests Frazzled may regulate DE-Cad turnover. DE-Cad turnover involves endocytosis of junctional DE-Cad followed by recycling back to the cell surface or to degradation, and it is the balance between these two pathways that defines the strength and integrity of ZA and other intercellular junctions (reviewed by Nanes

and Kowalczyk, 2012 [254]). Thus Frazzled might either inhibit the endocytosis of DE-Cad or facilitate exocytosis of recycled DE-Cad back into cell membrane. Given the results of clonal *frazzled* overexpression, which are discussed below, expression of a certain amount of the receptor in the epithelial cells might be required for maintenance of a reasonable balance between the endocytosed DE-Cad and DE-Cad anchored to ZA.

The effect of *fra.IR* expression on F-actin localization may be interrelated with the changes in DE-Cad localization. Actin filaments connect to junctional complexes, and are involved in regulation of AJ stability by mediating endocytosis processes, including the internalization of DE-Cad, vesicle formation, scission and transport (Yarar *et al.*, 2005 [255], Leibfried *et al.*, 2008 [256], Bu *et al.*, 2010 [257]). In *Drosophila* wing discs, the depletion of actin nucleation proteins, such as Wiskott-Aldrich syndrome proteins (WASp) and Arp2/3 complex components, causes discontinuity of junctionally associated actin filaments, and concomitant failure in the organization and stability of AJs. These defects occur due to disruption of normal DE-Cad endocytosis and accumulation of junctional structures on the cell surface (Georgiou *et al.*, 2008 [195]). Thus, the DE-Cad delocalization in tracheal cells expressing *fra.IR* construct might be due to failed F-actin polymerisation.

4.3.4 The mechanisms of Frazzled-induced F-actin polymerization

In this work, the ability of ectopic Frazzled to modulate the F-actin cytoskeleton in wing disc epithelial cells has been demonstrated repeatedly using various approaches and genetic environments. Unlike the cultured wing discs, where peripodial overexpression of *frazzled* promotes the formation of "stress fiber" like structures, the cells of stable epithelia, responding to high levels of the receptor, formed numerous long membrane protrusions on the basal side resembling filopodial extensions. Together with the prominent co-localization of Frazzled antibodies with F-actin filaments in the core of basal protrusions, these data suggest that the receptor signaling in-

duces polymerization of F-actin. This idea requires confirmation, as although the function of *Drosophila* Frazzled is well characterised in neural development, there is less known about other tissues. In contrast, DCC has been shown to promote actin polymerisation in several non-neural cell types, including epithelial cell lines (Shekarabi and Kennedy, 2002 [122], Martin *et al.*, 2006 [167]), fibroblasts (Li *et al.*, 2002 [198]), and stem cells (Lee *et al.*, 2014 [200]).

The studies of nervous system development have greatly contributed to our understanding of how Frazzled/DCC signaling pathways regulate the actin cytoskeleton. In the growing neural network, axons undergo constant elongation and turning, which are based on dynamic polymerization and remodelling of actin, myosin and microtubules (Dent *et al.*, 2011 [258]). In response to specific guidance cues, the actin-rich growth cones produce flat sheet-like protrusions, lamellipodia, and finger-like protrusions, filopodia, oriented in the direction of the target tissue (Tanaka and Sabry, 1995 [259], Dent and Gertler, 2003 [260]). The formation and retraction of membrane protrusions in growth cones as well as in other motile cells require intense remodelling of adhesion and cytoskeletal protein machinery (reviewed by Mitchison and Cramer, 1996 [261], and Lowery and Van Vactor, 2009 [262]). The regulation of actin, myosin and tubulin in neuronal and non-neuronal cells is fulfilled by the members of the Rho family of GTPases (reviewed by Hall, 1998 [263], Yamazaki *et al.*, 2005 [264], Machacek *et al.*, 2009 [265], Chauhan *et al.*, 2011 [266], and Ridley, 2015 [267]. Three main GTPases, RhoA, Cdc42 and Rac1, have been shown to mediate signaling between DCC and the actin cytoskeleton. For example, Rac1 and Cdc2 are activated by ectopic DCC expression in the presence of Netrin-1 in neuroblastoma cell lines (Li *et al.*, 2002 [198], Shekarabi and Kennedy, 2002 [122]). These two studies demonstrate that expression of dominant negative forms of Rac1 or Cdc42 greatly reduces lamellipodia or filopodia formation respectively. At the same time, inactivation of RhoA and Rho kinase by C3 transferase increases the ability of DCC to promote neurite outgrowth (Shekarabi and Kennedy, 2002 [122]). Also, the latter study showed that Netrin-1 attraction stimuli in cortical neurons results in Src-kinase-mediated phosphorylation of the Rac1 GEF Trio downstream

of DCC (DeGeer *et al.*, 2012 [268]). In *Drosophila*, Frazzled has also been shown to genetically and physically interact with Trio, which together with other actin polymerization factors, such as Abl and Ena, helps Frazzled drive commissure formation through axons crossing the midline (Forsthoefel *et al.*, 2005 [238]). Similar results were obtained in *Caenorhabditis elegans*, where UNC-40, the DCC ortholog, activates the Rac GEF TIAM-1 to induce growth cone protrusions in response to Netrin-based axon attraction signaling. In turn, TIAM-1 acts downstream of Cdc42 and upstream of CED-10 and MIG-2, the Rac-like GTPases (Demarco *et al.*, 2012 [269]).

Both, Rac1 and Cdc42, stimulate the formation of peripheral actin-rich protrusions forcing cells to move forward (Small *et al.*, 2002 [270], Raftopoulou and Hall, 2004 [271], Ridley, 2015 [267]). *De novo* actin nucleation in both, lamellipodia and filopodia, is dependent on the Arp2/3 complex (Mullins *et al.*, 1998 [272], Welch, 1999 [273]). However, in order to stimulate filopodia formation, Cdc42 uses Wiskott-tAldrich syndrome proteins (WASp) as signal transmitters to Arp2/3, whereas for lamellipodia Rac GTPase regulates Arp2/3 by WASp-family verprolin-homologous proteins complex (WAVE) (Sarmiento *et al.*, 2008 [274], Lebensohn and Kirschner, 2009 [275], Campellone and Welch, 2010 [276]). The efficiency of binding Arp2/3 to actin filaments and concominant nucleation in response to WASp/WAVE stimulation is mediated by other activators, including Ena/VASP (vasodilator-stimulated phosphoprotein) family proteins, formins and kinases (Campellone and Welch, 2010 [276], Breitsprecher *et al.*, 2011 [277], Havrylenko *et al.*, 2015 [278]). Enabled is a proven effector of Frazzled and UNC-40 function, and is recruited by the receptors to coordinate actin rearrangements in growth cones (Gitai *et al.*, 2003 [279], Forsthoefel *et al.*, 2005 [238]). Apparently, as was established for DCC, Ena/VASP gets phosphorylated by Ezrin-mediated activation of other DCC effectors, such as cAMP-dependent protein kinase and Protein kinase A anchoring proteins (AKAP) (Deming *et al.*, 2015 [280]).

4.3.5 Frazzled affects DE-Cadherin trafficking to the basolateral membrane

In addition to being localised to the ZA of the DP epithelium, DE-Cad and Armadillo are also distributed along the basolateral membrane. This basolateral pool has a gradient going from strong accumulation in the basal region to low levels in the middle of the lateral membrane. These populations of DE-Cad and Arm may be due to a process of Rab11-dependent endosomal trafficking towards the basolateral membrane (Lock and Stow, 2005 [281]). Molecules of DE-Cad that are sorted for recycling, as well as newly synthesized DE-Cad from the Golgi, can be captured by Rab11 recycling endosomes, and subsequently trafficked to the basolateral compartments of the cell (Lock and Stow, 2005 [281]; Desclozeaux *et al.*, 2008 [282]; Woichansky *et al.*, 2016 [193]), where it is exocytosed and integrated into the lateral membrane. Interaction of β-catenin/Armadillo with Rab11 and the exocyst components such as Sec5, Sec6 and Sec15, (Langevin *et al.*, 2005 [192]) is required for the targeted delivery of E-Cadherin to the membrane. One can imagine several ways by which basolateral E-Cadherin could be useful for an epithelial cell. Firstly, it could provide a reservoir of junctional components that can be redirected and used for dynamically re-building the ZA (Kusumi *et al.*, 1999 [283]). Secondly, lateral DE-Cad could increase lateral adhesion by creating intercellular contacts (Iino *et al.*, 2001 [284]). Thirdly, it is possible that some DE-Cad could undergo basal-to-apical flow to the ZA via actin filaments (Kametani and Takeichi, 2007 [285]; Woichansky *et al.*, 2016 [193]). These complex routes of DE-Cad trafficking are required for regulation of ZA stability (Desclozeaux *et al.*, 2008 [282]; Georgiou *et al.*, 2008 [195]; Cavey *et al.*, 2008 [286]; de Beco *et al.*, 2009 [287]). This dynamic feature of cellular junctions helps them to maintain intercellular adhesion during morphological changes in epithelial tissue (e.g. tissue invagination, EMTs, cell intercalation or cell extrusion, cell death; reviewed by Baum and Georgiou, 2011 [18], Nanes and Kowalczyk, 2012 [254]). Moreover, spot AJs distributed along the lateral membrane away from the apical ZA play a role a maintenance of the lateral actin cortex which

is important for preventing cells from being extruded from epithelial layers (Hong *et al.*, 2013 [288]; Wu *et al.*, 2014 [289]). Thus, in the case of the DP cells, the high intensity of DE-Cad and Arm along the basolateral membrane might be crucial for supporting the cuboidal morphology of the epithelium, as the densely distributed cell-cell junctions together with the actin cytoskeleton establish tension between the cells along the apical-basal axis.

Ectopic overexpression of *frazzled* in the DP cells causes a noticeable decrease of DE-Cad and Arm along the basolateral membrane compartment. I hypothesize that Frazzled disrupts the Rab-11-dependent endosomal trafficking of DE-Cad and Arm towards the lateral membrane, which might, in turn, lead to a restriction in the basal-to-apical supply of DE-Cad to the ZA from the basolateral pool. It is also possible that loss of lateral intercellular contacts alters cellular morphology creating the basal expansion that is seen. This hypothesis could also provide an explanation as to why PE cells do not exhibit any changes in DE-Cad distribution when they overexpress *frazzled*. Possibly, a pre-requisite for having a squamous morphology is an absence of additional basolateral intercellular contacts. For example, during *Drosophila* ovary development the cuboidal follicle cells transform to a flattened morphology by reduction of excess DE-Cad, DN-Cad and Arm in the membrane (Melani *et al.*, 2008 [290]). Computational analysis shows that elevation of lateral cell-cell contacts promotes cell elongation into a columnar morphology, and so, in squamous cells, they must be downregulated (Hannezo *et al.*, 2014 [291]). In PE cells, therefore, Frazzled inhibition of Rab11 would not be expected to show a phenotype as the basolateral pool of DE-Cad would not be present in the flattened PE cells.

Although the molecular mechanisms by which Frazzled could affect the endosomal trafficking of DE-Cad and Arm await further investigation, intriguing results have been obtained for Neogenin, the mammalian ortholog of Frazzled. Lee *et al.* (2016) have shown that knockdown of Neogenin in Caco-2 epithelial monolayers reduces the rate of E-cadherin internalization at AJs. Additionally Neogenin supports junctional tension by controlling assembly of stable actin rings at AJs (Lee *et al.*, 2016 [233]).

The ZA in wing disc epithelia appeared unaffected by *frazzled* overexpression in this study and given that the PE cell dissociation was inhibited I speculate that they retain integrity. It is possible that disruption of trafficking of basolateral junctional components that promote ZA stability, may be compensated for by the delivery of newly synthesized or recycled proteins to the ZA using apically directed routes (Yashiro *et al.*, 2014 [292]; Woichansky *et al.*, 2016 [193]). For example, in *rab11* mutants, the follicular epithelium displays a loss of apico-lateral exocytosis of DE-Cad but no significant changes in ZA structure (Woichansky *et al.*, 2016 [193]). Interestingly, the separation of two routes for DE-Cad trafficking appears to depend on Rho1 activity. Indeed, the depletion of Rho1 activity in the *Drosophila* eye epithelium reduces the density of Rab11-positive vesicles at the level of the apical AJ, whereas overexpressing Rho1 provides the opposite effect (Yashiro *et al.*, 2014 [292]). Inhibition of basal-to-apical flow of mammalian VE-Cadherin (vascular endothelial cadherin) by ML-7, an inhibitor of myosin light chain kinase, does not affect apical junctional structures. Conversely, treatment cells by Y-27632, the ROCK inhibitor, causes ZA disassembly while the lateral VE-Cadherin stays intact (Kametani and Takeichi, 2007 [285]). Presumably, cells overexpressing *frazzled* keep the activity of the Rho1 pathway in the apical regions, where it is able to maintain ZA stability. The majority of the receptor is accumulated in the basal regions, where it naturally induces Rac1 activity, whose signaling outcomes inhibit Rho1 and antagonize its cellular functions (Chauhan *et al.*, 2011 [266]). In this model, cells overexpressing *frazzled* would have a gradient of Rho1 activity, that goes down in the apical-to-basal direction, which helps the receptor to support ZA integrity. In turn, the more basally activated Rac1 could change the architecture of actin filaments along the basolateral membrane and thereby impede normal endosomal traffic and also basal-to-apical flow of DE-Cad.

4.3.6 Frazzled induces epithelial invagination

Groups of DP cells overexpressing *frazzled* have a distinct increase in the basal-to-apical diameter ratio, and often form an apical furrow and an expanded basal

region. These sorts of cell shape changes are associated with the process of tissue invagination (Sawyer *et al.*, 2010 [293], Kondo and Hayashi, 2015 [294]). Therefore, I suggest that increased levels of Frazzled are able to induce epithelial invagination. To speculate about possible effectors of Frazzled triggering invagination, one must consider what is known about the mechanisms underlying this process. Curvature of epithelial sheets depends primarily on apical constriction of individual epithelial cells. Shrinkage of apical regions leads to a change in cell morphology from cuboidal to wedge shape, which makes the basal surface larger than the apical. The larger the basal-to-apical surface ratio becomes, the deeper the invagination that results. Often, the formation of deep folds requires basal relaxation and cell shortening (reviewed by Kondo and Hayashi, 2015 [294]). Notably, the degree of increased cell-ECM adhesion surface area due to basal expansion or Cdc42-mediated filopodia formation, has been shown to determine the degree of apical constriction and curvature depth (Chauhan *et al.*, 2009 [295], Fernandes *et al.*, 2014 [296]). On a molecular level, apical constriction is driven by coordinated remodelling of non-muscle myosin, F-actin filaments and AJs, although the organization and dynamics of these three components may vary in different cell types and situations depending on the behaviour of the AJ and initial actomyosin network architecture (Mason and Martin, 2013 [297], Martin and Goldstein, 2014 [298]). As a rule, invagination is preceded by recruitment of Myosin II and F-actin to the apical medial surface (Brodu and Casanova, 2006 [299]). Then, the contractile force generated by Myosin II pulls F-actin filaments inward causing the cell to shrink on its apical side. Simultaneously, actin filaments maintain tight connections with the circumferential ZA by virtue of constant actin assembly mediated by Ena/VASP and Arp2/3 and interaction with the junctional components mediated by Vinculin and Afadin (the *Drosophila* Canoe homolog). Moreover, in order to support epithelial integrity during tissue bending apical actomyosin complexes together with actin-binding proteins Vinculin and Afadin are required for the maintenance of ZA stability (Leerberg *et al.*, 2014 [300], Choi *et al.*, 2016 [301]). Dynamics in ZA structure still remain obscure, however a very recent study of *Drosophila* gastrulation shows that the myosin contractile

pulses induce invaginating cells to reinforce intercellular junctions by shifting DE-Cad clusters towards more apical regions (Weng and Wieschaus, 2016 [302]).

In the majority of cases, actomyosin contractility relies upon RhoA/Rho1 signaling (Sawyer *et al.*, 2010 [293]). Firstly, RhoA/Rho1 activates actin polymerization proteins that promote filament assembly in the apical region. For example, during ventral furrow formation in *Drosophila* gastrulation Rho1 recruits the formin Diaphanous and Abelson kinase, and then the latter restricts its effector Enabled to the apical side (Fox and Peifer, 2007 [303], Homem and Peifer, 2008 [304]). Diaphanous is found to be activated by Rho1 signaling during the formation of a morphogenetic furrow in *Drosophila* eye imaginal disc (Homem and Peifer, 2008 [304]). Also, Rho1 plays a role in stimulating apical accumulation of myosin by recruiting Myosin II heavy chain Zipper and regulatory light chain Spaghetti Squash from the basal region (Nikolaidou and Barrett, 2004 [305]). It is worth mentioning that the intracellular transportation of F-actin and Myosin II polymerisation components as well as the other factors (such as RhoA and adhesion molecules) is implemented by the microtubule network, which becomes assembled along the apical-basal axis prior to tissue invagination (Corrigall *et al.*, 2007 [306], Nakaya *et al.*, 2008 [70], Harris and Peifer, 2007 [307]). Secondly, RhoA/Rho1 targets its effector ROCK, which promotes myosin contraction by both phosphorylating Myosin II light chain and inactivating Myosin II phosphatase (Kimura *et al.*, 1996 [308], Kawano *et al.*, 1999 [309]). In some systems, the activation of RhoA/Rho1 might require RhoGEF function. In *Drosophila rhoGEF2* mutants, the apical constriction is blocked and ventral furrow can not be formed, and Myosin II and F-actin fail to accumulate in the apical regions (Barrett *et al.*, 1997 [310], Nikolaidou and Barrett, 2004 [305], Grosshans *et al.*, 2005 [311]). However, the loss of RhoGEF2 does affect the invagination processes during eye morphogenesis (Corrigall *et al.*, 2007 [306]).

Currently, the relationship between Frazzled and Rho1 remains ambiguous. In mammals, Netrin-1/DCC signal transduction inhibits RhoA in neurons (Li *et al.*, 2002 [198]). On the other hand in *Drosophila*, the intracellular P3 motif of Frazzled is apparently required for initiating Rho1 activity (Dorsten *et al.*, 2007 [243]).

One of the putative cross-linkers between Frazzled and Rho1 is Moesin, which is thought to inhibit Rho1 via the Rho GAP protein Conundrum (Speck *et al.*, 2003 [172], Neisch *et al.*, 2013 [174]). Consistent with this, our study has shown that pMoe was downregulated in the basal regions of *frazzled* overexpressing cells suggesting activation of the Rho1 pathway. Perhaps, the increased activity of Rho1 is restricted only to the apical regions of the cell, where it induces apical constriction which can cause epithelial folding. Unfortunately, the MLC and Zipper immunostaining did not identify any obvious delocalization or increase of Myosin II components at the apical side of *frazzled* overexpressing cells. At the same time, on the basal side, the higher concentration of Frazzled could lead to increased activity of the other Rho GTPases, Rac1 and Cdc42, which are capable to inhibiting Rho1 function. Analogous mutual antagonism between Rho GTPases occurs in migrating cells where Rac1 and Cdc42 mediate protrusions on the front side, and RhoA is responsible for the actomyosin constriction under the back cortex (Chauhan *et al.*, 2011 [266]).

The hypothesis of spacial allocation of different Rho GTPases due to ectopic Frazzled overexpression is consistent with both phenotypes, the extended basal protrusions and the loss of basolateral DE-Cad. Apically activated Rho1 could induce actomyosin contractions, which in turn forces cells to strengthen their ZA, while basal activation of Rac1 and Cdc42 inhibits Rho1-dependent DE-Cad flow and reorganizes the F-actin network into protrusive structures. Cytoskeletal and junctional modifications along the basolateral cortex might also decrease intercellular tension, which results in the basal relaxation phenotype (see final model in Figure 7.1). The other possibility is that Frazzled induces apical constriction and invagination through a Rho1- and ROCK-independent pathway. Indeed, the lens pit invagination during eye development in vertebrates can occur even in the absence of RhoA, Rac1 or Cdc42 (Chauhan *et al.*, 2009 [295], Chauhan *et al.*, 2011 [266]). However, the other factors, which are able to initiate apical constriction bypassing RhoA signaling are yet to be elucidated.

Figure 4.1: **Loss of one copy of *frazzled* rescues *netA.IR* eversion failure.** Quantification of adult *netA.IR* eversion phenotypes for *UAS-netA.IR/+;Ubx-GAL4/+* (*Control*, n=180) and *UAS-netA.IR/Df(2R)BSC880;Ubx-GAL4/+* (*Df/+*, n=89) genotypes. The number of normal progeny was increased from 54% (*Control*) to 86.5% in *frazzled* deficiency line (p=0.0008). Error bars show 95% CI (by Wilson Score method).

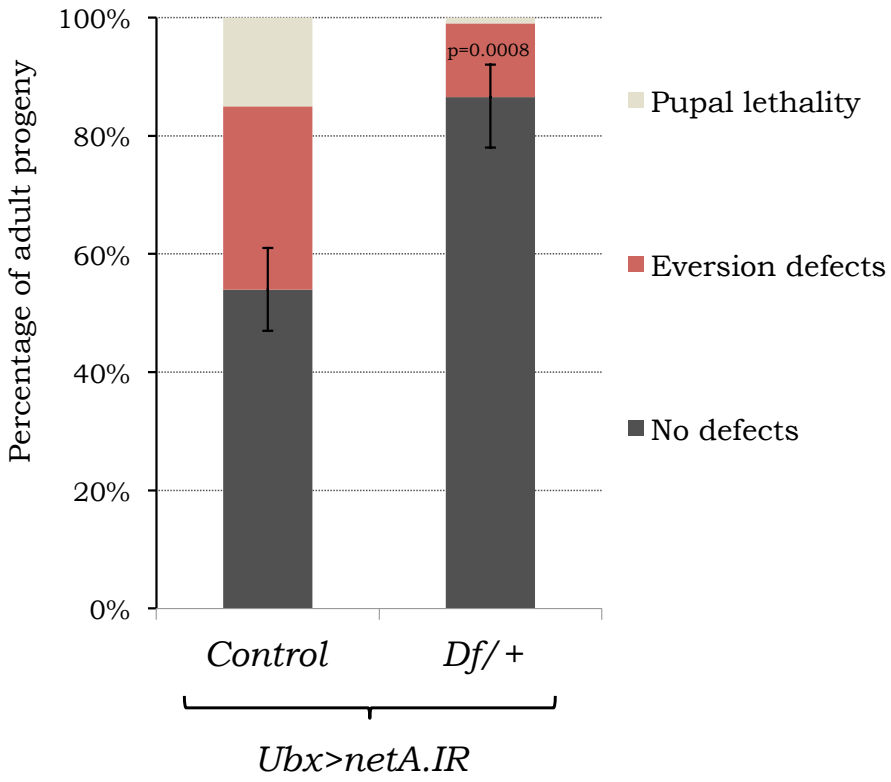
100%
80%
60%
40%
20%
0%
Percentage of adult progeny
p=0.0008
Pupal lethality
Eversion defects
No defects
Control
Df/+
Ubx>netA.IR

Figure 4.2: ***frazzled* knockdown accelerates EMT in cultured discs.** Quantification of eversion outcomes for *Ubx-GAL4,UAS-GFP/+* (*Control*, n=23) and *Ubx-GAL4,UAS-fra.IR,GFP/+* (*fra.IR*, n=18) wing discs after culturing for 7 hrs in ecdysone. The number of discs with intact ZA in PE was reduced from 61.1% (*Control*) to 21.8% in *fra.IR* probes (p=0.0225). Error bars show 95% CI (by Wilson Score method).

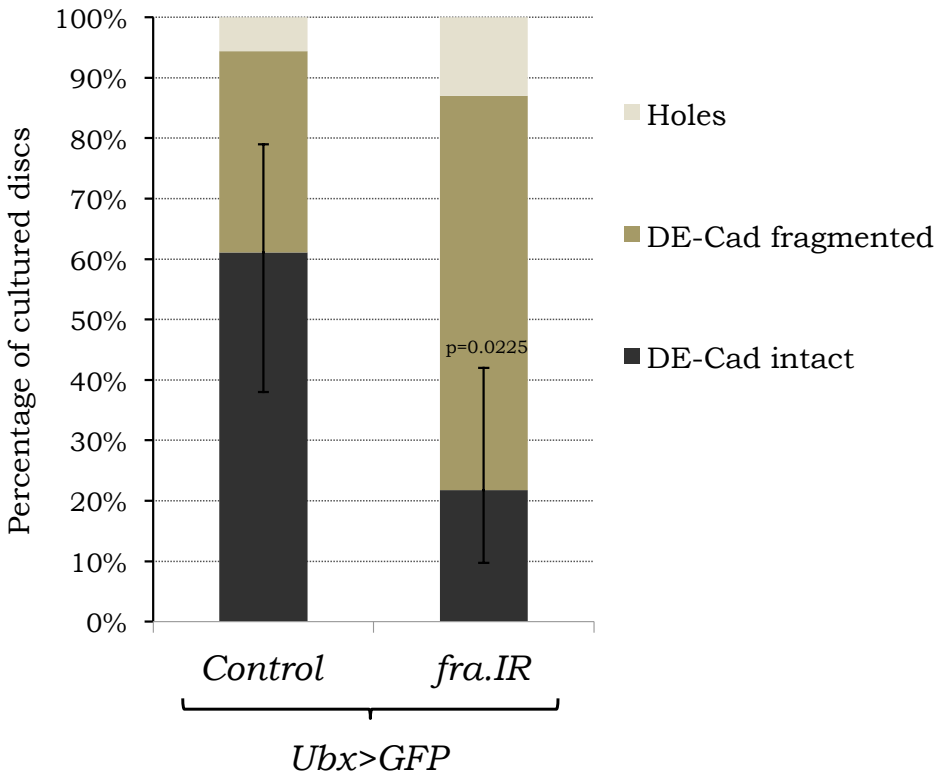
100%
90%
80%
70%
60%
50%
40%
30%
20%
10%
0%
Percentage of cultured discs
p=0.0225
Holes
DE-Cad fragmented
DE-Cad intact
Control
fra.IR
Ubx>GFP

Figure 4.3: **Flies transheterozygous for *fra*^{3} and *fra*^{4} exhibit adult eversion defects.** Quantification of control and *fra*^{3}/*fra*^{4} adult eversion phenotypes. Control flies include genotypes obtained in the same cross and heterozygous either for *fra*^{3} or for *fra*^{4} balanced over *CyO* (n=322). The calculation of total number of expected *fra*^{3}/*fra*^{4} progeny was based on Mendelian inheritance: n=146 for expected *fra*^{3}/*fra*^{4} adults that could emerge from the cross. The number of adult *fra*^{3}/*fra*^{4} escapers was 15. Among them, 7 flies had eversion defects. Thus, the number of *fra*^{3}/*fra*^{4} progeny with eversion defects was 4.8% ($p<0.0001$). Error bars show 95% CI (by Wilson Score method).

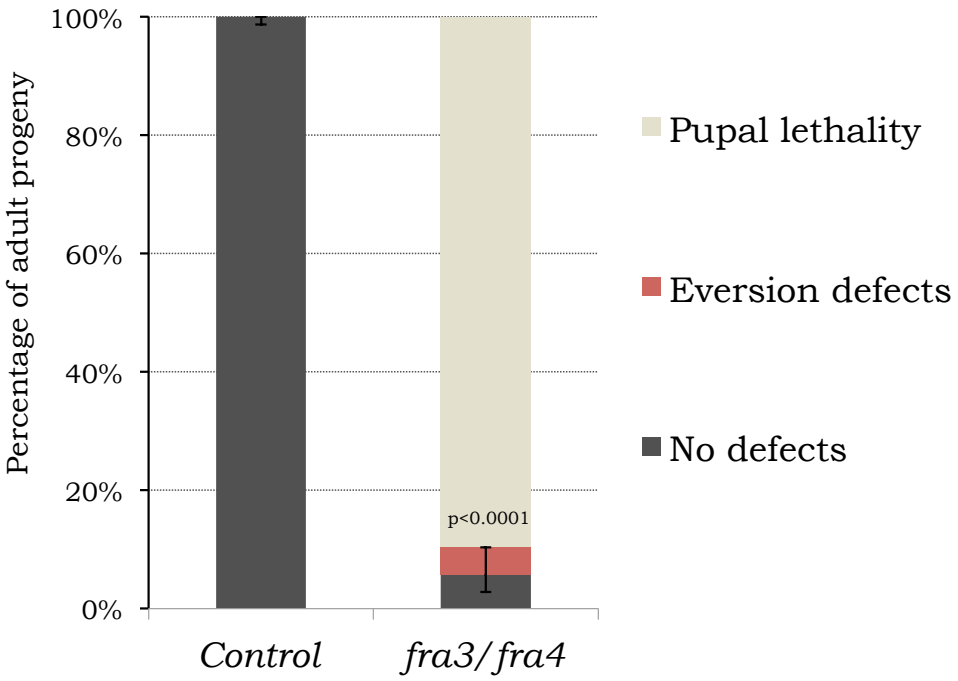
Percentage of adult progeny
100%
80%
60%
40%
20%
0%
p<0.0001
Control
fra3/fra4
Pupal lethality
Eversion defects
No defects

Figure 4.4: ***frazzled* mutant clones still express low levels of Frazzled.** (a-a') The *FLP/+, UAS-GFP/+; FRT42D,tub-GAL80/FRT42D,fra^{3}; tub-GAL4/+* wing disc with GFP-positive (green) *fra^{3}/fra^{3}* and GFP-negative, Fra-positive cells immunostained for Frazzled (red). These Frazzled-positive cells, which would be either be heterozygous (i.e. *fra^{3}/fra^{+}*) or homozygous wild type twin-spots (i.e. *fra^{+}/fra^{+}*) will be referred to as "control" cells hereafter. (b-b') Magnified area (indicated by dashed boxes on a-a') with *fra^{3}/fra^{3}* and wild type twin-spots. Green dashed line (b') indicates a border between the *frazzled* mutant and wild type clones. Frazzled expression is reduced but still persists within the *fra^{3}/fra^{3}* MARCM clones (b', arrows). Scale bars 10 μm.

fra^{3}/*fra*^{3} MARCM clones

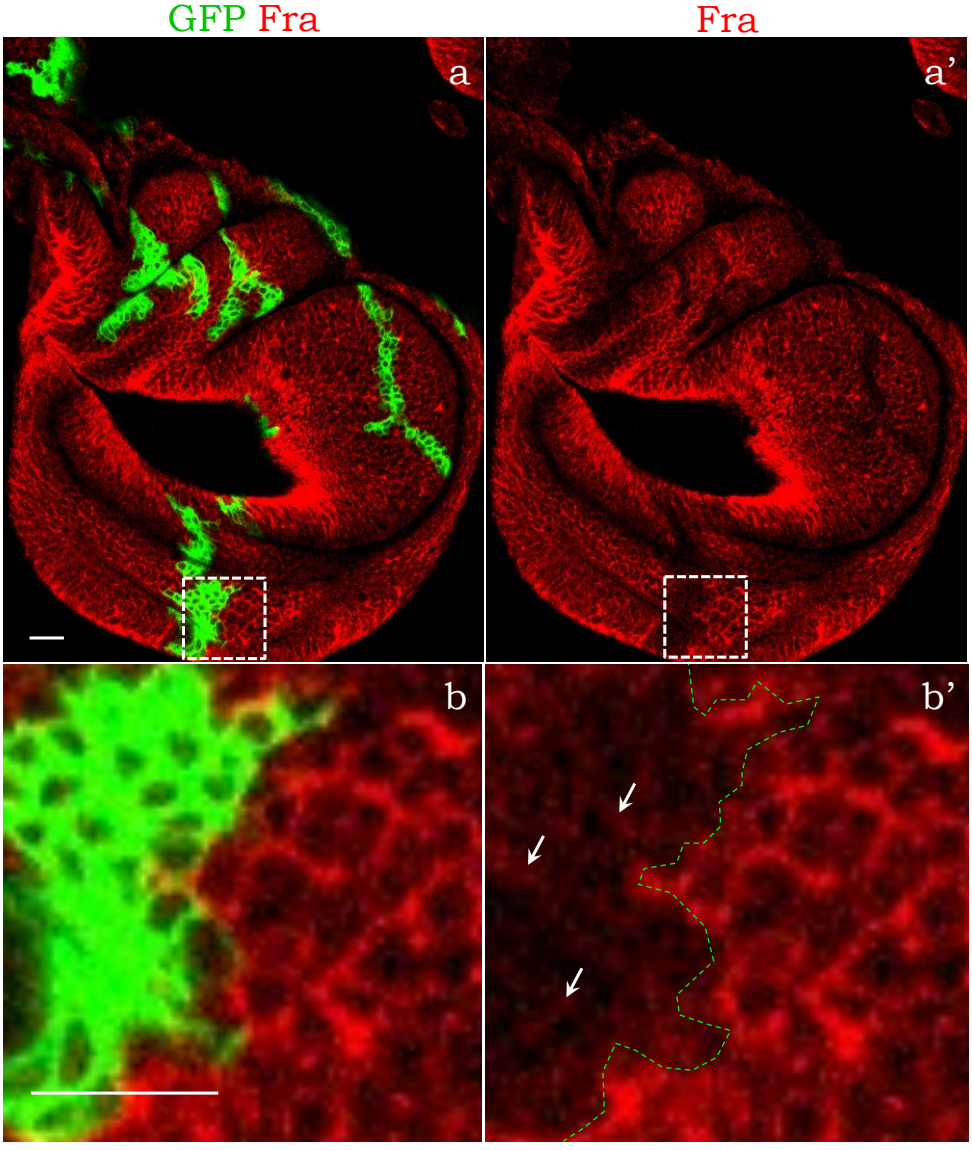

Figure 4.5: **DE-Cad localisation is not disrupted in *frazzled* mutant clones.** The *FLP/+, UAS-GFP/+; FRT42D,tub-GAL80/FRT42D,fra^{3}; tub-GAL4/+* wing disc with GFP-positive (green) *fra^{3}/fra^{3}* and GFP-negative, Frazzled-positive control cells immunostained for DE-Cad (grayscale). (a-a') The PE cells. (b-b') The DP cells. (c-c') Cross-sectional view of the disc. The apical-basal axis is marked by red double-headed arrow (c). Double-arrowhead (c) indicates ZA. Dashed lines (a', b', c') show the borders of the *fra*^{3}/*fra*^{3} MARCM clones. The intensity and localization of DE-Cad seem unchanged in *fra*^{3}/*fra*^{3} MARCM clones. Scale bars 10 μm.

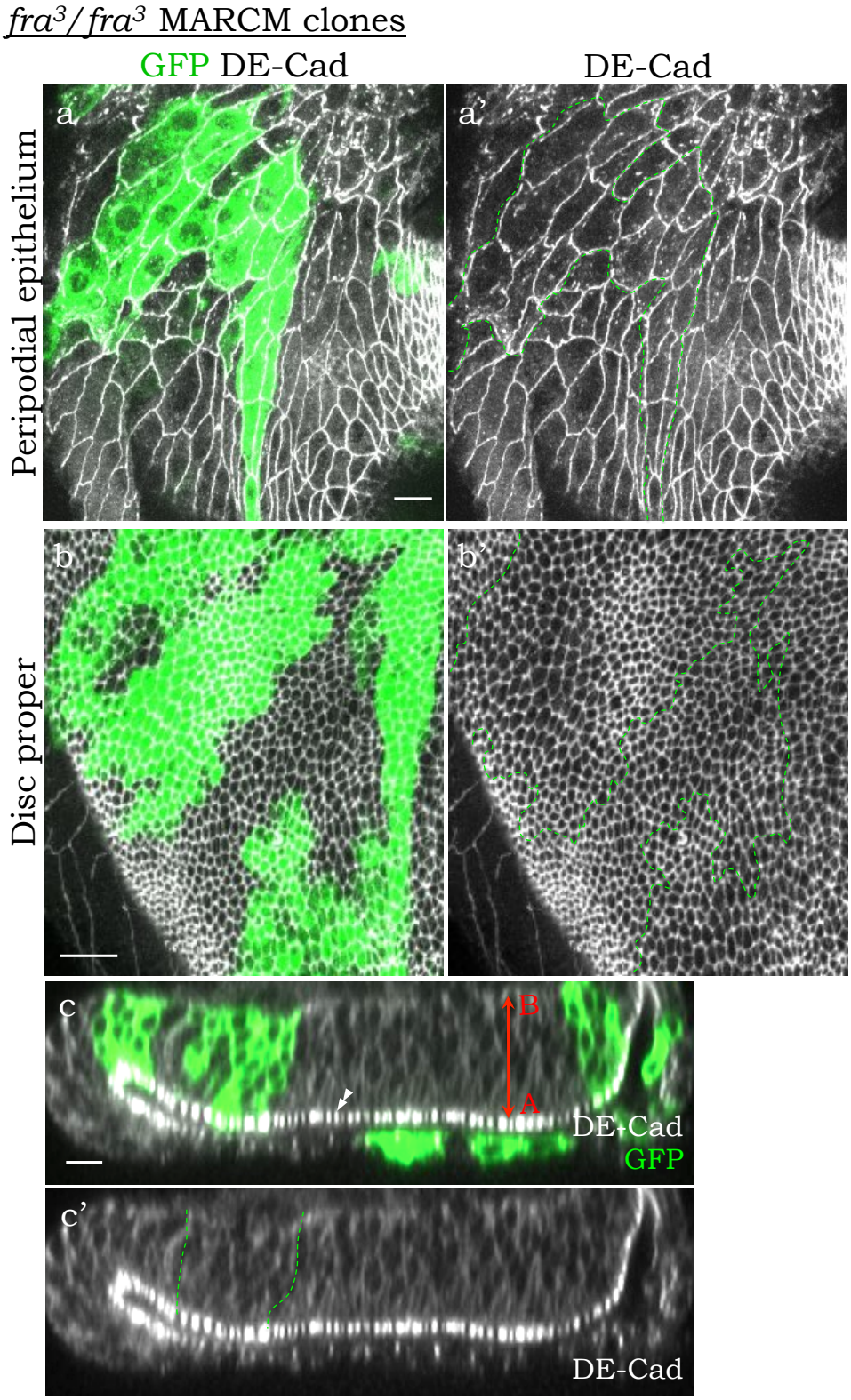
fra3/fra3 MARCM clones
GFP DE-Cad
DE-Cad
Peripodial epithelium
Disc proper
a
a'
b
b'
c
c'
B
A
DE-Cad
GFP
DE-Cad

Figure 4.6: **F-Actin appears normal in *frazzled* mutant clones.** The *FLP/+, UAS-GFP/+; FRT42D,tub-GAL80/FRT42D,fra^3; tub-GAL4/+* wing disc with GFP-positive (green) *fra^3/fra^3* and GFP-negative control cells stained for Rhodamine phalloidin (grayscale; marks F-actin). (a-a') The PE cells. (b-b') The DP cells. (c-c') Cross-sectional view of the disc. The apical-basal axis is marked by red double-headed arrow (c). Double-arrowhead (c) indicates ZA. Dashed lines (a', b', c') show the borders of the *fra^3/fra^3* MARCM clones. The intensity and localization of Rhodamine phalloidin seem unchanged in *fra^3/fra^3* MARCM clones. Scale bars 10 μm.

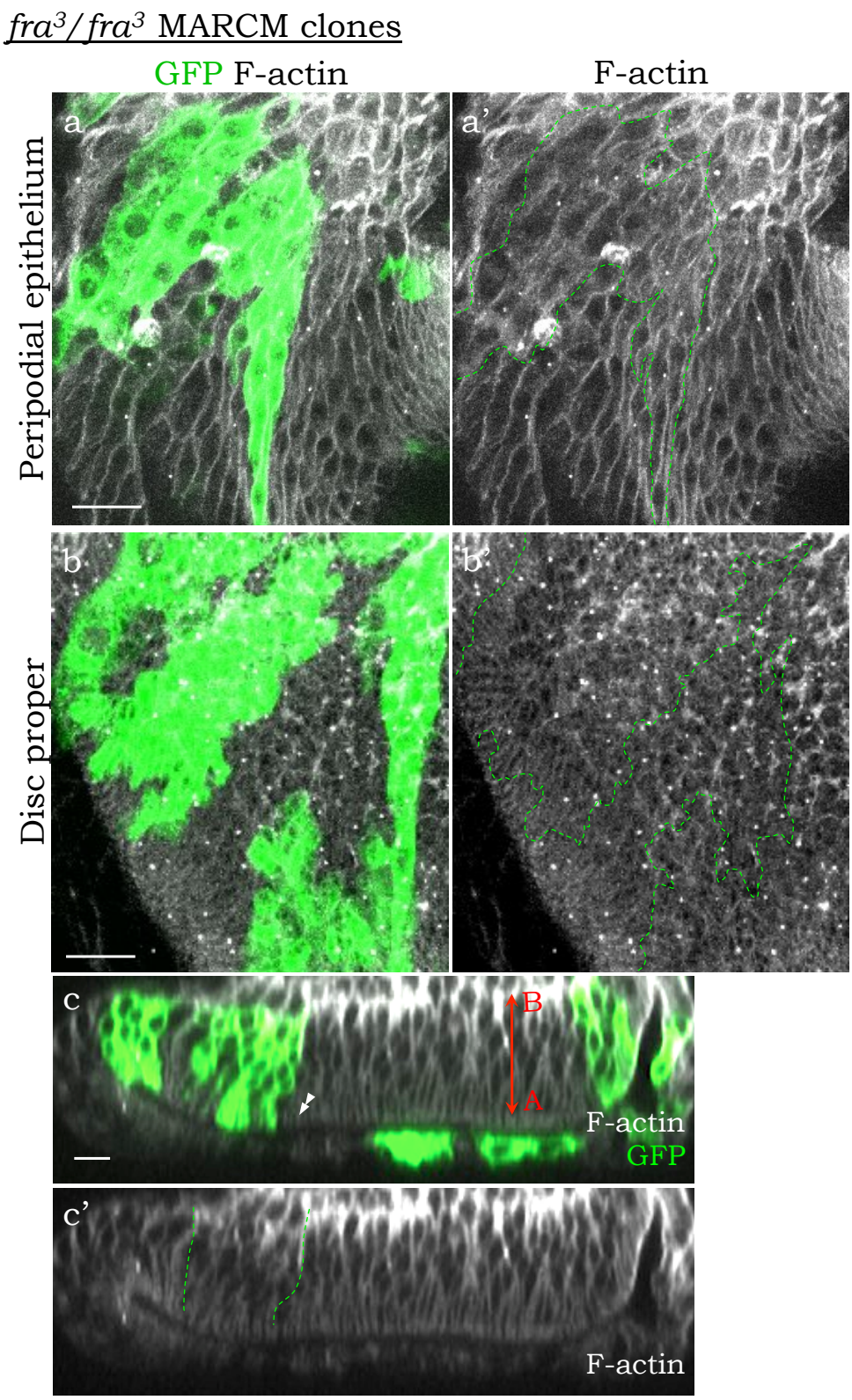
fra3/fra3 MARCM clones
GFP F-actin
F-actin
Peripodial epithelium
Disc proper
a
a'
b
b'
c
B
A
F-actin
GFP
c'
F-actin

Figure 4.7: **Moesin phosphorylation appears normal in *frazzled* mutant clones.** The *FLP/+, UAS-GFP/+; FRT42D,tub-GAL80/FRT42D,fra^{3}; tub-GAL4/+* wing disc with GFP-positive (green) *fra^{3}/fra^{3}* and GFP-negative control cells immunostained for pMoe (grayscale). (a-a') The PE cells. (b-b') The DP cells. (c-c') Cross-sectional view of the disc. The apical-basal axis is marked by red double-headed arrow (c). Double-arrowhead (c) indicates ZA. Dashed lines (a', b', c') show the borders of the *fra*^{3}/*fra*^{3} MARCM clones. The intensity and localization of pMoe seem unchanged in *fra*^{3}/*fra*^{3} MARCM clones. Scale bars 10 μm.

fra^3/*fra*^{3} MARCM clones

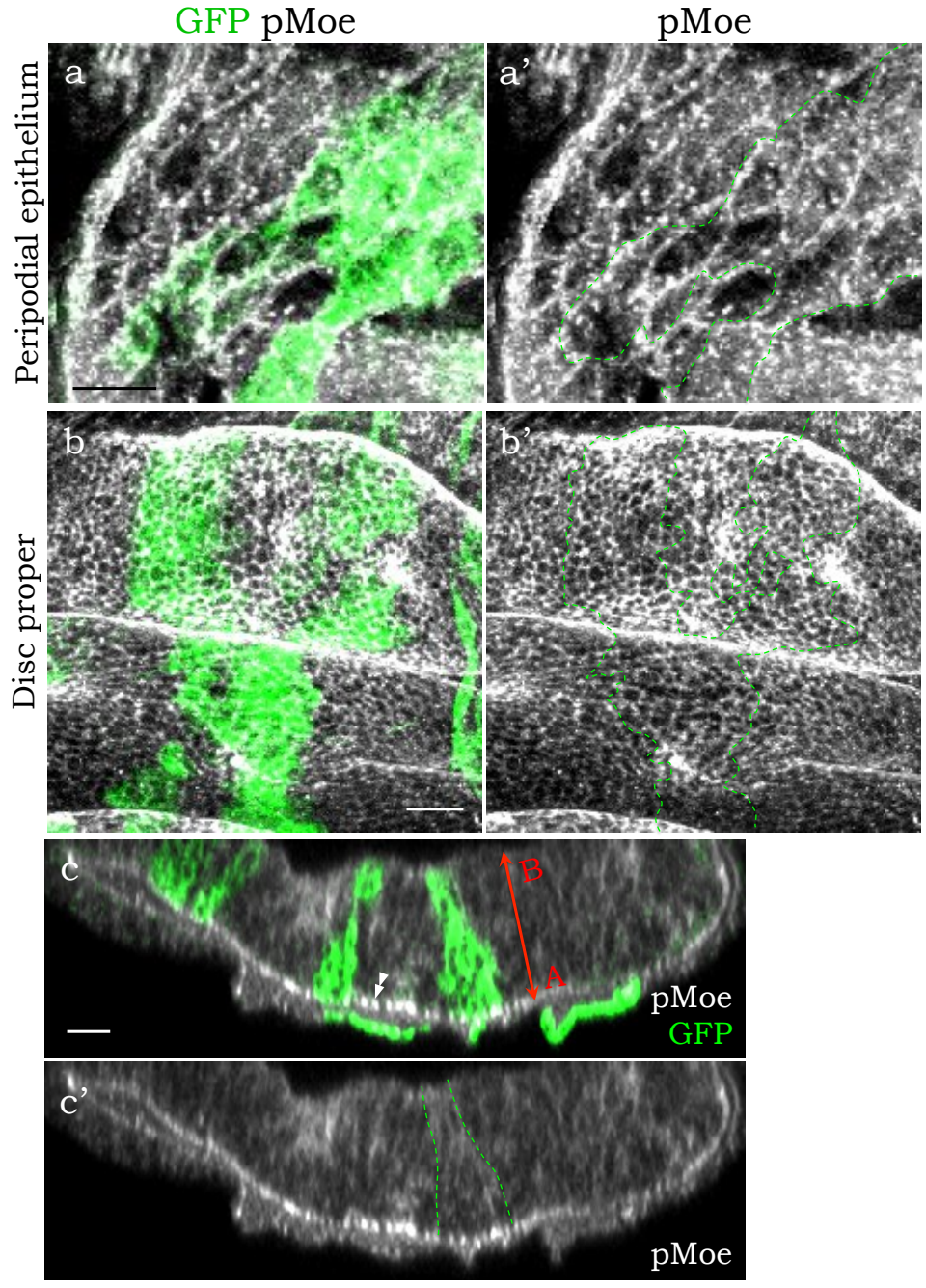

Figure 4.8: **Endogenous Frazzled is still expressed in cells with RNAi knockdown of *frazzled*.** The *FLP/+;UAS-dicer2;Act5C:CD2:GAL4/UAS-fra.IR,UAS-GFP* (a-a'), *FLP/+;UAS-gal4;Act5C:CD2:GAL4/UAS-fra.IR,UAS-GFP* (b-b') and *FLP/+;fra^3;Act5C:CD2:GAL4/UAS-fra.IR,UAS-GFP* (c-c') wing discs with GFP-positive (green) *frazzled* clones immunostained for Frazzled (grayscale). Frazzled is still presented in the GFP-positive cells (arrowheads, a', b', c'). Green dashed lines (a', b', c') indicate the borders of GFP-positive clones. Scale bars 10 μm.

FLP; UAS-dicer2; Act5C:CD2:GAL4, fraIR, RFP

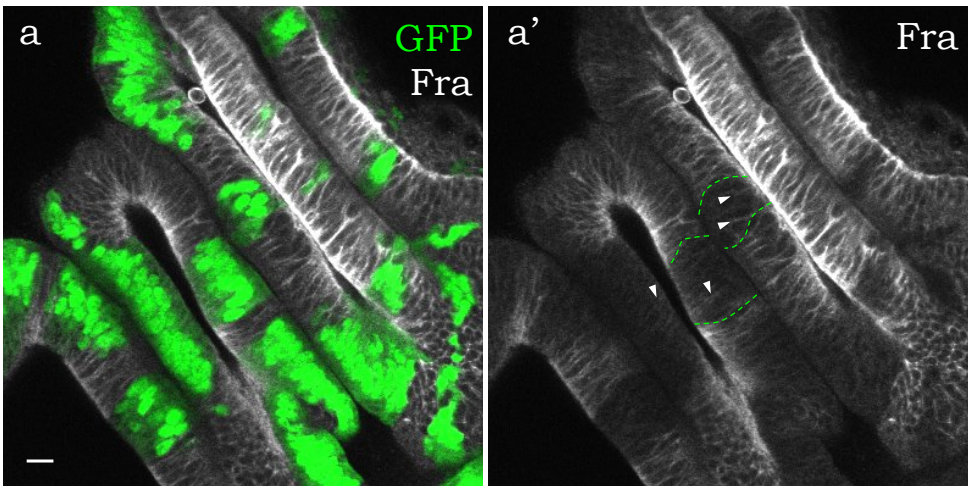

FLP; UAS-gal4; Act5C:CD2:GAL4, fraIR, RFP

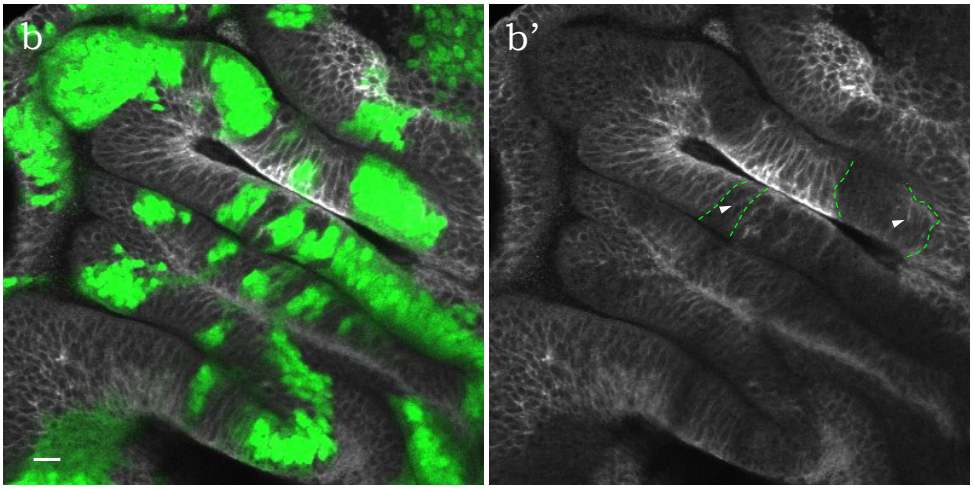

FLP; fra^3; Act5C:CD2:GAL4, fraIR, RFP

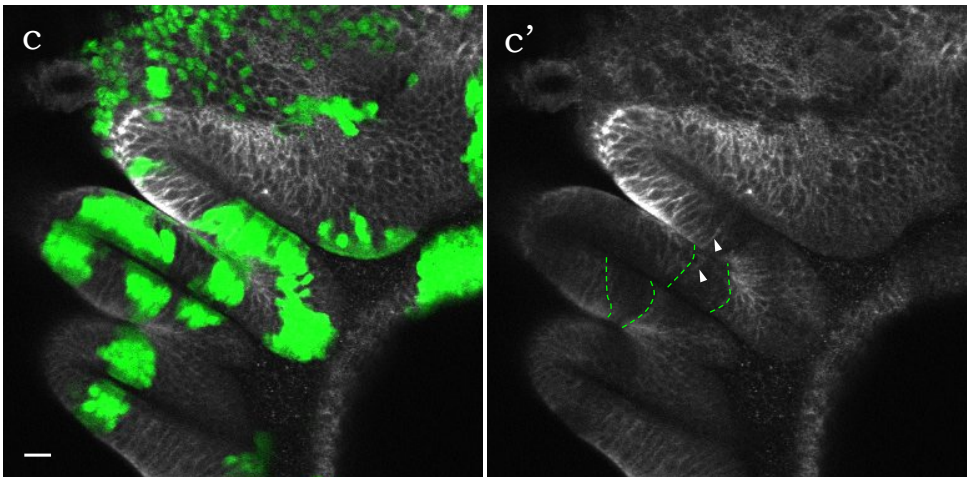

Figure 4.9: ***frazzled* knockdown in the trachea disrupts DE-Cad and F-actin distribution.** The tracheal epithelium *FLP/+; Act5C:CD2:GAL4/UAS-fra.IR,UAS-RFP* with RFP-positive (red) *fra.IR* clones stained for DE-Cad (blue (a, d, f) or grayscale (b)) and Rhodamine phalloidin (marks F-actin; green (a) or grayscale (c)). (a) The merged image of the disc. Dashed box indicates the magnified area depicted in d-f. (b) DE-Cad is distributed in the cytoplasm of *fra.IR* cells. (c) The level of F-actin is decreased in *fra.IR* cells. Red and yellow boxes indicate magnified areas depicted in b'-c' (*fra.IR*) and b"-c" (wild type) respectively. (b'-c') F-actin is downregulated at ZA in *fra.IR* cells (arrow). (b"-c") F-actin is localised at ZA line in wild type cells (arrow). Asterisks indicate ZA line. (d-f) The magnified view shows that the RFP (red) and DE-Cad (blue) dots (arrowheads) are not overlapped indicating that the DE-Cad cytoplasmic signal is not an artifact of the RFP signal showing up in the DE-Cad channel. Scale bars 10 μm.

Trachea *FLP; Act5C:CD2:GAL4, fra.IR, RFP*

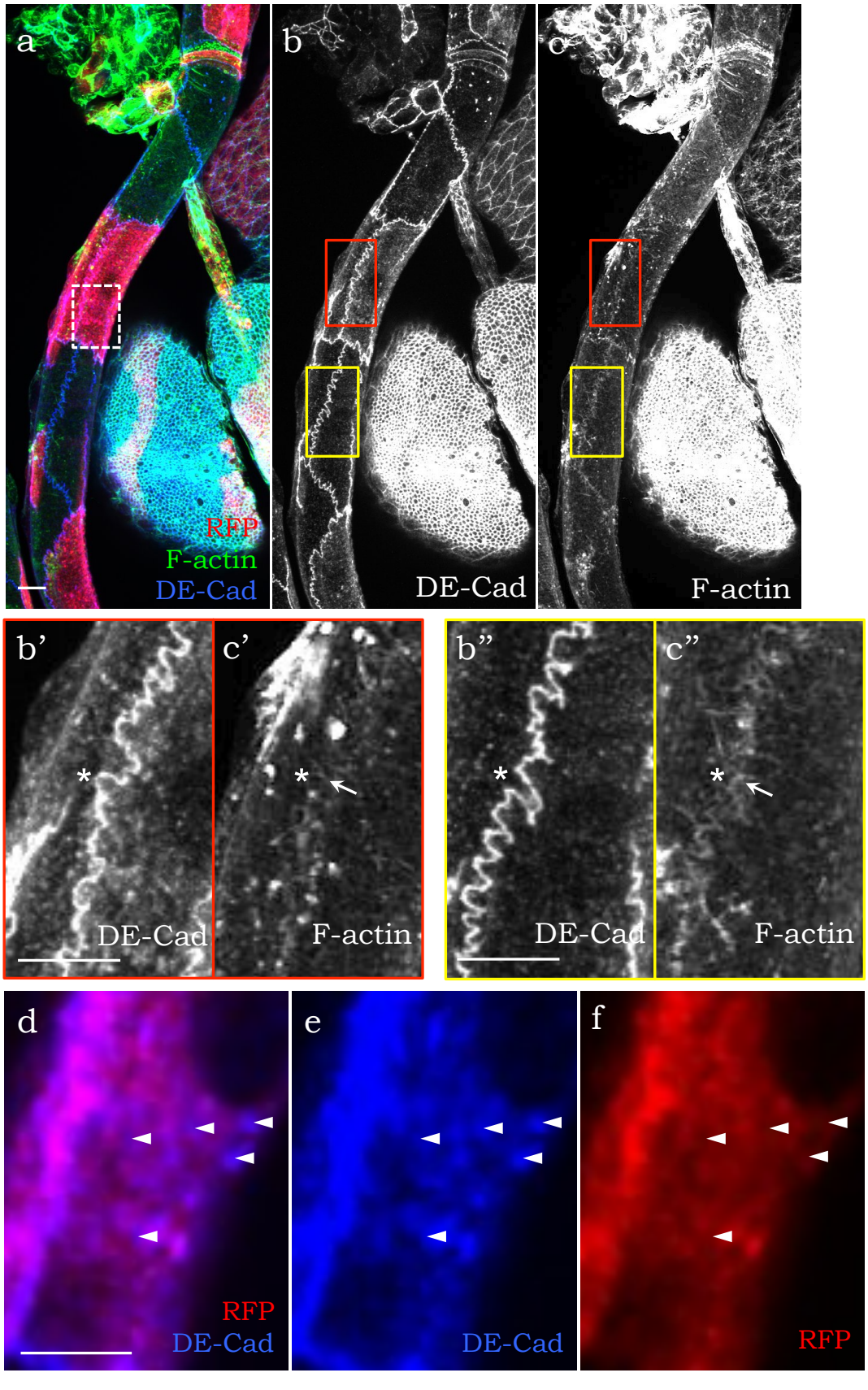

Figure 4.10: **Overexpression of *frazzled* promotes cellular protrusions in the PE and the DP epithelium.** The *FLP/+; Act5C:CD2:GAL4/UAS-fra,UAS-GFP* wing disc with GFP-positive (green) *frazzled* clones immunostained for DE-Cad (blue (a, c) and Frazzled (red (a, c) or grayscale (b-b', d-d')). (a, c) Merge images of the disc. (a, b, b') The PE cells overexpressing *frazzled*. (c, d, d') The DP cells overexpressing *frazzled*. Dashed boxes (b and d) indicate magnification areas depicted in b' and d' respectively. Frazzled (grayscale in b-b' and d-d') accumulates not only within the cytoplasm but also in extended protrusions (b', d', arrows). Scale bars 10 μm.

FLP; Act5C:CD2:GAL4, fra, GFP

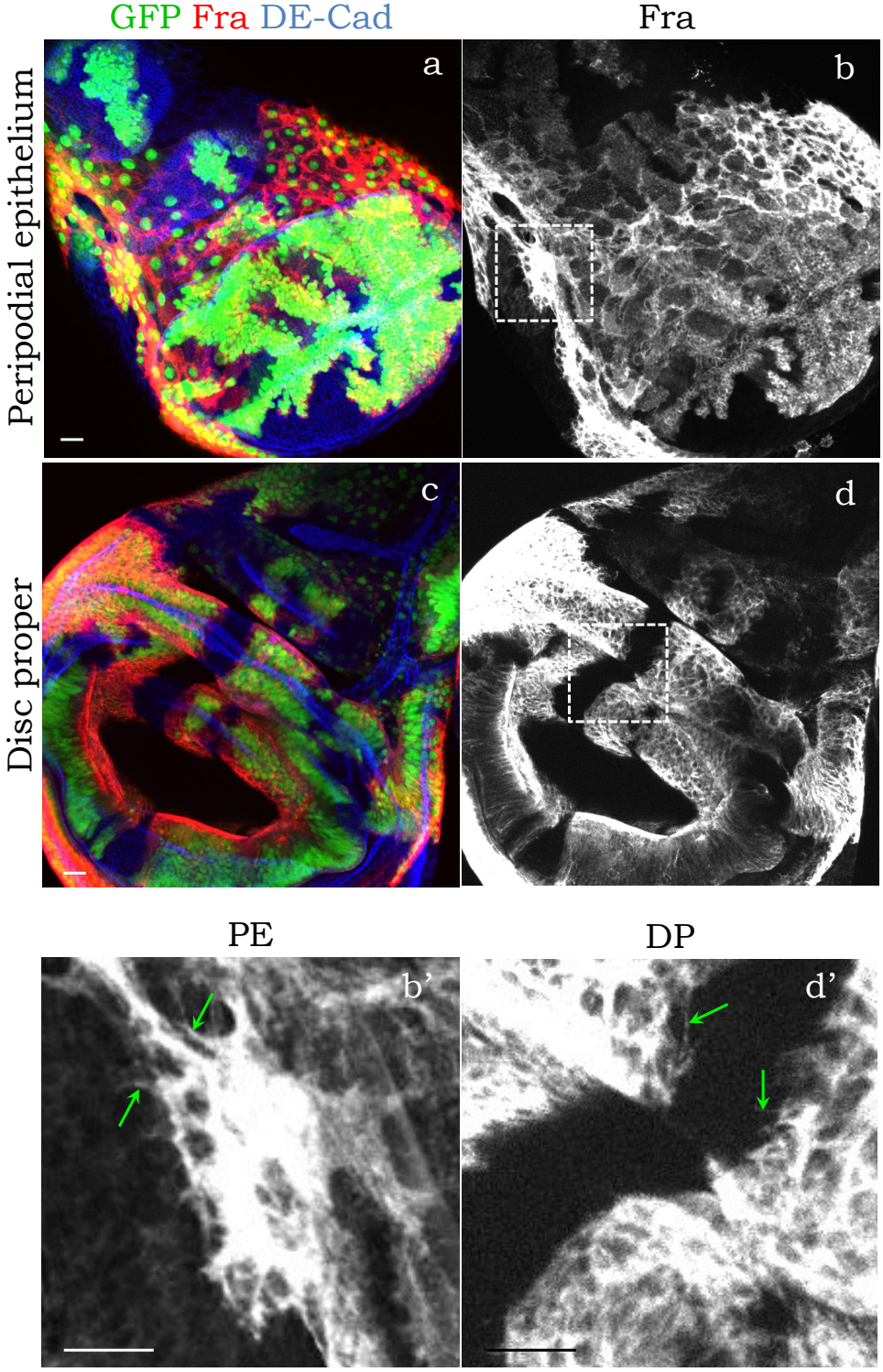

Figure 4.11: **Clonal expression of *frazzled* induces F-Actin rearrangements throughout the PE.** The fragments of the PE of *w1118/FLP; Act5C:CD2:GAL4/UAS-GFP* (*Control*) and *FLP/+; Act5C:CD2:GAL4/UAS-fra,UAS-GFP* wing discs stained for Rhodamine phalloidin (grayscale). (a-a') In control discs, F-actin has mainly peripheral localization in GFP-positive (green) as well as in GFP-negative clones. (b-b') In *frazzled*-overexpressing cells (GFP-positive, green), F-actin filaments are organized in thick extended bundles (arrows). In non-GFP wild type cells, F-actin filaments are also formed in multiple shorter protrusions spread along the cell cortex (arrowheads). Green dashed lines (a', b') indicate the borders of GFP-positive clones. Scale bars 10 μm.

Control

GFP F-actin

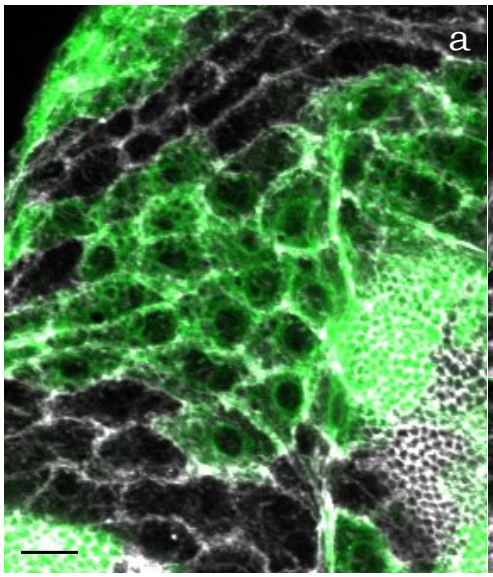

F-actin

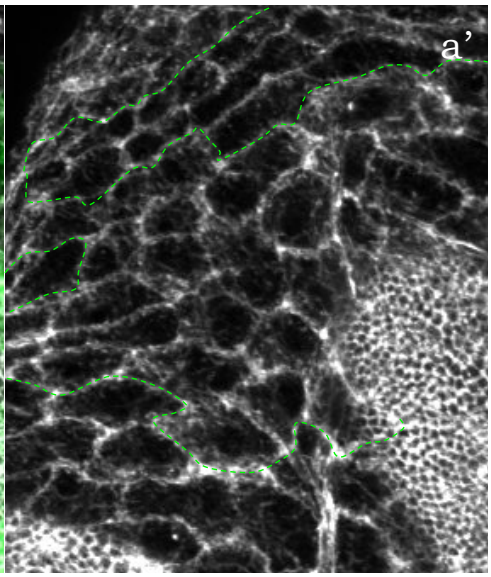

FLP; Act5C:CD2:GAL4, fra, GFP

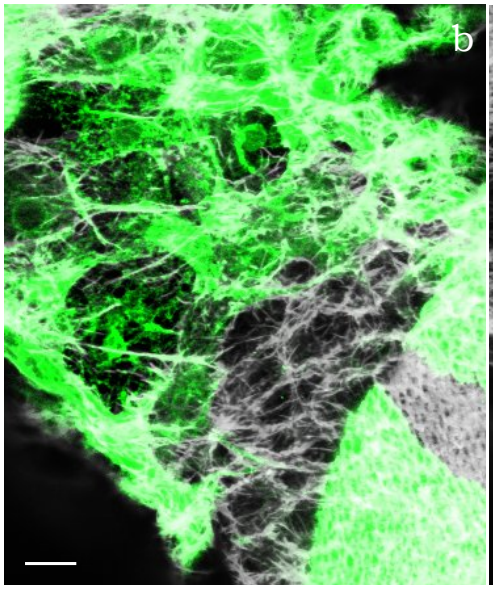

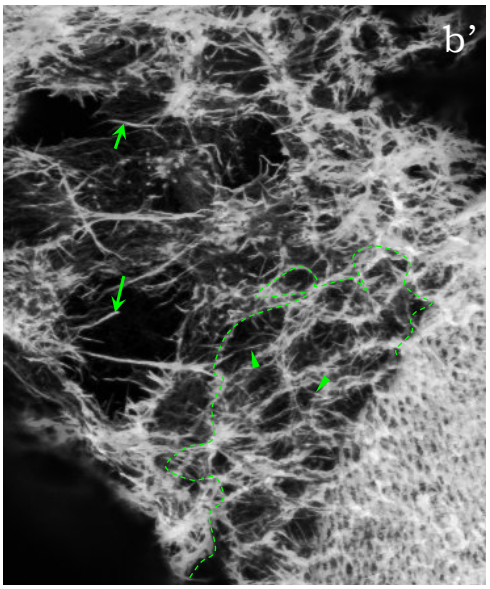

Figure 4.12: **DE-Cad localization and cell morphology in control *ptc>GFP* wing discs.** (a-a') The *ptc>GFP* wing disc (*Control*; GFP shown in green) immunostained for DE-Cad (grayscale). A dashed line (a) indicates the cross section depicted in c-c'. (b-b') Magnified area marked with dashed boxes (a-a'). (c-c') Cross-sectional view of the DP. Both, the GFP-positive (bordered by green dashed lines (a', b', c')) and non-GFP epithelium, display DE-Cad distributed at ZA (b', c', double-arrowheads), and on the basal (b', c', arrowheads) and lateral (b', c', arrows) sides of DP cells. (d) Schematic representation of a wing disc showing the disc proper (DP) and peripodial epithelium (PE) in frontal and cross-sectional views. In most cases, the width of apical side of the *ptc>GFP* stripe is equal or less to the width of basal side (red double-headed arrows, b, c, d; the quantification see in Figure 5.15). Hereafter the apical-basal (A-B) axis is marked by double-headed arrow (a, b, c, d). Scale bars 10 μm.

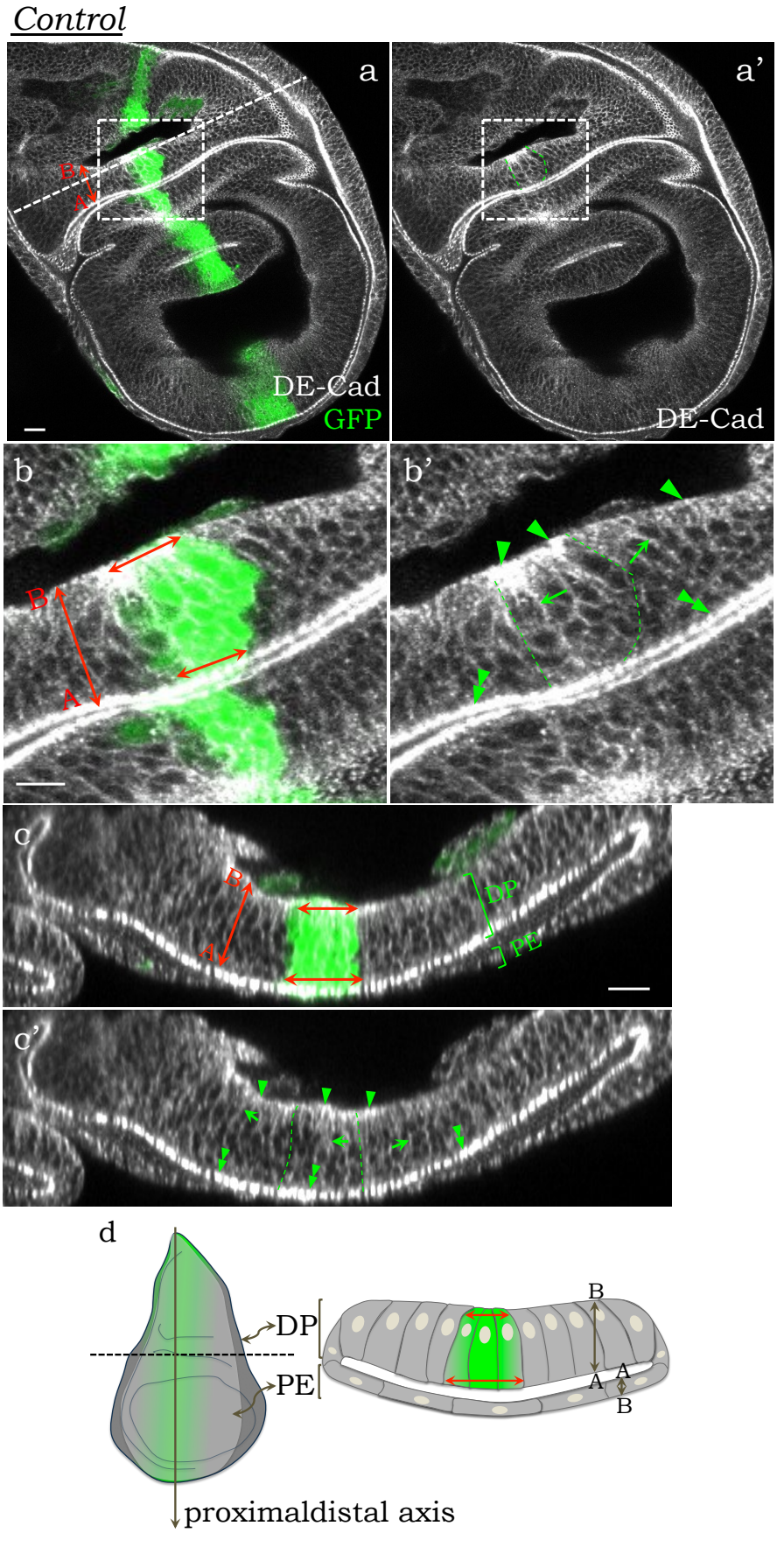
Control
a
a'
B
A
DE-Cad
GFP
DE-Cad
b
b'
B
A
c
c'
B
A
DP
PE
d
DP
PE
B
A
A
B
proximaldistal axis

Figure 4.13: **DE-Cad expression is reduced in basolateral regions of DP cells overexpressing *frazzled*.** (a-a') The *FLP/+; Act5C:CD2:GAL4/UAS-fra,UAS-GFP* wing disc (GFP shown in green) immunostained for DE-Cad (grayscale). A dashed line (a) indicates the cross section depicted in c-c'. (b-b') Magnified area marked with dashed boxes (a-a'). (c-c') Cross-sectional view of the DP. The non-GFP DP epithelium displays DE-Cad distributed at ZA (b', c', double-arrowheads), and on the basal (b', c', arrowheads) and lateral (b', c', arrows) sides of DP cells. The GFP-positive (green) DP epithelium (bordered by green dashed lines (a', b', c')) has reduced DE-Cad at the basal and lateral sides. Scale bars 10 μm.

FLP; Act5C:CD2:GAL4, fra, GFP

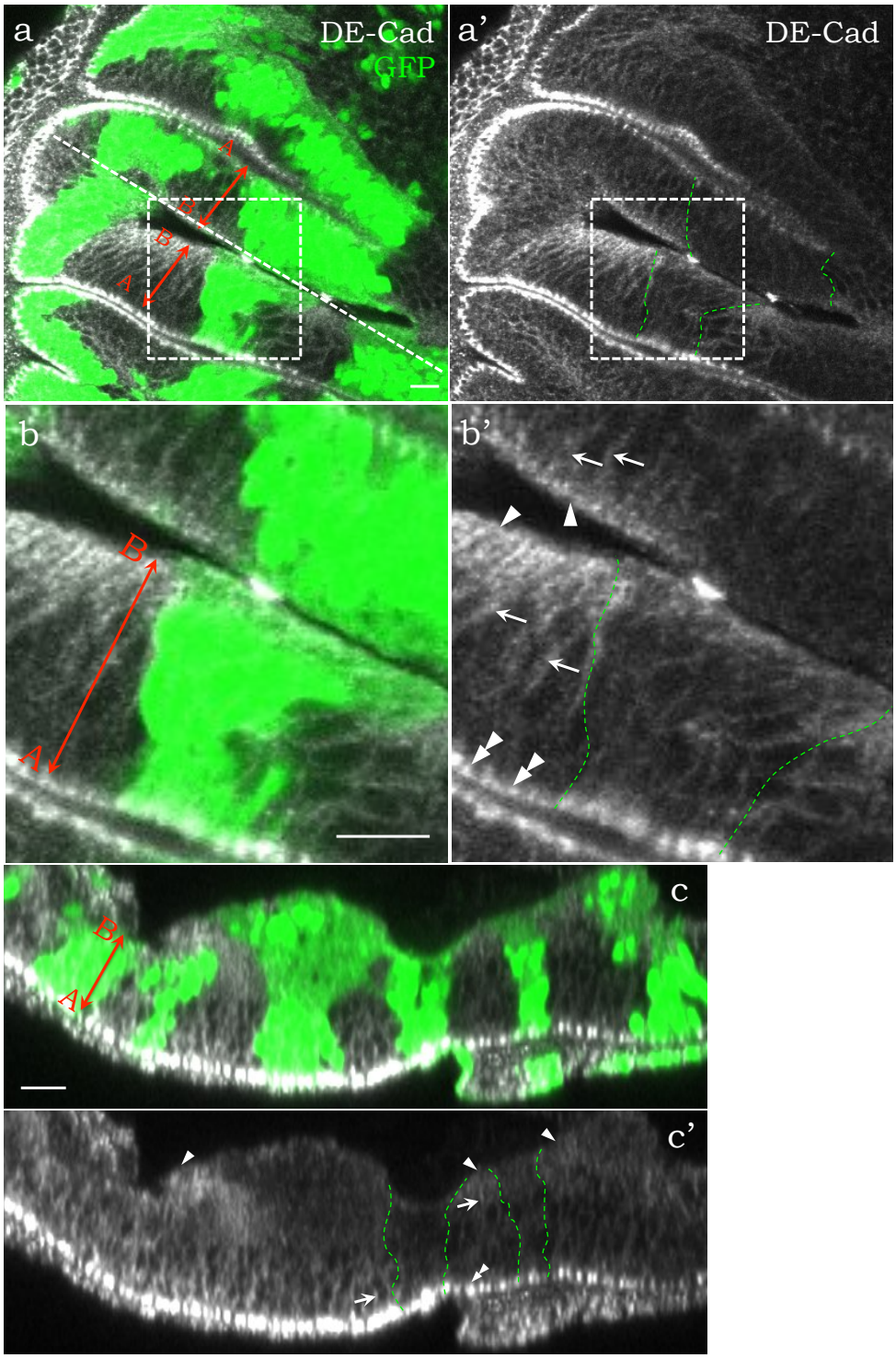

Figure 4.14: ***frazzled* overexpressing PE cells do not display detectable changes in DE-Cad expression.** The PE of a *FLP/+; Act5C:CD2:GAL4/UAS-fra,UAS-GFP* wing disc (GFP shown in green) immunostained for DE-Cad (grayscale). Green dashed line (b) indicates border of the *frazzled* overexpressing clone. Scale bars 10 μm.

PE *FLP; Act5C:CD2:GAL4, fra, GFP*

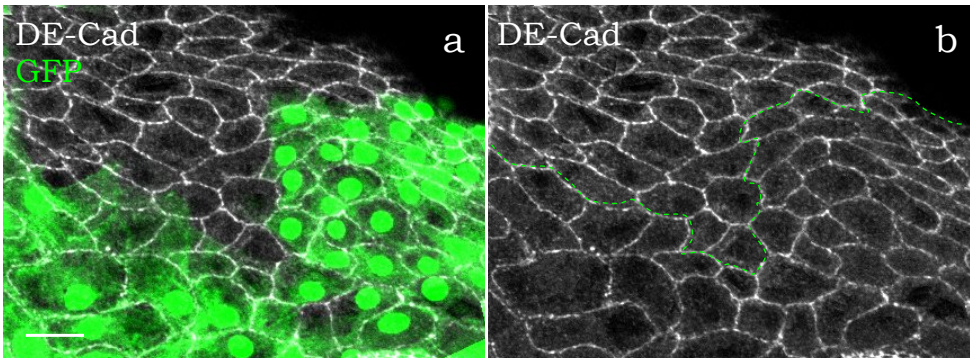

Figure 4.15: **The *ptc*-driven overexpression of *frazzled* reduces DE-Cad in basolateral regions of the DP epithelium.** (a-a') The *ptc>fra,GFP* wing disc (GFP shown in green) immunostained for DE-Cad (grayscale). A dashed line (a) indicates the cross section depicted in c-c'. (b-b') Magnified area marked with dashed boxes (a-a'). (c-c') Cross-sectional view of the DP. The non-GFP epithelium displays DE-Cad distributed at ZA (b', c', double-arrowheads), and on the basal (b', c', arrowheads) and lateral (b', c', arrows) sides of DP cells. The *ptc*-pattern (green) (bordered by green dashed lines (a', b', c')) had significantly reduced DE-Cad at the basal and lateral sides (the quantification see in Figure 5.15, a). Scale bars 10 μm.

ptc>fra,GFP

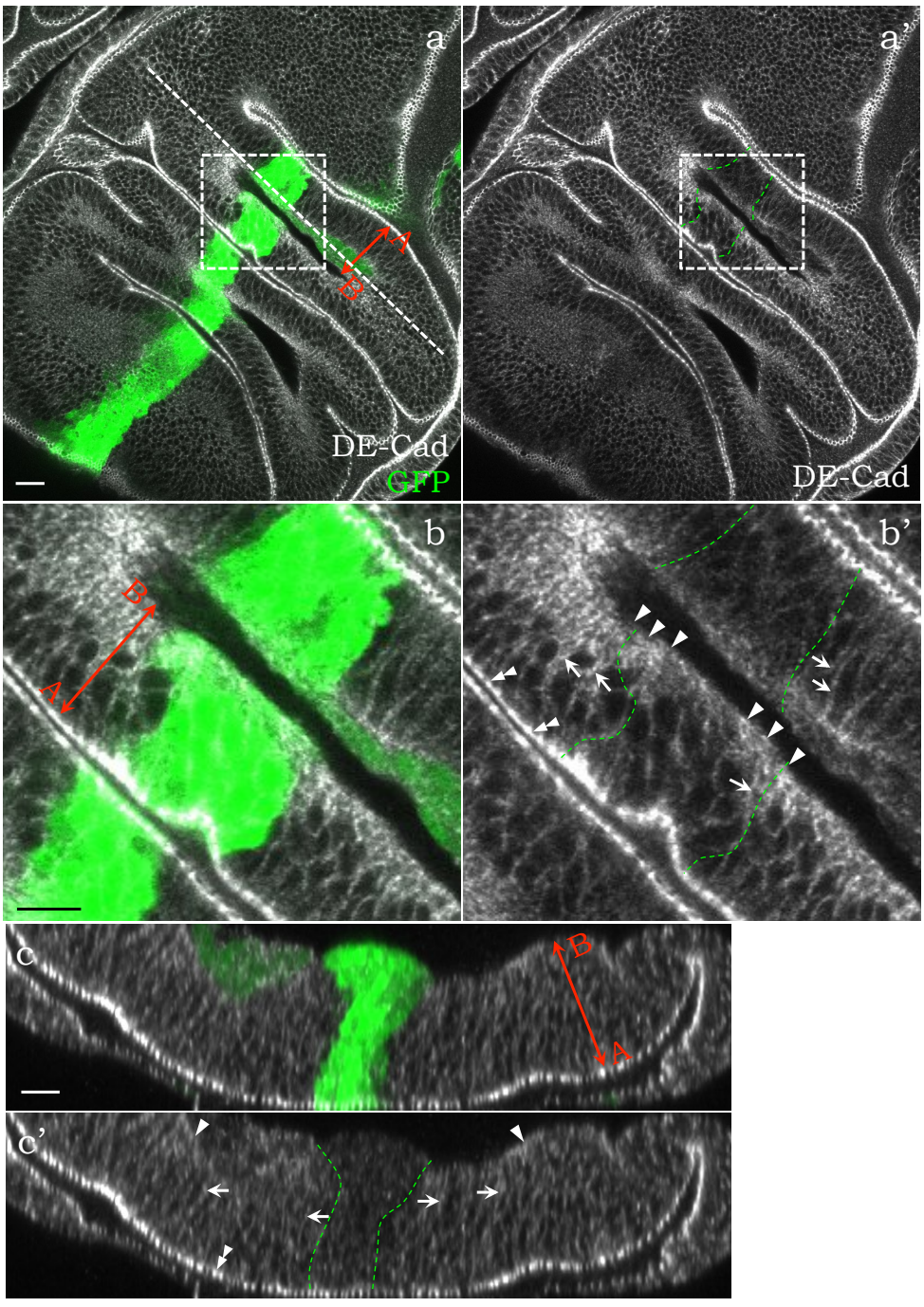

Figure 4.16: **Arm expression is reduced in basolateral regions of DP cells overexpressing *frazzled*.** (a-a') The *FLP/+; Act5C:CD2:GAL4/UAS-fra,UAS-GFP* wing disc (GFP shown in green) immunostained for Arm (grayscale). A dashed line (a) indicates the cross section depicted in c-c'. (b-b') Magnified area marked with dashed boxes (a-a'). (c-c') Cross-sectional view of the DP. The non-GFP DP epithelium displays Arm distributed at ZA (b', c', double-arrowheads), and on the basal (b', c', arrowheads) and lateral (b', c', arrows) sides of DP cells. The GFP-positive (green) DP epithelium (bordered by green dashed lines (a', b', c')) has reduced Arm at the basal and lateral sides. Scale bars 10 μm.

FLP; Act5C:CD2:GAL4, fra, GFP

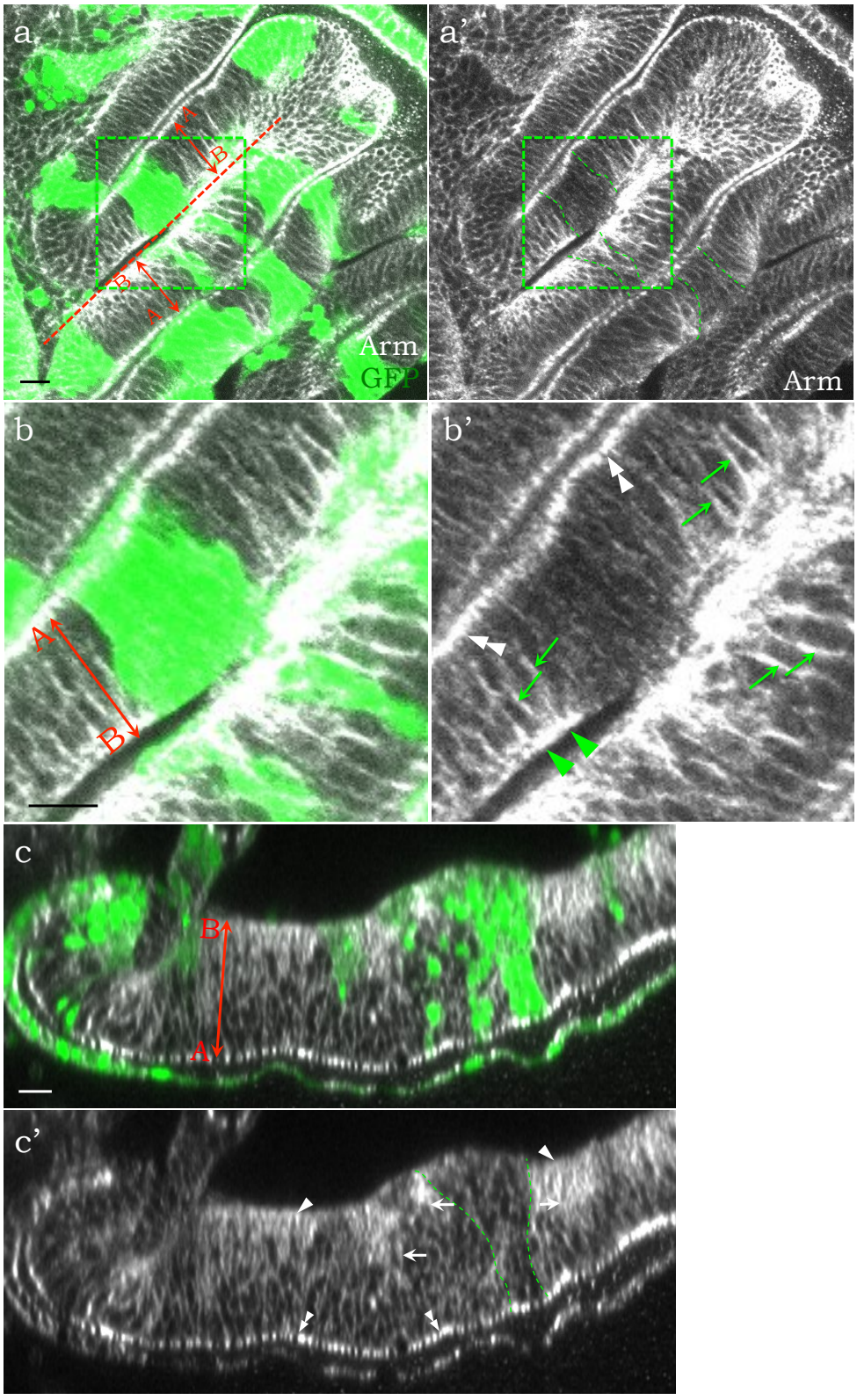

Figure 4.17: **Overexpression of *frazzled* causes basal expansion of the DP epithelium.** (a) The *FLP/+; Act5C:CD2:GAL4/UAS-fra,UAS-GFP* wing disc (GFP shown in green) immunostained for DE-Cad (grayscale). A dashed line indicates the cross-sectional view depicted in c. (b) Magnified area marked with a dashed box (a). (c) Cross-sectional view of the DP. The GFP-positive (green) *frazzled* overexpressing clones in the DP are wider on the basal side than on the apical side. (d) Three-dimensional view of the DP epithelium. Arrows indicate furrows formed within the *frazzled* overexpressing clones. (e) Schematic representation of control wing disc and a wing discs with clonal overexpression of *frazzled* (green) showing the DP and PE in frontal and cross-sectional views. The width of apical side of the *frazzled* overexpressing clone is wider than the width of basal side (c, e, red double-headed arrows). The apical side of the clone forms a fold (arrow). Scale bars 10 μm.

FLP; Act5C:CD2:GAL4, fra, GFP

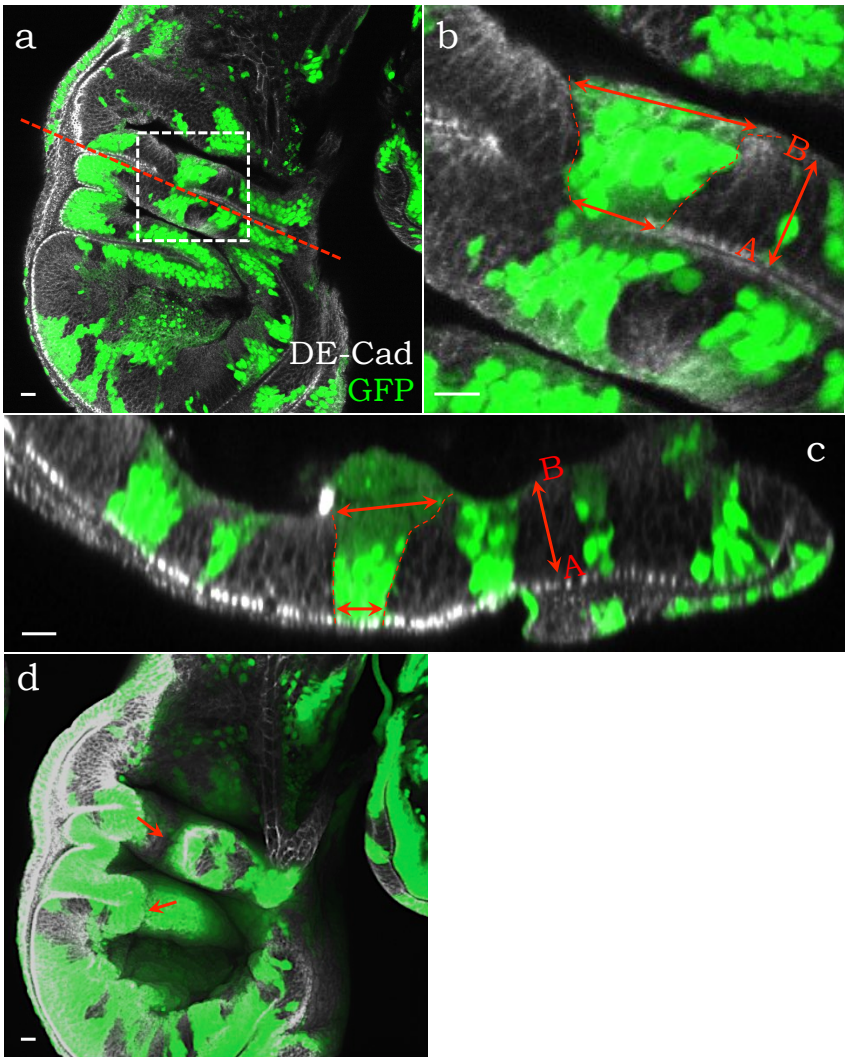

Figure 4.18: **pMLC expression seems unaffected in the DP cells over-expressing *frazzled*.** (a-a') The *FLP/+; Act5C:CD2:GAL4/UAS-fra,UAS-GFP* wing disc (GFP shown in green) immunostained for pMLC (grayscale). A dashed line (a) indicates the cross section depicted in c-c'. (b-b') Magnified area marked with dashed boxes (a-a'). (c-c') Cross-sectional view of the DP. The cytoplasmic pMLC puncta display a slight apical-basal polarization in the GFP-positive (bordered by green dashed lines (a', b', c')) as well as non-GFP DP cells. Scale bars 10 μm.

FLP; Act5C:CD2:GAL4, fra, GFP

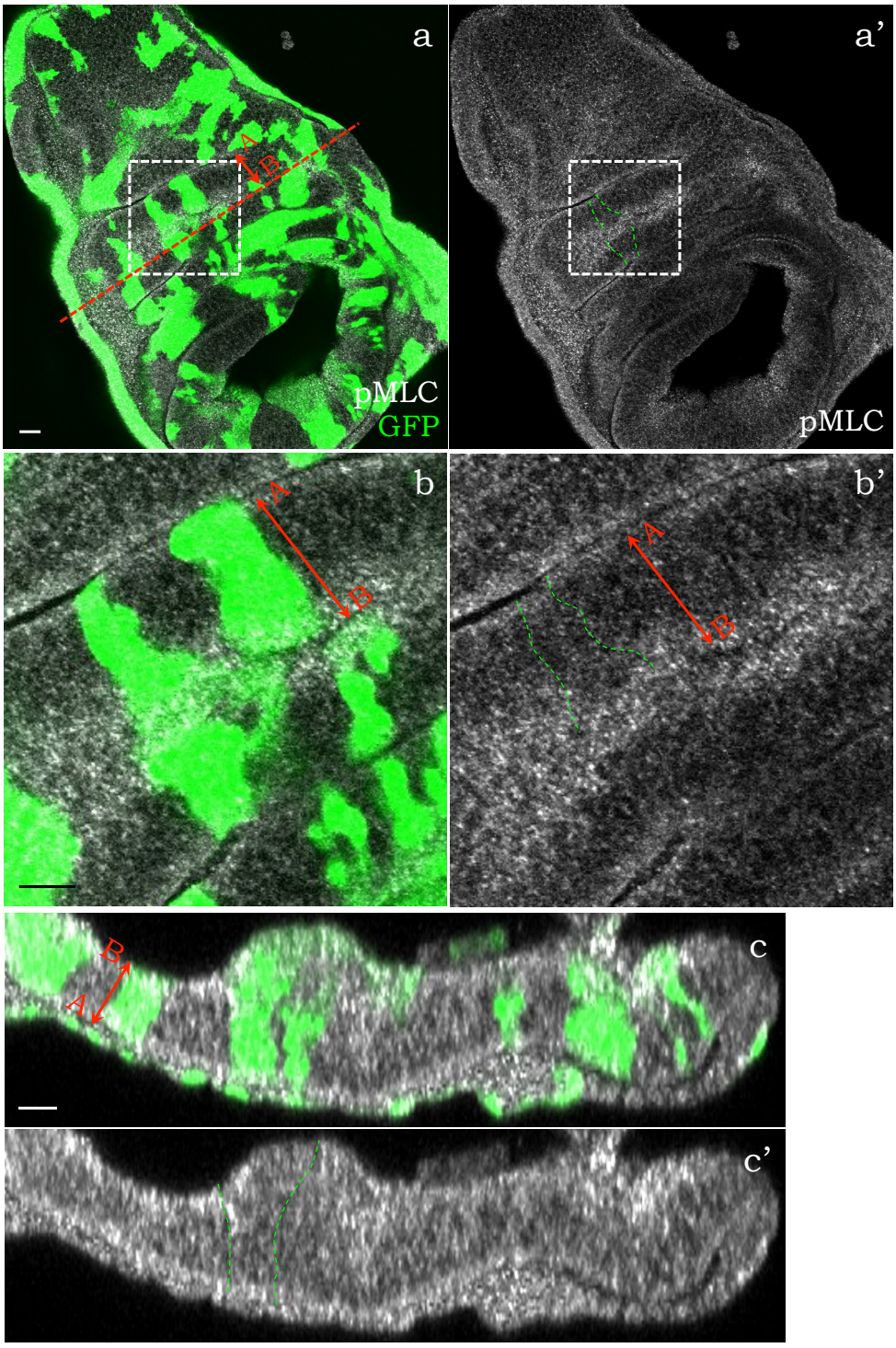

Figure 4.19: **The *ptc*-driven overexpression of *frazzled* causes basal expansion of the DP epithelium.** (a) The *ptc>fra,GFP* wing disc (GFP shown in green) immunostained for DE-Cad (grayscale). A dashed line indicates the cross section depicted in c. (b) Magnified area marked with a dashed box (a). (c) Cross-sectional view of the DP. Double-headed arrows indicate that *ptc>fra,GFP* pattern is wider on the basal side than on the apical side (the quantification see in Figure 5.15, b). Arrow (b, c) indicates a furrow formed due to *frazzled* overexpresion. Scale bars 10 μm.

ptc>fra,GFP

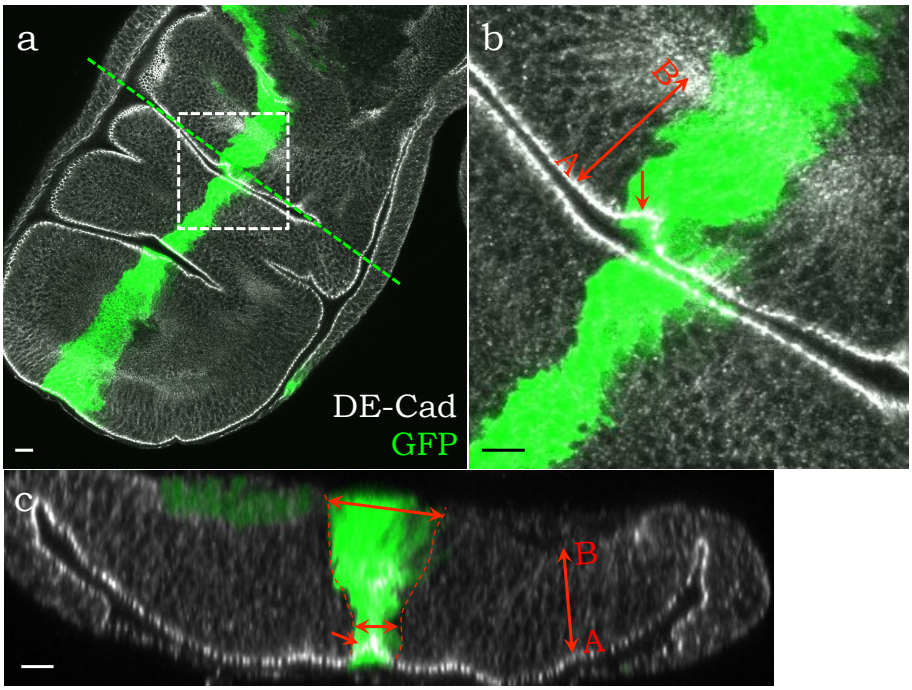

Figure 4.20: **pMoe localization in control *ptc>GFP* wing discs.** (a-a') The *ptc>GFP* wing disc (*Control*; GFP shown in green) immunostained for pMoe (grayscale). Dashed line (a) indicates the cross section depicted in c-c'. (b-b') Magnified area marked with dashed boxes (a-a'). (c-c') Cross-sectional view of the DP. Both, the GFP-positive (bordered by green dashed lines (a', b', c')) and non-GFP epithelium, display pMoe puncta distributing at ZA (b', c', double-arrowhead), and on the basal (b', c', arrowheads) and lateral (b', c', arrows) sides of DP cells. Scale bars 10 μm.

Control

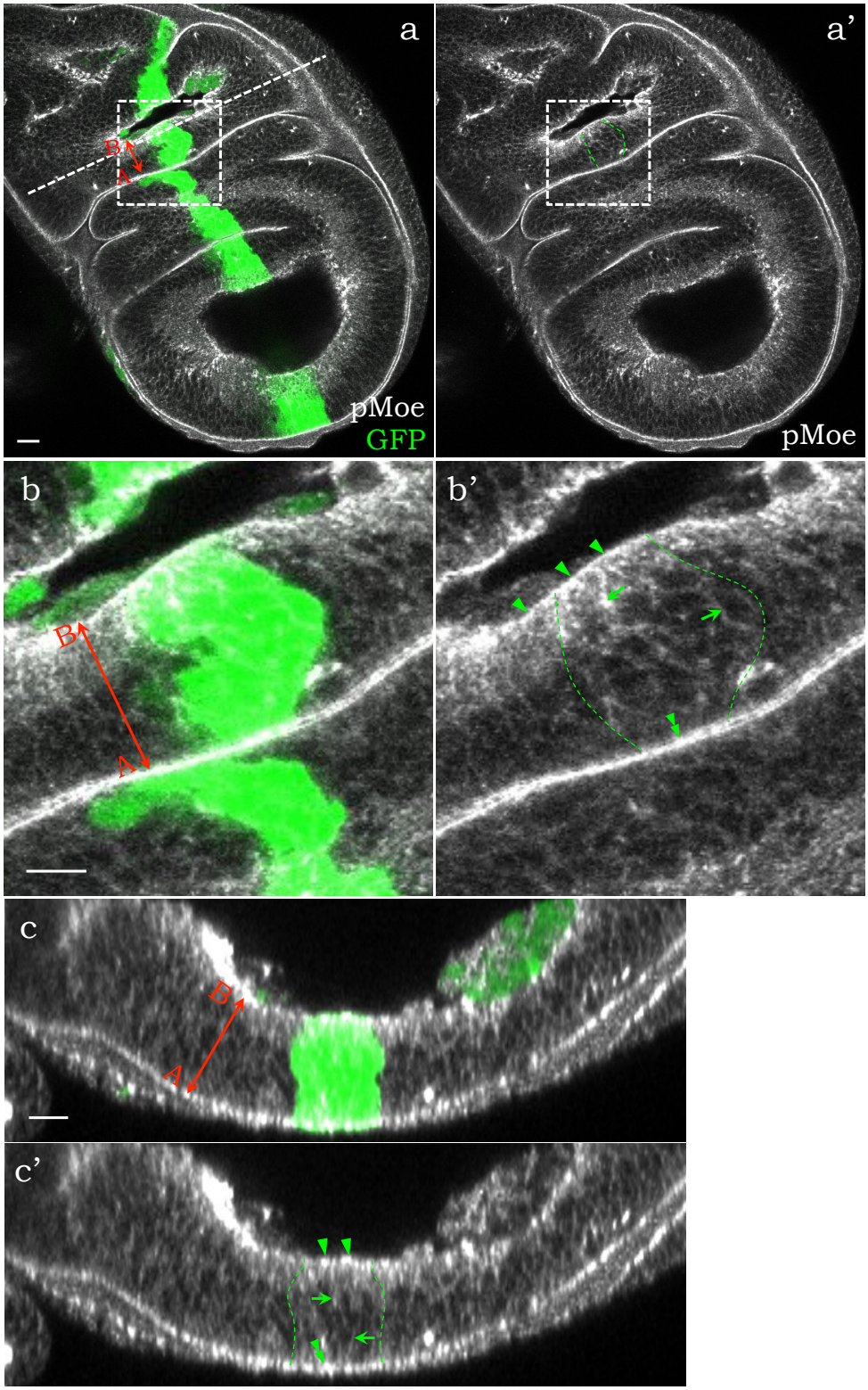

Figure 4.21: **pMoe is reduced in basolateral regions of DP cells overexpressing *frazzled*.** (a-a') The *FLP/+; Act5C:CD2:GAL4/UAS-fra,UAS-GFP* wing disc (GFP shown in green) immunostained for pMoe (grayscale). Dashed line (a) indicates the cross section depicted in c-c'. (b-b') Magnified area marked with dashed boxes (a-a'). (c-c') Cross-sectional view of the DP. Arrows indicate the areas where basally polarized pMoe was reduced in *frazzled* overexpressing clones (bordered by green dashed lines (a', b', c')). Scale bars 10 μm.

FLP; Act5C:CD2:GAL4, fra, GFP

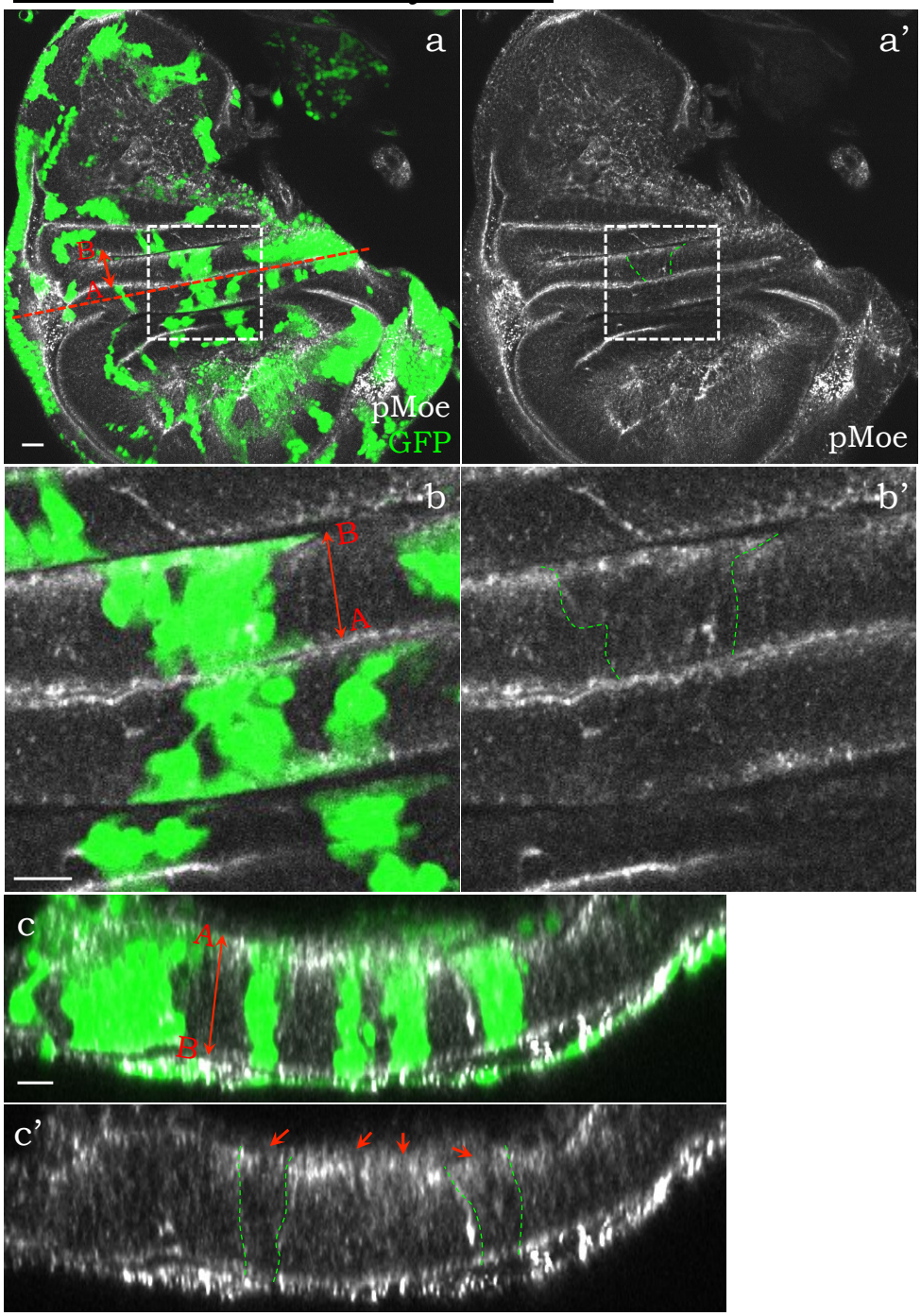

Figure 4.22: **The *ptc-GAL4*-driven overexpression of *frazzled* reduces pMoe in basolateral regions of the DP.** (a-a') The *ptc>fra,GFP* wing disc (GFP shown in green) immunostained for pMoe (grayscale). A dashed line (a) indicates the cross section depicted in c-c'. (b-b') Magnified area marked with dashed boxes (a-a'). (c-c') Cross-sectional view of the DP. The basally polarized pMoe is slightly reduced in the *ptc*-expression cells (bordered by green dashed lines (a', b', c'); (the quantification see in Figure 4.23). Scale bars 10 μm.

ptc>fra,GFP

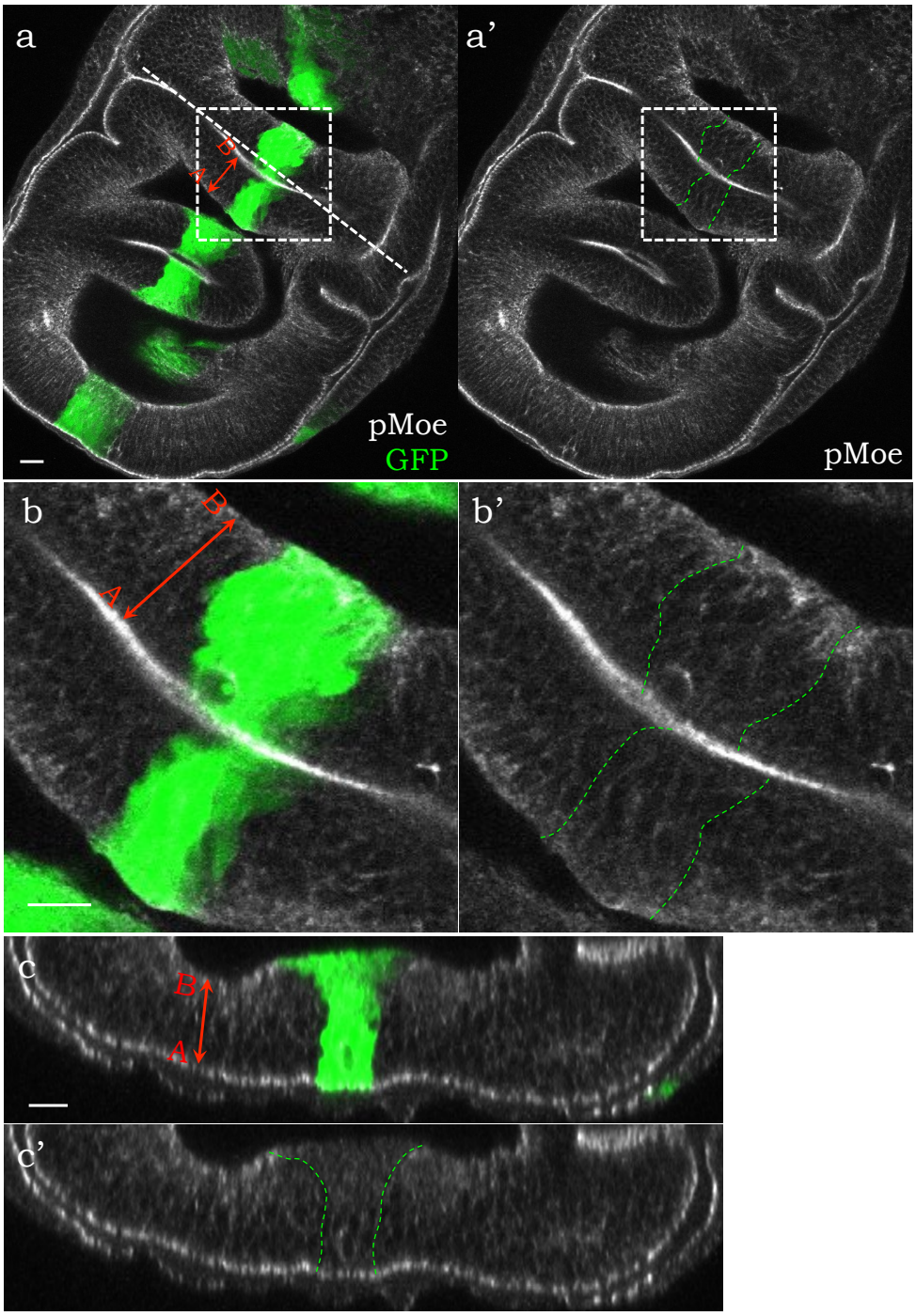

Figure 4.23: **Overexpression of *frazzled* reduces pMoe expression in the DP cells.** Mean intensity rates of pMoe staining in *ptc*-expression pattern relative to adjacent non-GFP areas in *ptc>fra,GFP* (*fra*; n=5) wing discs compared to *ptc>GFP* wing discs (*Control*; n=4). The mean intensity ratio significantly decreased from 1.07±0.04 in control down to 0.93±0.02 in *fra* discs (p=0.0025 by Student's t-test). Error bars equal to s.e.m.

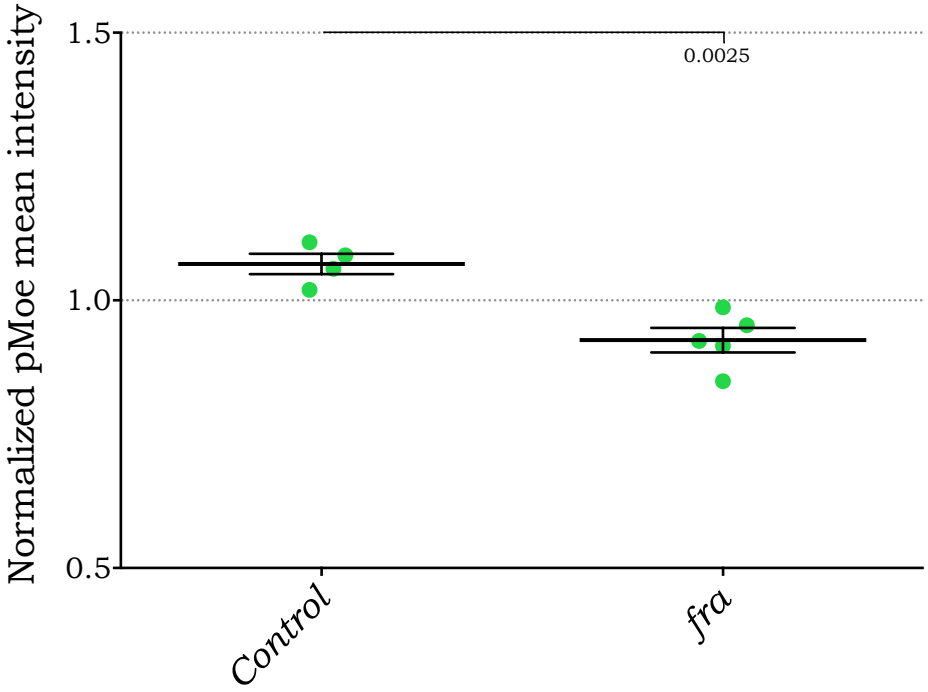
Normalized pMoe mean intensity
1.5
1.0
0.5
0.0025
Control
fra

Figure 4.24: **Changes in Conu expression were not detected in the DP cells overexpressing *frazzled*.** (a-a') The *FLP/+; Act5C:CD2:GAL4/UAS-fra,UAS-GFP* wing disc (GFP shown in green) immunostained for Conu (grayscale). A dashed line (a) indicates the cross section depicted in c-c'. (b-b') Magnified area marked with dashed boxes (a-a'). (c-c') Cross-sectional view of the DP. Conu puncta are distributed in the cytoplasm with a slight accumulation at the basal and apical sides in the GFP-positive (bordered by green dashed lines (a', b', c')) as well as non-GFP DP cells. Scale bars 10 μm.

FLP; Act5C:CD2:GAL4, fra, GFP

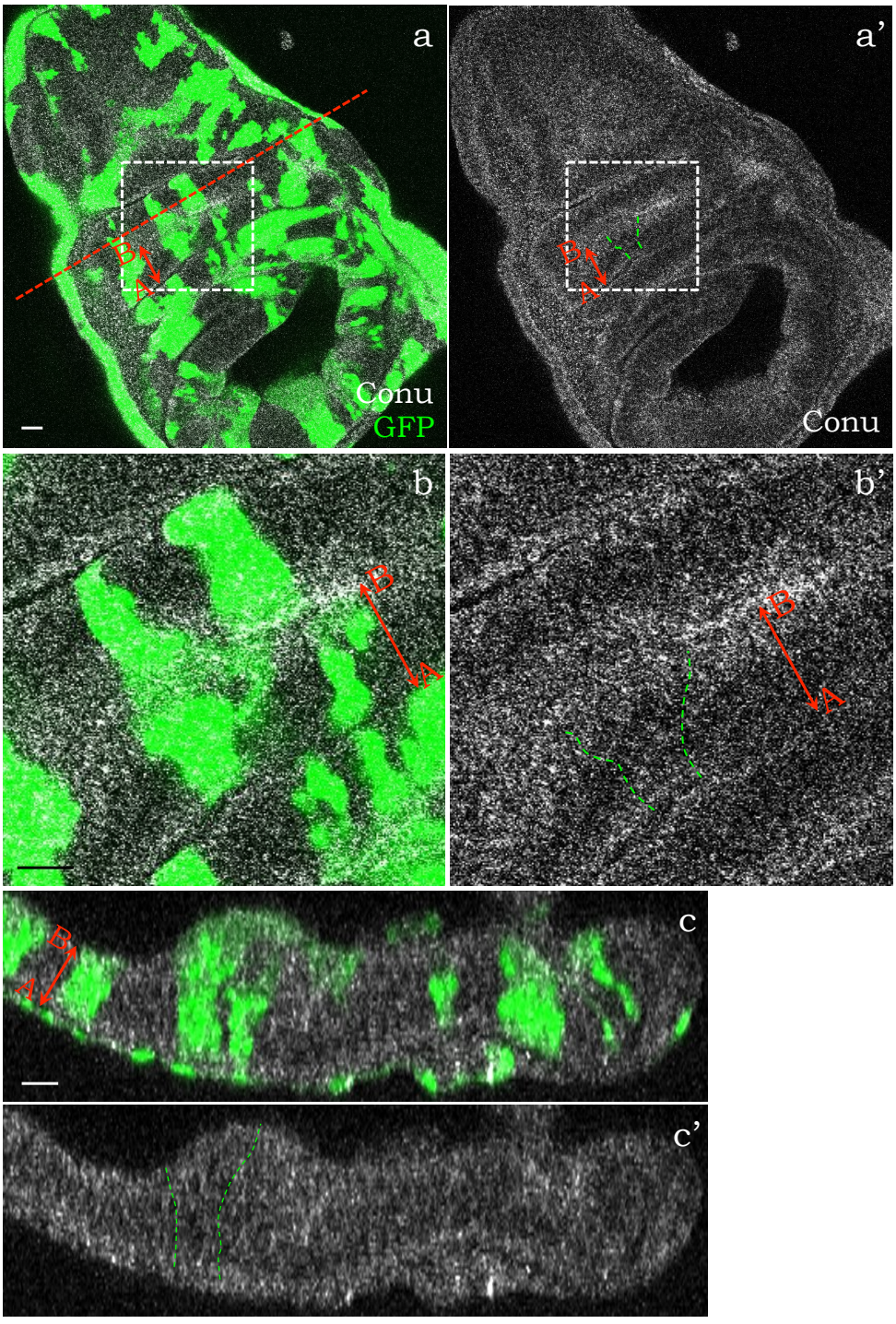

CHAPTER 5

Functional analysis of Frazzled intracellular domains

5.1 Introduction

5.1.1 Functions of intracellular domains of Frazzled

Transmission of Netrin chemoattractive signals in growing axons strongly depends upon the cytoplasmic region of Frazzled/DCC/UNC-40 receptors (Round and Stein, 2007 [312]). Intracellularly, all DCC family receptors contain three conserved amino acid motifs: P1, P2 and P3 (Kolodziej *et al.*, 1996 [135]; Figure 1.5). These motifs are required for the dimerization of the receptor and for crosstalk with other transmembrane receptors, and are also able to modulate the activity of extensive signaling complexes (reviewed by Guan and Rao, 2003 [313]). One study of a *C. elegans* UNC-40 gain-of-function phenotype showed that the P1 and P2 motifs, but not the P3, are required for excessive outgrowth, misguidance, branching, and deformed cell bodies of mechanosensory and motor neurons (Gitai *et al.*, 2003 [279]). Further analysis indicated that both the P1 and P2 motifs promote actin rearrangements but the P1 acts through the recruitment of Unc-34/Enabled, whereas the P2 acts via the activation of Ced-10/Rac1 and Unc-115 (an actin-binding protein) (Gitai

et al., 2003 [279]). *Drosophila* Ena and Trio, a Rac1 GEF, as well as the vertebrate Rac1 can also be activated by Frazzled/DCC during attractive midline axon guidance, but specific requirements of the cytoplasmic motifs have not been investigated (Shekarabi and Kennedy, 2002 [122]; Li *et al.*, 2002 [198]; Forsthoefel *et al.*, 2005 [238]). Besides the regulation of Ena, a distinct role for the P1 motif in axonal outgrowth and attraction may also rely upon its ability to regulate translational machinery by interaction with the eIFs and small ribosomal subunits (Tcherkezian *et al.*, 2010 [314]). Another study found that the contribution of the P2 domain to Netrin-induced commissural axon pathfinding is partly due to its involvement in microtubule dynamics control (Qu *et al.*, 2013 [241]): both the P2 and the P3 motifs of DCC were reported to bind directly to TUBB3, a neuronal β-tubulin isotype III, which is known to be an essential factor mediating axon guidance during the CNS development (Poirier *et al.*, 2010 [315]).

DCC gain-of-function analysis in *Xenopus laevis* spinal cord neurons indicated that the P3 motif is required for growth cone attraction to Netrin-1 (Stein *et al.*, 2001 [138]). Moreover, later studies proposed a mechanism whereby Rac1 is activated in response to Netrin-1-mediated phosphorylation of the Y1418 site of the P3 by Fyn/Src tyrosine kinases and recruitment of FAK (Li *et al.*, 2004 [202]; Liu *et al.*, 2004 [316]; Meriane *et al.*, 2004 [317]; Ren *et al.*, 2004 [242]). A structure function analysis of *Drosophila* Frazzled also confirmed the necessity of the Frazzled P3 motif for axon guidance: expression of *frazzled* transgenes could reconstitute the ability of *frazzled*-deficient commissural neurons to cross the midline, but only if the P3 motif was present (Garbe *et al.*, 2007 [139]). However, the authors determined that the LD site for binding FAK was not critical for Frazzled-mediated attraction to Netrins (Garbe *et al.*, 2007 [139]). Tyrosine phosphorylation of Frazzled does not seem to play an essential role in axon guidance in *Drosophila* (or in *C. elegans*) since the tyrosine residue in DCC is not conserved in its fly and worm orthologs and *frazzled* transgenes in which all 9 cytoplasmic Tyrosines are mutated to Phenylalanine can still rescue loss of function phenotypes (Garbe *et al.*, 2007 [139]; O'Donnell and Bashaw, 2013b [318]). One of the explanations for this discrepancy between DCC,

Frazzled and UNC-40 is that differences in the molecular mechanisms acting downstream of the receptors during Netrin-mediated attraction may have evolved between the species. Alternatively, the output of Netrin signaling may vary, depending on cell type or the extracellular environment (O'Donnell and Bashaw, 2013 [318]).

Another function of the P3 motif in promoting DCC-mediated attractive signals in vertebrates is the regulation of the activity of Myosin-X, an unconventional myosin required for establishment of cell polarity, adhesion and for formation of protrusive structures (Breshears *et al.*, 2010 [319]; Kerber and Cheney, 2011 [320]). An interaction of the FERM-domain of Myosin-X with the P3 motif recruits DCC to the tips of neurites growth cones, where the receptor regulates Myosin-X-mediated formation and elongation of basal filopodia (Zhu *et al.*, 2007 [321]). Further investigations suggested that DCC enhances the ability of Myosin-X to transport adhesion molecules (e.g. integrins) or actin-binding molecules (e.g. VASP) needed for extension of filopodial tips (Liu *et al.*, 2012 [322]). Whether a *Drosophila* isoform of Myosin-X (known as Myosin XV or Sisyphus; Liu *et al.*, 2008 [323]) is able to interact with Frazzled has not been elucidated, but it was shown that the P3 motif of *Drosophila* Frazzled is involved in the activation of another member of the myosin family, non-muscle myosin II (Dorsten *et al.*, 2007 [243]). Myosin II is a major contractile protein required for changing cell shape, cell adhesion, polarity and migration (Vicente-Manzanares *et al.*, 2009 [324]). Expression of *UAS-frazzled* alone or together with *UAS-ctMLCK* (coding an activated form of MLCK) strongly enhanced axonal projections crossing the midline incorrectly in ftz_{ng}>$Rho1^{v14}$ neurons (expressing an activated form of Rho1). The frequency of $Rho1^{v14}$-associated abnormal crossovers could be significantly reduced by expression of the *UAS-*sqh^{AA} (a mutated form of *spaghetti squash*, the regulatory light chain of *Drosophila* myosin II) as well as by expression of a *frazzled* transgene lacking the P3 motif. Similarly, the penetrance of crossover defects in ftz_{ng}>$Rho1^{v14}$*;frazzled* neurons could be increased by co-expression of a constitutively activated form of Abl kinase (Bcr^{210}-Abl), but the deletion of the P3 motif completely abolished this effect (Dorsten *et al.*, 2007 [243]). The authors speculated that the P3 motif of Frazzled controls

the ability of axons to cross the midline through the initiation of Rho1- and Abl-mediated myosin II activity (Dorsten *et al.*, 2007 [243]). With respect to Abl, there are several lines of evidence that Frazzled interacts with this tyrosine kinase and that it contributes to attractive axon guidance. However the specific requirement of a particular cytoplasmic domain for this interaction has not been clearly shown (Forsthoefel *et al.*, 2005 [238]; Dorsten *et al.*, 2007 [243]; Dorsten *et al.*, 2010 [239]). There is a possibility that Abl phosphorylates one of the tyrosine residues in a region between the P-motifs (Dorsten *et al.*, 2010 [239]).

The P3 motif is also thought to be critical for both self-association and interaction with the other receptors (e.g. Unc5 or Robo; Stein and Tessier-Lavigne, 2001 [143]; Stein *et al.*, 2001 [138]). However, in *Drosophila* the multimerization of Frazzled may not necessarily depend on the P3 motif (Garbe *et al.*, 2007 [139]).

5.1.2 This chapter

In this chapter I attempt to identify which Frazzled cytoplasmic domains are required for the *frazzled* overexpression phenotypes shown in previous chapters, namely: i) wing disc eversion defects in adult flies; ii) loss of basolateral DE-Cad; iii) increased protrusive membrane activity and iv) tissue invagination in the DP. To do this I conducted a structure function analysis using the *MYC*-tagged *frazzled* transgenes constructed by Garbe and colleagues (i.e. *UAS-fraFL-MYC* (full-length *frazzled*), (*UAS-fra*Δ*P1-MYC*, *UAS-fra*Δ*P2-MYC*, *UAS-fra*Δ*P1*Δ*P2-MYC*, *UAS-fra*Δ*P3-MYC* and *UAS-fra*Δ*P3.5-MYC*; Garbe *et al.*, 2007 [139]; Figures 5.1 and 5.16). This study will allow us to understand whether the adult eversion phenotype is associated with particular cellular phenotypes and whether the cellular phenotypes have the same requirements in terms of the P domains, and would therefore be likely to share the same molecular pathways. Note that the expression levels of these constructs has previously been reported to be similar, based on studies using the neuronal driver *elav-GAL4* (Garbe *et al.*, 2007 [139]) and this is borne out by MYC immunostaining in wing discs (this study - see below). Hence it is likely that the phenotypic differences that I observe are due to the different P-motif deletions

and not significant differences in expression levels.

5.2 Results

5.2.1 The P1 and P3 motifs of Frazzled are necessary for eversion failure in adult flies

As a first step in the Frazzled structural analysis, I confirmed that overexpression of a *MYC*-tagged full-length *frazzled* transgene (*fraFL*) resulted in eversion failures in adult flies. The *Ubx-GAL4*-driven expression of *UAS-fraFL-MYC* transgene, resulted in 8.3% of progeny having uneverted wings, and 9.2% displaying thoracic clefts (n=120; Figure 5.2, Table 5.1), and 13.3% lethality at pupal stages. This result confirms that the *MYC*-tagged *frazzled* can block eversion as efficiently as the normal *frazzled* transgene used previously (Manhire-Heath *et al.*, 2013 [133]).

Next, I tested how wing disc eversion was affected by peripodial overexpression of *MYC*-tagged *frazzled* transgenes lacking one of the intracellular P-motifs. Interestingly, only a version of Frazzled lacking the P2 motif (*UAS-fra*Δ*P2-MYC*) produced eversion phenotypes (Figure 5.2, Table 5.1), though the penetrance was only 5% (n=244). Of the adults expressing *UAS-fra*Δ*P2-MYC*, 0.8% of flies had a missing wing while 1.6% displayed defects in thorax formation. 2.5% of progeny were found lethal at pupal stages. Expression of *MYC*-tagged *frazzled* transgenes lacking either the P1 or P3 motif or a half of P3 motif (*UAS-fra*Δ*P1-MYC*, *UAS-fra*Δ*P3-MYC*, *UAS-fra*Δ*P3.5-MYC*) did not produce any eversion failure in adults (n=110, n=278, n=299 respectively). Also, expression of a transgene lacking both P1 and P2 domains (*UAS-fra*Δ*P1*Δ*P2-MYC*) did not result in eversion defects (n=396). Thus, transgenes lacking either the P1 or P3 motifs are unable to produce overexpression eversion phenotype in adults, suggesting that both the P1 and P3 motifs are necessary for eversion failure during wing development.

5.2.2 Role of P-motifs in producing *frazzled* overexpression cellular phenotypes

As demonstrated in Chapter 4, clonal overexpression of the wild type *frazzled* in wing disc epithelia induces multiple molecular and morphological changes such as: i) formation of extensive protrusions (in spite of the epithelial state of cells); ii) reduction of junctional proteins, DE-Cad and Armadillo, from the basolateral regions of the cell; and iii) cell shape changes. To determine the requirements of Frazzled P-motifs in these processes, all the *MYC*-tagged *frazzled* transgenes were clonally expressed in larval tissues using the heat shock induced flip-out of the *Act5C-FRT-CD2-FRT-GAL4* cassette (hereafter *Act5C:CD2:GAL4*).

5.2.2.1 The P3 motif of Frazzled is required for formation of protrusions in wing disc epithelial cells

I first examined the localisation of the Frazzled-MYC proteins using anti-MYC immunostaining. In DP cells, each version of the MYC-tagged Frazzled receptor was mostly accumulated basally and apically near the cell cortex (Figure 5.3, g'-i'). In both wing disc epithelia, DP and PE, the largest accumulation of MYC expression was observed on the basal side (Figure 5.3, g', arrow). A small amount of staining was also detected on the lateral membranes and as puncta within the cytoplasmic region (Figure 5.3, h', arrowheads). The anti-MYC immunostaining also strongly localised to the extensive protrusions that ectopic Frazzled produced, which allowed me to assess the role of individual P-motifs in protrusion formation. As was mentioned before, overexpression of *MYC*-tagged full-length *frazzled* produces long protrusions with apparently random orientations (Figure 5.4). Interestingly, these cellular protrusions were found not only in the clones of PE cells, but also on the basal side of DP cells (Figure 5.4, b', e', arrows).

Extensive protrusions in the PE and DP clones were also caused by overexpression of *MYC*-tagged *frazzled* with the individual or combined deletion of the P1 and P2 motifs (*fra*Δ*P1-MYC*, *fra*Δ*P2-MYC* or *fra*Δ*P1*Δ*P2-MYC*; Figure 5.4, a, a'-c, c',

arrows). However, the quantification analysis of basal DP protrusions in *ptc-GAL4* wing discs (Figure 5.5, f) revealed that average length of protrusions produced by expression of the *ptc>fra*Δ*P1-MYC* is slightly shorter than in *ptc>fraFL-MYC* cells: 6.69±0.49 and 8.08±0.4 μm respectively (p=0.0046; hereafter this and all other p-values in this chapter are based on a two-tailed Student's t-test). The *ptc>fra*Δ*P2-MYC* and *ptc>fra*Δ*P1*Δ*P2-MYC* wing discs displayed protrusions whose length was not significantly different from *fraFL-MYC*: 8.72±0.85 and 7.37±1.05 μm respectively (p>0.05). In contrast, expression of *UAS-fra*Δ*P3-MYC* resulted in noticeably shorter protrusions in FLP-out clones (Figure 5.4, d, d', arrowheads). The *ptc>fra*Δ*P3-MYC* DP cells also showed a substantial reduction in the length of protrusions down to 4.11±0.17 μm (p<0.0001 compared to both *ptc>fraFL-MYC* and *ptc>fra*Δ*P1-MYC*; Figure 5.5, f). Thus, these data suggest that the P2 motif is not required for the formation of membrane extensions in epithelial cells, whereas the P1 and P3 motifs are with the P3 domain being most important. Since both these motifs were required to block eversion, the results suggest that the formation of protrusions is a likely factor explaining the eversion defects associated with *frazzled* overexpression.

5.2.2.2 Each of three P-motifs of Frazzled is necessary for delocalisation of DE-Cad from the basolateral regions of disc proper cells

As expected, the overexpression of *fraFL-MYC* caused strong delocalisation of DE-Cad and Arm, from the basal and lateral sides of DP cells (Figures 5.6 and 5.7). Somewhat reduced DE-Cad and Arm staining could also be observed in the cytoplasmic area between the basal side and the AJ (Figures 5.6 and 5.7, b', c', arrows). As in Chapter 4, the intense DE-Cad and Arm signal at ZAs, made any changes in ZAs difficult to detect.

Surprisingly, clonal overexpression of *frazzled* transgenes lacking any of individual P-motifs (i.e. *UAS-fra*Δ*P1-MYC*, *UAS-fra*Δ*P2-MYC* and *UAS-fra*Δ*P3-MYC*) had no obvious affect on DE-Cad levels or localisation in DP cells or PE cells (Figure 5.8). The results suggest that only full length Frazzled has the ability to cause the

mislocalization of DE-Cad. Thus, given that only full length Frazzled was able to robustly cause eversion defects it raises the possibility that the eversion phenotypes may be related to changes in DE-Cad trafficking.

To quantify the reduction in non-junctional pools of DE-Cad in DP cells, I again used *ptc-GAL4*-driven expression of the *MYC*-tagged *frazzled* transgenes. As in Chapter 4, I measured the ratio of DE-Cad intensity in the *ptc*-expression zone versus the adjacent areas (see Materials and Methods, Figure 2.4), and then compared the results with calculations for control *ptc>GFP* wing discs (Figure 5.15, a). The *ptc*-driven expression of the *MYC*-tagged *fraFL* transgene caused significant loss of DE-Cad from basal and lateral sides of DP cells from 1.08±0.05 down to 0.94±0.05 (p=0.0043; Figure 5.9). Expression of any of the *frazzled* P-motif deletion transgenes did not show a significant difference from controls (p>0.2; Figures 5.10 and 5.15, a). Again, the results support the idea that Frazzled can regulate the localisation of junctional proteins in the cell compartment below the ZA line.

5.2.2.3 Both P1 and P3 motifs of Frazzled are required for basal expansion of disc proper cells

I next gave my attention to the effect of basal expansion in wing disc epithelia caused by overexpression of *frazzled*. Clonal overexpression of the *UAS-fraFL-MYC* in DP cells results in an expansion of the basal side of the epithelial cells (Figure 5.11, b-c). Often, one can also observe furrows or folds on the apical surface of the clone area indicating a tissue contraction event (Figure 5.11, b-c, arrows). Thus, I speculate that the basal expansion is likely due to a tissue invagination process. The invaginations were also apparent in the *ptc>fraFL-MYC* discs (Figure 5.13, b). Moreover, one could see a distinct furrow generated along a whole stripe of *frazzled* overexpression which was never seen in control *ptc>GFP* wing discs (Figure 5.14, a-b).

Clonal overexpression of *fraΔP1-MYC* did not result in basal expansion or apical contraction in DP cells (Figure 5.12, a), whereas the overexpression of *fraΔP2-MYC* did produce basal expansion combined with apical tissue folds similar to those seen

with full-length Frazzled (Figure 5.12, b). Overexpression of *UAS-fra*Δ*P1*Δ*P2-MYC* or *fra*Δ*P3-MYC* also promoted moderate basal expansion, though the severity of the phenotype was reduced (Figure 5.12, c, d; also see the quantification results in Figure 5.15, b). These results suggest that the tissue invagination mostly requires the P1 motif, whereas the P3 motif contributes to this process to a lesser degree.

The impact of each individual P-domain on the tissue invagination was also tested with the *ptc-GAL4*-driven expression of transgenes. To quantify the degree of basal expansion, I assessed the ratio of apical to basal length in the *ptc-GAL4*-expression area (see Material and Methods, Figure 2.4). Measurements for wing discs expressing *MYC*-tagged *frazzled* transgenes were compared to control *ptc>GFP* wing discs, in which the basal-apical ratio was equal to 0.88±0.09 (Figure 5.15, b). In *ptc>fraFL-MYC* discs the basal-apical ratio was increased to 1.63±0.11 ($p < 0.0001$ compared to *ptc>GFP*), whereas the ratio in *fra*Δ*P1-MYC* discs was not significantly different to control discs (0.95±0.13, $p > 0.3$; Figure 5.13, c, and Figure 5.14, c). The ratio in *fra*Δ*P2-MYC* discs was analogous to the *fraFL* phenotype (1.51±0.15; $p = 0.0001$ compared to *Control*, and $p > 0.2$ compared to the *fraFL*) (Figure 5.13, d, and Figure 5.14, d). Both *ptc>fra*ΔP1ΔP2-MYC and *ptc>fra*ΔP3-MYC wing discs had moderately increased basal-apical ratio (1.16±0.12 and 1.31±0.09 respectively), which was significantly higher than in *Control* ($p = 0.0038$ and $p = 0.0002$ respectively) but still significantly lower than in *fraFL* wing discs ($p = 0.0005$ and $p = 0.0048$ respectively), however furrows were not detected in any of the discs (Figure 5.13, e-f, and Figure 5.14, e-f). To sum up the observations, I suggest again that both the P1 and the P3 motifs of Frazzled play a role in the basal expansion of wing DP, however the contribution of the P1 to this process appears to be greater.

5.3 Discussion

In this chapter, I have demonstrated that both the P1 and P3 motifs are required for *frazzled* overexpression adult eversion phenotypes. By investigating the requirements of these motifs for the cellular overexpression phenotypes in the DP epithelium I

have also established that the tissue invagination phenotype is mostly dependent upon the P1 motif and, to a lesser degree, on the P3 motif, whereas the length of F-actin protrusions depends mostly on the P3 motif and slightly on the P1. These data also suggests that each P-motif contributes to the loss of DE-Cad from basolateral regions. The results and the final model are summarised in Figure 5.16.

5.3.1 *frazzled* overexpression eversion defects and reduction of basolateral DE-Cad are interrelated phenotypes

Both the P1 and P3 motifs are strongly required for the *frazzled* overexpression eversion phenotype as well as for DE-Cad redistribution from the basolateral cell side, whereas the P2 motif is also critical for DE-Cad redistribution, but contributes to eversion phenotypes to a lesser degree. These results suggest that control of DE-Cad localization is partly interconnected with the control of wing disc eversion. As discussed in the previous chapter, one likely possibility is that Frazzled might affect DE-Cad turnover, which supports the stability of intercellular adhesion in a changing environment. For example it is possible that basal-to-apical transport of DE-Cad is inhibited in cells overexpressing *frazzled*, whereas Rho1-dependent apical, endocytic transport of DE-Cad is reinforced. Such interruption of the balance between two DE-Cad traffic routes might lead to increased solidity of the ZA. If this were to occur in the PE, it would result in a delay of ZA breakdown during wing disc eversion. The results in Dorsten *et al.*, 2007 [243], which confirmed that the P3 motif of Frazzled regulates Rho1 activity, make this an attractive hypothesis for further testing. It is also possible that induction of a contractility pathway, in tissue overexpressing *frazzled*, might also contribute to ZA strengthening. For example, in MDCK cells AJs were strengthened due to E-Cadherin enrichment in response to elevated contractility (Choi *et al.*, 2016 [301]).

5.3.2 Tissue invagination is associated with eversion phenotypes, and is regulated independently of the delocalization of basolateral DE-Cad

Low penetrance eversion defects in *fra*Δ*P2* flies could originate from the tissue invagination phenotype. Indeed, the P2 motif does not seem to be involved in regulation of apico-basal morphology, whereas both the P1 and P3 motifs strongly contribute to this process. Given that the P2 motif is required for DE-Cad delocalization, the results suggest that tissue invagination and basolateral distribution of DE-Cad are produced by separate intracellular signals, but both processes are involved in the overall failure in eversion. The most critical upstream regulator of basal expansion appears to be the P1 motif. The P3 motif is also involved in this process, though its impact is slightly lower. The fact that *fra*Δ*P1*Δ*P2* epithelium remains more expanded at the basal side than the *fra*Δ*P1* epithelium may indicate that the deletion of both the P1 and P2 motifs is affecting the protein conformation, which is perhaps then affecting the ability of the P3 motif to control tissue invagination.

The most intriguing question is: what molecular mechanism is induced by the P1 and P3 motifs to promote epithelial invagination? In *Drosophila* axon growth cones, activity of non-muscle myosin II is has been shown to be regulated by both P1 and P3 motifs of Frazzled, however they function in opposite ways: the P1 motif has a repressive role in myosin II activation signaling, whereas the P3 motif should sustain myosin activity through a positive control of the upstream myosin regulator Rho1 (Dorsten *et al.*, 2007 [243]). Thus, how the P1 motif might contribute to invagination remains obscure.

5.3.3 Increased protrusion formation contributes to the eversion phenotype

Overexpression of full-length *frazzled* as well as the *frazzled* deletion transgenes results in prominent protrusions on the basal side of epithelium. As discussed in Chapter 4 and in the introduction to this chapter, Frazzled may activate Rac1, which is known to induce motile phenotypes in cells (Nobes and Hall, 1995 [217]). Formation of protrusions seem to play a role in promoting eversion failure, since significantly shorter protrusions were formed in *fra*Δ*P1* and *fra*Δ*P3* discs, where no eversion failure ensues. Overexpression of *UAS-fra*Δ*P3* transgene reduced the length of protrusions more strongly, consistent with previous reports where the P3 motif was critical for the growth cones attraction across the midline, whereas the other two P-motifs were dispensable (Garbe *et al.*, 2007 [139]). It is likely, that the length of formed protrusions depends on the ability of the P3 motif to activate non-muscle myosin, which is particularly involved in intra-filopodial elongation of F-actin filaments (Zhu *et al.*, 2007 [321]; Dorsten *et al.*, 2007 [243]; Breshears *et al.*, 2010 [319]; Kerber and Cheney, 2011 [320]; Liu *et al.*, 2008 [323]). The role of the P1 motif in protrusion formation could be associated with its likely ability to recruit Ena for cytoskeletal rearrangements, which was demonstrated for UNC40 (Gitai *et al.*, 2003 [279]). Ena protein is a well known actin anti-capping factor promoting actin-filament elongation during filopodium formation (Lebrand *et al.*, 2004 [325]; Barzik *et al.*, 2005 [326]).

5.3.4 Concluding remarks

Overall, the results suggest that the P1 and P3 motifs play the most essential role in *frazzled*-mediated maintenance of *Drosophila* epithelia. They seem to be involved in multiple cellular processes including cell adhesion and motility, and DE-Cad trafficking that together defines their essential role in wing disc eversion failure. These findings make the P1 and P3 motifs attractive for further, careful investigation of their molecular function in epithelia.

Table 5.1: **Adult wing disc eversion defects.**

All crosses performed at 25°C.

**v108577*

Genotype	No defects (%)	Eversion defects (%)	Early lethality (%)	Total (n)
+;+;Ubx-GAL4/+	100	0	0	214
+;UAS-netA.IR/+; Ubx-GAL4/+*	54	31	15	180
+;Df(2R)BSC880/UAS-netA.IR;Ubx-GAL4/+	86.5	12.5	1	89
fraFL-MYC/+;+;Ubx-GAL4/+	69.2	17.5	13.3	120
fraΔP1-MYC/+;+;Ubx-GAL4/+	100	0	0	110
fraΔP2-MYC/+;+;Ubx-GAL4/+	95.1	2.5	2.4	396
fraΔP1ΔP2-MYC/+;+;Ubx-GAL4/+	99.7	0.3	0	244
fraΔP3-MYC/+;+;Ubx-GAL4/+	99.7	0.3	0	278
fraΔP3.5-MYC/+;+;Ubx-GAL4/+	100	0	0	299

Figure 5.1: **Schematic representation of the Frazzled intracellular structure indicating conserved P-motifs.** Image is based on Garbe *et al.*, 2007 [139]. (a) Aminoacid sequence of the intracellular region of Frazzled. The P1, P2 and P3 motifs (indicated by red color; Kolodziej *et al.*, 1996 [135]) are deleted in the constructs shown in b. (b) Schematic diagram of the constructs designed by Garbe *et al.*, 2007 [139]. Each transgene contains a six-Myc epitope at its C-terminus. Ig, immunoglobulin. FN3, fibronectin type III.

a

1099 CRRKPQSSPEHTKKSYQKNNVGVPKPPDLWIHHDQMELKNIDKGLHTV **P1**
TPVCSDGASSSGALTLPRSVVHSEYEVETPVPGHVTNSLDKRSYVPGY
MTTSMNGTMERPQYPRTQYSHQNRSHMTMEAGLSQQSLTQPQSNSMAQ
TPEHPYGGYDANFCNAGNAAAGNGCVSTIESSKRGHPLKSFSVPGPPP **P2**
TGGATPVTKHTPAVTIRPQNQSPYKKPSFSAATPNRLQGGGSVVHSTD
EIQRLAPSTSTEELNQEMANLEGLMKDLSAITANEFEC **P3**

b

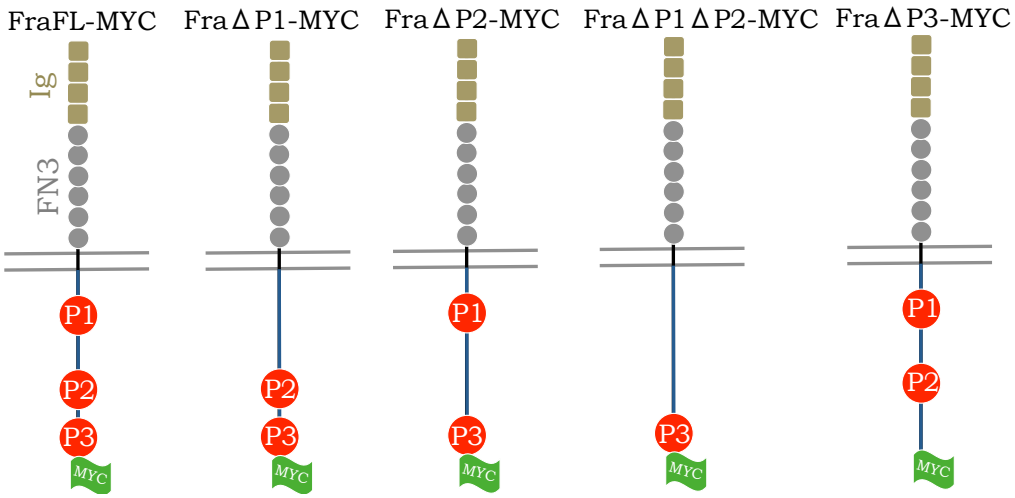

Figure 5.2: **The P1 and P3 motifs of Frazzled are required for eversion failure in adult flies.** Quantification of adult eversion phenotypes for *w1118/+;Ubx-GAL4/+* (*Control*; n=214), *UAS-fraFL-MYC/+;Ubx-GAL4/+* (*fraFL*; n=120), *UAS-fra*Δ*P1-MYC/+;Ubx-GAL4/+* (*fra*Δ*P1*; n=110), *UAS-fra*Δ*P2-MYC/+;Ubx-GAL4/+* (*fra*Δ*P2*; n=244), *UAS-fra*Δ*P1*Δ*P2-MYC/+;Ubx-GAL4/+* (*fra*Δ*P1*Δ*P2*; n=396), *UAS-fra*Δ*P3-MYC/+;Ubx-GAL4/+* (*fra*Δ*P3*; n=278), and *UAS-fra*Δ*P3.5-MYC/+;Ubx-GAL4/+* (*fra*Δ*P3.5* (deletion of a second half of the P3 motif; Garbe *et al.*, 2007 [139]); n=299) genotypes. Among *fraFL* progeny, 8.3% of flies had uneverted wings, and 9.2% had defects in thorax. Among *fra*Δ*P2*, 0.8% of flies had uneverted wings, and 1.6% had defects in thorax (two-tailed $p<0.0001$, by Fischer's exact test). The *fra*Δ*P1*Δ*P2*, *fra*Δ*P3* and *fra*Δ*P3.5* progeny was normal (two-tailed $p<0.0001$, by Fischer's exact test). Error bars show 95% CI of the proportion of normal progeny (by Wilson Score method).

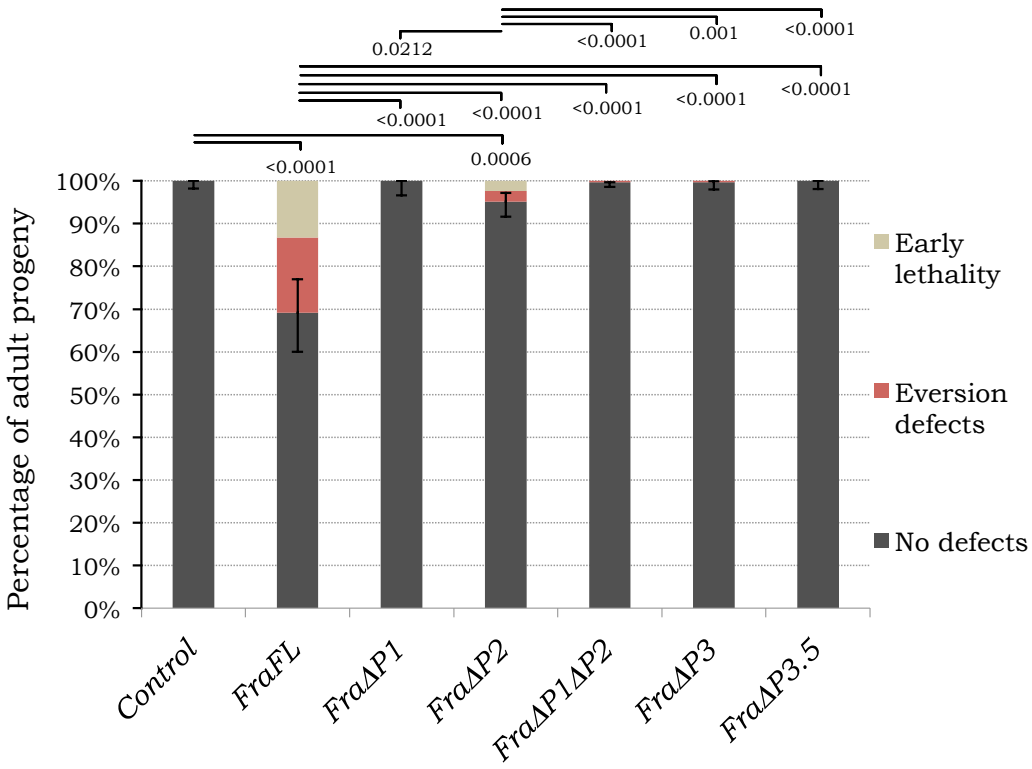
0.0212
<0.0001
0.001
<0.0001
<0.0001
<0.0001
<0.0001
<0.0001
<0.0001
<0.0001
0.0006
Percentage of adult progeny
100%
90%
80%
70%
60%
50%
40%
30%
20%
10%
0%
Early lethality
Eversion defects
No defects
Control
FraFL
FraΔP1
FraΔP2
FraΔP1ΔP2
FraΔP3
FraΔP3.5

Figure 5.3: **Overexpression of *fraFL-MYC* promotes cellular protrusions in the PE and the DP.** The *UAS-fraFL-MYC/FLP;Act5C:CD2:GAL4,UAS-GFP* wing disc with GFP-positive (green) *fraFL* clones stained for MYC (red (a-a', d-d', g-g') or grayscale (b-b', c-c', e-e', f-f', h-h', i-i')) and Rhodamine phalloidin (blue (a-a', d-d', g-g') or grayscale (b-b', c-c', e-e', f-f', h-h', i-i')). (a-c, a'-c') Maximum projections of the PE. Dashed boxes (a-c) indicate magnification areas depicted in a'-c' respectively. Anti-MYC antibodies (marking *fraFL* clones) were accumulated within the cytoplasm and in extended protrusions of the PE cells (b', arrows). (d-f, d'-f') Maximum projections of the DP. Dashed boxes (d-f) indicate magnification areas depicted in d'-f' respectively. Anti-MYC antibodies were accumulated within the cytoplasm and in extended protrusions of the DP cells (e', arrows). (g-i, g'-i') Cross-sectional view of the whole disc (indicated by a dashed line in a-c). Dashed boxes (g-i) indicate magnification areas depicted in g'-i' respectively. Anti-MYC antibodies were mostly accumulated at the basal side of the PE as well as the DP (nucleus (g', double-arrowhead) lies over the basal protrusions (g', arrow)). Much less anti-MYC antibodies were found on the apical and lateral surfaces (h', arrowheads). Hereafter the apical-basal (A-B) axis is marked by double-headed arrow (g-g'). Scale bars 10 μm.

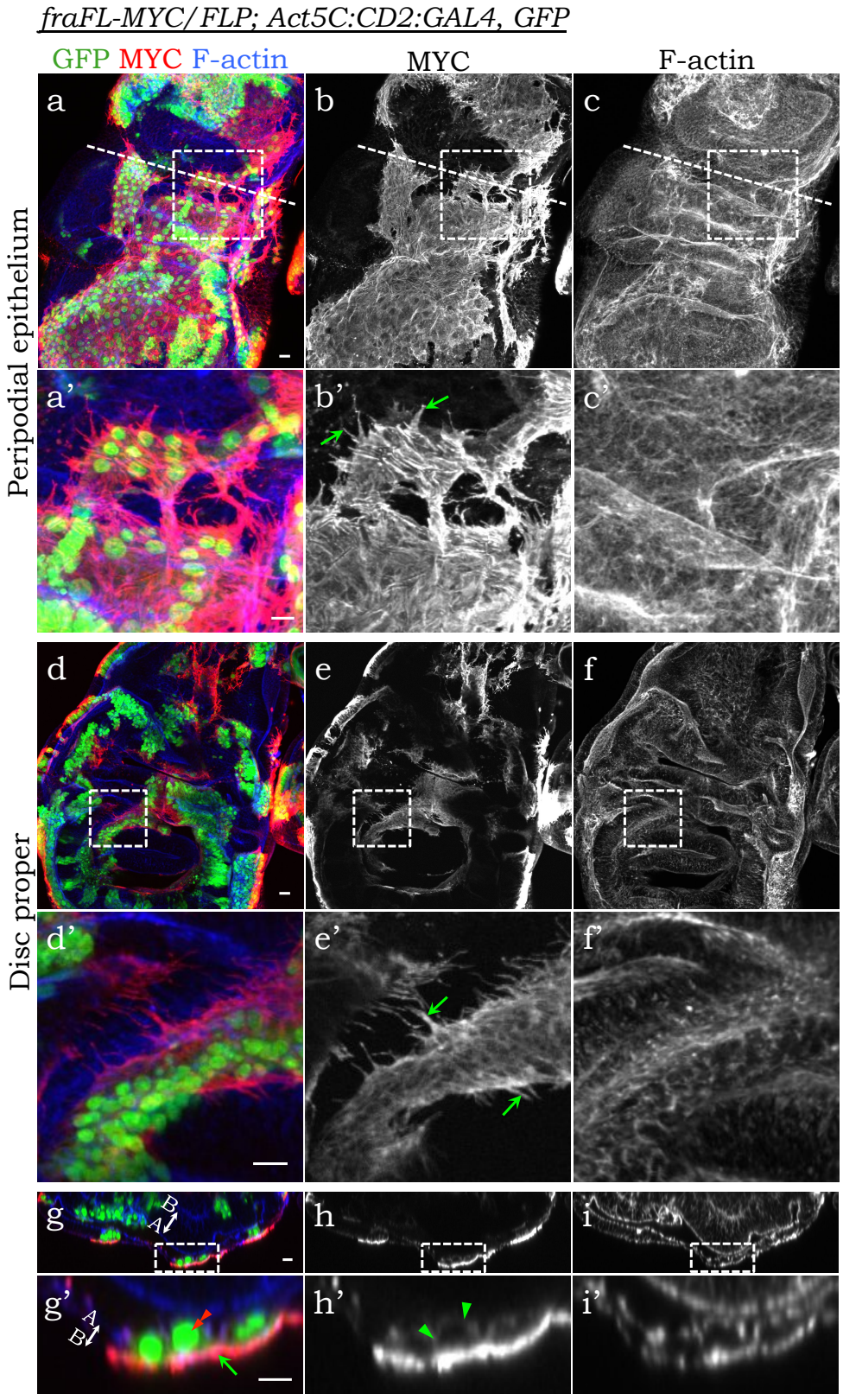
fraFL-MYC/FLP; Act5C:CD2:GAL4, GFP
GFP MYC F-actin
MYC
F-actin
Peripodial epithelium
Disc proper
a
b
c
a'
b'
c'
d
e
f
d'
e'
f'
g
h
i
g'
h'
i'
A
B

Figure 5.4: **The P3 motif is required for the induction of long protrusions by overexpression of *frazzled* transgenes.** Anti-MYC immunostaining (grayscale) of mosaic wing discs with clones expressing *frazzled*-deletion transgenes. (a-a') the DP (a) and the PE (a') of *UAS-fra*Δ*P1-MYC/FLP;Act5C:CD2:GAL4,UAS-GFP* wing disc. (b-b') the DP (b) and the PE (b') of *UAS-fra*Δ*P2-MYC/FLP;Act5C:CD2:GAL4,UAS-GFP* wing disc. (c-c') the DP (c) and the PE (c') of *UAS-fra*Δ*P1*Δ*P2-MYC/FLP;Act5C:CD2:GAL4,UAS-GFP* wing disc. Three genotypes were able to produce massive protrusions (arrows). (e-e') Fragments of the *UAS-fra*Δ*P3-MYC/FLP;Act5C:CD2:GAL4,UAS-GFP* DP (e) and the PE (e'). *fra*Δ*P3* clones extended much shorter protrusions (arrowheads). Scale bars 10 μm.

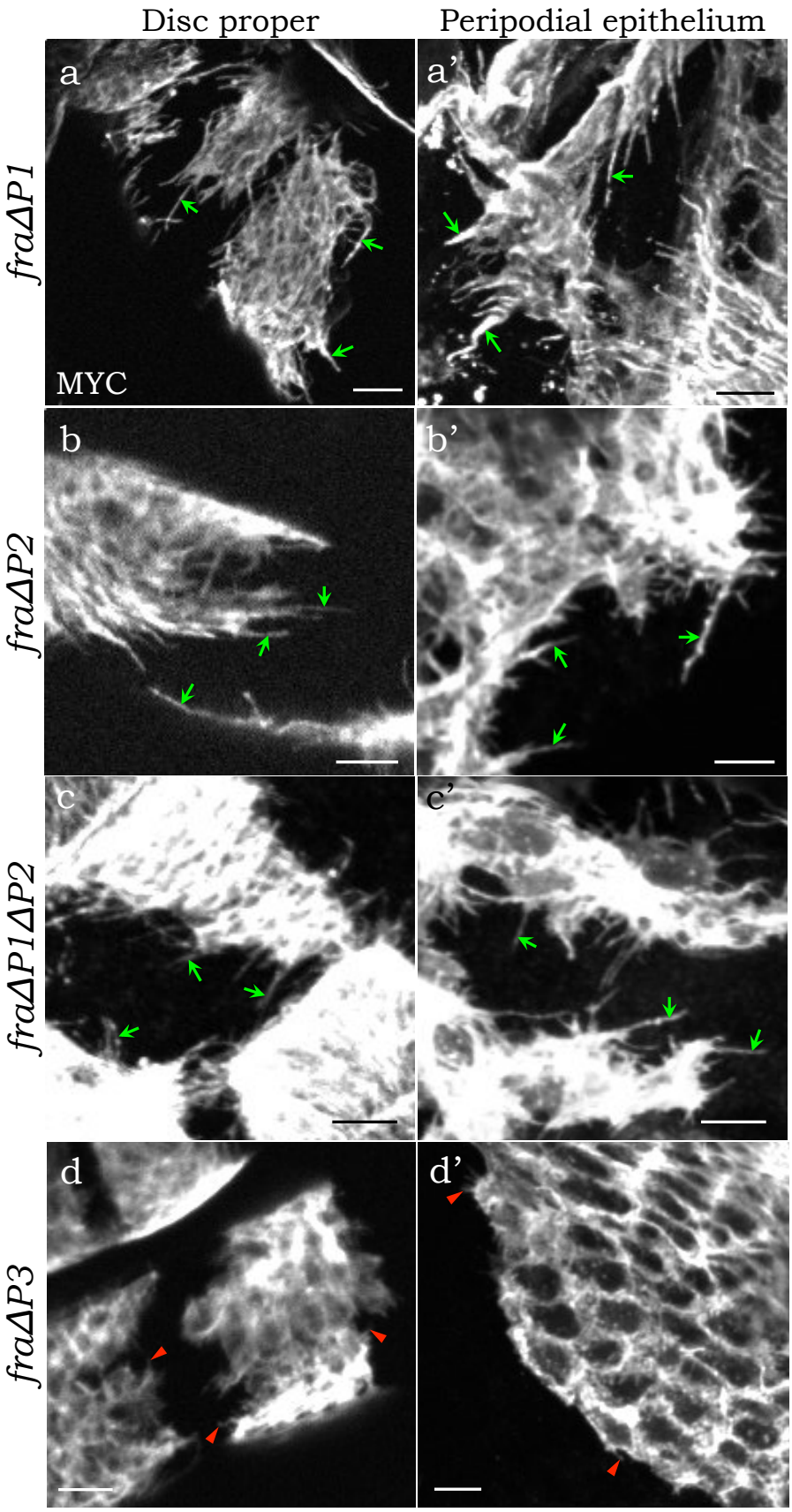
Disc proper
Peripodial epithelium
fraΔP1
fraΔP2
fraΔP1ΔP2
fraΔP3
a
a'
MYC
b
b'
c
c'
d
d'

Figure 5.5: ***ptc-GAL4*-driven expression of *fra*Δ*P1* and *fra*Δ*P3* produces shorter cellular protrusions in the DP compared to other *frazzled* transgenes.** (a-e) Basal protrusions of the DP stripe immunostained by MYC (grayscale). Average length of protrusions (arrows) was 8.08±0.4 μm for *ptc>fraFL-MYC* (n=4, a) and 6.69±0.49 μm for *ptc>fra*Δ*P1-MYC* (n=4, b), which were considered significantly different (p=0.0046). For *ptc>fra*Δ*P2-MYC* (n=4, c) and *ptc>fra*Δ*P1*Δ*P2-MYC* (n=5, d) wing discs, average length of protrusions was 8.72±0.85 μm and 7.37±1.05 μm respectively. These values did not differ significantly from the *ptc>fraFL-MYC* (p>0.05). The *ptc>fra*Δ*P3-MYC* expression (n=4, e) produced significantly shorter protrusions (arrowhead) of 4.11±0.17 μm (p<0.0001). (f) Scatter dot plots showing average length of protrusions, μm. *ptc*-driven combined expression of *fraFL-MYC* with *UAS-par6.IR* (n=5; see Chapter 6) produced basal protrusions as long as in *ptc>fraFL-MYC* DP: 7.68±0.39 μm (p>0.1). Error bars are represented as the mean±s.e.m. Two-tailed p-values based on the Students t-test are presented above the graph. Scale bars 10 μm.

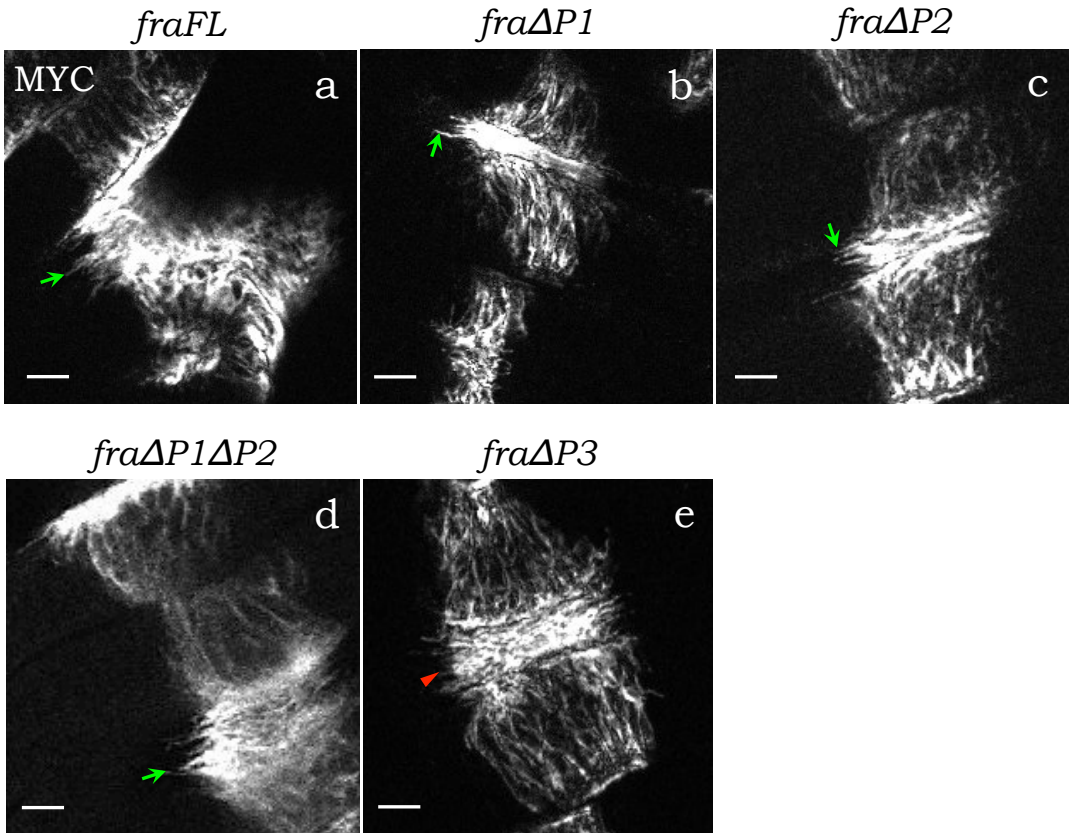
fraFL
fraΔP1
fraΔP2
MYC
a
b
c
fraΔP1ΔP2
fraΔP3
d
e

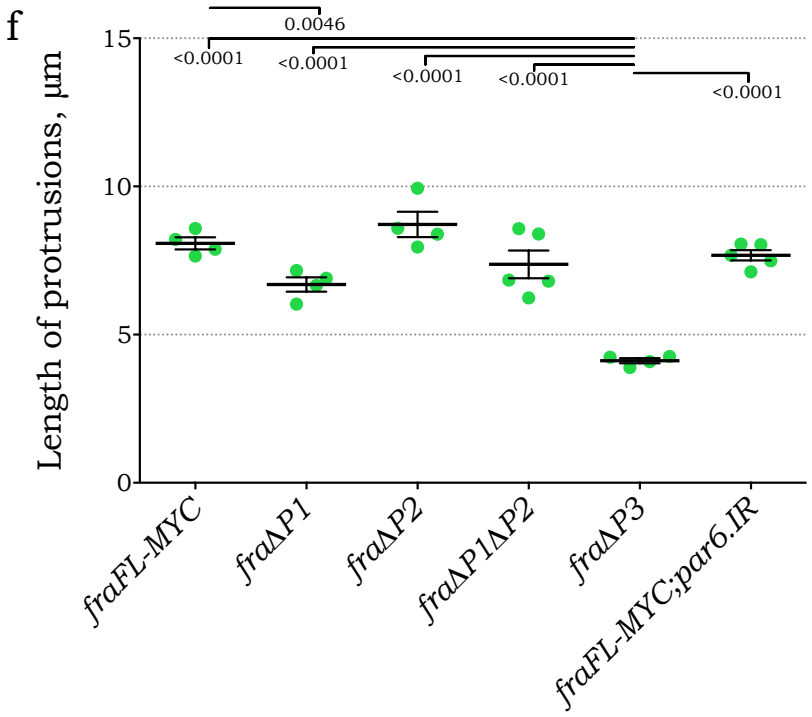
f
Length of protrusions, µm
15
10
5
0
0.0046
<0.0001
<0.0001
<0.0001
<0.0001
<0.0001
fraFL-MYC
fraΔP1
fraΔP2
fraΔP1ΔP2
fraΔP3
fraFL-MYC;par6.IR

Figure 5.6: **DE-Cad expression is reduced in basolateral regions of DP cells overexpressing *fraFL-MYC*.** (a-a') The *UAS-fraFL-MYC/FLP;Act5C:CD2:GAL4,UAS-GFP* wing disc (GFP shown in green) immunostained for DE-Cad (grayscale). A dashed line (a) indicates the cross section depicted in c-c'. (b-b') Magnified area marked with dashed boxes (a-a'). (c-c') Cross-sectional view of the DP. The non-GFP DP epithelium displays DE-Cad distributed at ZA (b', c', double-arrowheads), and on the basal (b', c', arrowheads) and lateral (b', c', arrows) sides of DP cells. The GFP-positive (green) DP epithelium (bordered by green dashed lines (a', b', c')) has reduced DE-Cad at the basal and lateral sides. Scale bars 10 μm.

fraFL-MYC/FLP; Act5C:CD2:GAL4, GFP

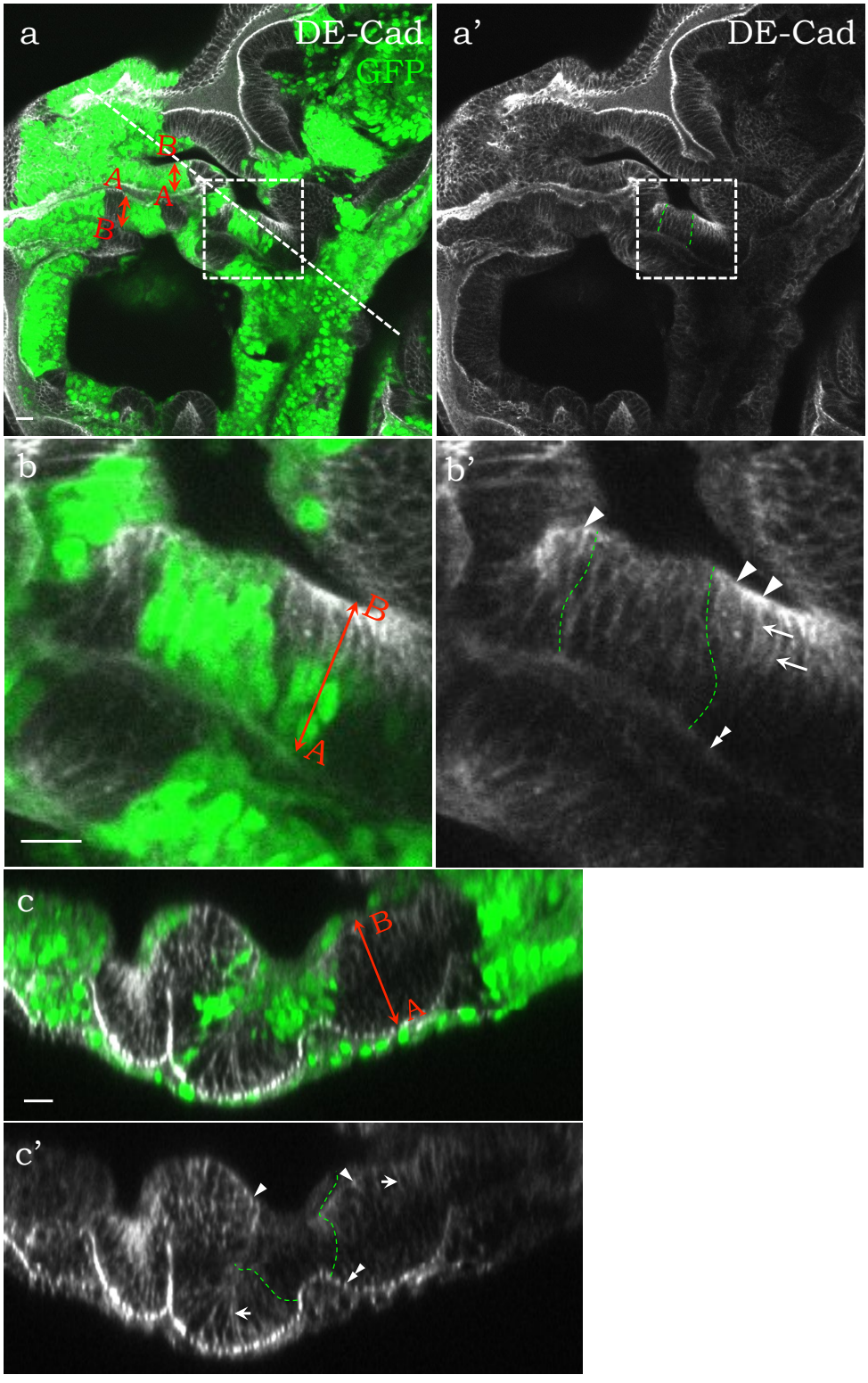

Figure 5.7: **Arm expression is reduced in basolateral regions of DP cells overexpressing *fraFL-MYC*.** (a-a') The *UAS-fraFL-MYC/FLP;Act5C:CD2:GAL4,UAS-GFP* wing disc (GFP shown in green) immunostained for Arm (grayscale). A dashed line (a) indicates the cross section depicted in c-c'. (b-b') Magnified area marked with dashed boxes (a-a'). (c-c') Cross-sectional view of the DP. The non-GFP DP epithelium displays Arm distributed at the ZA (b', c', double-arrowheads), and on the basal (b', c', arrowheads) and lateral (b', c', arrows) sides of DP cells. The GFP-positive (green) DP epithelium (bordered by green dashed lines (a', b', c')) has reduced Arm at the basal and lateral sides. Scale bars 10 μm.

fraFL-MYC/FLP; Act5C:CD2:GAL4, GFP

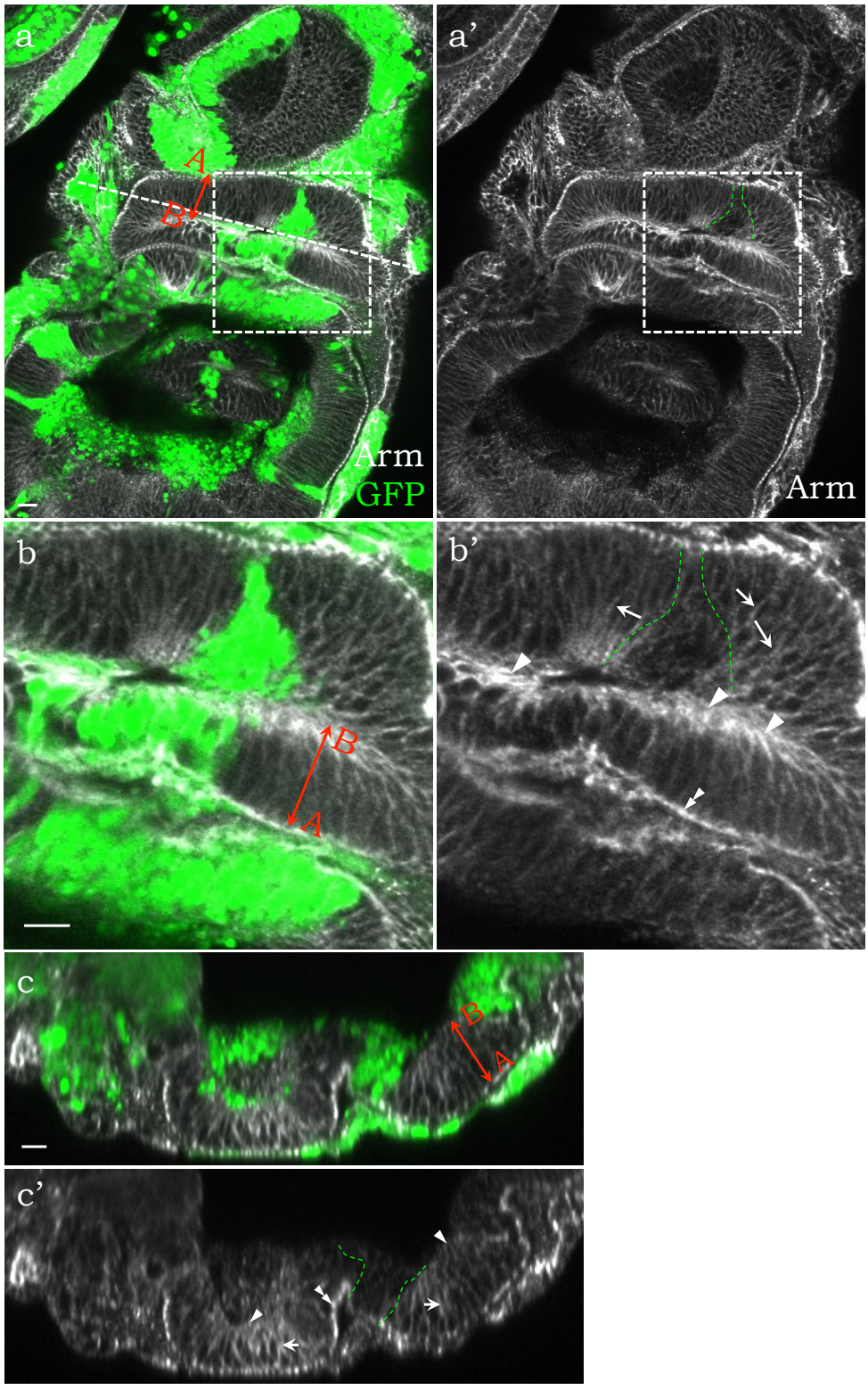

Figure 5.8: **Each P motif is required for delocalization of DE-Cad from basolateral side of the DP epithelium.** DE-Cad immunostaining (grayscale) of mosaic wing discs with GFP-positive (green) clones expressing *frazzled*-deletion transgenes. Dashed lines (a-d) indicate cross-sectional views displayed in a", a"' - d", d"' respectively. (a-a"') A fragment of the *UAS-fra*Δ*P1-MYC/FLP;Act5C:CD2:GAL4,UAS-GFP* DP. (b-b"') A fragment of the *UAS-fra*Δ*P2-MYC/FLP;Act5C:CD2:GAL4,UAS-GFP* DP. (c-c"') A fragment of the *UAS-fra*Δ*P1*Δ*P2-MYC/FLP;Act5C:CD2:GAL4,UAS-GFP* DP. (d-d"') A fragment of the *UAS-fra*Δ*P3-MYC/FLP;Act5C:CD2:GAL4,UAS-GFP* DP. DE-Cad seems unchanged in basolateral sides (arrowheads) and at the ZA (double-arrowheads) in all four genotypes. Scale bars 10 μm.

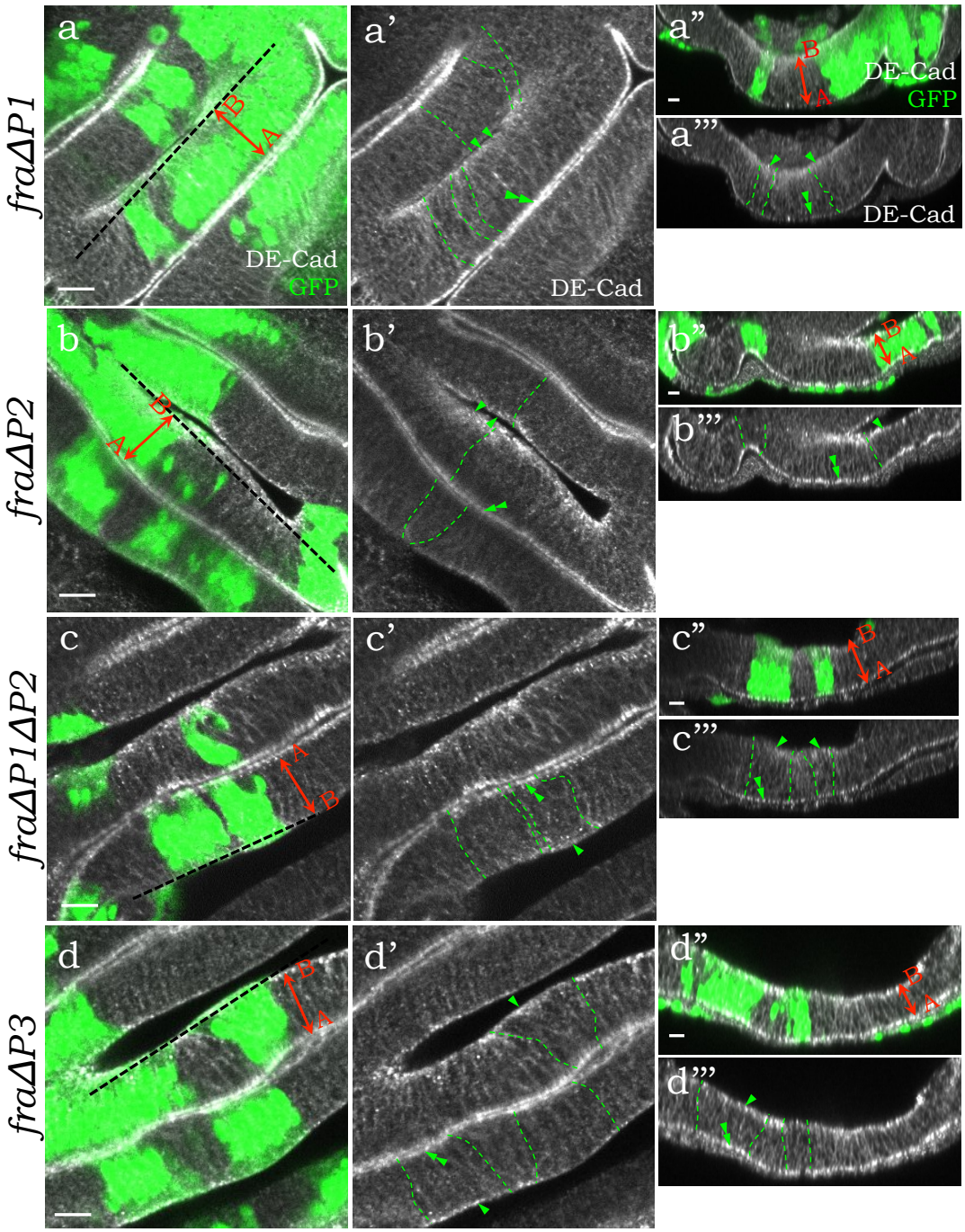
fraΔP1
fraΔP2
fraΔP1ΔP2
fraΔP3
a
a'
a"
a'''
b
b'
b"
b'''
c
c'
c"
c'''
d
d'
d"
d'''
DE-Cad
GFP
DE-Cad
DE-Cad
GFP
DE-Cad
A
B

Figure 5.9: ***ptc*-driven overexpression of *fraFL-MYC* reduces DE-Cad in basolateral regions of DP cells.** (a-a') The *ptc>fraFL-MYC,GFP* wing disc (GFP shown in green) immunostained for DE-Cad (grayscale). A dashed line (a) indicates the cross section depicted in c-c'. (b-b') Magnified area marked with dashed boxes (a-a'). (c-c') Cross-sectional view of the DP. The non-GFP epithelium displays DE-Cad distributed at the ZA (b', c', double-arrowheads), and on the basal (b', c', arrowheads) and lateral (b', c', arrows) sides of the DP cells. The *ptc*-pattern (green) (bordered by green dashed lines (a', b', c')) had significantly reduced DE-Cad at the basal and lateral sides (for quantification see Figure 5.15, a). Scale bars 10 μm.

ptc>fraFL-MYC

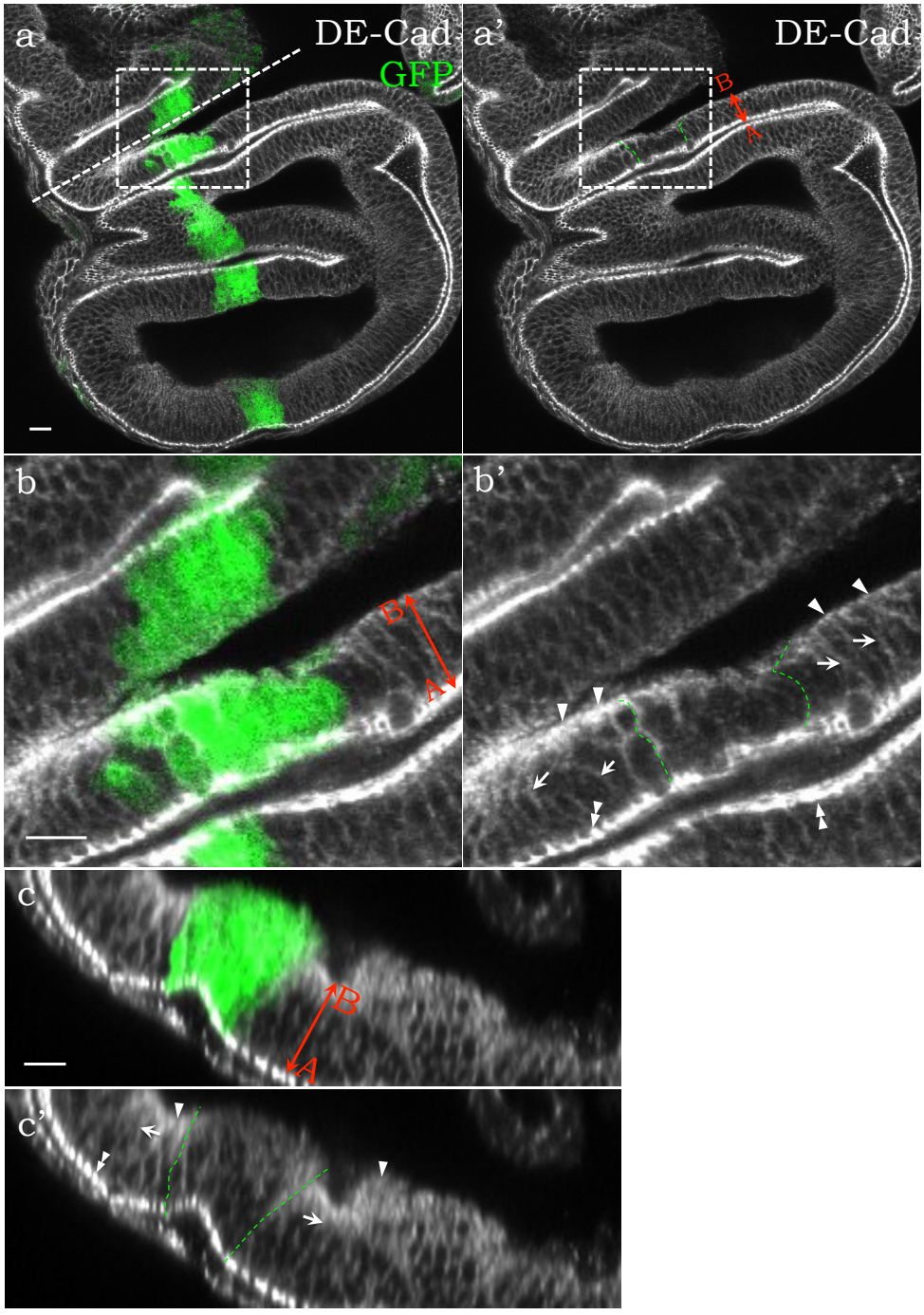

Figure 5.10: ***ptc*-driven overexpression of *frazzled*-deletion transgenes do not affect DE-Cad localization.** DE-Cad immunostaining (grayscale) of wing discs with *ptc*-driven expression of *frazzled*-deletion transgenes. *ptc*-expression pattern is GFP-positive (green). Dashed lines (a-d) indicate cross-sectional views displayed in a", a"' - d", d"' respectively. (a-a"') A fragment of the *ptc>fra*Δ*P1-MYC,GFP* DP. (b-b"') A fragment of the *ptc>fra*Δ*P2-MYC,GFP* DP. (c-c"') A fragment of the *ptc>fra*Δ*P1*Δ*P2-MYC,GFP* DP. (d-d"') A fragment of the *ptc>fra*Δ*P3-MYC,GFP* DP. DE-Cad is not significantly changed in basolateral sides (arrowheads) and at the ZA (double-arrowheads) in the *ptc*-expression patterns (bordered by green dashed lines) of all four genotypes (for quantification see in Figure 5.15, a). Scale bars 10 μm.

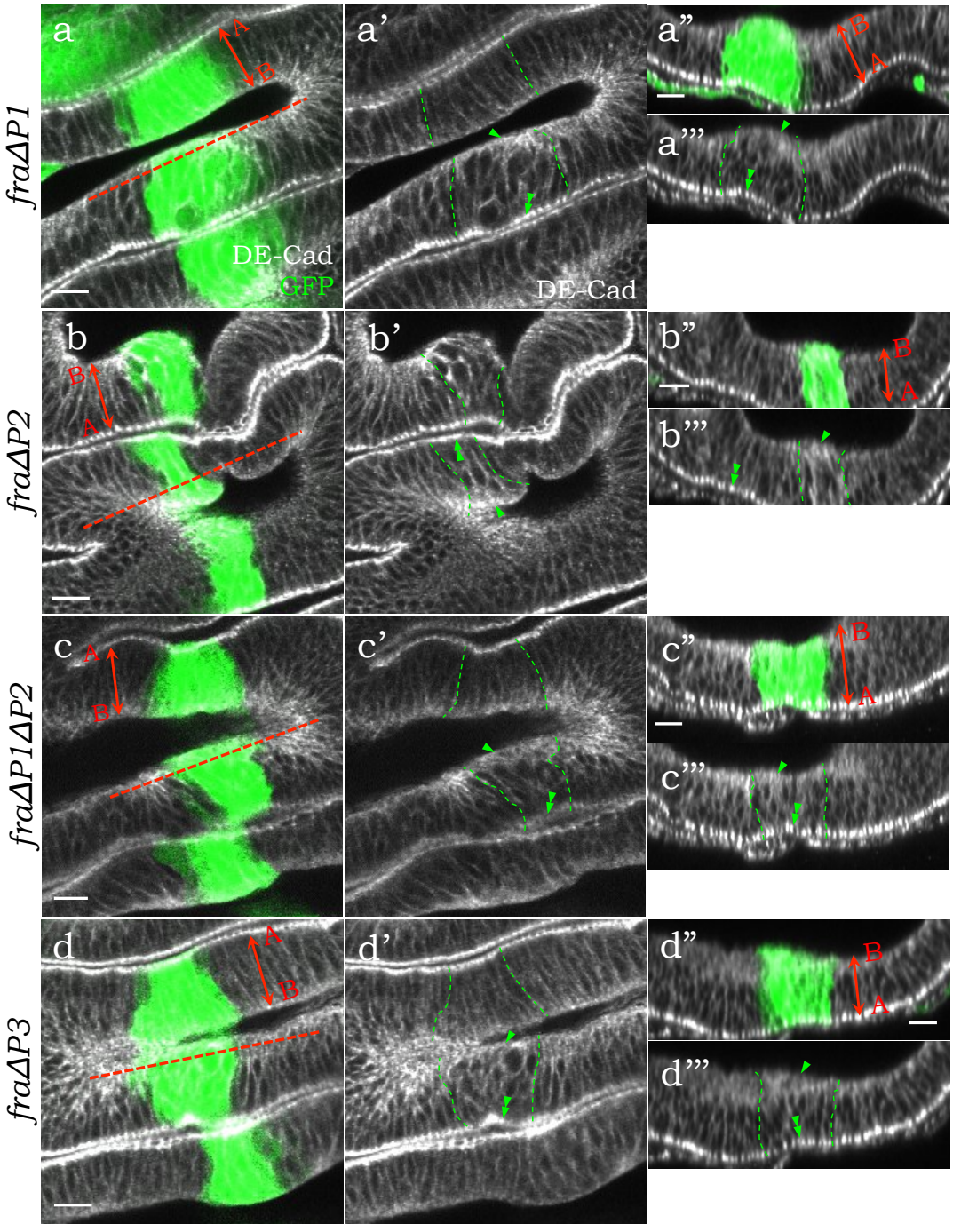
fraΔP1
fraΔP2
fraΔP1ΔP2
fraΔP3
a
a'
a"
a'''
b
b'
b"
b'''
c
c'
c"
c'''
d
d'
d"
d'''
A
B
DE-Cad
GFP
DE-Cad

Figure 5.11: **Overexpression of *fraFL-MYC* causes basal expansion of the epithelium.** (a) The *UAS-fraFL-MYC/FLP;Act5C:CD2:GAL4,UAS-GFP* wing disc (GFP shown in green) immunostained for DE-Cad (grayscale). A dashed line indicates the cross-sectional view depicted in c. (b) Magnified area marked with a dashed box (a). (c) Cross-sectional view of the DP. The GFP-positive (green) *fraFL-MYC* clones in the DP are wider on the basal side than on the apical side (b, c, red double-headed arrows). Arrows indicate furrows formed within the *fraFL-MYC* clones. Scale bars 10 μm.

fraFL-MYC/FLP; Act5C:CD2:GAL4, GFP

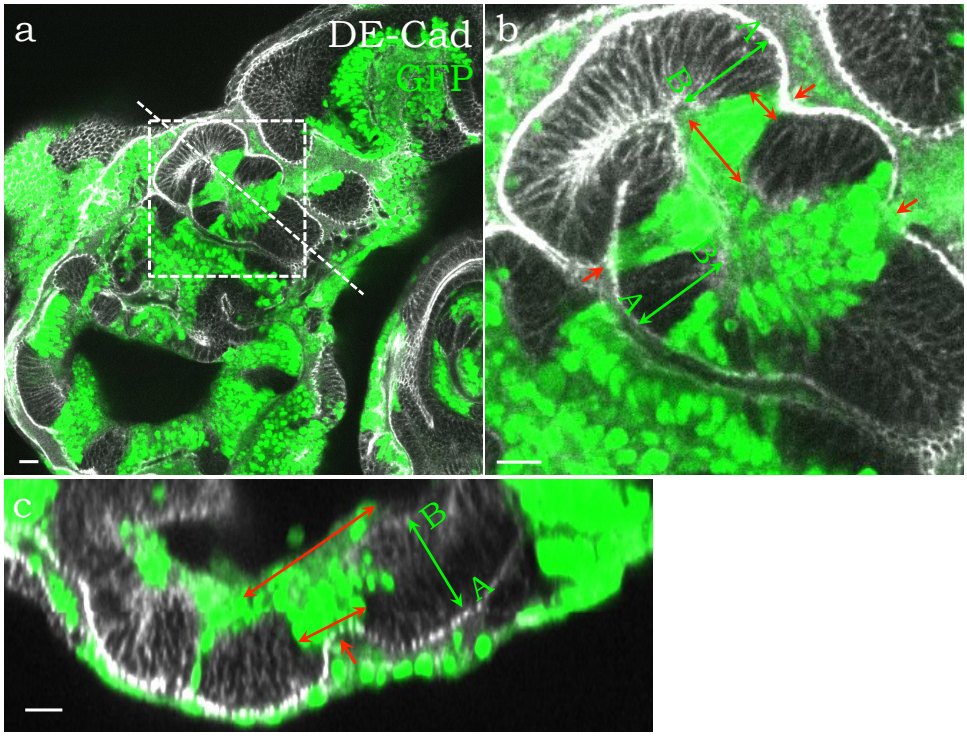

Figure 5.12: **Overexpression of *fra*Δ*P1* does not cause basal expansion.** Mosaic wing discs with GFP-positive (green) clones expressing *frazzled*-deletion transgenes immunostained for DE-Cad (grayscale). Dashed lines (a-d) indicate the cross-sectional views depicted in a'-d' respectively. (a-a') A fragment of the *UAS-fra*Δ*P1-MYC/FLP;Act5C:CD2:GAL4,UAS-GFP* DP. The width of apical side of the *fra*Δ*P1-MYC* clone was equal or less to the basal side (a-a', red double-headed arrows). (b-b') A fragment of the *UAS-fra*Δ*P2-MYC/FLP;Act5C:CD2:GAL4,UAS-GFP* DP. Basal-apical ratio of *fra*Δ*P2-MYC* clones appeared as high as in *fraFL* clones. (c-c') A fragment of the *UAS-fra*Δ*P1*Δ*P2-MYC/FLP;Act5C:CD2:GAL4,UAS-GFP* DP. (d-d') A fragment of the *UAS-fra*Δ*P3-MYC/FLP;Act5C:CD2:GAL4,UAS-GFP* DP. Basal-apical ratio in the *fra*Δ*P1*Δ*P2-MYC* and *fra*Δ*P3-MYC* clones appeared to be higher than in *Control* (for quantification see Figure 5.15, b). Scale bars 10 μm.

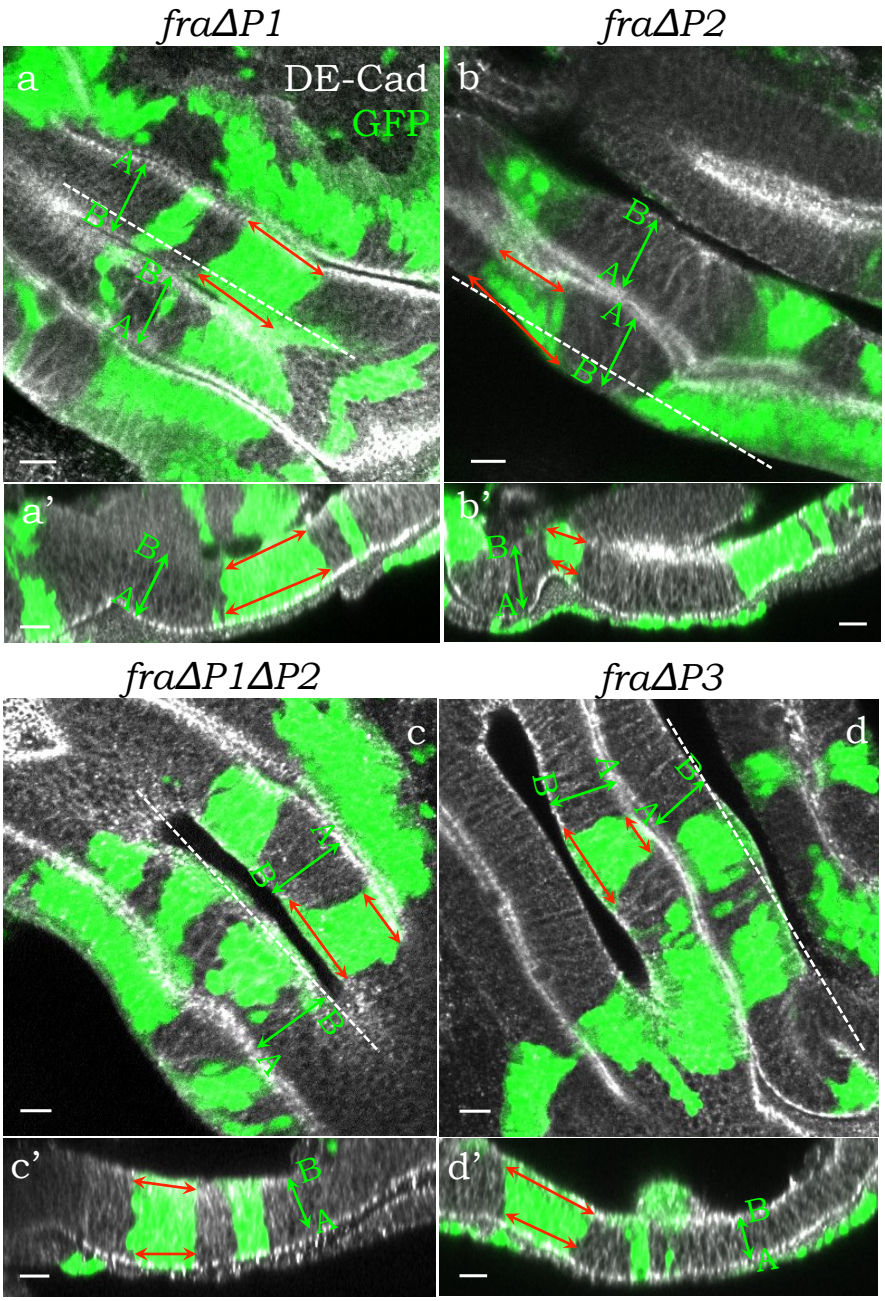
fraΔP1
fraΔP2
a
DE-Cad
GFP
b
a'
b'
fraΔP1ΔP2
fraΔP3
c
d
c'
d'

Figure 5.13: ***ptc*-driven overexpression of *fra*Δ*P1* does not cause basal expansion in the DP.** Wing discs with *ptc*-driven expression of *MYC*-tagged full-length *frazzled* or *frazzled*-deletion transgenes immunostained for DE-Cad (grayscale). *ptc*-expression pattern is GFP-positive (green). Dashed lines (a-f) indicate cross-sectional views displayed in a'-f' respectively. (a-a') The DP of a control *ptc>GFP* wing disc. Width of the apical side was equal or less to the basal side in *ptc*-expression area of a *Control* (for quantification see Figure 5.15, b). (b-b') The DP of a *ptc>fraFL-MYC,GFP* wing disc. Basal-apical ratio was increased significantly compared to *Control*. The apical side of the *ptc*-pattern could form a fold (arrows). (c-c') The DP of a *ptc>fra*Δ*P1-MYC,GFP* wing disc. Basal-apical ratio was not significantly different from *Control*. (d-d') The DP of a *ptc>fra*Δ*P2-MYC,GFP* wing disc. (e-e') The DP of a *ptc>fra*Δ*P1*Δ*P2-MYC,GFP* wing disc. (f-f') *ptc>fra*Δ*P3-MYC,GFP* wing disc. Basal expansion were observed in each genotype, whereas folds (c, arrow) were observed only within the *ptc*-areas expressing *fra*Δ*P2-MYC* transgene. Scale bars 10 μm.

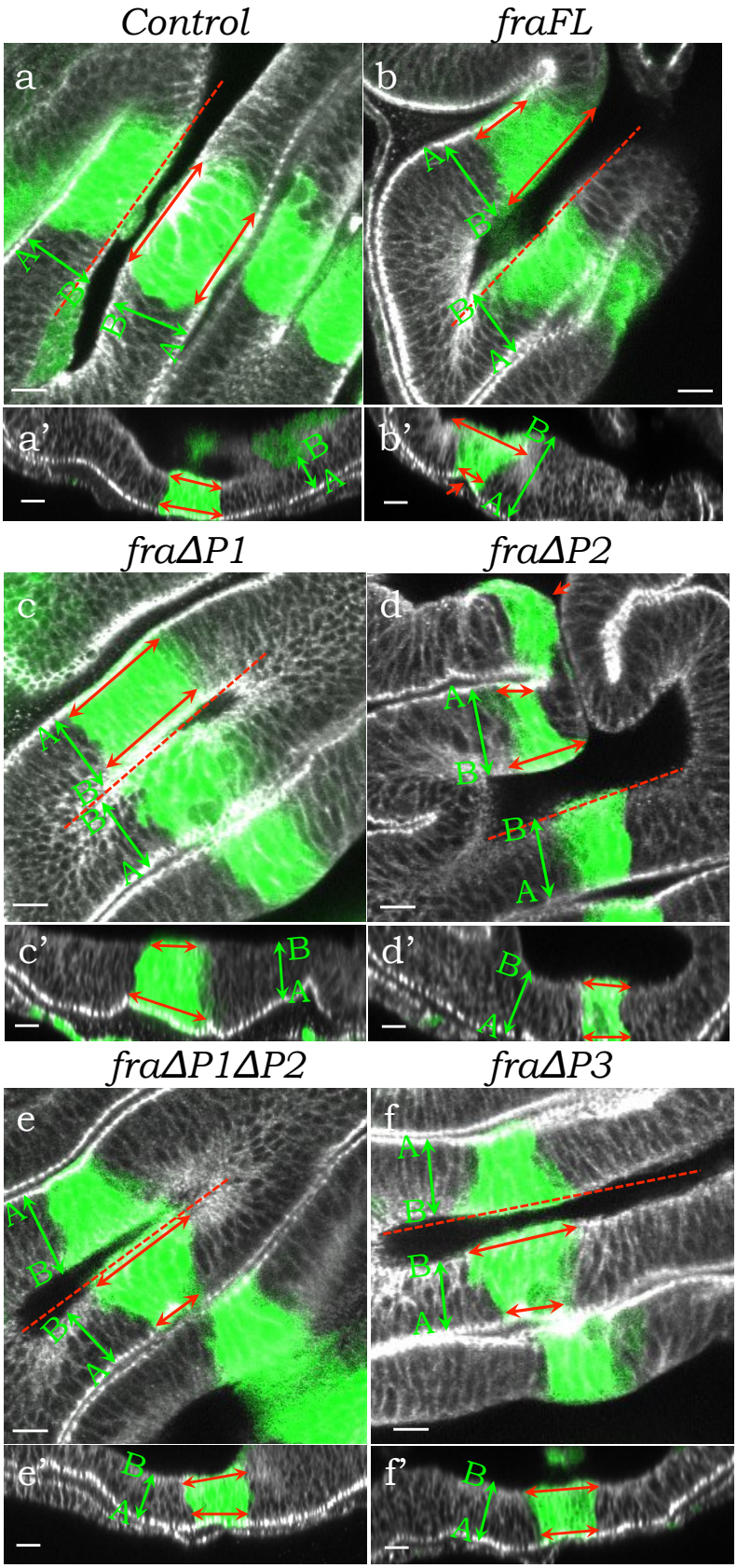
Control
fraFL
a
b
a'
b'
fraΔP1
fraΔP2
c
d
c'
d'
fraΔP1ΔP2
fraΔP3
e
f
e'
f'
A
B

Figure 5.14: ***ptc*-driven overexpression of *fraFL-MYC* and *fra*Δ*P2-MYC* transgenes promote furrow formation on the apical side.** Three-dimensional views of the wing discs with *ptc*-driven expression of *MYC*-tagged full-length *frazzled* or *frazzled*-deletion transgenes immunostained for DE-Cad (grayscale). *ptc*-expression pattern is GFP-positive (green). (a) Control *ptc>GFP* wing disc. (b) *ptc>fraFL-MYC,GFP* wing disc. (c) *ptc>fra*Δ*P1-MYC,GFP* wing disc. (d) *ptc>fra*Δ*P2-MYC,GFP* wing disc. (e) *ptc>fra*Δ*P1*Δ*P2-MYC,GFP* wing disc. (f) *ptc>fra*Δ*P1*Δ*P2-MYC,GFP* wing disc. Arrows (b, d) indicate a furrow generated along the *ptc*-expression stripe. Scale bars 10 μm.

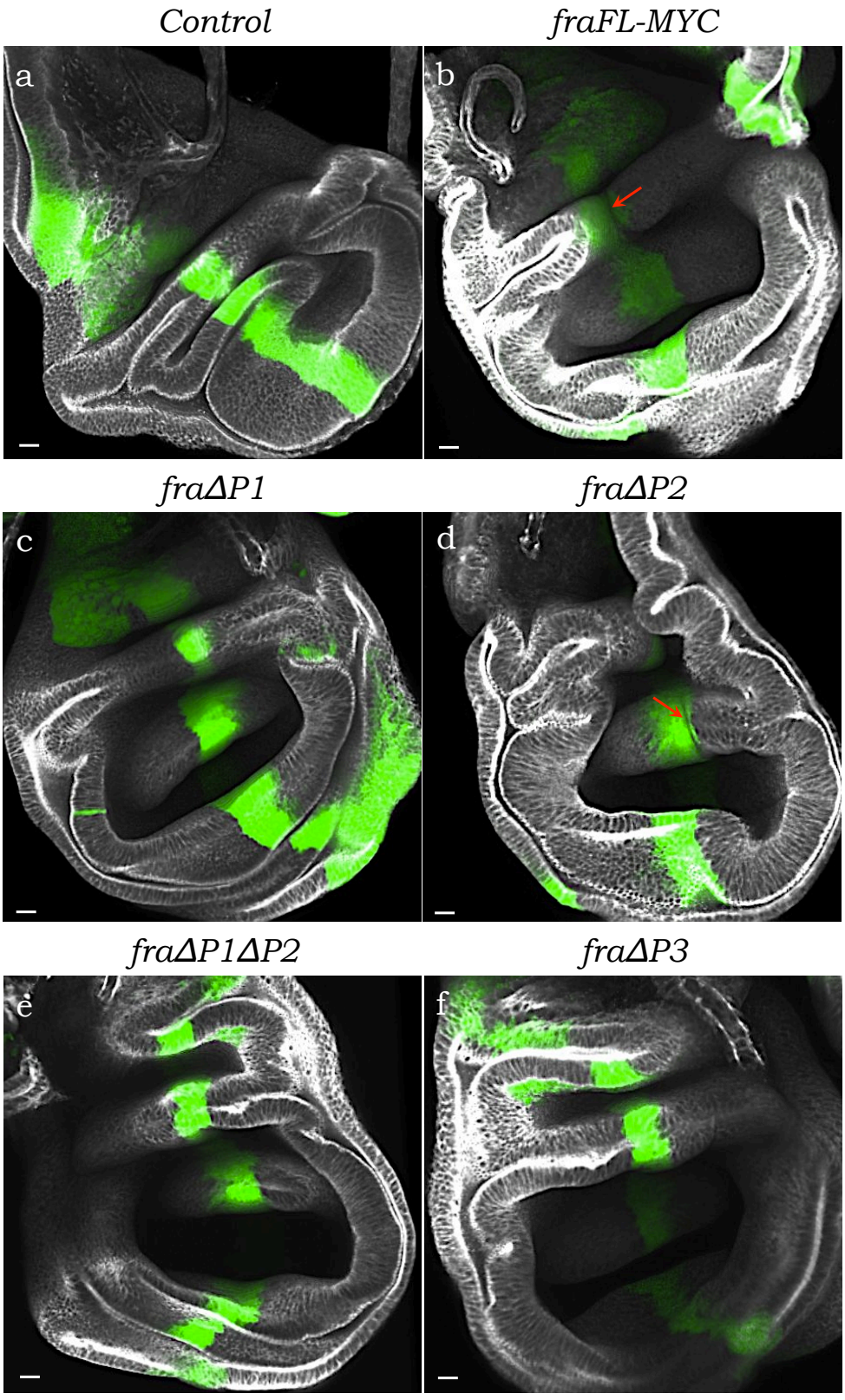
Control
fraFL-MYC
a
b
fraΔP1
fraΔP2
c
d
fraΔP1ΔP2
fraΔP3
e
f

Figure 5.15: **DE-Cad intensity and basal-apical ratio data for *ptc-GAL4*-expression wing discs.** (a) Normalized mean intensity rates of DE-Cad immunostaining in *ptc*-expression pattern relative to adjacent non-GFP areas in wing discs expressing *frazzled*-transgenes compared to *ptc>GFP* (*Control*) wing discs. (b) Basal-apical ratio in *ptc*-expression pattern in wing discs expressing *frazzled*-transgenes compared to *ptc>GFP* (*Control*) wing discs. Error bars are represented as the mean±s.e.m. Two-tailed p-values based on the Students t-test are presented above the graph.

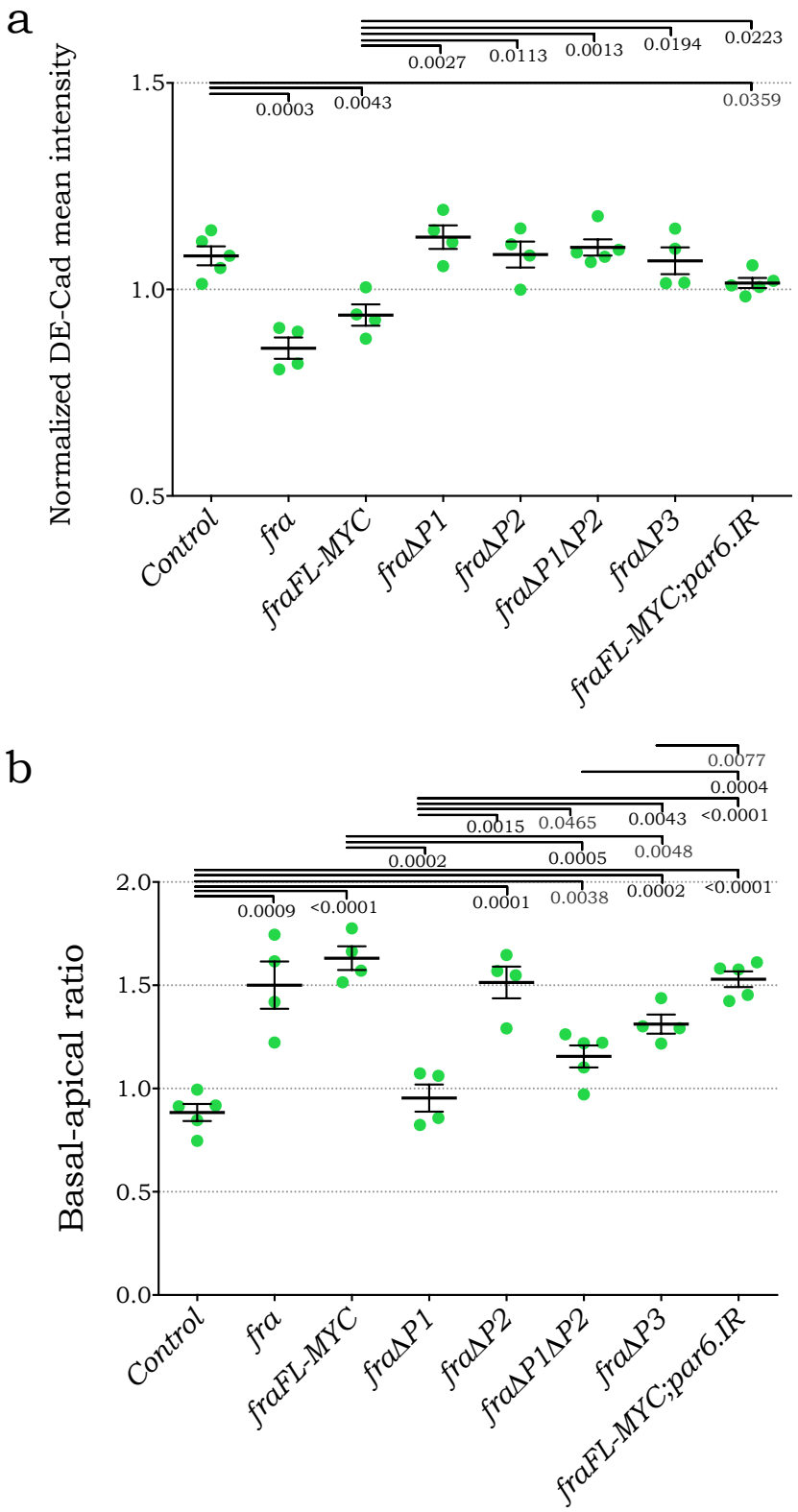
a
Normalized DE-Cad mean intensity
1.5
1.0
0.5
0.0003
0.0043
0.0359
0.0027
0.0113
0.0013
0.0194
0.0223
Control
fra
fraFL-MYC
fraΔP1
fraΔP2
fraΔP1ΔP2
fraΔP3
fraFL-MYC;par6.IR
b
Basal-apical ratio
2.0
1.5
1.0
0.5
0.0
0.0009
<0.0001
0.0001
0.0038
0.0002
<0.0001
0.0002
0.0005
0.0048
0.0015
0.0465
0.0043
<0.0001
0.0077
0.0004
Control
fra
fraFL-MYC
fraΔP1
fraΔP2
fraΔP1ΔP2
fraΔP3
fraFL-MYC;par6.IR

Figure 5.16: **Summarised data and the final model of Frazzled signaling.** (a) Table summarises the results from Frazzled structure function analysis. MYC-tags are neglected for simplicity. "✓✓", "✓" and "✗" symbolize either presence or partial presence or absence of a phenotype respectively in wing discs overexpressing *frazzled* deletion transgenes. (b) A model of Frazzled signaling pathways. Frazzled P-motifs affect three genetically independent processes: tissue invagination, DE-Cad trafficking and cell motility/adhesion. *frazzled* overexpression eversion phenotype could be associated with enhanced tissue invagination and disruptions in DE-Cad trafficking.

a Phenotypes produced by *frazzled* transgenes

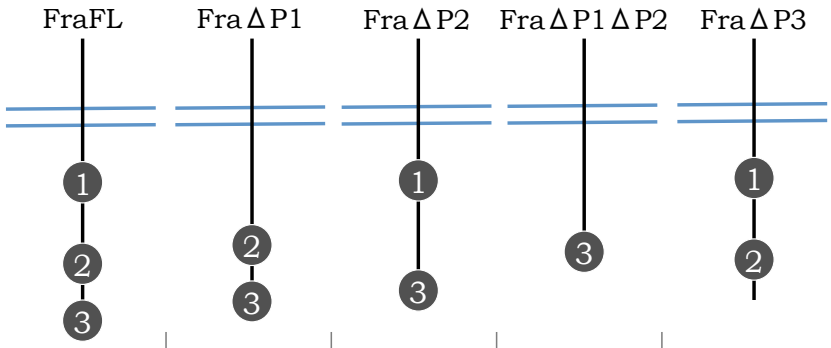

	FraFL	Fra Δ P1	Fra Δ P2	Fra Δ P1 Δ P2	Fra Δ P3
Eversion failure	✓✓	✗	✓	✗	✗
Long protrusions	✓✓	✓	✓✓	✓✓	✗
Loss of baso-lateral DE-Cad	✓✓	✗	✗	✗	✗
Basal expansion/ apical contraction	✓✓	✗	✓✓	✓	✓

b Possible cellular functions of Frazzled

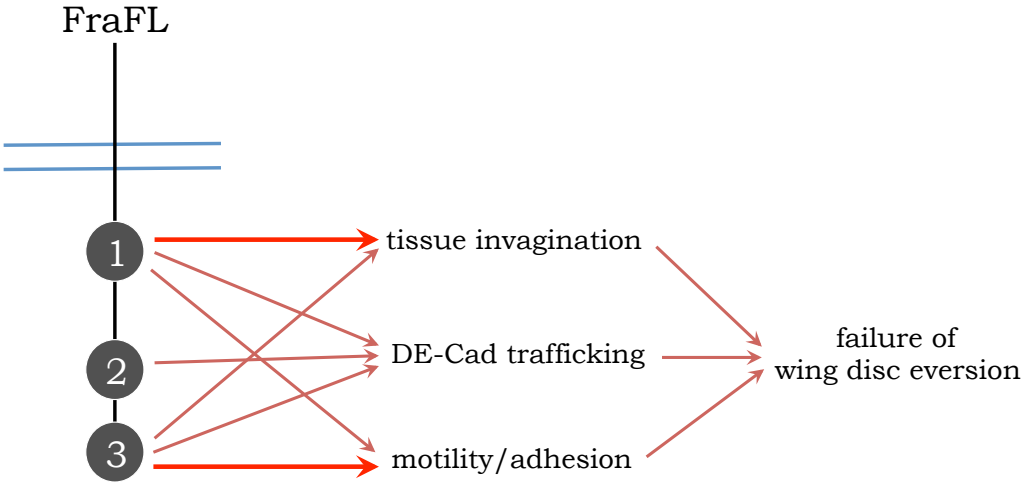

CHAPTER 6

Screening for candidates involved in the NetrinA/Frazzled signaling pathway

6.1 Introduction

6.1.1 RNAi screening

One of the future goals of this project is to identify factors acting downstream of NetrinA and Frazzled signaling during wing disc eversion. One way to do this would be to utilise the accessibility of adult eversion phenotypes to conduct a genome wide genetic screen for genes that can modulate the *netA.IR* and *frazzled* overexpression phenotypes, and then follow up with a cellular analysis as in Chapter 5. However, due to time constraints I was not able to undertake such a large screen within this work. Instead a pilot modifier RNAi screen of 49 genes was performed, whereby genes were knocked-down in the *UAS-netrinA.IR* or *frazzled* over-expression backgrounds, to see if they could suppress or enhance the eversion phenotypes.

Genes chosen for the screen were restricted to those that might be expected to take part in downstream NetrinA/ Frazzled signaling pathways. Regulatory factors that might act upstream, by regulating *netrinA* or *frazzled* gene expression, (e.g. transcription factors and miRNAs) were excluded.

Genes involved in the modifier screen can be roughly split into five groups according to their relationship to Netrins and Frazzled or their cellular function. The first group includes genes encoding components that have been shown to interact physically with Netrins or Netrin receptors. Two subgroups can be separated within this group: i) receptors of *Drosophila* netrins; and ii) other proteins known to interact physically or genetically with NetrinA and Frazzled. The second group contains genes encoding kinases that are reported to be able to phosphorylate Moesin, the hypothetical intermediate between Frazzled and Rho1. Small Rho GTPases were placed into the third group together with their regulators, GAPs and GEFs. Finally, the last group consisted of genes with cellular functions potentially needed for phenotypes produced by overexpressing *frazzled* such as regulation of epithelial polarity components, basal expansion and formation of protrusions. The genes were further divided into two sub-groups - genes encoding proteins that regulate cell adhesion and polarity in one subgroup, and genes encoding cytoskeleton associated proteins in the other subgroup.

6.1.1.1 The first group of genes: receptors of NetrinA and Frazzled interacting proteins

The first group of genes tested encode four types of netrins receptors: Frazzled, Unc5, DSCAMs and integrins. Previous work has shown that RNAi knockdown of *frazzled* in the PE significantly suppresses the *netA.IR* phenotype (Manhire-Heath *et al.*, 2013 [133]). None of the other receptors have been demonstrated to play a positive role in wing disc eversion except for one member of the Integrin family, the α-subunit Scab (Rose Manhire-Heath, PhD work). Nevertheless, Unc5 and DSCAMs are potentially able to interact with both NetrinA and Frazzled. During development of *Xenopus* spinal axons, Unc5 binds to DCC converting Netrin-1-induced attraction to repulsion (Hong *et al.*, 1999 [116]). In the same model, DSCAM collaborates with DCC mediating Netrin-1-induced attraction of axons (Ly *et al.*, 2008 [327]). Moreover, DSCAM may share downstream signaling pathways with DCC: like DCC the cytoplasmic domain of DSCAM binds to polymerized dynamic β-tubulin TUBB3

regulating axon branching (Qu *et al.*, 2013 [241]; Huang *et al.*, 2015 [328]). Integrins are required for cell migration promoting focal adhesion structures in complex with cytoskeletal and signaling proteins (e.g. talins, α-actinin, Vinculin, FAK, Src tyrosine kinase *etc.*), that makes their involvement in the NetrinA-mediated likely. For example, βIntν, βPS, If and Mew are essential during midgut primordia and salivary gland migration along the visceral mesoderm (Martin-Bermudo *et al.*, 1999 [329]; Bradley *et al.*, 2003 [330]; Devenport and Brown, 2004 [77]), the processes which are both regulated by NetrinA (Kolesnikov and Beckendorf, 2005 [331]; Pert *et al.*, 2015 [78]).

The gene *slit* is the ligand for the Robo receptor (Kidd *et al.*, 1999 [332]) and is the other major cue in axon guidance. Slit/Robo signaling mediates axon repulsion, whereas Netrin/Frazzled signaling mediates attraction (Garbe and Bashaw, 2004 [333]). Orchestrated chemo-repellent signaling of Slit/Robo and chemo-attractive signaling of Netrin/Frazzled also controls salivary gland migration parallel to the CNS (Kolesnikov and Beckendorf, 2005 [331]). The gene *trim9* codes a protein belonging to the TRIpartite Motif (TRIM) family. Trim9 functions as an E3 ubiquitin ligase, which tags transmembrane proteins for degradation (Meroni and Diez-Roux, 2005 [334]). In both nematode and flies, Trim9 is required for axons to migrate in response to the UNC-6/Netrin attraction signals, and this function of Trim9 is determined by its E3 ubiquitin ligase activity (Song *et al.*, 2011 [335]). The researchers demonstrated that overexpression of Frazzled diminishes axon guidance defects in *trim9* loss-of-function flies. Presumably, Trim9 modulates UNC-6/netrin signaling pathway ubiquitinating downstream effectors of UNC-40/Frazzled (Song *et al.*, 2011 [335]).

6.1.1.2 The second group of genes: putative Moe kinases

The second group of genes screened, encodes kinases with serine-threonine/tyrosine activity which are believed to mediate phosphorylation of the ERM protein Moesin. The repression of *netA.IR* phenotype by RNAi downregulation of *moe* has been shown previously in our lab (Manhire-Heath *et al.*, 2013 [133]). To date, the only

kinase shown to phosphorylate Moesin in *Drosophila* , is Slik kinase. Slik regulates Moesin to prevent Rho1-induced apoptosis in actively proliferating cells (Hipfner *et al.*, 2004 [173]). These studies also demonstrate that Slik is required for the organization and maintenance of apical actin structures (Hipfner *et al.*, 2004 [173]; Carreno *et al.*, 2008 [336]).

Tao kinase belongs to the same Sterile 20 family as Slik, however in contrast to other genes from this group, the loss of *tao* increases pMoe levels (Boggiano *et al.*, 2011 [337]). A very recent study revealed that the gene *tao* encodes two proteins, Tao-L and Tao-S, with and without a Sterile 20 kinase domain respectively. Both products participate in formation of actin-rich structures for regulating cell migration, but whereas Tao-L promotes lamellipodia-like cell protrusions needed for cell motion, Tao-S is responsible for filopodia-like structures required to stick cell to the surface (Pflanz *et al.*, 2015 [338]).

Two kinases, Src42a and Src64b, belong to the Src family of non-receptor tyrosine kinases and share redundant functions in fly development. In particular, both kinases regulate the actin cytoskeleton via physical or genetic interactions with actin-binding proteins (such as Cortactin, the formin DAAM, Focal Adhesion Kinase (FAK), Capping protein alpha (Cpa); Somogyi and Rørth, 2004 [339]; Matusek *et al.*, 2006 [340]; Tsai *et al.*, 2008 [341]; Fernandez *et al.*, 2014 [342]), cell-adhesion proteins (such as β-catenin and E-Cadherin; Takahashi *et al.*, 2005 [343]; Shindo *et al.*, 2008 [344]) or other kinases (such as DFer and Btk29a; Murray *et al.*, 2006 [345]; Guarnieri *et al.*, 1998 [346]; Roulier *et al.*, 1998 [347]) involved into cytoskeleton reorganization. A key finding in mammalian axon guidance research, was that Src kinase was biochemically required for phosphorylation of ERM-proteins in response to Netrin-1/DCC signaling (Antoine-Bertrand *et al.*, 2011 [168]).

DFer (known also as FER or Fps85d), is a member of the non-receptor protein kinase subfamily. Although there is no direct evidence that it phosphorylates Moesin, it is required for actin filament assembly and regulating cell-cell adhesion, both of which are likely to be mediated by Moesin (reviewed by Greer, 2002 [348]; El *et al.*, 2005 [349]). During *Drosophila* dorsal closure, DFer co-operates with Src42a to

promote actin cable built-up at the leading edge (Murray *et al.*, 2006 [345]).

Similar to DFer, a kinase Btk29a (also called Tec29) has not been shown to phosphorylate Moesin, but can regulate F-actin. It maintains a balance between monomeric G-actin and filamentous F-actin needed for normal salivary gland formation (Chandrasekaran and Beckendorf, 2005 [350]) and, together with Src64 kinase, regulates the growth of actin-rich ring canals in the ovary (Guarnieri *et al.*, 1998 [346]; Roulier *et al.*, 1998 [347]).

Lrrk is the homolog of mammalian LRRK2, the common determinant of Parkinson's disease. LRRK2 was shown to phosphorylate ERM proteins, Ezrin, Radixin and Moesin, to induce development of F-actin-enriched filopodia in growing neurites (Jaleel *et al.*, 2007 [351]; Parisiadou *et al.*, 2009 [352]). In *Drosophila*, Lrrk regulates the perinuclear position and clustering of lysosomes (Dodson *et al.*, 2012 [353]).

Serine/threonine-specific Akt kinases are able to phosphorylate different ERM-proteins. In mammalian PC12 cells, Akt1 interacts and phosphorylates Moe *in vivo* and *in vitro* downstream of PI3K and Rac1 (Jeon *et al.*, 2010 [354]). This process is essential for neurite elongation under Neural Growth Factor (NGF) induction. Akt2 phosphorylates and activates Ezrin to promote Na^+/H^+-exchanger exocytosis and translocation in Caco-2 cells (Shiue *et al.*, 2005 [355]). In *Drosophila*, Akt, together with PI3K, is involved in control of cell proliferation and organ growth (Verdu *et al.*, 1999 [356]; Kim *et al.*, 2004 [357]).

6.1.1.3 The third group of genes: small GTPases and their regulators

The third group of genes encodes small GTPases and their regulators, the GAPs and GEFs. Within the Rho subfamily of small GTPases, three *Drosophila* representatives, Rho1, Rac1 and Cdc42, are the most extensively studied because of their role in coordinating cytoskeletal dynamics and related processes such as cell movement, adhesion, polarity, morphogenesis and membrane trafficking (reviewed by Lu and Settleman, 1999 [358] and Johndrow *et al.*, 2004 [359]). Thus, small Rho GTPases are likely to function downstream of NetrinA/Frazzled signaling.

Two representatives of the Rab subfamily of small GTPases, Rab6 and Rab11,

were also included in the screen. Rab GTPases are known as key regulators of vesicular traffic of different intracellular substrates (reviewed by Hutagalung and Novick, 2011 [360] and Bhuin and Roy, 2014 [361]). Rab6 is associated with parts of the Golgi network, and considered to be involved in the vesicle transport from Golgi to endoplasmic reticulum and to membrane, and in the retrograde transport from early endosomes to Golgi (Del Nery *et al.*, 2006 [362], Grigoriev *et al.*, 2007 [363]). Rab6 also regulates cell polarity. Depletion of Rab6 (Drab6) results in defects in the organization and polarity of egg chambers due to disrupted membrane trafficking of oocyte specific secreted proteins Gurken and Yolkless, and mislocalization of the microtubule network (Coutelis and Ephrussi, 2007 [364]). Moreover, recent findings in photoreceptor cells show that Rab6 is specifically required for the apical vesicle transport between trans-Golgi cisternae and recycling endosomes (Satoh *et al.*, 2016 [365]; Iwanami *et al.*, 2016 [366]). Rab11 is well known as a marker of recycling endosomes. It regulates the transport of recycling endosomes and newly synthesized components from trans-Golgi structures to the membrane (Ullrich *et al.*, 1996 [367], Satoh *et al.*, 2005 [368]).

RhoGEF2, Pebble and Gef64C are putative upstream positive regulators (GEFs), and RhoGap68F is a negative regulator (GAP) of Rho1 GTPase (Häcker and Perrimon, 1998 [369], Prokopenko *et al.*, 1999 [370], Bashaw *et al.*, 2001 [371], Sanny *et al.*, 2006 [372]). RhoGEF2 induces Rho1-dependent apical contraction through activation of MLCK and inhibition of myosin phosphatase (Somlyo and Somlyo, 2003 [373]; Rogers *et al.*, 2004 [374]). Pebble (Pbl) activates Rho1 during *Drosophila* cytokinesis (Hime and Saint, 1992 [375]; Somers and Saint, 2003 [376]). It also is essential for the mesoderm EMT, where Pbl presumably also helps to activate the Rac1 pathway (Schumacher *et al.*, 2004 [377]; Smallhorn *et al.*, 2004 [378]; van Impel *et al.*, 2009 [379]; Murray *et al.*, 2012 [380]). Loss of Gef64C function enhanced axon guidance defects in *frazzled* mutant embryos (Bashaw *et al.*, 2001 [371]). This study provides a few lines of evidence suggesting Gef64C was a positive regulator of RhoA but not Rac1 or Cdc42, and altogether these results argue for a model in which RhoA mediates repulsion, while Rac1 mediates attraction.

Gef26 is a GEF that activates Rap1 GTPase (Lee *et al.*, 2002 [381]), a GTPase known for its ability to affect cell adhesion through the regulation of integrin activity and AJ localization (Bos *et al.*, 2003 [382], Knox and Brown, 2002 [383], Price *et al.*, 2004 [384]). In particular, Gef26 is required for the formation and maintenance of mature AJs that anchor stem cells to the niche, in the *Drosophila* testis (Wang *et al.*, 2006 [385]).

Tumbleweed (Tum) is a putative negative regulator of Rac1 GTPase (Goldstein *et al.*, 2005 [103]). Tum functions in conjunction with the kinesin-like protein Pavarotti forming a complex named Centralspindlin which plays an essential role in cytokinesis (Mishima *et al.*, 2002 [101], Goldstein *et al.*, 2005 [103]). *pannier-GAL4*-driven knockdown of *tum* in wing discs causes thoracic clefts and reduced number of bristles (Sfregola, 2014 [100]). Interestingly, similar to the effects of *frazzled* overexpression, the overexpression of Centralspindlin disrupts epithelial integrity and causes formation of filopodia, which together result in thoracic defects (Sfregola, 2014 [100]). The GEF Trio is a putative activator of Rac GTPases (Bateman *et al.*, 2000 [386]) and is known to cooperate with Frazzled during axon guidance (Forsthoefel *et al.*, 2005 [238]), therefore it is a likely candidate of NetrinA/Frazzled downstream signaling.

Schizo (Siz) is a homolog of vertebrate GEF for the Arf family of GTPases, which are known to regulate the Golgi-membrane vesicle trafficking and actin remodelling (Nie *et al.*, 2003 [387]). Siz was included in the screen due to its requirement for normal axon guidance and possible interaction with both *Drosophila* netrins and Frazzled (Hummel *et al.*, 1999 [388], Önel *et al.*, 2004 [389]).

6.1.1.4 The fourth group of genes: adhesion, polarity and cytoskeleton regulators

The fourth group of genes encode other proteins involved in the modulation of epithelial characteristics, and control of cell migration and EMT.

6.1.1.4.1 Genes controlling apical polarity

Drosophila Par6, atypical protein kinase C (aPKC), Cdc42, Crumbs (Crb), Baz (*Drosophila* Par3), Stardust (Sdt) and Pals1-associated TJ protein (Patj) are components of a network of apical polarity regulators (reviewed by Tepass, 2012 [2], and see Section 1.1.1 of this thesis). Bazooka, Par-6 and aPKC together with Cdc42 GTPase compose the Par complex, the major regulator of apical polarity (Goldstein and Macara, 2007 [3]). *par6* encodes one of the partitioning-defective proteins, which was originally discovered as a component of polarity complex required for the asymmetrical cell division in *C. elegans* (Kemphues *et al.*, 1988 [390]). For all metazoans, Par6 has been shown to mediate a range of cellular processes, such as regulation of apico-basal polarity, cytoskeleton organization, migration, endocytosis, growth, morphogenesis and proliferation (reviewed by Goldstein and Macara, 2007 [3]). One particularly interesting role of Par6 as well as Cdc42 and aPKC, in the context of this thesis, is regulation of endocytosis and endosomal recycling in both epithelial and non-epithelial (non-polarized) cells (Balklava *et al.*, 2007 [391]; Nishimura and Kaibuchi, 2007 [392]). For example, in the *Drosophila* notum epithelium Par6/Cdc42/aPKC complex is required for vesicle trafficking of DE-Cad at the level of the ZA where it is thought to promote vesicle scission and internalization of the junctional material. Loss of polarity components results in disintegration of AJs and subsequent cell dissemination (Georgiou *et al.*, 2008 [195]). The mechanism by which the polarity components are thought to control endocytosis is via the actin regulators WASp and the Arp2/3 complex (Georgiou *et al.*, 2008 [195]; Leibfried *et al.*, 2008 [256]).

The Par complex may also be also involved in the control of EMT. Breast and prostate cancers studies have shown that Par6 signaling is regulated by the central EMT mediator TGFβ and is associated with tumor metastasis (Viloria-Petit *et al.*, 2009 [393]; Mu *et al.*, 2015 [394]). In vertebrates, the regulation of Par6 signaling during EMT targets the dissolution of the TJ and induces cell motility (Ozdamar *et al.*, 2005 [44]; Barrios-Rodiles *et al.*, 2005 [395]; Viloria-Petit *et al.*, 2009 [393]).

Activated TGFβ acts through its type I receptor (TGFβRI), which directly binds Par6 at the occludin-complex of the TJ. The interaction of TGFβRI and Par6 induces TGFβ type II receptor (TGFβRII) mediated phosphorylation of both Par6 at Ser^{345} and TGFβRI by the TGFβ type II receptor (the latter process independently leads to the activation of Smad pathway of TGFβ signaling (see Chapter I)). In turn, phosphorylated Par6 associates with Smurf1, an E3 ubiquitin ligase, which directs RhoA for ubiquitination and degradation (Wang *et al.*, 2003 [396]). The localized degradation of RhoA results in loss of polarity, TJ dissociation and elevated protrusive activity (Ozdamar *et al.*, 2005 [44]). However, whether TGFβ-Par6 EMT initiation occurs in *Drosophila* is not clear since the Par6 phosphorylation site Ser^{345} was not found in flies (Ozdamar *et al.*, 2005 [44]).

6.1.1.4.2 Genes controlling cell adhesion and motility

Members of *Drosophila* Cadherins superfamily, DE-Cad/Shotgun and Dachsous (Ds) are known to provide intercellular interactions in epithelial and non-epithelial tissues (Clark *et al.*, 1995 [397]; Tepass *et al.*, 1996 [398]). Ds is best known as an alternative regulator of planar cell polarity, in addition to the well-known Frizzled pathway (Casal *et al.*, 2006 [399]; Lawrence *et al.*, 2007 [400]). One aspect of this regulation, is that Ds promotes actin-based protrusion formation at the posterior end of denticle producing cells of the ventral epidermis (Lawlor *et al.*, 2013 [401]). The gene *starry night* (*Stan*; also known as *flamingo*) functions downstream of the membrane receptor Frizzled in controlling planar cell polarity (Lee and Adler, 2002 [402]; Adler, 2012 [403]). Recently, Stan was demonstrated to assist Netrin/Frazzled signaling in axon guidance during midline development (Organisti *et al.*, 2015 [404]).

Focal adhesion kinase (FAK) is responsible for both cell-ECM adhesion and cell motility (Furuta *et al.*, 1995 [405]). It is believed that *Drosophila* Fak56d transduces signals from integrins, such as during synaptic growth in migrating motor axons (Tsai *et al.*, 2008 [341]). Interestingly, some vertebrate research suggests that FAK-mediated phosphorylation is necessary for Netrin-1 and DCC function in axon guidance, and moreover that DCC and FAK are able to interact directly via an

LD-like site of the P3 domain (Li *et al.*, 2004 [202]; Liu *et al.*, 2004 [316]; Ren *et al.*, 2004 [242]; Moore *et al.*, 2012 [406]).

Actin cytoskeleton regulators, such as Enabled (Ena), Abelson tyrosine kinase (Abl), Capping protein β subunit (Cpb) and SCAR are regulators of the F-actin cytoskeleton. SCAR and Ena proteins play a positive role in the polymerization of actin filaments on the free barbed ends promoting lamellipodial and filopodial formation (reviewed by Dent and Gertler, 2003 [260]). Ena functions together with Frazzled, Abl and Trio in modulating netrin-dependent signaling to control axon pathfinding, and the *Drosophila* embryos mutated for *enabled* or *abl* display broken, thinning or missed commissures in the CNS (Forsthoefel *et al.*, 2005 [238]; O'Donnell and Bashaw, 2013 [240]). In a study of ventral furrow formation, Ena subcellular localization and actin polymerization activity are defined by function of Abl, however the mechanism of Abl-Ena interaction is unclear (Grevengoed *et al.*, 2003 [407], Fox and Peifer, 2007 [303]).

Contrary to SCAR and Ena, a heterodimer of both α and β subunits of Capping protein (Cpa and Cpb) binds to the barbed ends of F-actin terminating further filament assembly and preventing loss of F-actin monomers (Hopmann *et al.*, 1996 [408]). Acting jointly with Ena/VASP, the Capping protein regulates elongation and branching of actin filaments (Barzik *et al.*, 2005 [326]). Loss of Capping proteins in the wing blade primordium results in the increased accumulation of F-actin filaments (Janody and Treisman, 2006 [409]). Besides the regulation of F-actin turnover, Capping proteins ensure an apical localization of DE-Cad and its stabilisation it at AJs (Jezowska *et al.*, 2011 [410]).

I also included the gene *disabled* (*dab*) as it is considered an upstream regulator of Abl and Ena, and presumably is needed for proper distribution of Abl within cells. The *dab* mutant embryos exhibit defects in cellularization, ventral furrow formation and dorsal closure, which are all presented in *abl* mutants, and the failures are presumably due to abnormal accumulation of F-actin (Song *et al.*, 2010 [411]). Moreover, the *Drosophila dab* mutants are shown to have disrupted Clathrin-mediated vesicle endocytosis in synapses, suggesting the requirements of

Dab in the endocytic trafficking (Kawasaki *et al.*, 2011 [412]).

Microtubules are key structures to establish cell polarity and enable cell migration (reviewed in Lee and Streuli, 2014 [413]). Axon outgrowth is presumably dependent on direct interaction of the P2 and P3 motifs of DCC and microtubules (Qu *et al.*, 2013 [241]). Two microtubule-associated proteins were included in the screen, Ensconsin (Ens) and Stathmin (Stai). Ens is ubiquitously bound to microtubules, where it recruits Kinesin-1 to facilitate vesicle and organelle transport towards the plus-ends (Sung *et al.*, 2008 [414], Barlan *et al.*, 2013 [415]). Stai is responsible for microtubule disassembly (Duncan *et al.*, 2013 [416]).

6.1.2 This chapter

The aim of this study was to identify downstream components of the NetrinA and Frazzled signaling pathways by looking for genes that, when knocked down, could suppress the adult eversion phenotypes of *netrinA* knockdown or *frazzled* overexpression.

UAS-gene.IR transgenes (see the Table 6.1) were co-expressed with *UAS-netrinA.IR* or *UAS-fraFL-MYC* under the control of the *Ubx-GAL4* driver, and the eversion phenotypes scored. Phenotypes were categorised into three classes:

i) normal development of wings and thorax;

ii) crumpled/missing wings and thoracic defects;

iii) early lethality.

Suppression or enhancement was defined as a significant reduction or increase, respectively, in the proportion of normal progeny versus abnormal (i.e. eversion defects or early lethality) (see the Table 6.1).

Surprisingly, of the 49 genes tested, many had a strong modulatory effect on

the phenotypes, with both strong enhancement and strong suppression of *netA.IR* and *frazzled* overexpression phenotypes, in some cases acting in opposite directions (Figure 6.1). The fact that so many genetic perturbations could so readily modify the phenotypes, suggests that the *netA.IR* and *frazzled* overexpression backgrounds create a sensitised eversion state, in which small changes can have large effects, making interpretations difficult.

Of all the genes, only RNAi lines for *par6* suppressed both *netA.IR* and *frazzled* overexpression eversion phenotypes. Therefore, in the final part of this study we tested whether RNAi downregulation of *par6* could also suppress the *frazzled* overexpression cellular phenotypes, i.e. DE-Cad delocalization, basal expansion and enhanced protrusion formation.

6.2 Results

The RNAi screening results are summarised in Figures 6.1, 6.2, 6.3, 6.4, 6.5, 6.6, 6.7 and in Table 6.1. Here, I will highlight the main outcomes of the screening.

6.2.1 RNAi lines that suppress *netA.IR* phenotypes

Expression of 30 RNAi lines significantly suppressed the *netA.IR* phenotype, suggesting that the function of the encoded proteins is repressed by NetrinA during wing disc eversion (Figure 6.1). It is also possible that these genes act upstream of *netrinA*, normally repressing its expression, though this is less likely given that regulatory factors, such as transcription factors and miRNAs, were excluded from the screen. Among these RNAi lines 17 had an opposite, enhancement effect on the *fraFL-MYC* overexpression phenotype (i.e. significantly reduced the number of normal flies): there were two representatives of the receptors of NetrinA ($\beta\nu$*.IR* and *dscam4.IR*), six RNAi constructs of the genes encoding putative Moe kinases (*slik.IR*, *btk29a.IR*, *fps82d.IR*, *lrrk.IR*, *src42a.IR* (BL17643) and *src64b.IR*), representatives of the small GTPases and their regulators (*rac1.IR*, *gef26.IR*, *rhogap68f.IR*), and six representatives from the fourth group of genes (*baz.IR*, *stan.IR*, *fak56d.IR*,

cpb.IR, *scar.IR* and *ens.IR*). For these genes the implication is that they normally play a positive role in eversion and are inhibited/repressed by Frazzled. The idea that these genes might be negatively regulated by both netrins and Frazzled, is at odds with the idea that *netrinA.IR* phenotypes are only due to up-regulation of Frazzled, and instead suggests that these genes may be acting in two distinct pathways or stages of eversion (see Discussion).

Co-expression of nine RNAi lines with *fraFL-MYC* did not significantly change the number of normal flies: there were four representatives of the first group of genes (*unc5*, *mew*, *dscam2.IR* and *sli.IR*), one Moe kinase (*fps82d.IR* (BL36053)), two GTPases and a GEF (*cdc42*, *rab6* and *gef64c*), and *abl.IR*. The fact that these RNAi lines could modulate the *netrinA.IR* phenotypes but not the *frazzled* overexpression phenotypes suggests that the *netrinA.IR* genotype might be more delicately balanced.

RNAi knockdown of the putative Moe kinase *tao1* and F-actin regulator *ena* caused complete early pupal lethality of progeny after crosses with *fraFL-MYC* (Figures 6.4 and 6.7). This could be due to the low viability of *Ubx>fraFL-MYC* crosses, or an extremely strong enhancement effect of *tao1.IR* and *ena.IR* on the *fraFL-MYC* overexpression phenotype.

Finally, the most interesting for us were crosses that demonstrated suppression of both the *netA.IR* and the *frazzled* overexpression phenotypes. In this study, I used a *fra.IR* line as a control, and confirmed that the proportion of normal flies increased from 40% to 98% by crossing to *netrinA.IR* females ($p<0.0001$; this and all other p-values in this chapter are based on a two-tailed Fischer's exact test), and from 83% to 97% by crossing to *fraFL-MYC* females ($p=0.012$; Figure 6.2). Interestingly, expression of *par6.IR* also repressed both the *netrinA.IR* phenotype (91% normal progeny; $p<0.0001$) and the *frazzled* overexpression phenotype (94% normal progeny; $p<0.025$; Figure 6.6). This result suggests that *par6* acts downstream of NetrinA/Frazzled pathway, and its function is up-regulated by Frazzled. Given this result, I tested whether expression of *par6.IR* is able to rescue *frazzled* overexpression cellular phenotypes (i.e. DE-Cad delocalization, tissue invagination

and protrusions; see Section 6.2.5).

6.2.2 RNAi lines that enhance *netA.IR* phenotypes

Expression of seven RNAi lines significantly enhanced the *netA.IR* phenotype, suggesting that the function of the encoded proteins is positively regulated by NetrinA during wing disc eversion (Figure 6.1). Four of them also significantly enhanced the *fraFL-MYC* overexpression phenotype: a representative of NetrinA receptors *dscam.IR*, a Rho1 GEF *rhogef2.IR*, a Rac1 GEF *trio.IR*, and E-Cadherin *shg.IR*. Likely, these genes are involved in the NetrinA/Frazzled downstream pathway, where their function is blocked by excess Frazzled activity.

Expression of three RNAi lines, *src42a.IR* (v100708), *pi3k.IR* and *stai.IR* in *fraFL-MYC* wing discs resulted in strong early lethality of progeny, suggesting that similarly to *shg.IR* these constructs have a negative effect on viability.

6.2.3 RNAi lines causing lethality of *netA.IR* progeny

Expression of 10 RNAi lines (*mys.IR*, *trim9.IR* (v21405 and v21405), *akt1.IR*, *rho1.IR*, *pbl.IR*, *rab11.IR*, *siz.IR*, *aPKC.IR*, *cadN.IR* and *cpa.IR*) caused strong lethality at the early stages in both *netA.IR* and *fraFL-MYC* crosses, suggesting these constructs are lethal by themselves (Figure 6.1).

A curious result was obtained for *tum.IR* line: its expression enhanced *netA.IR* phenotypes to complete lethality (0% normal flies; $p<0.0001$), and although flies overexpressing *fraFL-MYC* also had a high level of lethality, all the progeny were normal (52% normal progeny overall; $p=0.0001$; Figure 6.5). This second result suggests that Tum is an important effector of Frazzled signaling and is largely responsible for Frazzled eversion phenotypes.

6.2.4 RNAi lines having no effect on the *netA.IR* phenotypes

Expression of four RNAi lines did not produce effect on the *netA.IR* phenotype. Three of them (*trim9.IR* (v100767), *ds.IR* and *dab.IR*) also did not influence on the *fraFL-MYC* overexpression phenotype (Figure 6.1). This suggests either that these genes do not play a role in wing eversion, or that these RNAi construct are too weakly expressed by the *Ubx>GAL4*-driver. Expression of the fourth line (*IF.IR*) in *Ubx>fraFL-MYC* wing discs resulted in strong early lethality.

6.2.5 *par6.IR* partly rescues *frazzled*-associated reduction of basolateral DE-Cad

Of all the genes tested, only RNAi to *par6* was able to repress both *netA.IR* and *frazzled* overexpression phenotypes. To comprehend the possible interconnection between adult eversion phenotypes and cellular phenotypes, I tested whether RNAi knockdown of *par6* could also rescue cellular phenotypes of *frazzled* overexpression. Both *fraFL-MYC* and *par6.IR* were co-expressed using the *ptc-GAL4* driver, which allowed me to quantify the length of protrusions, the intensity of basolateral DE-Cad and the basal-apical ratio. Expression of *par6* expression partly reconstituted the level of basolateral DE-Cad (Figures 5.15, a and 6.8, c', c"): the mean antibody intensity (1.01±0.07) was significantly higher than in *ptc>FraFL-MYC* cells (0.9±0.09, p<0.0001 by Student's t-test), but lower than in control *ptc>GFP* cells (1.09±0.12, p=0.0072). The length of basal DP protrusions and basal-apical ratio in *ptc>FraFL-MYC;par6.IR* wing discs did not significantly differ from the same data in *ptc>FraFL-MYC* discs (Figures 5.5, f, 5.15, b, and 6.8, a', a", b', d): average length of protrusions was 7.7±1.98 μm (*ptc>FraFL-MYC* had protrusions of 7.8±1.95 μm, p >0.7), and basal-apical ratio was 1.53±0.26 (*ptc>FraFL-MYC* had protrusions of 1.63±0.43, p >0.3). Thus, *par6* is apparently involved into the *frazzled*-mediated control of DE-Cad trafficking. This result also supports the

hypothesis that DE-Cad trafficking is regulated independently from other *frazzled*-induced pathways (i.e. tissue invagination and protrusion formation).

6.3 Discussion

In this chapter an RNAi screen was conducted to test which genes are potentially acting in the downstream pathway through which NetrinA/Frazzled signaling controls the EMT in everting wing discs. Surprisingly, the majority of the genes (30 out of 49 genes) significantly suppressed eversion phenotypes in *netA.IR* flies. There are two possible explanations for this. One is that there is a decrease in the efficiency of RNAi to *netrinA* when co-expressing another *UAS-gene.IR* due to competition for the GAL4 activator. Arguing against this, co-expression of an unrelated *UAS* construct, *UAS-GFP*, does not suppress the *UAS-netrinA.IR* phenotypes (personal communication, M. J. Murray). On the other hand, it is possible that *netrinA* plays a fundamental role in controlling the epithelial state of the peripodial cells through signaling pathways regulating polarity, cell-cell adhesion, cell-ECM adhesion and cytoskeletal structure. In this case the loss of NetrinA affects multiple aspects of the cell, all of which are required to inhibit the EMT. Downregulation of just a single gene involved in this system would then be enough to tip the balance back to a normal eversion process.

At the same time, co-expression of a high portion of RNAi lines (in total 22 out of 49 genes) with *UAS-fraFL-MYC* resulted in a significant enhancement effect on eversion phenotypes. A complicating factor in this analysis is that the productivity/fecundity of *UAS-fraFL-MYC* crosses was quite low (Table 6.1, column 6) suggesting a high level of embryonic/larval lethality. This was exacerbated by many of the RNAi lines, in that the level of early pupal lethality was increased. In fact, for 14 of the 17 RNAi lines that suppressed *netA.IR* phenotypes but enhanced *frazzled* overexpression phenotypes, the enhancement was due to increased early pupal lethality. When lethals are excluded from the analysis (i.e. only the proportion of normal progeny versus progeny with disrupted wing/thorax is considered) only 3

genes (*gef26*, *rhogap68f*, *src64b*) significantly enhance (Table 6.1, column 8).

For these 3 RNAi lines at least, however, the results still suggest that these genes are being inhibited downstream of both NetrinA and Frazzled, raising the possibility of two pathways. It is worth remembering that disc eversion is a complex process with successive stages, which takes place over several hours, and that even Frazzled itself appears to play both positive and negative roles at different times. Thus these genes may play dual roles, which are revealed by the two genetic backgrounds employed in the screen.

Knockdown of four genes, *dscam*, *rhogef2*, *shg* and *trio*, had a significant enhancement effect on both *netA.IR* and *frazzled* overexpression phenotypes, suggesting their function is repressed by Frazzled and can be activated in response to NetrinA signaling. This result for *shg* is surprising since one might expect it to be inhibited during the EMT rather than being induced by NetrinA. Likely, expression of *shg.IR* strongly affects progeny by itself which means the results are confounded by a high degree of lethality (only 34 progeny were able to be analysed in both *netA.IR* and *fraFL-MYC* crosses; Table 6.1). Nevertheless, the results might also be pointing to a real positive role for E-Cadherin during eversion, perhaps during the latter stages of invasion and sheet migration, where it might be required to maintain tissue integrity. NetrinA signaling in the PE during eversion is easier to imagine as the tissue is known to undergo myosin II-mediated contraction (Aldaz *et al.*, 2013 [417]). On the other hand, there is also a possibility that RhoGEF2 is activated independently to induce the JNK pathway (Khoo *et al.*, 2013 [418]) which presumably acts upstream or parallel to NetrinA/Frazzled signaling (Manhire-Heath *et al.*, 2013 [133]). Therefore, the enhancement effect here could be associated with the complementary repression of wing disc eversion. The enhancement effect of *trio.IR* could, like *shg.IR*, be partly due to low fertility of *fraFL-MYC* females (19 of counted progeny respectively). However, as a potential Frazzled-interacting protein (Forsthoefel *et al.*, 2005 [238]), Trio could also be induced during thorax closure to regulate actin dynamics in the leading edge cells (Bateman and Van Vactor, 2000 [386]), where the receptor presumably plays a positive role.

A strong enhancement effect was also seen for *tum*, which is consistent with its proven role in wing disc eversion (Sfregola, 2014 [100]). However, again there was an extremely high level of lethality which makes interpretation difficult. Perhaps the most striking result is that all of the non-lethal progeny in the Frazzled overexpression genotype, were normal suggesting Tum is a potent factor acting downstream of Frazzled which inhibits eversion.

One gene, *par6*, a gene coding apical polarity protein, had a consistent effect on both *netA.IR* and *frazzled* overexpression and might therefore act downstream of both NetrinA and its receptor Frazzled. To elucidate possible mechanisms of *par6.IR*-induced suppression of *fraFL-MYC* eversion defects, I investigated the cellular phenotypes when expressing *par6.IR* in *ptc>fraFL-MYC* wing discs.

6.3.1 Downregulation of *par6* partially restores basolateral expression of DE-Cad in *frazzled* overexpressing cells

I have shown that *ptc-GAL4*-driven co-expression of *par6.IR* and *fraFL-MYC* partly reduces the loss of basolateral DE-Cad, whereas the tissue invagination phenotype and protrusion formation were unaffected. There is a possibility that rescue of *netA.IR* and *frazzled* overexpression eversion phenotypes by depletion of *par6* may be due to promotion of the EMT in mutant PE. This effect might rely on enhanced ZA breakdown in *par6.IR* cells, where disruption of DE-Cad vesicular trafficking to ZA probably underlies this process (Georgiou *et al.*, 2008 [195]; Leibfried *et al.*, 2008 [256]). Overall the results support a model in which basal-to-apical transport of DE-Cad is inhibited in cells overexpressing *frazzled*, whereas apical endocytic transport of the main junctional protein is supported. I hypothesize that in DP cells *frazzled* overexpression results in increased *par6*- and Rho1-mediated maintenance of ZA leading apparently to a deficiency of basolateral DE-Cad trafficking. The reduction of *par6* expression therefore could partly return the equilibrium between two routes of DE-Cad transport by depleting apical trafficking together with reconstitution of basolateral trafficking. If the same mechanism was occurring in the PE, where the

basolateral DE-Cad trafficking is naturally reduced due to the squamous morphology of the PE, the reduction of *par6* expression could attenuate maintenance of the ZA resulting in more efficient ZA breakdown during wing disc eversion.

Table 6.1: **Raw data from epistatic RNAi screening.**

All crosses were performed at 29°C.

N/C indicates "not counted" and refers to larval/embryonic lethality cases.

Values in column 7 represent Fisher's exact test values of normal progeny *vs* abnormal (i.e eversion defects or early pupal lethality). Values in column 8 represent Fisher's exact test values of normal progeny *vs* eversion defects (i.e. early pupal lethals were excluded.)

* *v108577*

Female genotype	Male genotype	No defects (%)	Eversion defects (%)	Early lethality (%)	Total (n)	P-value (normal *vs* abnormal)	P-value (normal *vs* eversion defects)
Ubx>netA.IR; GAL80^{ts}*	*w1118*	40	30	30	128		
	abl.IR (BL41710)	95	5	0	40	8.75E-11	8.07E-06
	akt1.IR (BL33615)	0	0	100	N/C	9.76E-16	1.00E+00
	aPKC.IR (BL34332)	0	0	100	N/C	9.76E-16	1.00E+00
	baz.IR (BL35002)	88	5	7	31	1.71E-06	2.39E-04
	btk29a.IR (v25615)	93	5	2	96	1.87E-17	1.54E-09
	cadN.IR (BL41982)	0	2	98	46	7.01E-09	4.33E-01
	cdc42d.IR (BL42861)	71	23	6	95	6.70E-06	1.70E-02
	cpa.IR (BL41685)	0	0	100	N/C	9.76E-16	1.00E+00

cpb.IR (BL41952)	91	5	4	150	6.56E-21	5.73E-12
dab.IR (BL42646)	51	2	47	45	2.21E-01	2.04E-04
ds.IR (BL28008)	43	10	47	13	7.69E-01	2.35E-01
dscam.IR (BL38945)	0	6	94	36	2.51E-07	1.90E-01
dscam2.IR (BL51839)	91	4	5	107	1.15E-16	3.37E-11
dscam4.IR (BL51508)	88	7	5	148	1.78E-17	2.28E-10
ena.IR (BL39034)	85	9	6	108	4.65E-13	2.45E-07
ens.IR (BL40825)	87	9	4	119	3.90E-15	4.97E-08
fak56d.IR (BL33617)	98	1	1	67	3.51E-18	2.18E-10
fra.IR (BL31469)	98	2	0	83	3.01E-20	5.69E-11
fra.IR (BL40826)	83	17	0	64	1.57E-08	8.57E-04
fps82d.IR (BL36053)	89	3.5	7.5	80	8.34E-13	3.92E-09
fps82d.IR (v107266)	56	28.5	15.5	141	1.02E-02	1.95E-01
gef26.IR (BL28928)	83.5	5.5	11	104	7.17E-12	7.80E-09
gef64c.IR (BL31130)	81	9	10	81	2.46E-09	2.71E-06
IF.IR (BL38958)	53	35	12	34	1.78E-01	8.34E-01
lrrk.IR (BL32457)	84	8	8	155	9.92E-15	1.74E-09
lrrk.IR (v105630)	68	10	22	95	2.60E-05	3.32E-05
mew.IR (BL44553)	92	8	0	73	4.44E-14	4.55E-07

mys.IR	0	0	100	N/C	9.76E-16	1.00E+00
par6.IR (BL35000)	95	4	1	73	5.56E-16	4.58E-09
pbl.IR (BL28343)	0	3	97	145	2.22E-20	3.83E-02
pi3k.IR (v107390)	2	8	90	84	2.84E-11	7.57E-02
rab6.IR (BL35744)	80	8	12	83	1.01E-08	2.71E-06
rab11.IR (BL27730)	0	0	100	N/C	9.76E-16	1.00E+00
rac1.IR (BL34910)	94	2	4	102	3.16E-19	1.02E-12
rho1.IR (BL32383)	0	0	100	N/C	9.76E-16	1.00E+00
rhogap68f.IR (BL41990)	94	6	0	110	1.00E-19	1.18E-09
rhoGEF2.IR (BL34643)	18	18	64	103	5.12E-04	5.59E-01
scar.IR (BL51803)	92	4	4	116	4.99E-19	2.80E-11
shg.IR (BL32904)	10	12	78	34	4.17E-04	6.95E-01
siz.IR (BL39060)	0	33	67	12	4.00E-03	3.83E-02
sli.IR (BL31467)	92	1	7	104	5.93E-18	9.19E-14
slik.IR (BL35719)	98	1	1	168	2.50E-32	2.73E-18
slik.IR (BL43783)	92	4	2	119	1.02E-18	2.57E-11
slik.IR (BL43784)	74	15	11	103	3.31E-07	1.47E-04
src42a.IR (v17643)	89	11	0	168	5.86E-20	9.39E-09
src42a.IR (v100708)	11	31	58	178	7.93E-09	1.30E-04

	src64b.IR (BL30517)	92	6	2	142	4.32E-21	5.18E-11
	stai.IR (BL53925)	21	12	67	43	2.72E-02	7.73E-01
	stan.IR (BL35050)	97	2	1	45	3.49E-13	1.47E-07
	tao1.IR (BL34881)	70.5	4.5	25	89	8.56E-06	1.30E-07
	trim9.IR (v21405)	0	0	100	N/C	9.76E-16	1.00E+00
	trim9.IR (v21406)	0	0	100	N/C	9.76E-16	1.00E+00
	trim9.IR (v100767)	49	33	18	131	1.69E-01	7.72E-01
	trio.IR (BL43549)	9	23.5	67.5	103	3.39E-08	4.14E-03
	tum.IR (BL35007)	0	0	100	156	2.41E-21	1.00E+00
	unc5.IR (BL33756)	87	8.5	4.5	106	8.36E-14	7.24E-08
	βIntν.IR (BL28601)	84	10	6	127	1.54E-13	2.04E-07
Ubx>fraFL-MYC;GAL80^{ts}	*w1118*	83	13	4	75		
	abl.IR (BL41710)	65	20	15	20	1.21E-01	4.57E-01
	akt1.IR (BL33615)	0	0	100	N/C	7.91E-35	1.00E+00
	aPKC.IR (BL34332)	0	0	100	N/C	7.91E-35	1.00E+00
	baz.IR (BL35002)	45	10	45	31	2.46E-04	7.08E-01
	btk29a.IR (v25615)	49	8	43	49	1.20E-04	1.00E+00
	cadN.IR (BL41982)	0	0	100	N/C	7.91E-35	1.00E+00
	cdc42.IR (BL42861)	75	25	0	12	6.88E-01	3.87E-01

cpa.IR (BL41685)	0	0	100	N/C	7.91E-35	1.00E+00
cpb.IR (BL41952)	61.3	6.4	32.3	31	2.45E-02	7.28E-01
dab.IR (BL42646)	94	6	0	17	4.54E-01	6.83E-01
ds.IR (BL28008)	77	0	23	13	6.98E-01	3.50E-01
dscam.IR (BL38945)	13.5	13.5	73	37	1.26E-12	1.55E-02
dscam2.IR (BL51839)	76.5	0	23.5	17	5.10E-01	3.48E-01
dscam4.IR (BL51508)	42	0	58	19	7.54E-04	5.86E-01
ena.IR (BL39034)	0	0	100	N/C	7.91E-35	1.00E+00
ens.IR (BL40825)	46	18	36	28	4.56E-04	1.70E-01
fak56d.IR (BL33617)	55	15	30	67	4.79E-04	3.23E-01
fra.IR (BL31469)	97	0	3	60	1.20E-02	2.21E-03
fps82d.IR (BL36053)	61.5	10	28.5	21	6.96E-02	1.00E+00
fps82d.IR (v107266)	55	21	24	38	3.06E-03	1.49E-01
gef26.IR (BL28928)	29	33	38	24	2.31E-06	2.03E-03
gef64c.IR (BL31130)	68	5	27	90	3.23E-02	2.81E-01
IF.IR (BL38958)	0	0	100	N/C	7.91E-35	1.00E+00
lrrk.IR (BL32457)	55.5	11	33.5	18	2.48E-02	6.79E-01
mew.IR (BL44553)	65	9	26	23	8.73E-02	1.00E+00
mys.IR	0	0	100	N/C	7.91E-35	1.00E+00

par6.IR (BL35000)	94	0	6	100	2.55E-02	1.61E-04
pbl.IR (BL28343)	0	3	97	60	1.18E-25	2.44E-02
pi3k.IR (v107390)	0	0	100	N/C	7.91E-35	1.00E+00
scar.IR (BL51803)	48	4	48	27	9.13E-04	6.83E-01
shg.IR (BL32904)	41	27	32	34	2.93E-05	1.49E-02
siz.IR (BL39060)	0	0	100	N/C	7.91E-35	1.00E+00
sli.IR (BL31467)	71	0	29	34	2.05E-01	6.18E-02
slik.IR (BL35719)	56	16	28	43	2.43E-03	3.85E-01
slik.IR (BL43783)	0	0	100	N/C	7.91E-35	1.00E+00
slik.IR (BL43784)	56	8	36	59	1.03E-03	1.00E+00
src42a.IR (v17643)	51.4	22.8	25.8	35	1.10E-03	7.65E-02
src42a.IR (v100708)	0	0	100	N/C	7.91E-35	1.00E+00
src64b.IR (BL30517)	43	21	36	61	1.76E-06	2.58E-02
stai.IR (BL53925)	0	0	100	N/C	7.91E-35	1.00E+00
stan.IR (BL35050)	38	0	62	45	9.42E-07	1.98E-01
rab6.IR (BL35744)	72	20	8	25	2.60E-01	5.11E-01
rab11.IR (BL27730)	0	0	100	N/C	7.91E-35	1.00E+00
rac1.IR (BL34910)	47.5	12.5	40	40	1.91E-04	5.17E-01
rho1.IR (BL32383)	0	0	100	N/C	7.91E-35	1.00E+00

rhogap68f.IR (BL41990)	31	18	50	44	3.78E-08	2.93E-02
rhoGEF2.IR (BL34643)	12	47	41	34	1.37E-12	4.76E-08
tao1.IR (BL34881)	0	0	100	N/C	7.91E-35	1.00E+00
trim9.IR (v21405)	0	0	100	N/C	7.91E-35	1.00E+00
trim9.IR (v21406)	0	0	100	N/C	7.91E-35	1.00E+00
trim9.IR (v100767)	53	27	20	15	3.56E-02	1.09E-01
trio.IR (BL43549)	53	15.5	31.5	19	1.25E-02	4.11E-01
tum.IR (BL35007)	52	0	48	65	1.29E-04	2.85E-02
unc5.IR (BL33756)	57	0	43	14	6.82E-02	5.86E-01
βIntν.IR (BL28601)	46	16	38	85	1.46E-06	1.07E-01

Figure 6.1: **Relationships of NetrinA and Frazzled with putative downstream effectors during wing disc eversion.** (a) Schematic summarising the possible regulatory relationships between NetrinA and Frazzled with a potential downstream target that might explain the phenotypic outcomes. Note: it is also theoretically possible that an interacting Protein X could act upstream by regulating expression of NetrinA of Frazzled levels, but for simplicity this is not shown in this diagram. (b) Table summarising RNAi lines expression results by their effects on *netA.IR* or *frazzled* overexpression eversion phenotypes. Classification of enhancement, suppression is based on the Fisher's exact test of normal progeny with respect to abnormal (i.e. eversion defects or early pupal lethality). RNAi lines were placed in the lethal category if the proportion of early pupal lethals was greater than 90%.

a

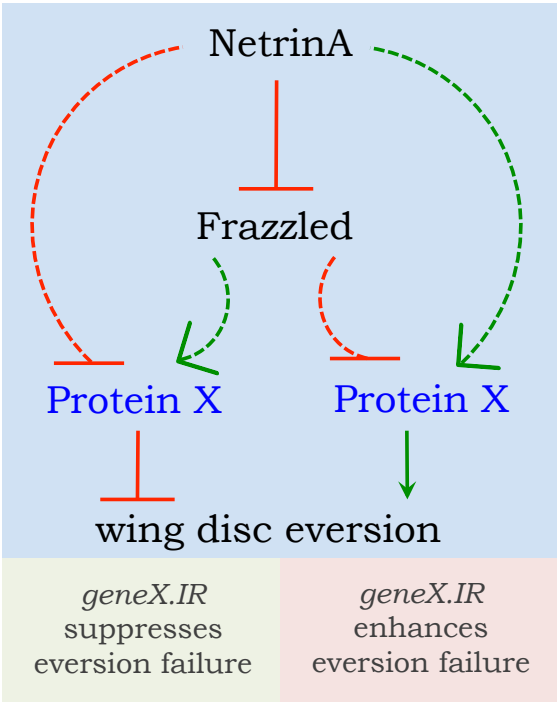

b

fraFL-MYC \ netrinA.IR	suppress	enhance	lethal	no effect
suppress	*fra*, *par6*			
enhance	*β η*, *baz*, *btk29a*, *cpb*, *dscam4*, *ens*, *fak56d*, *fps82d*, *gef26*, *lrrk*, *rac1*, *rhogef68f*, *scar*, *slik*, *src42a (17643)*, *src64b*, *stan*	*dscam*, *rhogef2*, *shg*, *trio*	*tum*	
lethal	*ena*, *tao1*	*pi3k*, *src42a (100708)*, *stai*	*akt1*, *aPKC*, *cadN*, *cpa*, *mys*, *pbl*, *rab11*, *rho1*, *siz*, *trim9 (21405, 21406)*	*IF*
no effect	*abl*, *cdc42*, *dscam2*, *fps82d (36053)*, *gef64c*, *mew*, *rab6*, *sli*, *unc5*			*dab*, *ds*, *trim9 (100767)*

Figure 6.2: **Genetic interaction analysis of genes encoding receptors of NetrinA.** (a) Crosses to *netA.IR* females. (b) Crosses to *fraFL-MYC* females. P-values represent Fisher's exact test values of normal progeny vs abnormal (i.e. eversion defects or early pupal lethality) (Table 6.1, column 8). Values of less than significance level (0.05) are presented above the graphs. Error bars show 95% CI for the proportion of normal progeny vs abnormal (by Wilson Score method).

a

Group 1. Receptors of NetrinA

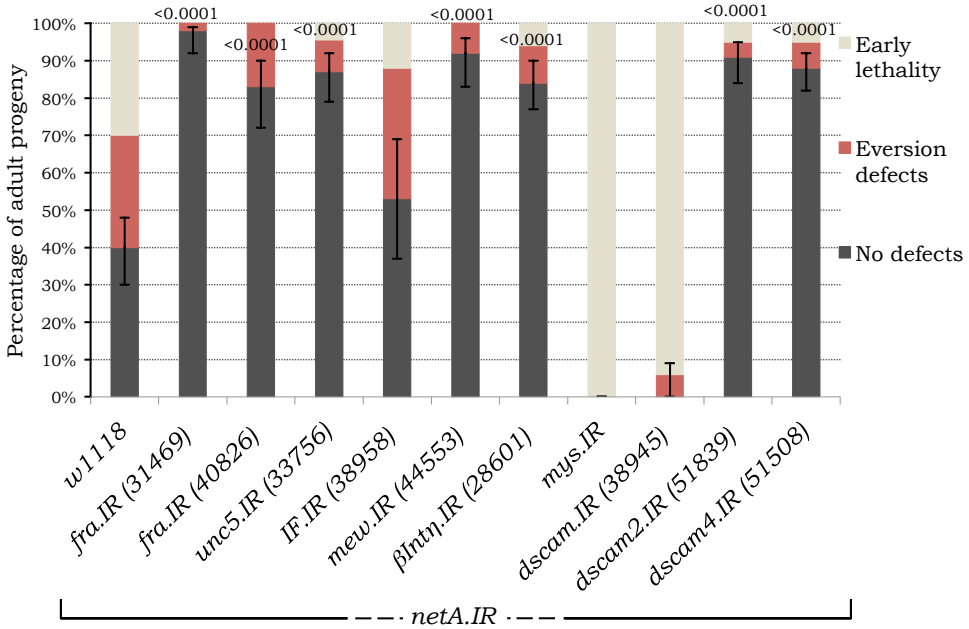

b

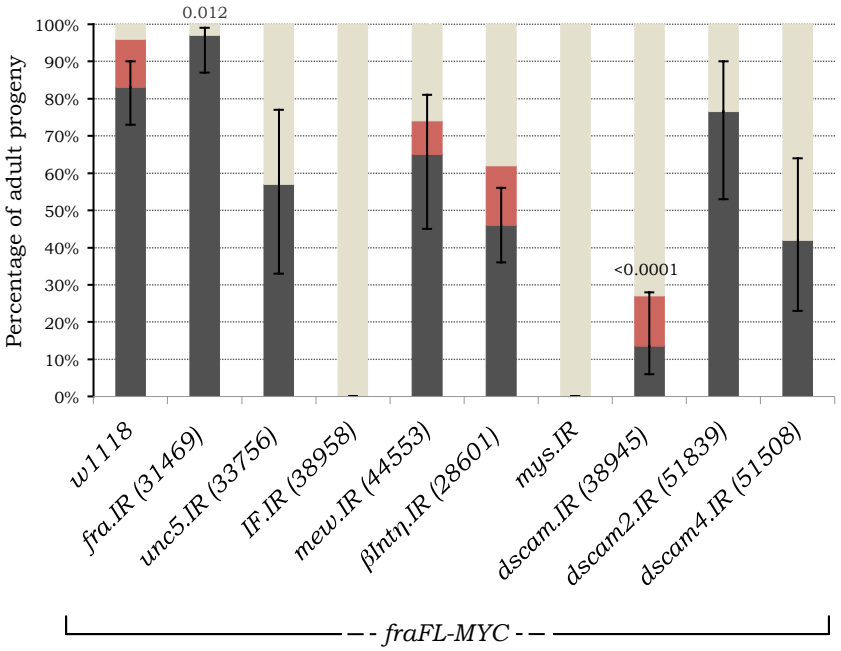

Figure 6.3: **Genetic interaction analysis of genes encoding proteins interacting with Frazzled.**(a) Crosses to *netA.IR* females. (b) Crosses to *fraFL-MYC* females. P-values represent Fisher's exact test values of normal progeny vs abnormal (i.e. eversion defects or early pupal lethality) (Table 6.1, column 8). Values of less than significance level (0.05) are presented above the graphs. Error bars show 95% CI for the proportion of normal progeny vs abnormal (by Wilson Score method).

Group 1. Frazzled interacting proteins

a

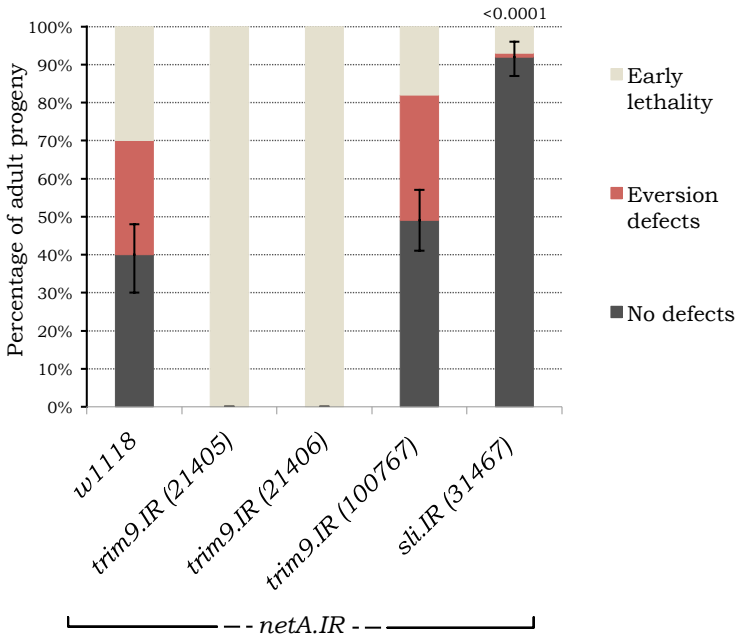

b

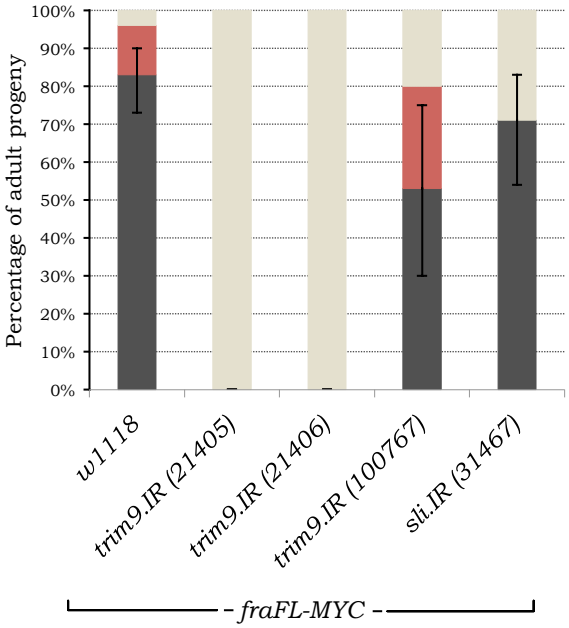

Figure 6.4: **Genetic interaction analysis of genes encoding potential Moe kinases.**(a) Crosses to *netA.IR* females. (b) Crosses to *fraFL-MYC* females. P-values represent Fisher's exact test values of normal progeny vs abnormal (i.e. eversion defects or early pupal lethality) (Table 6.1, column 8). Values of less than significance level (0.05) are presented above the graphs. Error bars show 95% CI for the proportion of normal progeny vs abnormal (by Wilson Score method).

Group 2. Kinases

a

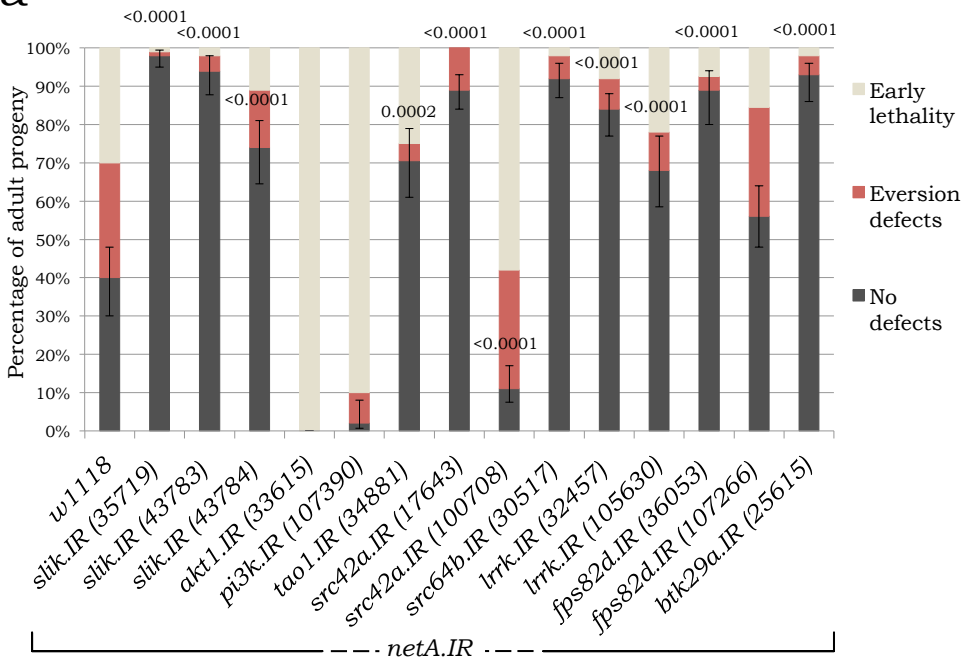

b

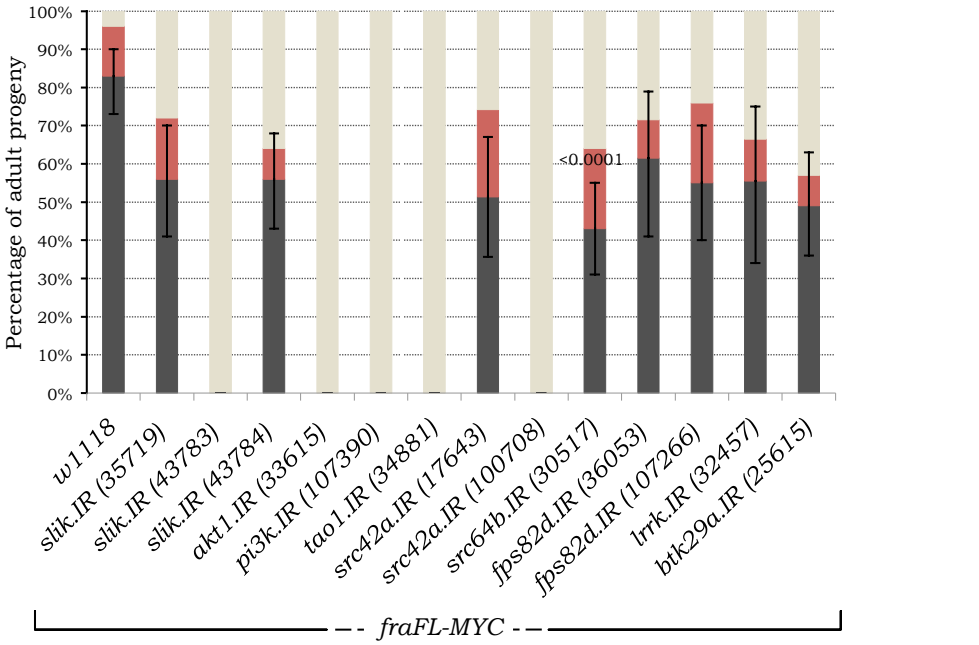

Figure 6.5: **Genetic interaction analysis of genes encoding small GTPases.**(a) Crosses to *netA.IR* females. (b) Crosses to *fraFL-MYC* females. P-values represent Fisher's exact test values of normal progeny vs abnormal (i.e. eversion defects or early pupal lethality) (Table 6.1, column 8). Values of less than significance level (0.05) are presented above the graphs. Error bars show 95% CI for the proportion of normal progeny vs abnormal (by Wilson Score method).

Group 3. GTPases and their regulators

a

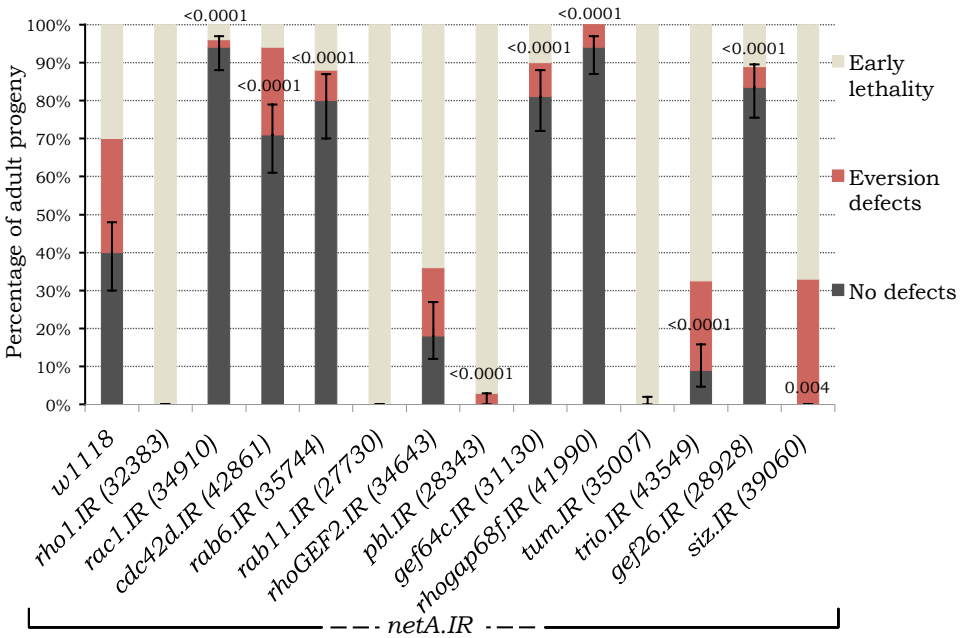

b

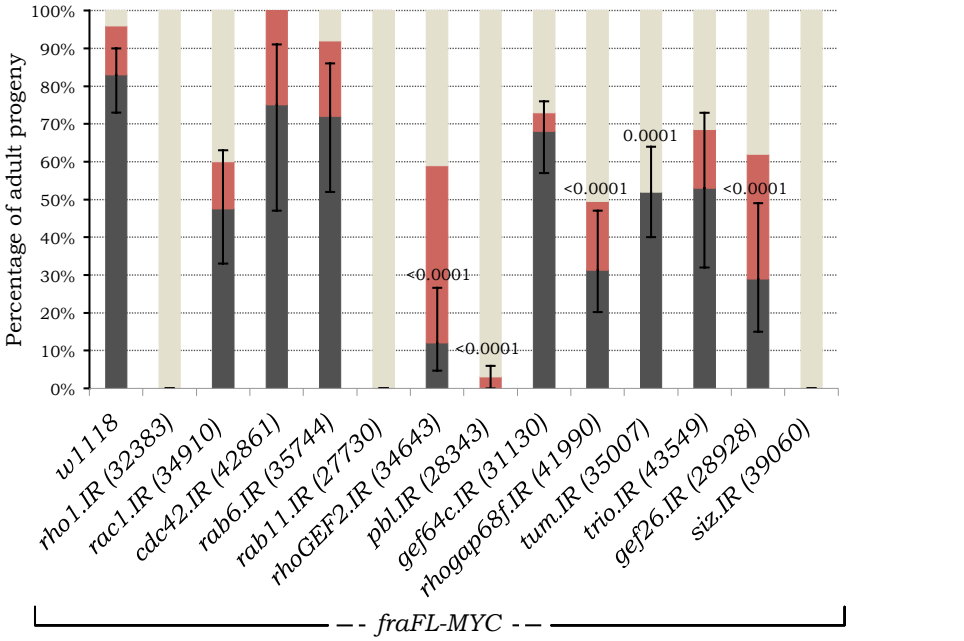

Figure 6.6: **Genetic interaction analysis of genes encoding adhesion and polarity proteins.**(a) Crosses to *netA.IR* females. (b) Crosses to *fraFL-MYC* females. P-values represent Fisher's exact test values of normal progeny vs abnormal (i.e. eversion defects or early pupal lethality) (Table 6.1, column 8). Values of less than significance level (0.05) are presented above the graphs. Error bars show 95% CI for the proportion of normal progeny vs abnormal (by Wilson Score method).

Group 4. Polarity & adhesion regulators

a

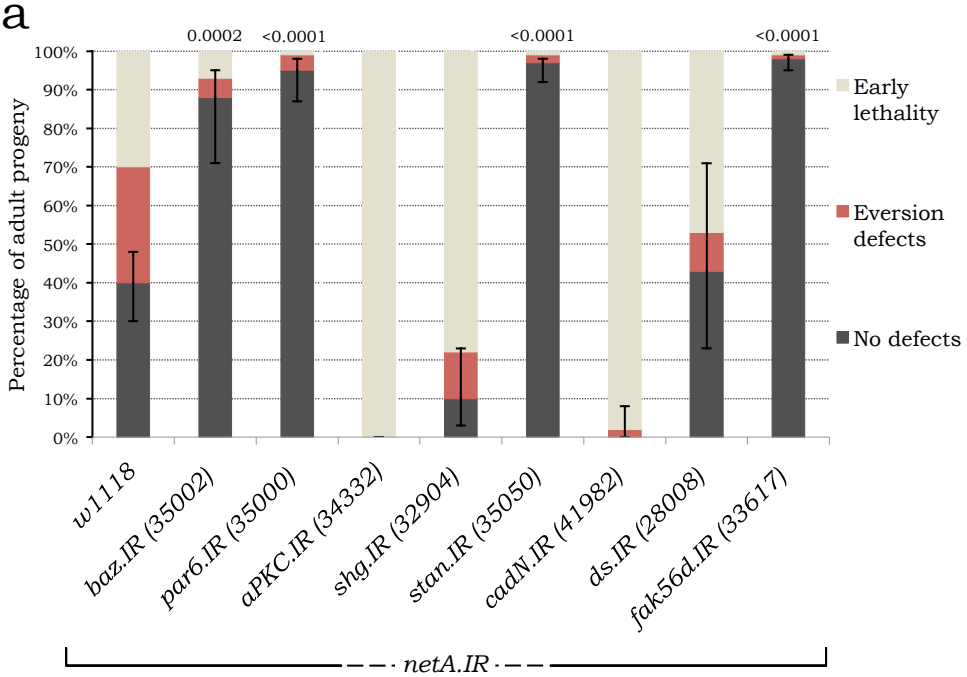

b

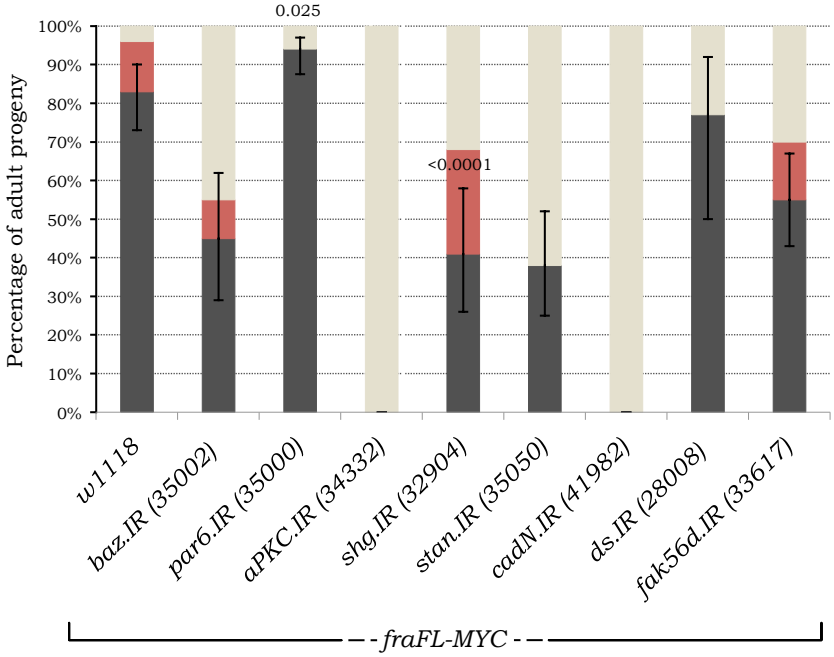

Figure 6.7: **Genetic interaction analysis of genes encoding cytoskeleton regulators.**(a) Crosses to *netA.IR* females. (b) Crosses to *fraFL-MYC* females. P-values represent Fisher's exact test values of normal progeny vs abnormal (i.e. eversion defects or early pupal lethality) (Table 6.1, column 8). Values of less than significance level (0.05) are presented above the graphs. Error bars show 95% CI for the proportion of normal progeny vs abnormal (by Wilson Score method).

Group 4. Cytoskeleton regulators

a

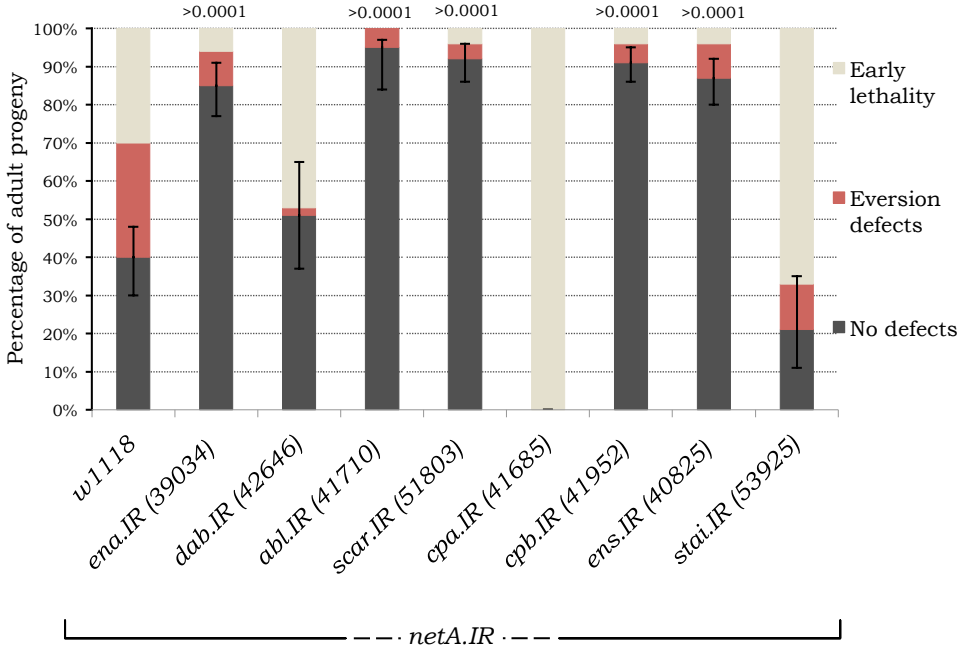

b

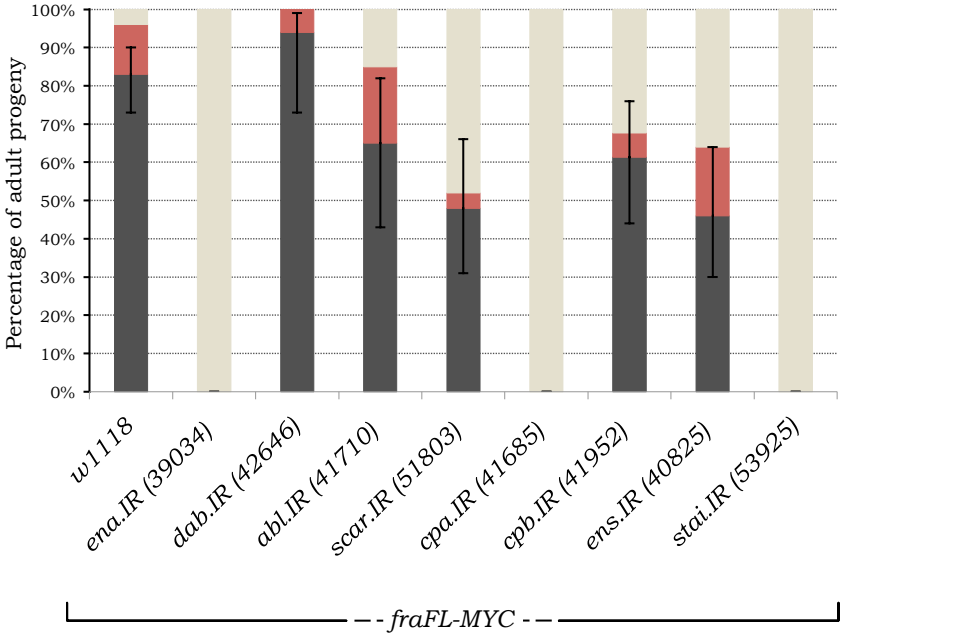

Figure 6.8: ***par6.IR* partly rescues *fraFL-MYC*-associated reduction of basolateral DE-Cad.** The *ptc>FraFL-MYC;par6.IR;GFP* wing disc immunostained for Fra (red in a, a', a", or grayscale in b, b', b") and DE-Cad (blue in a, a', a", or grayscale in c, c', c" and d). (a-c) Frontal view of the DP of *ptc>FraFL-MYC;par6.IR;GFP* disc. Dashed boxes indicate magnified area depicted in a'-c'. Dashed lines indicate the cross-sectional views depicted in a"-c". (a'-c' and a"-c") Magnified area and cross section of the DP showing GFP-positive *ptc*-expression stripe (green, a' and a") surrounded by wild type GFP-negative cells. The *ptc>FraFL-MYC;par6.IR* cells display strong basal expansion (black double-headed arrows, a' and a") and basal protrusions associated with Frazzled (arrows, b'). The intensity of basolateral DE-Cad in *ptc>FraFL-MYC;par6.IR* cells appeared to be visibly comparable with the intensity in wild type cells (arrowheads, c' and c"). ZA are indicated by double arrowheads (c' and c"). The apical-basal (A-B) axis is marked by double-headed arrow (a' and a"). (d) Three-dimensional view of the same disc. A furrow (arrow) formed along the GFP-positive (green) *ptc>FraFL-MYC;par6.IR* stripe. Scale bars 10 μm.

ptc>fraFL-MYC; par6.IR; GFP

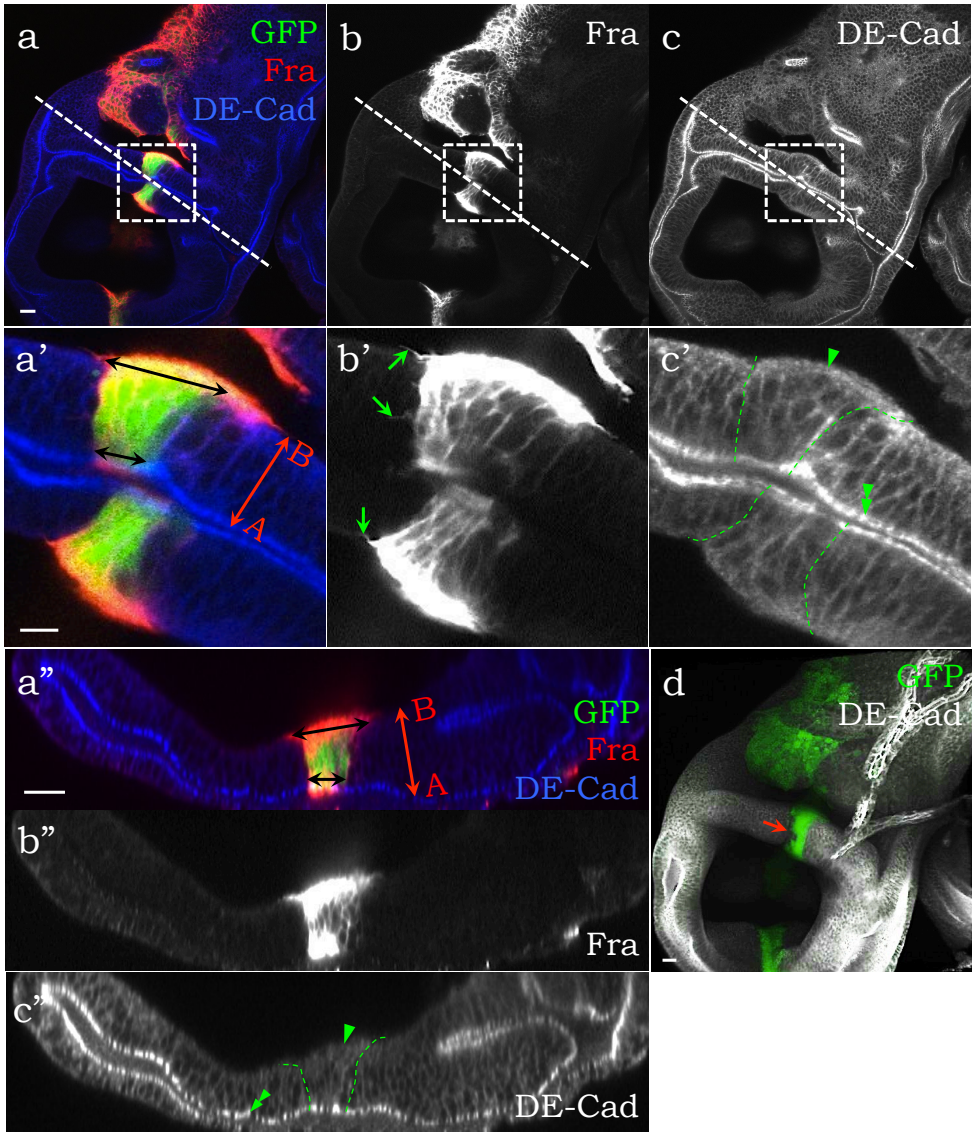

CHAPTER 7

Final discussion

This PhD project investigated the role of NetrinA and its receptor Frazzled in *Drosophila* epithelial plasticity. The findings contribute to our understanding of the genetic control of the EMT, a key event underlying developmental (germ layers and organ formation), physiological (i.e. fibrosis, regeneration) and pathophysiological (i.e. tumor dissemination and metastasis) processes in the majority of metazoans. NetrinA and Frazzled belong to highly conserved families of proteins best known for their role in the controlling axon guidance during CNS development (Hong *et al.*, 1999 [116]; Lai Wing Sun *et al.*, 2011 [108]) and also play an important role in organ development outside of the nervous system (Yebra *et al.*, 2003 [120]; Srinivasan *et al.*, 2003 [121]; Ziel *et al.*, 2009 [126]; Castets and Mehlen, 2010 [124]; Pert *et al.*, 2015 [78]). Netrin signaling is also strongly linked to cancer. Some netrins are over-expressed in many common cancers (Papanastasiou *et al.*, 2011 [128], Fitamant *et al.*, 2008 [129], Huang *et al.*, 2014 [130], Kong *et al.*, 2013 [131], Ramesh *et al.*, 2011 [132]) while the receptor, DCC, is lost in a high percentage of colorectal and other cancer types (Fearon *et al.*, 1990 [146]; Mehlen and Fearon, 2004 [147]). DCC's role in cancer progression is controversial, however, since only a few studies have shown it can act as a tumour suppressor and suppress metastatic growth (Castets *et al.*, 2011 [153]; Krimpenfort *et al.*, 2012 [232]; Duman-Scheel, 2012 [145]).

This study now adds new insight into Netrin signaling and metastasis, by pro-

viding evidence of a novel role for NetrinA as a positive regulator of EMT. This part of the research, covered in Chapter 3, was included in Manhire-Heath *et al.*, 2013 [133]. In Chapters 4 and 5, a more detailed study of Frazzled provided evidence that it could have dual effects on epithelial cells. In the PE and trachea it was able to support the epithelial state, while in the stable DP epithelium, it could induce motile protrusions, cell shape changes and disrupt sub-cellular localisation of junctional proteins. In this final section I integrate these results to arrive at a model for Frazzled function in epithelia.

7.1 A final model for NetrinA/Frazzled signaling in regulation of *Drosophila* epithelia

At the beginning of this study, we discovered that wing disc eversion was disrupted in adult flies expressing *netA.IR* (31% of progeny) or overexpressing *frazzled* (11%) in the PE (Manhire-Heath *et al.*, 2013 [133]). To better visualise the cellular basis for this, I established an *in vitro* approach for wing disc eversion. With this system, in ≈90% of the control discs the PE underwent partial EMT after 8 hrs of culture with ecdysone. During the EMT, peripodial cells displayed breakdown of E-Cadherin-associated ZA, cell dissociation and hole formation. The dissociated peripodial cells surrounding the hole reorganized their cytoskeletal structure, becoming enriched for F-actin bundles, and acquiring a more rounded, mesenchymal morphology. These cellular modifications were accompanied by degradation of the ECM surrounding the wing disc.

Consistent with the adult eversion defects, RNAi knockdown of *netrinA* in the PE inhibited ZA breakdown in 47% of the cultured discs, whereas in discs overexpressing *frazzled*, the rate was 35%. We speculated that NetrinA promotes ZA degradation, by downregulating Frazzled in the PE. This hypothesis was supported by findings that Frazzled levels decrease in the PE as the time of eversion approaches, and that the loss of NetrinA results in elevation of Frazzled in the PE (Manhire-Heath *et al.*,

2013 [133]). Moreover, RNAi knockdown of *frazzled* and loss of one copy of *frazzled* rescued the *netA.IR* eversion phenotype (Manhire-Heath *et al.*, 2013 [133] and this study, Chapter 4). Furthermore, *fra.IR* accelerated fragmentation of E-Cadherin in the PE in cultured wing discs, and also caused disruption of ZA-associated F-actin and redistribution of E-Cadherin in tracheal cells. Then, using a series of *frazzled* transgenes, I found that overexpression of Frazzled causes epithelial cells to expand basally and extend protrusions, undergo apical furrowing, and lose E-Cadherin and other junction-related proteins in basolateral regions.

Of these three phenotypes, the formation of protrusions is perhaps most readily understood. A number of *Drosophila* and vertebrate studies have demonstrated that the cytoplasmic regions of the Frazzled/DCC receptors activate the motility regulators Rac1 and Cdc42 (Shekarabi and Kennedy, 2002 [122]; Li *et al.*, 2002 [198]; Gitai *et al.*, 2003 [279]; Ren *et al.*, 2004 [242]; Forsthoefel *et al.*, 2005 [238]; Demarco *et al.*, 2012 [269]; Figure 7.1). Here, I found that cultured wing discs expressing *netA.IR* or *frazzled* in the PE produced elevated F-actin levels, a part of which was organized into basal straight bundles resembling stress fibers, the typical structures involved in cell-matrix adhesion (Tojkander *et al.*, 2012 [211]). Thus, at the EMT stage elevated levels of Frazzled could potentially cause excessive adhesion to the BM and inhibit eversion. The role of protrusions in blocking eversion is unclear since *fra*Δ*P1* and *fra*Δ*P3* transgenes were fully competent for protrusion formation but were unable to disrupt eversion. Previously, the P3 motif of Frazzled was suggested to be the only motif which is essential for commissural axons to cross the midline (Garbe *et al.*, 2007 [139]). Additionally, the P3 motif of DCC is known for its interaction with the Myosin-X, which is also required for elongation of filopodia (Zhu *et al.*, 2007 [321]). My results suggest that the P1 is also required for F-actin nucleation, and this seems plausible due to likely ability of the P1 to recruit actin polymerization factor Ena (Gitai *et al.*, 2003 [279]; Lebrand *et al.*, 2004 [325]). Out results also suggest that some Frazzled-induced motility might actually be required for invasion, migration and thorax closure, since fra^3/fra^4 escapers exhibited strong thoracic clefts.

Overexpression of Frazzled also caused furrows to form on the apical side the DP tissue (Figure 7.1). I speculate that this is indicative of excess Rho1 activity. Numerous studies have demonstrated that Rho1/RhoA is a major regulator of this sort of tissue invagination. During this process, activated Rho1 recruits F-actin polymerization regulators (i.e. formin Diaphanous, Abelson kinase) and non-muscle myosin to the apical side promoting actomyosin constriction and furrow formation (Fox and Peifer, 2007 [303], Homem and Peifer, 2008 [304]; Sawyer *et al.*, 2010 [293]). How Rho1 activity might be increased is not known but perhaps Frazzled-dependent Rac1 activation in basal regions restricts Rho1 activity to the other end of the cells. Whatever factors are causing Frazzled-induced invagination, they are also likely to inhibit eversion since the only ΔP transgene fully competent to cause tissue invagination, *fra*Δ*P2*, was also the only one to cause eversion defects.

Finally, Frazzled was able to deplete basolateral levels of E-Cadherin and Armadillo, and also pMoe which is known to co-localize with the junctional complexes and regulate their assembly (Hipfner *et al.*, 2004 [173]; Arpin *et al.*, 2011 [419]). I think this phenotype may lie at the heart of eversion failure for two reasons: i) only full-length Frazzled could efficiently block adult eversion and only E-Cadherin delocalisation required full-length Frazzled; and ii) *par6*, which is likely to play a key role in eversion failure given its knockdown rescued both *netA.IR* and *frazzled* overexpression defects, is only necessary for E-Cadherin delocalisation. The idea that Frazzled might regulate E-Cadherin is plausible given that Neogenin has been shown to regulate E-Cadherin trafficking in human epithelial cells (Lee *et al.*, 2016 [233]).

I hypothesise that Frazzled supports epithelial integrity by regulating vesicle transport of junctional material towards the ZA via Rho1 and Par6, which are known to positively regulate sub-apical vesicle trafficking of E-Cadherin (Yashiro *et al.*, 2014 [292]; Georgiou *et al.*, 2008 [195]; Leibfried *et al.*, 2008 [256]; Figure 7.1). In this model, elevated Frazzled supports the apical endocytic routes of E-Cadherin and Armadillo in the DP, and simultaneously inhibits the basolateral route, resulting in reduced basolateral pools of junctional complexes. Similar loss of lateral cell-cell adhesion are seen when epithelial cells flatten and reinforce their ZA contacts (Melani

et al., 2008 [290]; Hannezo *et al.*, 2014 [291]). Apparently, Frazzled also intensifies apical transport of junctional components in flat PE cells, where, however, the loss of basolateral pools is not detectable.

To conclude, NetrinA and Frazzled play a fundamental role in morphogenic events of *Drosophila* epithelia. Based on my results from RNAi screening, NetrinA apparently does this via multiple signaling pathways including cell adhesion, polarity, motility and endocytic transport. Since NetrinA and Frazzled function in opposite ways, it is likely that NetrinA downregulates its receptor in the PE during early stages of wing disc eversion. However Frazzled activity appears to play a positive role in the latter stages as thorax closure proceeds. Frazzled likely has its influence on cellular phenotypes via the small Rho GTPases. I hypothesise that ectopic expression of *frazzled* in the cuboidal epithelium creates localized Rho1 activity in the apical regions, promoting ZA reinforcement and apical constriction. Basally, where the receptor is most richly accumulated, Frazzled activates Rac1 and Cdc42 thereby promoting cell motility. How Frazzled switches from its function as an epithelial supporter to promoting cell motility is a question for future studies.

7.2 Future directions

This study opens a variety of possibilities for future investigation. Firstly, it would be of interest to analyse peripodial cell behaviour during thorax closure to determine whether NetrinA and Frazzled are required for motility at the leading edge during epithelial sheet migration. Secondly, it remains to be determined how NetrinA/Frazzled signaling is related to the other main regulators of the eversion process (i.e. JNK and Dpp). Another key study area is the *frazzled* loss-of-function phenotype in cultured and non-cultured wing discs. Given the apparent perdurance of Frazzled in fra^{-}/fra^{-} clones, an approach that targets the actual Frazzled protein, such as deGradFP technology (Caussinus *et al.*, 2012 [420]) may be more effective. Given my proposal that Frazzled regulates junctional trafficking, cell contractility and motility, the involvement of appropriate signaling pathways (i.e. Rab GTPases,

Rho1/ROCK, myosin, tubulins, Rac1, Cdc42, Dia, Ena, Abl *etc.*) must now be established. As cellular motility and constriction are dynamic processes, live cell imaging could also be conducted to better understand the cell behaviour. Finally, more work is required to understand how Frazzled is downregulated by NetrinA and whether this involves ubiquitination and/or lysosomal degradation pathways.

Through such studies, *Drosophila* will no doubt continue to shed light on the complex molecular pathways affected by NetrinA/Frazzled signaling and the rich range of biological processes they regulate. This, in turn, will contribute to the most topical subject of biomedical research, cancer progression and metastasis. Currently, most studies develop and improve cancer treatments based on the ability of DCC to suppress metastatic growth through its apoptotic activity. The data from this work identifies another two major roles of Frazzled/DCC in epithelial cells - support of epithelial stability, and regulation of epithelial cell morphology. Further understanding the biology of these Frazzled/DCC functions and how they contribute to cancer progression would help to generate more effective therapeutic approaches for cancer cure.

Figure 7.1: **Final model for Frazzled signaling.** (a) The upper image displays normal epithelial cells. There are shown two routes by which junctional material (both recycled and newly synthesised) can be transported between the Golgi and the ZA (Woichansky *et al.*, 2016 [193]): i) apical (possibly mediated by Par6 and Rho1); and ii) basolateral. The plasma membrane has a limited amount of Frazzled. Interaction between NetrinA and Frazzled induces endocytic degradation of the receptor. The box on the right displays the signaling pathways proposed to be activated by different cytoplasmic regions of Frazzled. (b) The lower image displays epithelial cells overexpressing *frazzled*. In apical regions of the cell Rho1 is activated, resulting in actomyosin contraction. Also, apical Rho1 reinforces apical E-Cadherin trafficking (also supported by Par6), which results in attenuation of the basolateral route. On the basal side, activation of Rac1 and Cdc42 by GEFs (Chauhan *et al.*, 2011 [266]) activates F-actin polymerization factors (e.g. Arp2/3, WASp) and inhibits Rho1.

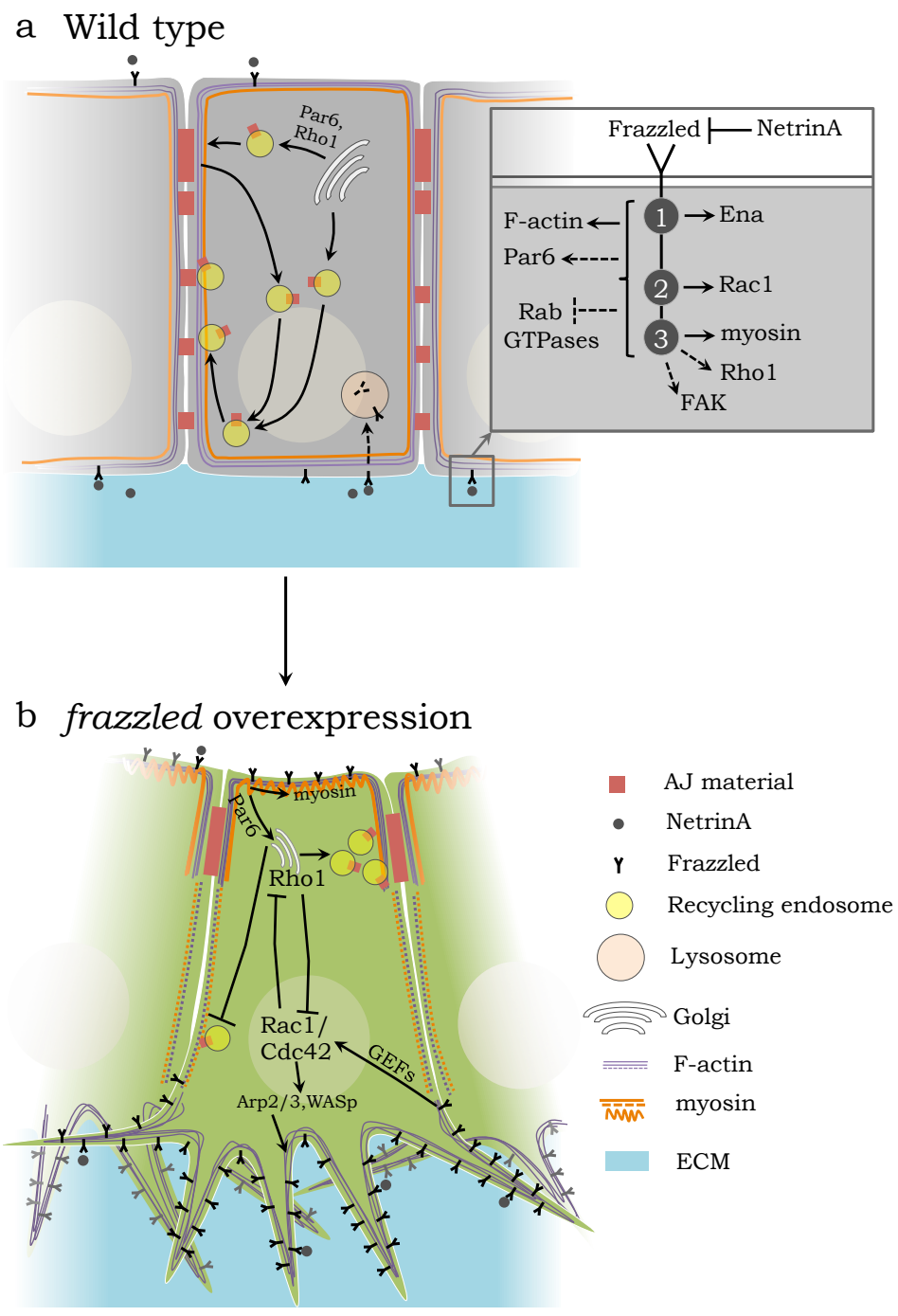
a Wild type
Par6,
Rho1
Frazzled
NetrinA
F-actin
Par6
Rab
GTPases
1
Ena
2
Rac1
3
myosin
Rho1
FAK
b frazzled overexpression
myosin
Par6
Rho1
Rac1/
Cdc42
GEFs
Arp2/3,WASp
AJ material
NetrinA
Frazzled
Recycling endosome
Lysosome
Golgi
F-actin
myosin
ECM

Bibliography

[1] Kai Simons and Stephen D Fuller. Cell surface polarity in epithelia. *Annual review of cell biology*, 1(1):243–288, 1985. (Cited on page 22.)

[2] Ulrich Tepass. The apical polarity protein network in *Drosophila* epithelial cells: regulation of polarity, junctions, morphogenesis, cell growth, and survival. *Annual review of cell and developmental biology*, 28:655–685, 2012. (Cited on pages 22, 23, 24, and 125.)

[3] Bob Goldstein and Ian G Macara. The PAR proteins: fundamental players in animal cell polarization. *Developmental cell*, 13(5):609–622, 2007. (Cited on pages 23 and 125.)

[4] Emeline Assémat, Elsa Bazellières, Emilie Pallesi-Pocachard, André Le Bivic, and Dominique Massey-Harroche. Polarity complex proteins. *Biochimica et Biophysica Acta (BBA)-Biomembranes*, 1778(3):614–630, 2008. (Cited on pages 23 and 24.)

[5] Andrea Hutterer, Joerg Betschinger, Mark Petronczki, and Juergen A Knoblich. Sequential roles of Cdc42, Par-6, aPKC, and Lgl in the establishment of epithelial polarity during *Drosophila* embryogenesis. *Developmental cell*, 6(6):845–854, 2004. (Cited on pages 23 and 24.)

[6] Scott X Atwood, Chiswili Chabu, Rhiannon R Penkert, Chris Q Doe, and Kenneth E Prehoda. Cdc42 acts downstream of bazooka to regulate neuroblast polarity through Par-6-aPKC. *Journal of cell science*, 120(18):3200–3206, 2007. (Cited on page 23.)

[7] Tony JC Harris and Mark Peifer. Adherens junction-dependent and -independent steps in the establishment of epithelial cell polarity in *Drosophila* . *The Journal of cell biology*, 167(1):135–147, 2004. (Cited on page 23.)

[8] Tony JC Harris and Mark Peifer. The positioning and segregation of apical cues during epithelial polarity establishment in *Drosophila* . *The Journal of cell biology*, 170(5):813–823, 2005. (Cited on page 23.)

[9] Melanie A McGill, RF Andrew McKinley, and Tony JC Harris. Independent cadherin-catenin and Bazooka clusters interact to assemble adherens junctions. *The Journal of cell biology*, 185(5):787–796, 2009. (Cited on page 23.)

[10] Andreas Wodarz, Uwe Hinz, Martin Engelbert, and Elisabeth Knust. Expression of *crumbs* confers apical character on plasma membrane domains of ectodermal epithelia of *Drosophila*. *Cell*, 82(1):67–76, 1995. (Cited on pages 23 and 24.)

[11] Ulrich Tepass, Carin Theres, and Elisabeth Knust. *crumbs* encodes an EGF-like protein expressed on apical membranes of *Drosophila* epithelial cells and required for organization of epithelia. *Cell*, 61(5):787–799, 1990. (Cited on page 23.)

[12] Ulrich Tepass and Elisabeth Knust. Crumbs and Stardust act in a genetic pathway that controls the organization of epithelia in *Drosophila melanogaster*. *Developmental biology*, 159(1):311–326, 1993. (Cited on page 24.)

[13] David Bilder and Norbert Perrimon. Localization of apical epithelial determinants by the basolateral PDZ protein Scribble. *Nature*, 403(6770):676–680, 2000. (Cited on page 24.)

[14] Tomoyuki Yamanaka, Yosuke Horikoshi, Yuki Sugiyama, Chikako Ishiyama, Atsushi Suzuki, Tomonori Hirose, Akihiro Iwamatsu, Azusa Shinohara, and Shigeo Ohno. Mammalian Lgl forms a protein complex with PAR-6 and aPKC

independently of PAR-3 to regulate epithelial cell polarity. *Current biology*, 13(9):734–743, 2003. (Cited on page 24.)

[15] Mireille Montcouquiol, Rivka A Rachel, Pamela J Lanford, Neal G Copeland, Nancy A Jenkins, and Matthew W Kelley. Identification of Vangl2 and Scrb1 as planar polarity genes in mammals. *Nature*, 423(6936):173–177, 2003. (Cited on page 24.)

[16] Jean-Remy Courbard, Alexandre Djiane, Jun Wu, and Marek Mlodzik. The apical/basal-polarity determinant Scribble cooperates with the PCP core factor Stbm/Vang and functions as one of its effectors. *Developmental biology*, 333(1):67–77, 2009. (Cited on page 24.)

[17] CR Green. Intercellular junctions. In *Biology of the Integument*, pages 5–16. Springer, 1984. (Cited on page 24.)

[18] Buzz Baum and Marios Georgiou. Dynamics of adherens junctions in epithelial establishment, maintenance, and remodeling. *The Journal of cell biology*, 192(6):907–917, 2011. (Cited on pages 24, 71, and 100.)

[19] Mitsuko Watabe-Uchida, Naoshige Uchida, Yuzo Imamura, Akira Nagafuchi, Kazushi Fujimoto, Tadashi Uemura, Stefan Vermeulen, Frans Van Roy, Eileen D Adamson, and Masatoshi Takeichi. α-Catenin-vinculin interaction functions to organize the apical junctional complex in epithelial cells. *The Journal of cell biology*, 142(3):847–857, 1998. (Cited on page 25.)

[20] Agnieszka Kobielak, H Amalia Pasolli, and Elaine Fuchs. Mammalian Formin-1 participates in adherens junctions and polymerization of linear actin cables. *Nature cell biology*, 6(1):21–30, 2004. (Cited on page 25.)

[21] Kentaro Abe and Masatoshi Takeichi. EPLIN mediates linkage of the cadherin–catenin complex to F-actin and stabilizes the circumferential actin belt. *Proceedings of the National Academy of Sciences*, 105(1):13–19, 2008. (Cited on page 25.)

[22] Buzz Baum and Norbert Perrimon. Spatial control of the actin cytoskeleton in *Drosophila* epithelial cells. *Nature cell biology*, 3(10):883–890, 2001. (Cited on page 25.)

[23] Matthias Behr, Dietmar Riedel, and Reinhard Schuh. The claudin-like megatrachea is essential in septate junctions for the epithelial barrier function in *Drosophila* . *Developmental cell*, 5(4):611–620, 2003. (Cited on page 25.)

[24] Ulrich Tepass. Claudin complexities at the apical junctional complex. *Nature cell biology*, 5(7):595–597, 2003. (Cited on page 25.)

[25] Kenzi Oshima and Richard G Fehon. Analysis of protein dynamics within the septate junction reveals a highly stable core protein complex that does not include the basolateral polarity protein Discs large. *Journal of cell science*, 124(16):2861–2871, 2011. (Cited on page 25.)

[26] Patrick Laprise, Kimberly M Lau, Kathryn P Harris, Nancy F Silva-Gagliardi, Sarah M Paul, Slobodan Beronja, Greg J Beitel, C Jane McGlade, and Ulrich Tepass. Yurt, Coracle, Neurexin IV and the Na+, K+-ATPase form a novel group of epithelial polarity proteins. *Nature*, 459(7250):1141–1145, 2009. (Cited on page 25.)

[27] Barry M Gumbiner. Cell adhesion: the molecular basis of tissue architecture and morphogenesis. *Cell*, 84(3):345–357, 1996. (Cited on page 25.)

[28] Valerie S LeBleu, Brian MacDonald, and Raghu Kalluri. Structure and function of basement membranes. *Experimental biology and medicine*, 232(9):1121–1129, 2007. (Cited on page 25.)

[29] Richard O Hynes. Integrins: bidirectional, allosteric signaling machines. *Cell*, 110(6):673–687, 2002. (Cited on pages 25 and 77.)

[30] Richard O Hynes. Integrins: versatility, modulation, and signaling in cell adhesion. *Cell*, 69(1):11–25, 1992. (Cited on page 25.)

[31] Aki Manninen. Epithelial polarity-generating and integrating signals from the ECM with integrins. *Experimental cell research*, 334(2):337–349, 2015. (Cited on page 26.)

[32] Jormay Lim and Jean Paul Thiery. Epithelial-mesenchymal transitions: insights from development. *Development*, 139(19):3471–3486, 2012. (Cited on page 26.)

[33] Raghu Kalluri and Robert A Weinberg. The basics of epithelial-mesenchymal transition. *The Journal of clinical investigation*, 119(6):1420–1428, 2009. (Cited on page 26.)

[34] Aristidis Moustakas and Carl-Henrik Heldin. Signaling networks guiding epithelial–mesenchymal transitions during embryogenesis and cancer progression. *Cancer science*, 98(10):1512–1520, 2007. (Cited on page 27.)

[35] Yoko Katsuno, Samy Lamouille, and Rik Derynck. TGF-β signaling and epithelial-mesenchymal transition in cancer progression. *Current opinion in oncology*, 25(1):76–84, 2013. (Cited on page 27.)

[36] David M Gonzalez and Damian Medici. Signaling mechanisms of the epithelial-mesenchymal transition. *Science signaling*, 7(344):re8, 2014. (Cited on pages 27 and 28.)

[37] Aristidis Moustakas and Carl-Henrik Heldin. Mechanisms of TGFβ-induced epithelial-mesenchymal transition. *Journal of Clinical Medicine*, 5(7):63, 2016. (Cited on page 27.)

[38] Sean Lawler, Xin-Hua Feng, Ruey-Hwa Chen, E Miko Maruoka, Christoph W Turck, Irene Griswold-Prenner, and Rik Derynck. The type II transforming growth factor-β receptor autophosphorylates not only on serine and threonine but also on tyrosine residues. *Journal of Biological Chemistry*, 272(23):14850–14859, 1997. (Cited on page 27.)

[39] Rik Derynck and Xin-Hua Feng. TGF-β receptor signaling. *Biochimica et Biophysica Acta (BBA)-Reviews on Cancer*, 1333(2):F105–F150, 1997. (Cited on page 27.)

[40] Carl-Henrik Heldin and Aristidis Moustakas. Signaling receptors for TGF-β family members. *Cold Spring Harbor Perspectives in Biology*, 8(8):a022053, 2016. (Cited on page 27.)

[41] Yigong Shi and Joan Massagué. Mechanisms of TGF-β signaling from cell membrane to the nucleus. *Cell*, 113(6):685–700, 2003. (Cited on page 27.)

[42] Theresa Vincent, Etienne PA Neve, Jill R Johnson, Alexander Kukalev, Federico Rojo, Joan Albanell, Kristian Pietras, Ismo Virtanen, Lennart Philipson, Philip L Leopold, Crystal G Ronald, de Herreros Antonio Garcia, Moustakas Aristidis, Pettersson F Ralf, and Fuxe Jonas. A SNAIL1-SMAD3/4 transcriptional repressor complex promotes TGF-β mediated epithelial-mesenchymal transition. *Nature cell biology*, 11(8):943–950, 2009. (Cited on page 28.)

[43] Aristidis Moustakas and Carl-Henrik Heldin. Non-Smad TGF-β signals. *J Cell Sci*, 118(16):3573–3584, 2005. (Cited on page 28.)

[44] Barish Ozdamar, Rohit Bose, Miriam Barrios-Rodiles, Hong-Rui Wang, Yue Zhang, and Jeffrey L Wrana. Regulation of the polarity protein Par6 by TGFβ receptors controls epithelial cell plasticity. *Science*, 307(5715):1603–1609, 2005. (Cited on pages 28, 125, and 126.)

[45] Nicol Hutchison, Bruce M Hendry, and Claire C Sharpe. Rho isoforms have distinct and specific functions in the process of epithelial to mesenchymal transition in renal proximal tubular cells. *Cellular signalling*, 21(10):1522–1531, 2009. (Cited on page 28.)

[46] Samy Lamouille, Jian Xu, and Rik Derynck. Molecular mechanisms of epithelial-mesenchymal transition. *Nature reviews Molecular cell biology*, 15(3):178–196, 2014. (Cited on pages 28, 62, and 73.)

[47] Nick Barker. The canonical wnt/β-catenin signalling pathway. *Wnt Signaling: Pathway Methods and Mammalian Models*, pages 5–15, 2008. (Cited on page 28.)

[48] Victoria Bolós, Moisés Blanco, Vanessa Medina, Guadalupe Aparicio, Silvia Díaz-Prado, and Enrique Grande. Notch signalling in cancer stem cells. *Clinical and Translational Oncology*, 11(1):11–19, 2009. (Cited on page 28.)

[49] Jussi Taipale and Philip A Beachy. The Hedgehog and Wnt signalling pathways in cancer. *nature*, 411(6835):349–354, 2001. (Cited on page 28.)

[50] Elizabeth C Finger and Amato J Giaccia. Hypoxia, inflammation, and the tumor microenvironment in metastatic disease. *Cancer and Metastasis Reviews*, 29(2):285–293, 2010. (Cited on page 28.)

[51] Rebecca L Heise, Vandy Stober, Chaitra Cheluvaraju, John W Hollingsworth, and Stavros Garantziotis. Mechanical stretch induces epithelial-mesenchymal transition in alveolar epithelia via hyaluronan activation of innate immunity. *Journal of Biological Chemistry*, 286(20):17435–17444, 2011. (Cited on page 28.)

[52] Paola Nisticò, Mina J Bissell, and Derek C Radisky. Epithelial-mesenchymal transition: general principles and pathological relevance with special emphasis on the role of matrix metalloproteinases. *Cold Spring Harbor perspectives in biology*, 4(2):a011908, 2012. (Cited on page 28.)

[53] Amparo Cano, Mirna A Pérez-Moreno, Isabel Rodrigo, Annamaria Locascio, María J Blanco, Marta G del Barrio, Francisco Portillo, and M Angela Nieto. The transcription factor Snail controls epithelial–mesenchymal transitions by repressing E-cadherin expression. *Nature cell biology*, 2(2):76–83, 2000. (Cited on pages 28 and 71.)

[54] EL Whiteman, CJ Liu, ER Fearon, and B Margolis. The transcription factor Snail represses Crumbs3 expression and disrupts apico-basal polarity complexes. *Oncogene*, 27(27):3875–3879, 2008. (Cited on page 28.)

[55] M Leptin and B Grunewald. Cell shape changes during gastrulation in *Drosophila* . *Development*, 110(1):74–84, 1990. (Cited on pages 29 and 30.)

[56] Jing Yang, Sendurai A Mani, Joana Liu Donaher, Sridhar Ramaswamy, Raphael A Itzykson, Christophe Come, Pierre Savagner, Inna Gitelman, Andrea Richardson, and Robert A Weinberg. Twist, a master regulator of morphogenesis, plays an essential role in tumor metastasis. *cell*, 117(7):927–939, 2004. (Cited on page 29.)

[57] Esmeralda Casas, Jihoon Kim, Andrés Bendesky, Lucila Ohno-Machado, Cecily J Wolfe, and Jing Yang. Snail2 is an essential mediator of Twist1-induced epithelial mesenchymal transition and metastasis. *Cancer research*, 71(1):245–254, 2011. (Cited on page 29.)

[58] Muh-Hwa Yang, Dennis Shin-Shian Hsu, Hsei-Wei Wang, Hsiao-Jung Wang, Hsin-Yi Lan, Wen-Hao Yang, Chi-Hung Huang, Shou-Yen Kao, Cheng-Hwai Tzeng, Shyh-Kuan Tai, Shyue-Yih Chang, Oscar Kuang-Sheng Lee, and Kou-Juey Wu. BMI1 is essential in Twist1-induced epithelial-mesenchymal transition. *Nature cell biology*, 12(10):982–992, 2010. (Cited on page 29.)

[59] Fen Yang, Luyang Sun, Qian Li, Xiao Han, Liandi Lei, Hua Zhang, and Yongfeng Shang. SET8 promotes epithelial-mesenchymal transition and confers TWIST dual transcriptional activities. *The EMBO journal*, 31(1):110–123, 2012. (Cited on page 29.)

[60] Edwin A Clark, Todd R Golub, Eric S Lander, and Richard O Hynes. Genomic analysis of metastasis reveals an essential role for RhoC. *Nature*, 406(6795):532–535, 2000. (Cited on page 29.)

[61] Héctor Peinado, David Olmeda, and Amparo Cano. Snail, Zeb and bHLH factors in tumour progression: an alliance against the epithelial phenotype? *Nature Reviews Cancer*, 7(6):415–428, 2007. (Cited on page 29.)

[62] Ester Sánchez-Tilló, Laura Siles, Oriol De Barrios, Miriam Cuatrecasas, Eva C Vaquero, Antoni Castells, and Antonio Postigo. Expanding roles of ZEB factors in tumorigenesis and tumor progression. *Am J Cancer Res*, 1(7):897–912, 2012. (Cited on page 29.)

[63] Kwonseop Kim, Zifan Lu, and Elizabeth D Hay. Direct evidence for a role of β-catenin/LEF-1 signaling pathway in induction of EMT. *Cell biology international*, 26(5):463–476, 2002. (Cited on page 29.)

[64] Colin Jamora, Ramanuj DasGupta, Pawel Kocieniewski, and Elaine Fuchs. Links between signal transduction, transcription and adhesion in epithelial bud development. *Nature*, 422(6929):317–322, 2003. (Cited on page 29.)

[65] Catherine D Nobes and Alan Hall. Rho GTPases control polarity, protrusion, and adhesion during cell movement. *The Journal of cell biology*, 144(6):1235–1244, 1999. (Cited on page 29.)

[66] Mahmut Yilmaz and Gerhard Christofori. EMT, the cytoskeleton, and cancer cell invasion. *Cancer and Metastasis Reviews*, 28(1-2):15–33, 2009. (Cited on pages 29 and 73.)

[67] Jacqueline Cherfils and Mahel Zeghouf. Regulation of small GTPases by GEFs, GAPs, and GDIs. *Physiological reviews*, 93(1):269–309, 2013. (Cited on page 30.)

[68] Orane Visvikis, Madhavi P Maddugoda, and Emmanuel Lemichez. Direct modifications of Rho proteins: deconstructing GTPase regulation. *Biology of the Cell*, 102(7):377–389, 2010. (Cited on page 30.)

[69] Mark A McNiven. Breaking away: matrix remodeling from the leading edge. *Trends in cell biology*, 23(1):16–21, 2013. (Cited on page 30.)

[70] Yukiko Nakaya, Erike W Sukowati, Yuping Wu, and Guojun Sheng. RhoA and microtubule dynamics control cell-basement membrane interaction in EMT during gastrulation. *Nature cell biology*, 10(7):765–775, 2008. (Cited on pages 30 and 104.)

[71] Michael J Murray. *Drosophila* models of metastasis. *AIMS Genetics*, 2(1):25–53, 2015. (Cited on page 30.)

[72] Dari Sweeton, Suki Parks, Michael Costa, and Eric Wieschaus. Gastrulation in *Drosophila* : the formation of the ventral furrow and posterior midgut invaginations. *Development*, 112(1):775–789, 1991. (Cited on page 30.)

[73] Angelike Stathopoulos and Michael Levine. Linear signaling in the Toll-Dorsal pathway of *Drosophila* : activated Pelle kinase specifies all threshold outputs of gene expression while the bHLH protein Twist specifies a subset. *Development*, 129(14):3411–3419, 2002. (Cited on page 30.)

[74] Amy McMahon, Gregory T Reeves, Willy Supatto, and Angelike Stathopoulos. Mesoderm migration in *Drosophila* is a multi-step process requiring FGF signaling and integrin activity. *Development*, 137(13):2167–2175, 2010. (Cited on page 30.)

[75] R Reuter. The gene *serpent* has homeotic properties and specifies endoderm versus ectoderm within the *Drosophila* gut. *Development*, 120(5):1123–1135, 1994. (Cited on pages 30 and 31.)

[76] Ulrich Tepass and Volker Hartenstein. The development of cellular junctions in the *Drosophila* embryo. *Developmental biology*, 161(2):563–596, 1994. (Cited on pages 31 and 96.)

[77] Danelle Devenport and Nicholas H. Brown. Morphogenesis in the absence of integrins: mutation of both *Drosophila* β-subunits prevents midgut migration. 131(21):5405–5415, 2004. (Cited on pages 31 and 120.)

[78] Melissa Pert, Miao Gan, Robert Saint, and Michael J Murray. Netrins and Frazzled/DCC promote the migration and mesenchymal to epithelial transition of *Drosophila* midgut cells. *Biology open*, 4(2):233–243, 2015. (Cited on pages 31, 40, 84, 94, 120, and 137.)

[79] Denise J Montell, Wan Hee Yoon, and Michelle Starz-Gaiano. Group choreography: mechanisms orchestrating the collective movement of border cells. *Nature Reviews Molecular Cell Biology*, 13(10):631–645, 2012. (Cited on page 31.)

[80] Véronique Van De Bor, Geordie Zimniak, Delphine Cérézo, Sébastien Schaub, and Stéphane Noselli. Asymmetric localisation of cytokine mRNA is essential for JAK/STAT activation during cell invasiveness. *Development*, 138(7):1383–1393, 2011. (Cited on page 31.)

[81] Henry J Wehman. Fine structure of *Drosophila* wing imaginal discs during early stages of metamorphosis. *Wilhelm Roux'Archiv für Entwicklungsmechanik der Organismen*, 163(4):375–390, 1969. (Cited on page 32.)

[82] José Carlos Pastor-Pareja, Ferdinand Grawe, Enrique Martin-Blanco, and Antonio Garcia-Bellido. Invasive cell behavior during *Drosophila* imaginal disc eversion is mediated by the JNK signaling cascade. *Developmental cell*, 7(3):387–399, 2004. (Cited on pages 32, 33, 34, 64, 70, and 74.)

[83] Geoff Richards. Insect hormones in development. *Biological Reviews*, 56(4):501–549, 1981. (Cited on page 32.)

[84] Silvia Aldaz, Luis M Escudero, and Matthew Freeman. Live imaging of *Drosophila* imaginal disc development. *Proceedings of the National Academy of Sciences*, 107(32):14217–14222, 2010. (Cited on pages 33, 42, 54, 61, 63, and 70.)

[85] Enrique Martín-Blanco, Alexandra Gampel, Jenny Ring, Kanwar Virdee, Nikolai Kirov, Aviva M Tolkovsky, and Alfonso Martinez-Arias. *puckered* encodes a phosphatase that mediates a feedback loop regulating JNK activity

during dorsal closure in *Drosophila* . *Genes & development*, 12(4):557–570, 1998. (Cited on pages 33 and 34.)

[86] Julia Zeitlinger and Dirk Bohmann. Thorax closure in *Drosophila* : involvement of Fos and the JNK pathway. *Development*, 126(17):3947–3956, 1999. (Cited on pages 33, 34, and 35.)

[87] François Agnès, Magali Suzanne, and Stéphane Noselli. The *Drosophila* JNK pathway controls the morphogenesis of imaginal discs during metamorphosis. *Development*, 126(23):5453–5462, 1999. (Cited on page 33.)

[88] Minoru Tateno, Yasuyoshi Nishida, and Takashi Adachi-Yamada. Regulation of JNK by Src during *Drosophila* development. *Science*, 287(5451):324–327, 2000. (Cited on pages 33 and 35.)

[89] François Agnès, Magali Suzanne, and Stéphane Noselli. The *Drosophila* JNK pathway controls the morphogenesis of imaginal discs during metamorphosis. *Development*, 126(23):5453–5462, 1999. (Cited on page 34.)

[90] Ajay Srivastava, Jose Carlos Pastor-Pareja, Tatsushi Igaki, Raymond Pagliarini, and Tian Xu. Basement membrane remodeling is essential for *Drosophila* disc eversion and tumor invasion. *Proceedings of the National Academy of Sciences*, 104(8):2721–2726, 2007. (Cited on pages 34, 70, 76, and 78.)

[91] Enrique Martín-Blanco, José C Pastor-Pareja, and Antonio García-Bellido. JNK and decapentaplegic signaling control adhesiveness and cytoskeleton dynamics during thorax closure in *Drosophila* . *Proceedings of the National Academy of Sciences*, 97(14):7888–7893, 2000. (Cited on pages 34 and 35.)

[92] Fisun Hamaratoglu, Markus Affolter, and George Pyrowolakis. Dpp/BMP signaling in flies: From molecules to biology. In *Seminars in cell & developmental biology*, volume 32, pages 128–136. Elsevier, 2014. (Cited on page 34.)

[93] George Pyrowolakis, Britta Hartmann, Bruno Müller, Konrad Basler, and Markus Affolter. A simple molecular complex mediates widespread BMP-induced repression during *Drosophila* development. *Developmental cell*, 7(2):229–240, 2004. (Cited on page 35.)

[94] Forrest A Spencer, F Michael Hoffmann, and William M Gelbart. Decapentaplegic: a gene complex affecting morphogenesis in *Drosophila melanogaster*. *Cell*, 28(3):451–461, 1982. (Cited on page 35.)

[95] Hai Huang, Guiping Du, Hanqing Chen, Xuehong Liang, Changqing Li, Nannan Zhu, Lei Xue, Jun Ma, and Renjie Jiao. *Drosophila* Smt3 negatively regulates JNK signaling through sequestering Hipk in the nucleus. *Development*, 138(12):2477–2485, 2011. (Cited on page 35.)

[96] Richelle Sopko and Norbert Perrimon. Receptor tyrosine kinases in *Drosophila* development. *Cold Spring Harbor perspectives in biology*, 5(6), 2013. (Cited on page 36.)

[97] Satoshi Ishimaru, Ryu Ueda, Yoshimi Hinohara, Mayumi Ohtani, and Hidesaburo Hanafusa. PVR plays a critical role via JNK activation in thorax closure during *Drosophila* metamorphosis. *The EMBO journal*, 23(20):3984–3994, 2004. (Cited on page 36.)

[98] Koichi Eguchi, Yasuhide Yoshioka, Hideki Yoshida, Kazushige Morishita, Seiji Miyata, Hiroshi Hiai, and Masamitsu Yamaguchi. The *Drosophila* DOCK family protein sponge is involved in differentiation of R7 photoreceptor cells. *Experimental cell research*, 319(14):2179–2195, 2013. (Cited on page 36.)

[99] Kazushige Morishita, Fumito Ozasa, Koichi Eguchi, Yasuhide Yoshioka, Hideki Yoshida, Hiroshi Hiai, and Masamitsu Yamaguchi. *Drosophila* DOCK family protein Sponge regulates the JNK pathway during thorax development. *Cell structure and function*, 2014. (Cited on page 36.)

[100] Michael Sfregola. Centralspindlin is required for thorax development during *Drosophila* metamorphosis. *genesis*, 52(5):387–398, 2014. (Cited on pages 36, 37, 124, and 135.)

[101] Masanori Mishima, Susanne Kaitna, and Michael Glotzer. Central spindle assembly and cytokinesis require a Kinesin-like protein/RhoGAP complex with microtubule bundling activity. *Developmental cell*, 2(1):41–54, 2002. (Cited on pages 36 and 124.)

[102] Michael Zavortink, Nelida Contreras, Tracie Addy, Amy Bejsovec, and Robert Saint. Tum/RacGAP50C provides a critical link between anaphase microtubules and the assembly of the contractile ring in *Drosophila melanogaster*. *Journal of Cell Science*, 118(22):5381–5392, 2005. (Cited on page 36.)

[103] Ann YN Goldstein, Yuh-Nung Jan, and Liqun Luo. Function and regulation of Tumbleweed (RacGAP50C) in neuroblast proliferation and neuronal morphogenesis. *Proceedings of the National Academy of Sciences of the United States of America*, 102(10):3834–3839, 2005. (Cited on pages 37 and 124.)

[104] Richard R Adams, Alvaro AM Tavares, Adi Salzberg, Hugo J Bellen, and David M Glover. Pavarotti encodes a kinesin-like protein required to organize the central spindle and contractile ring for cytokinesis. *Genes & development*, 12(10):1483–1494, 1998. (Cited on page 37.)

[105] Li Tao, Barbara Fasulo, Brandt Warecki, and William Sullivan. Tum/RacGAP functions as a switch activating the Pav/kinesin-6 motor. *Nature communications*, 7, 2016. (Cited on page 37.)

[106] Andrea H Brand and Norbert Perrimon. Targeted gene expression as a means of altering cell fates and generating dominant phenotypes. *Development*, 118(2):401–415, 1993. (Cited on page 37.)

[107] SK Pallavi and LS Shashidhara. Egfr/Ras pathway mediates interactions between peripodial and disc proper cells in *Drosophila* wing discs. *Development*, 130(20):4931–4941, 2003. (Cited on pages 37 and 53.)

[108] Karen Lai Wing Sun, James P Correia, and Timothy E Kennedy. Netrins: versatile extracellular cues with diverse functions. *Development*, 138(11):2153–2169, 2011. (Cited on pages 38, 39, 43, and 137.)

[109] Robin Harris, Laura Moore Sabatelli, and Mark A Seeger. Guidance cues at the *Drosophila* CNS midline: identification and characterization of two *Drosophila* Netrin/UNC-6 homologs. *Neuron*, 17(2):217–228, 1996. (Cited on pages 38 and 39.)

[110] Kevin J Mitchell, Jennifer L Doyle, Tito Serafini, Timothy E Kennedy, Marc Tessier-Lavigne, Corey S Goodman, and Barry J Dickson. Genetic analysis of Netrin genes in *Drosophila* : Netrins guide CNS commissural axons and peripheral motor axons. *Neuron*, 17(2):203–215, 1996. (Cited on page 39.)

[111] László Bányai and László Patthy. The NTR module: domains of Netrins, secreted Frizzled related proteins, and type I procollagen C-proteinase enhancer protein are homologous with tissue inhibitors of metalloproteases. *Protein science*, 8(08):1636–1642, 1999. (Cited on page 39.)

[112] Timothy E Kennedy, Tito Serafini, Josér De La Torre, and Marc Tessier-Lavigne. Netrins are diffusible chemotropic factors for commissural axons in the embryonic spinal cord. *Cell*, 78(3):425–435, 1994. (Cited on page 39.)

[113] Tito Serafini, Timothy E Kennedy, Michael J Gaiko, Christine Mirzayan, Thomas M Jessell, and Marc Tessier-Lavigne. The netrins define a family of axon outgrowth-promoting proteins homologous to *C. elegans* UNC-6. *Cell*, 78(3):409–424, 1994. (Cited on page 39.)

[114] Gunnar Newquist, Jesse Hogan, Kirsti Walker, Matthew Lamanuzzi, Micah Bowser, and Thomas Kidd. Control of male and female fertility by the netrin axon guidance genes. *PloS one*, 8(8):e72524, 2013. (Cited on page 39.)

[115] Sophia A Colamarino and Marc Tessier-Lavigne. The axonal chemoattractant Netrin-1 is also a chemorepellent for trochlear motor axons. *Cell*, 81(4):621–629, 1995. (Cited on page 39.)

[116] Kyonsoo Hong, Lindsay Hinck, Makoto Nishiyama, Mu-ming Poo, Marc Tessier-Lavigne, and Elke Stein. A ligand-gated association between cytoplasmic domains of UNC5 and DCC family receptors converts netrin-induced growth cone attraction to repulsion. *Cell*, 97(7):927–941, 1999. (Cited on pages 39, 44, 119, and 137.)

[117] Christian M von Hilchen, Irina Hein, Gerhard M Technau, and Benjamin Altenhein. Netrins guide migration of distinct glial cells in the *Drosophila* embryo. *Development*, 137(8):1251–1262, 2010. (Cited on page 39.)

[118] Yan Jiang, Min-tsai Liu, and Michael D Gershon. Netrins and DCC in the guidance of migrating neural crest-derived cells in the developing bowel and pancreas. *Developmental biology*, 258(2):364–384, 2003. (Cited on page 39.)

[119] Elyanne M Ratcliffe, Suhas U Setru, Jason J Chen, Zhishan S Li, Fabien D'Autréaux, and Michael D Gershon. Netrin/DCC-mediated attraction of vagal sensory axons to the fetal mouse gut. *Journal of Comparative Neurology*, 498(5):567–580, 2006. (Cited on page 39.)

[120] Mayra Yebra, Anthony MP Montgomery, Giuseppe R Diaferia, Thomas Kaido, Steve Silletti, Brandon Perez, Margaret L Just, Simone Hildbrand, Rosemary Hurford, Elin Florkiewicz, Marc Tessier-Lavigne, and Vincenzo Cirulli. Recognition of the neural chemoattractant Netrin-1 by integrins $\alpha 6\beta 4$ and $\alpha 3\beta 1$ regulates epithelial cell adhesion and migration. *Developmental cell*, 5(5):695–707, 2003. (Cited on pages 39 and 137.)

[121] Karpagam Srinivasan, Phyllis Strickland, Ana Valdes, Grace C Shin, and Lindsay Hinck. Netrin-1/Neogenin interaction stabilizes multipotent progenitor cap cells during mammary gland morphogenesis. *Developmental cell*, 4(3):371–382, 2003. (Cited on pages 40 and 137.)

[122] Masoud Shekarabi and Timothy E Kennedy. The netrin-1 receptor DCC promotes filopodia formation and cell spreading by activating Cdc42 and Rac1. *Molecular and Cellular Neuroscience*, 19(1):1–17, 2002. (Cited on pages 40, 82, 98, 107, and 139.)

[123] Yuru Liu, Elke Stein, Timothy Oliver, Yong Li, William J Brunken, Manuel Koch, Marc Tessier-Lavigne, and Brigid LM Hogan. Novel role for Netrins in regulating epithelial behavior during lung branching morphogenesis. *Current biology*, 14(10):897–905, 2004. (Cited on page 40.)

[124] Marie Castets and Patrick Mehlen. Netrin-1 role in angiogenesis: to be or not to be a pro-angiogenic factor? *Cell Cycle*, 9(8):1466–1471, 2010. (Cited on pages 40 and 137.)

[125] Katrina M Welch-Reardon, Nan Wu, and Christopher CW Hughes. A role for partial endothelial-mesenchymal transitions in angiogenesis? *Arteriosclerosis, thrombosis, and vascular biology*, 35(2):303–308, 2015. (Cited on page 40.)

[126] Joshua W Ziel, Elliott J Hagedorn, Anjon Audhya, and David R Sherwood. UNC-6 (netrin) orients the invasive membrane of the anchor cell in *C. elegans*. *Nature Cell Biology*, 11(2):183–189, 2009. (Cited on pages 40, 41, and 137.)

[127] David R Sherwood and Paul W Sternberg. Anchor cell invasion into the vulval epithelium in *C. elegans*. *Developmental cell*, 5(1):21–31, 2003. (Cited on page 41.)

[128] Anastasios D Papanastasiou, Georgios Pampalakis, Dionyssios Katsaros, and Georgia Sotiropoulou. Netrin-1 overexpression is predictive of ovarian malignancies. *Oncotarget*, 2(5):363, 2011. (Cited on pages 41 and 137.)

[129] Julien Fitamant, Céline Guenebeaud, Marie-May Coissieux, Catherine Guix, Isabelle Treilleux, Jean-Yves Scoazec, Thomas Bachelot, Agnès Bernet, and Patrick Mehlen. Netrin-1 expression confers a selective advantage for tumor cell survival in metastatic breast cancer. *Proceedings of the National Academy of Sciences*, 105(12):4850–4855, 2008. (Cited on pages 41 and 137.)

[130] Qian Huang, Hong-wei Hua, Feng Jiang, Dai-he Liu, and Gang Ding. Netrin-1 promoted pancreatic cancer cell proliferation by upregulation of Mdm2. *Tumor Biology*, 35(10):9927–9934, 2014. (Cited on pages 41 and 137.)

[131] Chui-ze Kong, Jiao Liu, Lin Liu, Zhe Zhang, and Kun-feng Guo. Interactional expression of Netrin-1 and its dependence receptor UNC5B in prostate carcinoma. *Tumor Biology*, 34(5):2765–2772, 2013. (Cited on pages 41 and 137.)

[132] Ganesan Ramesh, Arthur Berg, and Calpurnia Jayakumar. Plasma Netrin-1 is a diagnostic biomarker of human cancers. *Biomarkers*, 16(2):172–180, 2011. (Cited on pages 41 and 137.)

[133] Rosemary Manhire-Heath, Sofia Golenkina, Robert Saint, and Michael J Murray. Netrin-dependent downregulation of Frazzled/DCC is required for the dissociation of the peripodial epithelium in *Drosophila* . *Nature communications*, 4, 2013. (Cited on pages 41, 43, 45, 46, 61, 63, 72, 73, 74, 84, 88, 92, 93, 94, 110, 119, 120, 134, 138, and 139.)

[134] Marko Brankatschk and Barry J Dickson. Netrins guide *Drosophila* commissural axons at short range. *Nature neuroscience*, 9(2):188–194, 2006. (Cited on page 42.)

[135] Peter A Kolodziej, Leslie C Timpe, Kevin J Mitchell, Sharon R Fried, Corey S Goodman, Lily Yeh Jan, and Yuh Nung Jan. *frazzled* encodes a *Drosophila* member of the DCC immunoglobulin subfamily and is required for CNS and motor axon guidance. *Cell*, 87(2):197–204, 1996. (Cited on pages 43, 44, 51, 81, 84, 85, 106, and 120.)

[136] Brian V Geisbrecht, Kimberly A Dowd, Ronald W Barfield, Patti A Longo, and Daniel J Leahy. Netrin binds discrete subdomains of DCC and UNC5 and mediates interactions between DCC and Heparin. *Journal of Biological Chemistry*, 278(35):32561–32568, 2003. (Cited on page 43.)

[137] Robert P Kruger, Jeeyong Lee, Weiquan Li, and Kun-Liang Guan. Mapping netrin receptor binding reveals domains of Unc5 regulating its tyrosine phosphorylation. *The Journal of neuroscience*, 24(48):10826–10834, 2004. (Cited on page 43.)

[138] Elke Stein, Yimin Zou, Mu-ming Poo, and Marc Tessier-Lavigne. Binding of DCC by Netrin-1 to mediate axon guidance independent of Adenosine A2B receptor activation. *Science*, 291(5510):1976–1982, 2001. (Cited on pages 44, 107, and 109.)

[139] David S Garbe, Mike O'Donnell, and Greg J Bashaw. Cytoplasmic domain requirements for Frazzled-mediated attractive axon turning at the *Drosophila* midline. *Development*, 134(24):4325–4334, 2007. (Cited on pages 44, 53, 107, 109, 117, 120, 122, and 139.)

[140] Kazuko Keino-Masu, Masayuki Masu, Lindsay Hinck, E David Leonardo, Shirley S-Y Chan, Joseph G Culotti, and Marc Tessier-Lavigne. Deleted in Colorectal Cancer (DCC) encodes a netrin receptor. *Cell*, 87(2):175–185, 1996. (Cited on page 44.)

[141] SS-Y Chan, H Zheng, M-W Su, R Wilk, MT Killeen, EM Hedgecock, and JG Culotti. UNC-40, a *C. elegans* homolog of DCC (Deleted in Colorectal Cancer), is required in motile cells responding to UNC-6 netrin cues. *Cell*, 87(2):187–195, 1996. (Cited on page 44.)

[142] Masaki Hiramoto, Yasushi Hiromi, Edward Giniger, and Yoshiki Hotta. The *Drosophila* Netrin receptor Frazzled guides axons by controlling Netrin distribution. *Nature*, 406(6798):886–889, 2000. (Cited on pages 44 and 95.)

[143] Elke Stein and Marc Tessier-Lavigne. Hierarchical organization of guidance receptors: silencing of netrin attraction by Slit through a Robo/DCC receptor complex. *Science*, 291(5510):1928–1938, 2001. (Cited on pages 44 and 109.)

[144] Krystyna Keleman and Barry J Dickson. Short- and long-range repulsion by the *Drosophila* Unc5 netrin receptor. *Neuron*, 32(4):605–617, 2001. (Cited on page 44.)

[145] Molly Duman-Scheel. Deleted in colorectal cancer DCC pathfinding: axon guidance gene finally turned tumor suppressor. *Current drug targets*, 13(11):1445, 2012. (Cited on pages 44, 80, and 137.)

[146] Eric R Fearon, Kathleen R Cho, Janice M Nigro, Scott E Kern, Jonathan W Simons, J Michael Ruppert, AC Preisinger, G Thomas, and KW Kinzler. Identification of a chromosome 18q gene that is altered in colorectal cancers. *Science*, 247(4938):49–56, 1990. (Cited on pages 44 and 137.)

[147] Patrick Mehlen and Eric R Fearon. Role of the dependence receptor DCC in colorectal cancer pathogenesis. *Journal of clinical oncology*, 22(16):3420–3428, 2004. (Cited on pages 44, 81, and 137.)

[148] David C Gotley, Jennifer A Reeder, Jonathan Fawcett, Michael D Walsh, Paul Bates, David L Simmons, and Toni M Antalis. The deleted in colon cancer (DCC) gene is consistently expressed in colorectal cancers and metastases. *Oncogene*, 13(4):787–795, 1996. (Cited on page 44.)

[149] LM Arantes, AC de Carvalho, ME Melendez, CC Centrone, JF Góis-Filho, TN Toporcov, DN Caly, EH Tajara, EM Goloni-Bertollo, and AL Carvalho. Validation of methylation markers for diagnosis of oral cavity cancer. *European Journal of Cancer*, 51(5):632–641, 2015. (Cited on page 44.)

[150] Xiaoyu Qu, Jerry Davison, Liping Du, Barry Storer, Derek L Stirewalt, Shelly Heimfeld, Elihu Estey, Frederick R Appelbaum, and Min Fang. Identification of differentially methylated markers among cytogenetic risk groups of

acute myeloid leukemia. *Epigenetics*, just-accepted(0):00–00, 2015. (Cited on page 44.)

[151] Adrienne VanZomeren-Dohm, Joseph Sarro, Ellen Flannery, and Molly Duman-Scheel. The *Drosophila* Netrin receptor Frazzled/DCC functions as an invasive tumor suppressor. *BMC developmental biology*, 11(1):41, 2011. (Cited on pages 44, 46, 81, 82, 83, 85, 93, and 95.)

[152] Patrick Mehlen, Shahrooz Rabizadeh, Scott J Snipas, Nuria Assa-Munt, Guy S Salvesen, and Dale E Bredesen. The DCC gene product induces apoptosis by a mechanism requiring receptor proteolysis. *Nature*, 395(6704):801–804, 1998. (Cited on page 44.)

[153] Marie Castets, Laura Broutier, Yann Molin, Marie Brevet, Guillaume Chazot, Nicolas Gadot, Armelle Paquet, Laetitia Mazelin, Loraine Jarrosson-Wuilleme, Jean-Yves Scoazec, et al. DCC constrains tumour progression via its dependence receptor activity. *Nature*, 482(7386):534–537, 2011. (Cited on pages 45, 81, and 137.)

[154] Fabien Llambi, Frédéric Causeret, Evelyne Bloch-Gallego, and Patrick Mehlen. Netrin-1 acts as a survival factor via its receptors UNC5H and DCC. *The EMBO journal*, 20(11):2715–2722, 2001. (Cited on page 45.)

[155] Céline Furne, Véronique Corset, Zoltán Hérincs, Nathalie Cahuzac, Anne-Odile Hueber, and Patrick Mehlen. The dependence receptor DCC requires lipid raft localization for cell death signaling. *Proceedings of the National Academy of Sciences of the United States of America*, 103(11):4128–4133, 2006. (Cited on page 45.)

[156] Yoshihito Taniguchi, Helena Karlström, Johan Lundkvist, Tomohiko Mizutani, Akira Otaka, Monica Vestling, Alan Bernstein, Dorit Donoviel, Urban Lendahl, and Tasuku Honjo. Notch receptor cleavage depends on but is not directly executed by presenilins. *Proceedings of the National Academy of Sciences*, 99(6):4014–4019, 2002. (Cited on page 45.)

[157] David Goldschneider, Nicolas Rama, Catherine Guix, and Patrick Mehlen. The neogenin intracellular domain regulates gene transcription via nuclear translocation. *Molecular and cellular biology*, 28(12):4068–4079, 2008. (Cited on page 45.)

[158] Alexandra Neuhaus-Follini and Greg J Bashaw. The intracellular domain of the Frazzled/DCC receptor is a transcription factor required for commissural axon guidance. *Neuron*, 87(4):751–763, 2015. (Cited on page 45.)

[159] Gang Hu, Sheng Zhang, Marc Vidal, Joshua La Baer, Tian Xu, and Eric R Fearon. Mammalian homologs of Seven in absentia regulate DCC via the ubiquitin-proteasome pathway. *Genes & development*, 11(20):2701–2714, 1997. (Cited on page 45.)

[160] Tae-Hong Kim, Hyun Kyoung Lee, In Seo, Hae Rahn Bae, Duk Joon Suh, Jane Wu, Yi Rao, Kyu-Geun Hwang, and Hwan Tae Park. Netrin induces down-regulation of its receptor, Deleted in Colorectal Cancer, through the ubiquitin-proteasome pathway in the embryonic cortical neuron. *Journal of neurochemistry*, 95(1):1–8, 2005. (Cited on pages 45 and 94.)

[161] Tianzhi Shu, Kimberly M Valentino, Clare Seaman, Helen M Cooper, and Linda J Richards. Expression of the Netrin-1 receptor, Deleted in colorectal cancer (DCC), is largely confined to projecting neurons in the developing forebrain. *Journal of Comparative Neurology*, 416(2):201–212, 2000. (Cited on page 45.)

[162] Kevin A Edwards, Ruth A Montague, S Shepard, Bruce A Edgar, Raymond L Erikson, and Daniel P Kiehart. Identification of *Drosophila* cytoskeletal proteins by induction of abnormal cell shape in fission yeast. *Proceedings of the National Academy of Sciences*, 91(10):4589–4593, 1994. (Cited on page 46.)

[163] Brooke M McCartney and Richard G Fehon. Distinct cellular and subcellular patterns of expression imply distinct functions for the *Drosophila* homologues

of Moesin and the Neurofibromatosis 2 tumor suppressor, Merlin. *The Journal of Cell Biology*, 133(4):843–852, 1996. (Cited on page 46.)

[164] Sophie Louvet-Vallée. ERM proteins: from cellular architecture to cell signaling. *Biology of the Cell*, 92(5):305–316, 2000. (Cited on page 47.)

[165] Anthony Bretscher, Kevin Edwards, and Richard G Fehon. ERM proteins and Merlin: integrators at the cell cortex. *Nature reviews Molecular cell biology*, 3(8):586–599, 2002. (Cited on page 47.)

[166] Richard G Fehon, Andrea I McClatchey, and Anthony Bretscher. Organizing the cell cortex: the role of ERM proteins. *Nature reviews Molecular cell biology*, 11(4):276–287, 2010. (Cited on page 47.)

[167] Mercè Martín, Patricia Simon-Assmann, Michèle Kedinger, Marianne Martin, Paul Mangeat, Francisco X Real, and Myriam Fabre. DCC regulates cell adhesion in human colon cancer derived HT-29 cells and associates with Ezrin. *European journal of cell biology*, 85(8):769–783, 2006. (Cited on pages 47, 81, 82, and 98.)

[168] Judith Antoine-Bertrand, Atefeh Ghogha, Vilayphone Luangrath, Fiona K Bedford, and Nathalie Lamarche-Vane. The activation of Ezrin-Radixin-Moesin proteins is regulated by Netrin-1 through Src kinase and RhoA/Rho kinase activities and mediates Netrin-1–induced axon outgrowth. *Molecular biology of the cell*, 22(19):3734–3746, 2011. (Cited on pages 47 and 121.)

[169] Kevin A Edwards, Maddy Demsky, Ruth A Montague, Nate Weymouth, and Daniel P Kiehart. GFP-Moesin illuminates Actin cytoskeleton dynamics in living tissue and demonstrates cell shape changes during morphogenesis in *Drosophila* . *Developmental biology*, 191(1):103–117, 1997. (Cited on page 47.)

[170] James W Bloor and Daniel P Kiehart. *Drosophila* RhoA regulates the cytoskeleton and cell-cell adhesion in the developing epidermis. *Development*, 129(13):3173–3183, 2002. (Cited on page 47.)

[171] Cédric Polesello, Isabelle Delon, Philippe Valenti, Pierre Ferrer, and François Payre. Dmoesin controls actin-based cell shape and polarity during *Drosophila melanogaster* oogenesis. *Nature cell biology*, 4(10):782–789, 2002. (Cited on page 47.)

[172] Olga Speck, Sarah C Hughes, Nicole K Noren, Rima M Kulikauskas, and Richard G Fehon. Moesin functions antagonistically to the Rho pathway to maintain epithelial integrity. *Nature*, 421(6918):83–87, 2003. (Cited on pages 47, 76, and 105.)

[173] David R Hipfner, Nadine Keller, and Stephen M Cohen. Slik Sterile-20 kinase regulates Moesin activity to promote epithelial integrity during tissue growth. *Genes & development*, 18(18):2243–2248, 2004. (Cited on pages 47, 121, and 140.)

[174] Amanda L Neisch, Etienne Formstecher, and Richard G Fehon. Conundrum, an ARHGAP18 orthologue, regulates RhoA and proliferation through interactions with Moesin. *Molecular biology of the cell*, 24(9):1420–1433, 2013. (Cited on pages 47, 51, 92, and 105.)

[175] Amanda L Neisch, Olga Speck, Beth Stronach, and Richard G Fehon. Rho1 regulates apoptosis via activation of the JNK signaling pathway at the plasma membrane. *The Journal of cell biology*, 189(2):311–323, 2010. (Cited on page 47.)

[176] Tzumin Lee and Liqun Luo. Mosaic analysis with a repressible cell marker (MARCM) for *Drosophila* neural development. *Trends in neurosciences*, 24(5):251–254, 2001. (Cited on page 55.)

[177] Kimberly D McClure and Gerold Schubiger. Developmental analysis and squamous morphogenesis of the peripodial epithelium in *Drosophila* imaginal discs. *Development*, 132(22):5033–5042, 2005. (Cited on page 56.)

[178] Christiane Guillermet and Paul Mandaron. *In vitro* imaginal disc development and moulting hormone. *Journal of embryology and experimental morphology*, 57(1):107–118, 1980. (Cited on page 60.)

[179] Junichi Ikenouchi, Miho Matsuda, Mikio Furuse, and Shoichiro Tsukita. Regulation of tight junctions during the epithelium-mesenchyme transition: direct repression of the gene expression of claudins/occludin by Snail. *Journal of cell science*, 116(10):1959–1967, 2003. (Cited on page 61.)

[180] Tracey A Martin and Wen G Jiang. Loss of tight junction barrier function and its role in cancer metastasis. *Biochimica et Biophysica Acta (BBA)-Biomembranes*, 1788(4):872–891, 2009. (Cited on page 61.)

[181] Victoria Aranda, Marissa E Nolan, and Senthil K Muthuswamy. Par complex in cancer: a regulator of normal cell polarity joins the dark side. *Oncogene*, 27(55):6878–6887, 2008. (Cited on page 62.)

[182] C Royer and X Lu. Epithelial cell polarity: a major gatekeeper against cancer&quest. *Cell Death & Differentiation*, 18(9):1470–1477, 2011. (Cited on page 62.)

[183] Fernando Martin-Belmonte and Mirna Perez-Moreno. Epithelial cell polarity, stem cells and cancer. *Nature Reviews Cancer*, 12(1):23–38, 2012. (Cited on page 62.)

[184] Shuh Narumiya, Masahiro Tanji, and Toshimasa Ishizaki. Rho signaling, ROCK and mDia1, in transformation, metastasis and invasion. *Cancer and Metastasis Reviews*, 28(1-2):65–76, 2009. (Cited on page 62.)

[185] Elena Llano, Alberto M Pendás, Pedro Aza-Blanc, Thomas B Kornberg, and Carlos López-Otin. Dm1-MMP, a matrix metalloproteinase from *Drosophila* with a potential role in extracellular matrix remodeling during neural development. *Journal of Biological Chemistry*, 275(46):35978–35985, 2000. (Cited on page 62.)

[186] Elena Llano, Geza Adam, Alberto M Pendás, Vıctor Quesada, Luis M Sánchez, Iñigo Santamaria, Stéphane Noselli, and Carlos López-Otin. Structural and enzymatic characterization of *Drosophila* Dm2-MMP, a membrane-bound matrix metalloproteinase with tissue-specific expression. *Journal of Biological Chemistry*, 277(26):23321–23329, 2002. (Cited on page 62.)

[187] Xavier Morin, Richard Daneman, Michael Zavortink, and William Chia. A protein trap strategy to detect GFP-tagged proteins expressed from their endogenous loci in *Drosophila* . *Proceedings of the National Academy of Sciences*, 98(26):15050–15055, 2001. (Cited on page 62.)

[188] Jean Paul Thiery, Hervé Acloque, Ruby YJ Huang, and M Angela Nieto. Epithelial-mesenchymal transitions in development and disease. *Cell*, 139(5):871–890, 2009. (Cited on page 63.)

[189] Chaturvedula Tripura, Nulu-Prafulla Chandrika, Vutukuru-Nagalakshmi Susmitha, Stéphane Noselli, and LS Shashidhara. Regulation and activity of JNK signaling in the wing disc peripodial membrane during adult morphogenesis in *Drosophila* . *International Journal of Developmental Biology*, 55(6):583, 2011. (Cited on page 64.)

[190] Anne J Ridley and Alan Hall. The small GTP-binding protein Rho regulates the assembly of focal adhesions and actin stress fibers in response to growth factors. *Cell*, 70(3):389–399, 1992. (Cited on pages 67 and 75.)

[191] Hiroki Oda, Shoichiro Tsukita, and Masatoshi Takeichi. Dynamic behavior of the cadherin-based cell–cell adhesion system during *Drosophila* gastrulation. *Developmental biology*, 203(2):435–450, 1998. (Cited on page 71.)

[192] Johanna Langevin, Matthew J Morgan, Carine Rossé, Victor Racine, Jean-Baptiste Sibarita, Sandra Aresta, Mala Murthy, Thomas Schwarz, Jacques Camonis, and Yohanns Bellaïche. *Drosophila* exocyst components Sec5, Sec6, and Sec15 regulate DE-Cadherin trafficking from recycling endosomes to the

plasma membrane. *Developmental cell*, 9(3):365–376, 2005. (Cited on pages 71 and 100.)

[193] Innokenty Woichansky, Carlo Antonio Beretta, Nicola Berns, and Veit Riechmann. Three mechanisms control E-cadherin localization to the zonula adherens. *Nature communications*, 7, 2016. (Cited on pages 71, 100, 102, and 144.)

[194] Weijia Zhu, Brian Leber, and David W Andrews. Cytoplasmic *O*-glycosylation prevents cell surface transport of E-cadherin during apoptosis. *The EMBO journal*, 20(21):5999–6007, 2001. (Cited on page 71.)

[195] Marios Georgiou, Eliana Marinari, Jemima Burden, and Buzz Baum. Cdc42, Par6, and aPKC regulate Arp2/3-mediated endocytosis to control local adherens junction stability. *Current Biology*, 18(21):1631–1638, 2008. (Cited on pages 71, 97, 100, 125, 135, and 140.)

[196] Kathryn P Harris and Ulrich Tepass. Cdc42 and Par proteins stabilize dynamic adherens junctions in the *Drosophila* neuroectoderm through regulation of apical endocytosis. *The Journal of cell biology*, 183(6):1129–1143, 2008. (Cited on page 72.)

[197] Ruth Kroschewski, Alan Hall, and Ira Mellman. Cdc42 controls secretory and endocytic transport to the basolateral plasma membrane of MDCK cells. *Nature cell biology*, 1(1):8–13, 1999. (Cited on page 72.)

[198] Xiaodong Li, Etienne Saint-Cyr-Proulx, Klaus Aktories, and Nathalie Lamarche-Vane. Rac1 and Cdc42 but not Rhoa or Rho kinase activities are required for neurite outgrowth induced by the Netrin-1 receptor DCC (deleted in colorectal cancer) in N1E-115 neuroblastoma cells. *Journal of Biological Chemistry*, 277(17):15207–15214, 2002. (Cited on pages 72, 82, 98, 104, 107, and 139.)

[199] Elzbieta Janda, Ma Nevolo, Kerstin Lehmann, Julian Downward, Hartmut Beug, and Michele Grieco. Raf plus TGFβ-dependent EMT is initiated by endocytosis and lysosomal degradation of E-cadherin. *Oncogene*, 25(54):7117–7130, 2006. (Cited on page 72.)

[200] Sei-Jung Lee, Young Hyun Jung, Sang Yub Oh, Min Sik Yong, Jung Min Ryu, and Ho Jae Han. Netrin-1 induces MMP-12-dependent E-cadherin degradation via the distinct activation of PKCα and FAK/Fyn in promoting mesenchymal stem cell motility. *Stem cells and development*, 23(16):1870–1882, 2014. (Cited on pages 72, 82, and 98.)

[201] Qiangqiang Jia, Yang Liu, Hanhan Liu, and Sheng Li. Mmp1 and Mmp2 cooperatively induce *Drosophila* fat body cell dissociation with distinct roles. *Scientific reports*, 4, 2014. (Cited on page 72.)

[202] Weiquan Li, Jeeyong Lee, Haris G Vikis, Seung-Hee Lee, Guofa Liu, Jennifer Aurandt, Tang-Long Shen, Eric R Fearon, Jun-Lin Guan, and Min Han. Activation of FAK and Src are receptor-proximal events required for netrin signaling. *Nature neuroscience*, 7(11):1213–1221, 2004. (Cited on pages 72, 107, and 127.)

[203] Yi Shen, Dianne S Hirsch, Christy A Sasiela, and Wen Jin Wu. Cdc42 regulates E-cadherin ubiquitination and degradation through an epidermal growth factor receptor to Src-mediated pathway. *Journal of Biological Chemistry*, 283(8):5127–5137, 2008. (Cited on page 72.)

[204] Panos Z Anastasiadis, Sun Y Moon, Molly A Thoreson, Debbie J Mariner, Howard C Crawford, Yi Zheng, and Albert B Reynolds. Inhibition of RhoA by p120 catenin. *Nature cell biology*, 2(9):637–644, 2000. (Cited on page 73.)

[205] Manel Bosch, Florenci Serras, Enrique Martín-Blanco, and Jaume Baguñà. JNK signaling pathway required for wound healing in regenerating *Drosophila* wing imaginal discs. *Developmental biology*, 280(1):73–86, 2005. (Cited on page 74.)

[206] Lynn Cooley, Esther Verheyen, and Kathleen Ayers. *chickadee* encodes a profilin required for intercellular cytoplasm transport during *Drosophila* oogenesis. *Cell*, 69(1):173–184, 1992. (Cited on page 74.)

[207] Changsong Yang, Minzhou Huang, John DeBiasio, Martin Pring, Michael Joyce, Hiroaki Miki, Tadaomi Takenawa, and Sally H Zigmond. Profilin enhances Cdc42-induced nucleation of actin polymerization. *The Journal of cell biology*, 150(5):1001–1012, 2000. (Cited on page 74.)

[208] Heinrich Jasper, Vladimir Benes, Christian Schwager, Silvia Sauer, Sandra Clauder-Münster, Wilhelm Ansorge, and Dirk Bohmann. The genomic response of the *Drosophila* embryo to JNK signaling. *Developmental cell*, 1(4):579–586, 2001. (Cited on page 74.)

[209] Stéphanie Pellegrin and Harry Mellor. Actin stress fibres. *Journal of cell science*, 120(20):3491–3499, 2007. (Cited on page 74.)

[210] Perttu Naumanen, Pekka Lappalainen, and Pirta Hotulainen. Mechanisms of actin stress fibre assembly. *Journal of microscopy*, 231(3):446–454, 2008. (Cited on page 74.)

[211] Sari Tojkander, Gergana Gateva, and Pekka Lappalainen. Actin stress fibers–assembly, dynamics and biological roles. *Journal of cell science*, 125(8):1855–1864, 2012. (Cited on pages 74, 75, and 139.)

[212] Keith Burridge. Are stress fibres contractile? *Nature*, 294, 1981. (Cited on page 75.)

[213] Wen-Tien Chen. Mechanism of retraction of the trailing edge during fibroblast movement. *The Journal of cell biology*, 90(1):187–200, 1981. (Cited on page 75.)

[214] Caroline S Hill, Judy Wynne, and Richard Treisman. The Rho family GTPases RhoA, Racl, and CDC42Hs regulate transcriptional activation by SRF. *Cell*, 81(7):1159–1170, 1995. (Cited on page 75.)

[215] Pirta Hotulainen and Pekka Lappalainen. Stress fibers are generated by two distinct actin assembly mechanisms in motile cells. *The Journal of cell biology*, 173(3):383–394, 2006. (Cited on page 75.)

[216] Midori Maekawa, Toshimasa Ishizaki, Shuken Boku, Naoki Watanabe, Akiko Fujita, Akihiro Iwamatsu, Takashi Obinata, Kazumasa Ohashi, Kensaku Mizuno, and Shuh Narumiya. Signaling from Rho to the actin cytoskeleton through protein kinases ROCK and LIM-kinase. *Science*, 285(5429):895–898, 1999. (Cited on page 75.)

[217] Catherine D Nobes and Alan Hall. Rho, Rac, and Cdc42 GTPases regulate the assembly of multimolecular focal complexes associated with actin stress fibers, lamellipodia, and filopodia. *Cell*, 81(1):53–62, 1995. (Cited on pages 75 and 117.)

[218] Thomas D Pollard. Regulation of actin filament assembly by Arp2/3 complex and formins. *Annu. Rev. Biophys. Biomol. Struct.*, 36:451–477, 2007. (Cited on page 75.)

[219] Fukun Guo, Marcella Debidda, Linda Yang, David A Williams, and Yi Zheng. Genetic deletion of Rac1 GTPase reveals its critical role in actin stress fiber formation and focal adhesion complex assembly. *Journal of Biological Chemistry*, 281(27):18652–18659, 2006. (Cited on page 75.)

[220] Danny L Brower and Sharon M Jaffe. Requirement for integrins during *Drosophila* wing development. *Nature*, 342(6247):285–287, 1989. (Cited on page 77.)

[221] Paloma Domínguez-Giménez, Nicholas H Brown, and María D Martín-Bermudo. Integrin-ECM interactions regulate the changes in cell shape driving the morphogenesis of the *Drosophila* wing epithelium. *Journal of cell science*, 120(6):1061–1071, 2007. (Cited on page 77.)

[222] Jason G Homsy, Heinrich Jasper, Xomalin G Peralta, Hai Wu, Daniel P Kiehart, and Dirk Bohmann. JNK signaling coordinates integrin and actin functions during *Drosophila* embryogenesis. *Developmental dynamics*, 235(2):427–434, 2006. (Cited on page 77.)

[223] Isabelle Delon and Nicholas H Brown. The integrin adhesion complex changes its composition and function during morphogenesis of an epithelium. *Journal of cell science*, 122(23):4363–4374, 2009. (Cited on page 77.)

[224] Joni D Mott and Zena Werb. Regulation of matrix biology by matrix metalloproteinases. *Current opinion in cell biology*, 16(5):558–564, 2004. (Cited on page 78.)

[225] Laura J Stevens and Andrea Page-McCaw. A secreted MMP is required for reepithelialization during wound healing. *Molecular biology of the cell*, 23(6):1068–1079, 2012. (Cited on page 78.)

[226] Andrés Dekanty, Lara Barrio, Mariana Muzzopappa, Herbert Auer, and Marco Milán. Aneuploidy-induced delaminating cells drive tumorigenesis in *Drosophila* epithelia. *Proceedings of the National Academy of Sciences*, 109(50):20549–20554, 2012. (Cited on page 78.)

[227] David E Levy and JE Darnell. STATs: transcriptional control and biological impact. *Nature reviews Molecular cell biology*, 3(9):651–662, 2002. (Cited on page 78.)

[228] Caroline Medioni and Stéphane Noselli. Dynamics of the basement membrane in invasive epithelial clusters in *Drosophila* . *Development*, 132(13):3069–3077, 2005. (Cited on page 79.)

[229] Qian Dong, Breanna Brenneman, Christopher Fields, and Ajay Srivastava. A Cathepsin-L is required for invasive behavior during Air Sac Primordium development in *Drosophila melanogaster*. *FEBS letters*, 2015. (Cited on page 79.)

[230] B Lv, C Song, L Wu, Q Zhang, D Hou, P Chen, S Yu, Z Wang, Y Chu, and J Zhang. Netrin-4 as a biomarker promotes cell proliferation and invasion in gastric cancer. *Oncotarget*, 2015. (Cited on page 79.)

[231] Akio Shimizu, Hironao Nakayama, Priscilla Wang, Courtney König, Tomoshige Akino, Johanna Sandlund, Silvia Coma, Joseph E Italiano, Akiko Mammoto, and Diane R *et al.* Bielenberg. Netrin-1 promotes glioblastoma cell invasiveness and angiogenesis by multiple pathways including activation of Rhoa, Cathepsin B, and cAMP-response element-binding protein. *Journal of Biological Chemistry*, 288(4):2210–2222, 2013. (Cited on page 79.)

[232] Paul Krimpenfort, Ji-Ying Song, Natalie Proost, John Zevenhoven, Jos Jonkers, and Anton Berns. Deleted in colorectal carcinoma suppresses metastasis in p53-deficient mammary tumours. *Nature*, 482(7386):538–541, 2012. (Cited on pages 81 and 137.)

[233] Natalie K Lee, Ka Wai Fok, Amanda White, Nicole H Wilson, Conor J OLeary, Hayley L Cox, Magdalene Michael, Alpha S Yap, and Helen M Cooper. Neogenin recruitment of the WAVE regulatory complex maintains adherens junction stability and tension. *Nature communications*, 7, 2016. (Cited on pages 81, 101, and 140.)

[234] Jun R Huh, Ming Guo, and Bruce A Hay. Compensatory proliferation induced by cell death in the *Drosophila* wing disc requires activity of the apical cell death caspase Dronc in a nonapoptotic role. *Current Biology*, 14(14):1262–1266, 2004. (Cited on page 82.)

[235] Hyung Don Ryoo, Travis Gorenc, and Hermann Steller. Apoptotic cells can induce compensatory cell proliferation through the JNK and the Wingless signaling pathways. *Developmental cell*, 7(4):491–501, 2004. (Cited on page 82.)

[236] Ainhoa Pérez-Garijo, Francisco A Martín, Gary Struhl, and Ginés Morata. Dpp signaling and the induction of neoplastic tumors by caspase-inhibited

apoptotic cells in *Drosophila*. *Proceedings of the National Academy of Sciences of the United States of America*, 102(49):17664–17669, 2005. (Cited on page 82.)

[237] Vivek A Rudrapatna, Erdem Bangi, and Ross L Cagan. Caspase signalling in the absence of apoptosis drives Jnk-dependent invasion. *EMBO reports*, 14(2):172–177, 2013. (Cited on pages 82 and 95.)

[238] David J Forsthoefel, Eric C Liebl, Peter A Kolodziej, and Mark A Seeger. The Abelson tyrosine kinase, the Trio GEF and Enabled interact with the Netrin receptor Frazzled in *Drosophila* . *Development*, 132(8):1983–1994, 2005. (Cited on pages 82, 99, 107, 109, 124, 127, 134, and 139.)

[239] Joy N Dorsten, Bridget E Varughese, Stephanie Karmo, Mark A Seeger, and Mark FA VanBerkum. In the absence of $frazzled$ over-expression of Abelson tyrosine kinase disrupts commissure formation and causes axons to leave the embryonic CNS. *PloS one*, 5(3):e9822, 2010. (Cited on pages 82 and 109.)

[240] Michael P O′Donnell and Greg J Bashaw. Distinct functional domains of the Abelson tyrosine kinase control axon guidance responses to Netrin and Slit to regulate the assembly of neural circuits. *Development*, 140(13):2724–2733, 2013a. (Cited on pages 82 and 127.)

[241] Chao Qu, Trisha Dwyer, Qiangqiang Shao, Tao Yang, Huai Huang, and Guofa Liu. Direct binding of TUBB3 with DCC couples Netrin-1 signaling to intracellular microtubule dynamics in axon outgrowth and guidance. *J Cell Sci*, 126(14):3070–3081, 2013. (Cited on pages 82, 107, 120, and 128.)

[242] Xiu-rong Ren, Guo-li Ming, Yi Xie, Yan Hong, Dong-mei Sun, Zhong-qiu Zhao, Zhu Feng, Qiang Wang, Sangwoo Shim, Zhou-feng Chen, et al. Focal adhesion kinase in Netrin-1 signaling. *Nature neuroscience*, 7(11):1204–1212, 2004. (Cited on pages 82, 107, 127, and 139.)

[243] Joy N Dorsten, Peter A Kolodziej, and Mark FA VanBerkum. Frazzled regulation of myosin ii activity in the *Drosophila* embryonic CNS. *Developmental biology*, 308(1):120–132, 2007. (Cited on pages 82, 85, 104, 108, 109, 115, 116, and 117.)

[244] Joy S Wu and Liqun Luo. A protocol for mosaic analysis with a repressible cell marker (MARCM) in *Drosophila* . *Nature protocols*, 1(6):2583–2589, 2007. (Cited on page 85.)

[245] Georg Dietzl, Doris Chen, Frank Schnorrer, Kuan-Chung Su, Yulia Barinova, Michaela Fellner, Beate Gasser, Kaolin Kinsey, Silvia Oppel, and Susanne Scheiblauer. A genome-wide transgenic RNAi library for conditional gene inactivation in *Drosophila* . *Nature*, 448(7150):151–156, 2007. (Cited on page 87.)

[246] Toshiyasu Mikuma, Hiroaki Kawasaki, Yasuhiko Yamamoto, and Kazunari Taira. Overexpression of Dicer enhances RNAi-mediated gene silencing by short-hairpin RNAs (shRNAs) in human cells. *Nucleic acids symposium series*, 48(1):191–192, 2004. (Cited on page 87.)

[247] Dong-Ho Kim, Mark A Behlke, Scott D Rose, Mi-Sook Chang, Sangdun Choi, and John J Rossi. Synthetic dsRNA Dicer substrates enhance RNAi potency and efficacy. *Nature biotechnology*, 23(2):222–226, 2005. (Cited on page 87.)

[248] S Rodrigues, Olivier De Wever, Erik Bruyneel, RJ Rooney, and C Gespach. Opposing roles of Netrin-1 and the dependence receptor DCC in cancer cell invasion, tumor growth and metastasis. *Oncogene*, 26(38):5615–5625, 2007. (Cited on page 93.)

[249] Joy N Dorsten and Mark FA VanBerkum. Frazzled cytoplasmic P-motifs are differentially required for axon pathway formation in the *Drosophila* embryonic CNS. *International Journal of Developmental Neuroscience*, 26(7):753–761, 2008. (Cited on page 95.)

[250] Alex Mauss, Marco Tripodi, Jan Felix Evers, and Matthias Landgraf. Midline signalling systems direct the formation of a neural map by dendritic targeting in the *Drosophila* motor system. *PLoS Biol*, 7(9):e1000200, 2009. (Cited on page 95.)

[251] Rei K Morikawa, Takahiro Kanamori, Kei-ichiro Yasunaga, and Kazuo Emoto. Different levels of the Tripartite motif protein, Anomalies in sensory axon patterning (Asap), regulate distinct axonal projections of *Drosophila* sensory neurons. *Proceedings of the National Academy of Sciences*, 108(48):19389–19394, 2011. (Cited on page 95.)

[252] Timothy A Evans, Celine Santiago, Elise Arbeille, and Greg J Bashaw. Robo2 acts in trans to inhibit Slit-Robo1 repulsion in pre-crossing commissural axons. *Elife*, 4(na):e08407, 2015. (Cited on page 95.)

[253] Joan M Whitten. The post-embryonic development of the tracheal system in *Drosophila melanogaster*. *Journal of Cell Science*, 3(41):123–150, 1957. (Cited on page 96.)

[254] Andrew P Kowalczyk and Benjamin A Nanes. Adherens junction turnover: regulating adhesion through cadherin endocytosis, degradation, and recycling. In *Adherens Junctions: from Molecular Mechanisms to Tissue Development and Disease*, pages 197–222. Springer, 2012. (Cited on pages 97 and 100.)

[255] Defne Yarar, Clare M Waterman-Storer, and Sandra L Schmid. A dynamic actin cytoskeleton functions at multiple stages of Clathrin-mediated endocytosis. *Molecular biology of the cell*, 16(2):964–975, 2005. (Cited on page 97.)

[256] Andrea Leibfried, Robert Fricke, Matthew J Morgan, Sven Bogdan, and Yohanns Bellaiche. *Drosophila* Cip4 and WASp define a branch of the Cdc42-Par6-aPKC pathway regulating E-cadherin endocytosis. *Current Biology*, 18(21):1639–1648, 2008. (Cited on pages 97, 125, 135, and 140.)

[257] Wenyu Bu, Kim Buay Lim, Yuan Hong Yu, Ai Mei Chou, Thankiah Sudhaharan, and Sohail Ahmed. Cdc42 interaction with N-WASP and Toca-1 regulates membrane tubulation, vesicle formation and vesicle motility: implications for endocytosis. *PLoS One*, 5(8):e12153, 2010. (Cited on page 97.)

[258] Erik W Dent, Stephanie L Gupton, and Frank B Gertler. The growth cone cytoskeleton in axon outgrowth and guidance. *Cold Spring Harbor perspectives in biology*, 3(3):a001800, 2011. (Cited on page 98.)

[259] Elly Tanaka and James Sabry. Making the connection: cytoskeletal rearrangements during growth cone guidance. *Cell*, 83(2):171–176, 1995. (Cited on page 98.)

[260] Erik W Dent and Frank B Gertler. Cytoskeletal dynamics and transport in growth cone motility and axon guidance. *Neuron*, 40(2):209–227, 2003. (Cited on pages 98 and 127.)

[261] TJ Mitchison and LP Cramer. Actin-based cell motility and cell locomotion. *Cell*, 84(3):371–379, 1996. (Cited on page 98.)

[262] Laura Anne Lowery and David Van Vactor. The trip of the tip: understanding the growth cone machinery. *Nature reviews Molecular cell biology*, 10(5):332–343, 2009. (Cited on page 98.)

[263] Alan Hall. Rho GTPases and the actin cytoskeleton. *Science*, 279(5350):509–514, 1998. (Cited on page 98.)

[264] Daisuke Yamazaki, Shusaku Kurisu, and Tadaomi Takenawa. Regulation of cancer cell motility through actin reorganization. *Cancer science*, 96(7):379–386, 2005. (Cited on page 98.)

[265] Matthias Machacek, Louis Hodgson, Christopher Welch, Hunter Elliott, Olivier Pertz, Perihan Nalbant, Amy Abell, Gary L Johnson, Klaus M Hahn, and Gaudenz Danuser. Coordination of Rho GTPase activities during cell protrusion. *Nature*, 461(7260):99–103, 2009. (Cited on page 98.)

[266] Bharesh K Chauhan, Ming Lou, Yi Zheng, and Richard A Lang. Balanced Rac1 and RhoA activities regulate cell shape and drive invagination morphogenesis in epithelia. *Proceedings of the National Academy of Sciences*, 108(45):18289–18294, 2011. (Cited on pages 98, 102, 105, and 144.)

[267] Anne J Ridley. Rho GTPase signalling in cell migration. *Current opinion in cell biology*, 36:103–112, 2015. (Cited on pages 98 and 99.)

[268] Jonathan DeGeer, Jérôme Boudeau, Susanne Schmidt, Fiona Bedford, Nathalie Lamarche-Vane, and Anne Debant. Tyrosine phosphorylation of the RhoGEF Trio regulates Netrin-1/DCC-mediated cortical axon outgrowth. *Molecular and cellular biology*, pages MCB–01264, 2012. (Cited on page 99.)

[269] Rafael S Demarco, Eric C Struckhoff, and Erik A Lundquist. The Rac GTP exchange factor TIAM-1 acts with CDC-42 and the guidance receptor UNC-40/DCC in neuronal protrusion and axon guidance. *PLoS Genet*, 8(4):e1002665, 2012. (Cited on pages 99 and 139.)

[270] J Victor Small, Theresia Stradal, Emmanuel Vignal, and Klemens Rottner. The lamellipodium: where motility begins. *Trends in cell biology*, 12(3):112–120, 2002. (Cited on page 99.)

[271] Myrto Raftopoulou and Alan Hall. Cell migration: Rho GTPases lead the way. *Developmental biology*, 265(1):23–32, 2004. (Cited on page 99.)

[272] R Dyche Mullins, John A Heuser, and Thomas D Pollard. The interaction of Arp2/3 complex with actin: nucleation, high affinity pointed end capping, and formation of branching networks of filaments. *Proceedings of the National Academy of Sciences*, 95(11):6181–6186, 1998. (Cited on page 99.)

[273] Matthew D Welch. The world according to Arp: regulation of actin nucleation by the Arp2/3 complex. *Trends in cell biology*, 9(11):423–427, 1999. (Cited on page 99.)

[274] Corina Sarmiento, Weigang Wang, Athanassios Dovas, Hideki Yamaguchi, Mazen Sidani, Mirvat El-Sibai, Vera DesMarais, Holly A Holman, Susan Kitchen, and Jonathan M Backer. WASP family members and Formin proteins coordinate regulation of cell protrusions in carcinoma cells. *The Journal of cell biology*, 180(6):1245–1260, 2008. (Cited on page 99.)

[275] Andres M Lebensohn and Marc W Kirschner. Activation of the WAVE complex by coincident signals controls actin assembly. *Molecular cell*, 36(3):512–524, 2009. (Cited on page 99.)

[276] Kenneth G Campellone and Matthew D Welch. A nucleator arms race: cellular control of actin assembly. *Nature reviews Molecular cell biology*, 11(4):237–251, 2010. (Cited on page 99.)

[277] Dennis Breitsprecher, Antje K Kiesewetter, Joern Linkner, Marlene Vinzenz, Theresia EB Stradal, John Victor Small, Ute Curth, Richard B Dickinson, and Jan Faix. Molecular mechanism of Ena/VASP-mediated actin-filament elongation. *The EMBO Journal*, 30(3):456–467, 2011. (Cited on page 99.)

[278] Svitlana Havrylenko, Philippe Noguera, Majdouline Abou-Ghali, John Manzi, Fahima Faqir, Audrey Lamora, Christophe Guérin, Laurent Blanchoin, and Julie Plastino. WAVE binds Ena/VASP for enhanced Arp2/3 complex-based actin assembly. *Molecular biology of the cell*, 26(1):55–65, 2015. (Cited on page 99.)

[279] Zemer Gitai, W Yu Timothy, Erik A Lundquist, Marc Tessier-Lavigne, and Cornelia I Bargmann. The netrin receptor UNC-40/DCC stimulates axon attraction and outgrowth through enabled and, in parallel, Rac and UNC-115/AbLIM. *Neuron*, 37(1):53–65, 2003. (Cited on pages 99, 106, 107, 117, and 139.)

[280] Paula B Deming, Shirley L Campbell, Jamie B Stone, Robert L Rivard, Alison L Mercier, and Alan K Howe. Anchoring of Protein Kinase A by ERM (Ezrin-Radixin-Moesin) proteins is required for proper Netrin signaling

through DCC (Deleted in colorectal cancer). *Journal of Biological Chemistry*, 290(9):5783–5796, 2015. (Cited on page 99.)

[281] John G Lock and Jennifer L Stow. Rab11 in recycling endosomes regulates the sorting and basolateral transport of E-cadherin. *Molecular biology of the cell*, 16(4):1744–1755, 2005. (Cited on page 100.)

[282] Marion Desclozeaux, Juliana Venturato, Fiona G Wylie, Jason G Kay, Shannon R Joseph, Huong T Le, and Jennifer L Stow. Active Rab11 and functional recycling endosome are required for E-cadherin trafficking and lumen formation during epithelial morphogenesis. *American Journal of Physiology-Cell Physiology*, 295(2):C545–C556, 2008. (Cited on page 100.)

[283] Akihiro Kusumi, Kenichi Suzuki, and Kotaro Koyasako. Mobility and cytoskeletal interactions of cell adhesion receptors. *Current opinion in cell biology*, 11(5):582–590, 1999. (Cited on page 100.)

[284] Ryota Iino, Ikuko Koyama, and Akihiro Kusumi. Single molecule imaging of green fluorescent proteins in living cells: E-cadherin forms oligomers on the free cell surface. *Biophysical Journal*, 80(6):2667–2677, 2001. (Cited on page 100.)

[285] Yoshiko Kametani and Masatoshi Takeichi. Basal-to-apical cadherin flow at cell junctions. *Nature cell biology*, 9(1):92–98, 2007. (Cited on pages 100 and 102.)

[286] Matthieu Cavey, Matteo Rauzi, Pierre-François Lenne, and Thomas Lecuit. A two-tiered mechanism for stabilization and immobilization of E-cadherin. *Nature*, 453(7196):751–756, 2008. (Cited on page 100.)

[287] Simon de Beco, Charles Gueudry, François Amblard, and Sylvie Coscoy. Endocytosis is required for E-cadherin redistribution at mature adherens junctions. *Proceedings of the National Academy of Sciences*, 106(17):7010–7015, 2009. (Cited on page 100.)

[288] Soonjin Hong, Regina B Troyanovsky, and Sergey M Troyanovsky. Binding to F-actin guides cadherin cluster assembly, stability, and movement. *The Journal of cell biology*, 201(1):131–143, 2013. (Cited on page 101.)

[289] Selwin K Wu, Guillermo A Gomez, Magdalene Michael, Suzie Verma, Hayley L Cox, James G Lefevre, Robert G Parton, Nicholas A Hamilton, Zoltan Neufeld, and Alpha S Yap. Cortical F-actin stabilization generates apical-lateral patterns of junctional contractility that integrate cells into epithelia. *Nature cell biology*, 16(2):167–178, 2014. (Cited on page 101.)

[290] Mariana Melani, Kaylene J Simpson, Joan S Brugge, and Denise Montell. Regulation of cell adhesion and collective cell migration by hindsight and its human homolog RREB1. *Current Biology*, 18(7):532–537, 2008. (Cited on pages 101 and 141.)

[291] Edouard Hannezo, Jacques Prost, and Jean-Francois Joanny. Theory of epithelial sheet morphology in three dimensions. *Proceedings of the National Academy of Sciences*, 111(1):27–32, 2014. (Cited on pages 101 and 141.)

[292] Hanako Yashiro, Andrew J Loza, James B Skeath, and Gregory D Longmore. Rho1 regulates adherens junction remodeling by promoting recycling endosome formation through activation of Myosin II. *Molecular biology of the cell*, 25(19):2956–2969, 2014. (Cited on pages 102 and 140.)

[293] Jacob M Sawyer, Jessica R Harrell, Gidi Shemer, Jessica Sullivan-Brown, Minna Roh-Johnson, and Bob Goldstein. Apical constriction: a cell shape change that can drive morphogenesis. *Developmental biology*, 341(1):5–19, 2010. (Cited on pages 103, 104, and 140.)

[294] Takefumi Kondo and Shigeo Hayashi. Mechanisms of cell height changes that mediate epithelial invagination. *Development, growth & differentiation*, 57(4):313–323, 2015. (Cited on page 103.)

[295] Bharesh K Chauhan, Andrea Disanza, Sue-Yeon Choi, Sonya C Faber, Ming Lou, Hilary E Beggs, Giorgio Scita, Yi Zheng, and Richard A Lang. Cdc42- and IRSp53-dependent contractile filopodia tether presumptive lens and retina to coordinate epithelial invagination. *Development*, 136(21):3657–3667, 2009. (Cited on pages 103 and 105.)

[296] Vilaiwan M Fernandes, Kasandra McCormack, Lindsay Lewellyn, and Esther M Verheyen. Integrins regulate apical constriction via microtubule stabilization in the *Drosophila* eye disc epithelium. *Cell reports*, 9(6):2043–2055, 2014. (Cited on page 103.)

[297] Frank M Mason, Michael Tworoger, and Adam C Martin. Apical domain polarization localizes actin-myosin activity to drive ratchet-like apical constriction. *Nature cell biology*, 15(8):926–936, 2013. (Cited on page 103.)

[298] Adam C Martin and Bob Goldstein. Apical constriction: themes and variations on a cellular mechanism driving morphogenesis. *Development*, 141(10):1987–1998, 2014. (Cited on page 103.)

[299] Véronique Brodu and Jordi Casanova. The RhoGAP *crossveinless-c* links *trachealess* and EGFR signaling to cell shape remodeling in *Drosophila* tracheal invagination. *Genes & development*, 20(13):1817–1828, 2006. (Cited on page 103.)

[300] Joanne M Leerberg, Guillermo A Gomez, Suzie Verma, Elliott J Moussa, Selwin K Wu, Rashmi Priya, Brenton D Hoffman, Carsten Grashoff, Martin A Schwartz, and Alpha S Yap. Tension-sensitive actin assembly supports contractility at the epithelial zonula adherens. *Current Biology*, 24(15):1689–1699, 2014. (Cited on page 103.)

[301] Wangsun Choi, Bipul R Acharya, Grégoire Peyret, Marc-Antoine Fardin, René-Marc Mège, Benoit Ladoux, Alan S Fanning, and Mark Peifer. Remodeling the zonula adherens in response to tension and the role of Afadin

in this response. *The Journal of cell biology*, 213(2):243–260, 2016. (Cited on pages 103 and 115.)

[302] Mo Weng and Eric Wieschaus. Myosin-dependent remodeling of adherens junctions protects junctions from Snail-dependent disassembly. *The Journal of cell biology*, 212(2):219–229, 2016. (Cited on page 104.)

[303] Donald T Fox and Mark Peifer. Abelson kinase (Abl) and RhoGEF2 regulate actin organization during cell constriction in *Drosophila* . *Development*, 134(3):567–578, 2007. (Cited on pages 104, 127, and 140.)

[304] Catarina CF Homem and Mark Peifer. Diaphanous regulates myosin and adherens junctions to control cell contractility and protrusive behavior during morphogenesis. *Development*, 135(6):1005–1018, 2008. (Cited on pages 104 and 140.)

[305] Kelly K Nikolaidou and Kathy Barrett. A Rho GTPase signaling pathway is used reiteratively in epithelial folding and potentially selects the outcome of Rho activation. *Current Biology*, 14(20):1822–1826, 2004. (Cited on page 104.)

[306] Douglas Corrigall, Rhian F Walther, Lilia Rodriguez, Pierre Fichelson, and Franck Pichaud. Hedgehog signaling is a principal inducer of Myosin-II-driven cell ingression in *Drosophila* epithelia. *Developmental cell*, 13(5):730–742, 2007. (Cited on page 104.)

[307] Tony JC Harris and Mark Peifer. aPKC controls microtubule organization to balance adherens junction symmetry and planar polarity during development. *Developmental cell*, 12(5):727–738, 2007. (Cited on page 104.)

[308] Kazushi Kimura, Masaaki Ito, Mutsuki Amano, and Kazuyasu Chihara. Regulation of myosin phosphatase by Rho and Rho-associated kinase (Rho-kinase). *Science*, 273(5272):245, 1996. (Cited on page 104.)

[309] Yoji Kawano, Yuko Fukata, Noriko Oshiro, Mutsuki Amano, Toshikazu Nakamura, Masaaki Ito, Fumio Matsumura, Masaki Inagaki, and Kozo Kaibuchi.

Phosphorylation of myosin-binding subunit (MBS) of myosin phosphatase by Rho-kinase *in vivo*. *The Journal of cell biology*, 147(5):1023–1038, 1999. (Cited on page 104.)

[310] Kathy Barrett, Maria Leptin, and Jeffrey Settleman. The Rho GTPase and a putative RhoGEF mediate a signaling pathway for the cell shape changes in *Drosophila* gastrulation. *Cell*, 91(7):905–915, 1997. (Cited on page 104.)

[311] Jörg Großhans, Christian Wenzl, Hans-Martin Herz, Slawomir Bartoszewski, Frank Schnorrer, Nina Vogt, Heinz Schwarz, and H-Arno Müller. RhoGEF2 and the formin Dia control the formation of the furrow canal by directed actin assembly during *Drosophila* cellularisation. *Development*, 132(5):1009–1020, 2005. (Cited on page 104.)

[312] Jennifer Round and Elke Stein. Netrin signaling leading to directed growth cone steering. *Current opinion in neurobiology*, 17(1):15–21, 2007. (Cited on page 106.)

[313] Kun-Liang Guan and Yi Rao. Signalling mechanisms mediating neuronal responses to guidance cues. *Nature Reviews Neuroscience*, 4(12):941–956, 2003. (Cited on page 106.)

[314] Joseph Tcherkezian, Perry A Brittis, Franziska Thomas, Philippe P Roux, and John G Flanagan. Transmembrane receptor DCC associates with protein synthesis machinery and regulates translation. *Cell*, 141(4):632–644, 2010. (Cited on page 107.)

[315] Karine Poirier, Yoann Y Saillour, Nadia Bahi-Buisson, Xavier H Jaglin, Catherine Fallet-Bianco, Rima Nabbout, Laetitia Castelnau-Ptakhine, Agathe Roubertie, Tania Attie-Bitach, Isabelle Desguerre, et al. Mutations in the neuronal beta tubulin subunit TUBB3 result in malformation of cortical development and neuronal migration defects. *Human molecular genetics*, page ddq377, 2010. (Cited on page 107.)

[316] Guofa Liu, Hilary Beggs, Claudia Jürgensen, Hwan-Tae Park, Hao Tang, Jessica Gorski, Kevin R Jones, Louis F Reichardt, Jane Wu, and Yi Rao. Netrin requires focal adhesion kinase and Src family kinases for axon outgrowth and attraction. *Nature neuroscience*, 7(11):1222–1232, 2004. (Cited on pages 107 and 127.)

[317] Mayya Meriane, Joseph Tcherkezian, Christine A Webber, Eric I Danek, Ibtissem Triki, Sarah McFarlane, Evelyne Bloch-Gallego, and Nathalie Lamarche-Vane. Phosphorylation of DCC by Fyn mediates Netrin-1 signaling in growth cone guidance. *The Journal of cell biology*, 167(4):687–698, 2004. (Cited on page 107.)

[318] Michael P O'Donnell and Greg J Bashaw. Src inhibits midline axon crossing independent of Frazzled/Deleted in Colorectal Carcinoma (DCC) receptor tyrosine phosphorylation. *The Journal of Neuroscience*, 33(1):305–314, 2013b. (Cited on pages 107 and 108.)

[319] Laura M Breshears, Deborah Wessels, David R Soll, and Margaret A Titus. An unconventional myosin required for cell polarization and chemotaxis. *Proceedings of the National Academy of Sciences*, 107(15):6918–6923, 2010. (Cited on pages 108 and 117.)

[320] Michael L Kerber and Richard E Cheney. Myosin-X: a MyTH-FERM myosin at the tips of filopodia. *J Cell Sci*, 124(22):3733–3741, 2011. (Cited on pages 108 and 117.)

[321] Xiao-Juan Zhu, Cheng-Zhong Wang, Peng-Gao Dai, Yi Xie, Ning-Ning Song, Yu Liu, Quan-Sheng Du, Lin Mei, Yu-Qiang Ding, and Wen-Cheng Xiong. Myosin X regulates netrin receptors and functions in axonal path-finding. *Nature Cell Biology*, 9(2):184–192, 2007. (Cited on pages 108, 117, and 139.)

[322] Yu Liu, Yun Peng, Peng-Gao Dai, Quan-Sheng Du, Lin Mei, and Wen-Cheng Xiong. Differential regulation of Myosin X movements by its cargos, DCC and Neogenin. *J Cell Sci*, 125(3):751–762, 2012. (Cited on page 108.)

[323] Raymond Liu, Sarah Woolner, James E Johndrow, David Metzger, Adriana Flores, and Susan M Parkhurst. Sisyphus, the *Drosophila* myosin XV homolog, traffics within filopodia transporting key sensory and adhesion cargos. *Development*, 135(1):53–63, 2008. (Cited on pages 108 and 117.)

[324] Miguel Vicente-Manzanares, Xuefei Ma, Robert S Adelstein, and Alan Rick Horwitz. Non-muscle myosin ii takes centre stage in cell adhesion and migration. *Nature reviews Molecular cell biology*, 10(11):778–790, 2009. (Cited on page 108.)

[325] Cecile Lebrand, Erik W Dent, Geraldine A Strasser, Lorene M Lanier, Matthias Krause, Tatyana M Svitkina, Gary G Borisy, and Frank B Gertler. Critical role of Ena/VASP proteins for filopodia formation in neurons and in function downstream of Netrin-1. *Neuron*, 42(1):37–49, 2004. (Cited on pages 117 and 139.)

[326] Melanie Barzik, Tatyana I Kotova, Henry N Higgs, Larnele Hazelwood, Dorit Hanein, Frank B Gertler, and Dorothy A Schafer. Ena/VASP proteins enhance actin polymerization in the presence of barbed end capping proteins. *Journal of Biological Chemistry*, 280(31):28653–28662, 2005. (Cited on pages 117 and 127.)

[327] Alice Ly, Anatoly Nikolaev, Geetha Suresh, Yufang Zheng, Marc Tessier-Lavigne, and Elke Stein. DSCAM is a netrin receptor that collaborates with DCC in mediating turning responses to Netrin-1. *Cell*, 133(7):1241–1254, 2008. (Cited on page 119.)

[328] H Huang, Q Shao, C Qu, T Yang, T Dwyer, and G Liu. Coordinated interaction of Down syndrome cell adhesion molecule and Deleted in colorectal cancer with dynamic TUBB3 mediates Netrin-1-induced axon branching. *Neuroscience*, 293:109–122, 2015. (Cited on page 120.)

[329] Maria D Martin-Bermudo, Ines Alvarez-Garcia, and Nicholas H Brown. Migration of the *Drosophila* primordial midgut cells requires coordination of di-

verse PS integrin functions. *Development*, 126(22):5161–5169, 1999. (Cited on page 120.)

[330] Pamela L Bradley, Monn Monn Myat, Christy A Comeaux, and Deborah J Andrew. Posterior migration of the salivary gland requires an intact visceral mesoderm and integrin function. *Developmental biology*, 257(2):249–262, 2003. (Cited on page 120.)

[331] Tereza Kolesnikov and Steven K Beckendorf. Netrin and Slit guide salivary gland migration. *Developmental biology*, 284(1):102–111, 2005. (Cited on page 120.)

[332] Thomas Kidd, Kimberly S Bland, and Corey S Goodman. Slit is the midline repellent for the Robo receptor in *Drosophila*. *Cell*, 96(6):785–794, 1999. (Cited on page 120.)

[333] David S Garbe and Greg J Bashaw. Axon guidance at the midline: from mutants to mechanisms. *Critical reviews in biochemistry and molecular biology*, 39(5-6):319–341, 2004. (Cited on page 120.)

[334] Germana Meroni and Graciana Diez-Roux. TRIM/RBCC, a novel class of single protein RING finger E3 ubiquitin ligases. *Bioessays*, 27(11):1147–1157, 2005. (Cited on page 120.)

[335] Song Song, Qinglan Ge, Jinbo Wang, Haiyang Chen, Sanyuan Tang, Junfeng Bi, Xia Li, Qi Xie, and Xun Huang. TRIM-9 functions in the UNC-6/UNC-40 pathway to regulate ventral guidance. *Journal of Genetics and Genomics*, 38(1):1–11, 2011. (Cited on page 120.)

[336] Sébastien Carreno, Ilektra Kouranti, Edith Szafer Glusman, Margaret T Fuller, Arnaud Echard, and François Payre. Moesin and its activating kinase Slik are required for cortical stability and microtubule organization in mitotic cells. *The Journal of cell biology*, 180(4):739–746, 2008. (Cited on page 121.)

[337] Julian C Boggiano, Pamela J Vanderzalm, and Richard G Fehon. Tao-1 phosphorylates Hippo/MST kinases to regulate the Hippo-Salvador-Warts tumor suppressor pathway. *Developmental cell*, 21(5):888–895, 2011. (Cited on page 121.)

[338] Ralf Pflanz, Aaron Voigt, Toma Yakulov, and Herbert Jäckle. *Drosophila* gene *tao-1* encodes proteins with and without a Ste20 kinase domain that affect cytoskeletal architecture and cell migration differently. *Open biology*, 5(1):140161, 2015. (Cited on page 121.)

[339] Kálmán Somogyi and Pernille Rørth. Cortactin modulates cell migration and ring canal morphogenesis during *Drosophila* oogenesis. *Mechanisms of development*, 121(1):57–64, 2004. (Cited on page 121.)

[340] Tamás Matusek, Alexandre Djiane, Ferenc Jankovics, Damian Brunner, Marek Mlodzik, and József Mihály. The *Drosophila* formin DAAM regulates the tracheal cuticle pattern through organizing the actin cytoskeleton. *Development*, 133(5):957–966, 2006. (Cited on page 121.)

[341] Pei-I Tsai, Hsiu-Hua Kao, Caroline Grabbe, Yu-Tao Lee, Aurnab Ghose, Tzu-Ting Lai, Kuan-Po Peng, David Vactor, Ruth H Palmer, Ruey-Hwa Chen, et al. Fak56 functions downstream of integrin αPS3$\beta\nu$ and suppresses MAPK activation in neuromuscular junction growth. (Cited on pages 121 and 126.)

[342] BG Fernandez, B Jezowska, and F Janody. *Drosophila* Actin-Capping Protein limits JNK activation by the Src proto-oncogene. *Oncogene*, 33(16):2027–2039, 2014. (Cited on page 121.)

[343] Mayuko Takahashi, Fumitaka Takahashi, Kumiko Ui-Tei, Tetsuya Kojima, and Kaoru Saigo. Requirements of genetic interactions between Src42A, *armadillo* and *shotgun*, a gene encoding E-Cadherin, for normal development in *Drosophila* . *Development*, 132(11):2547–2559, 2005. (Cited on page 121.)

[344] Masayo Shindo, Housei Wada, Masako Kaido, Minoru Tateno, Toshiro Aigaki, Leo Tsuda, and Shigeo Hayashi. Dual function of Src in the maintenance of adherens junctions during tracheal epithelial morphogenesis. *Development*, 135(7):1355–1364, 2008. (Cited on page 121.)

[345] Michael J. Murray, Catherine M. Davidson, Neil M. Hayward, and Andrea H. Brand. The Fes/Fer non-receptor tyrosine kinase cooperates with Src42A to regulate dorsal closure in *Drosophila*. *Development*, 133(16):3063–3073, 2006. (Cited on pages 121 and 122.)

[346] Douglas J Guarnieri, G Steven Dodson, and Michael A Simon. SRC64 regulates the localization of a Tec-family kinase required for *Drosophila* ring canal growth. *Molecular cell*, 1(6):831–840, 1998. (Cited on pages 121 and 122.)

[347] Erica M Roulier, Scott Panzer, and Steven K Beckendorf. The Tec29 tyrosine kinase is required during *Drosophila* embryogenesis and interacts with Src64 in ring canal development. *Molecular cell*, 1(6):819–829, 1998. (Cited on pages 121 and 122.)

[348] Peter Greer. Closing in on the biological functions of Fps/Fes and Fer. *Nature Reviews Molecular Cell Biology*, 3(4):278–289, 2002. (Cited on page 121.)

[349] Tarek Y El Sayegh, Pamela D Arora, Lingzhi Fan, Carol A Laschinger, Peter A Greer, Christopher A McCulloch, and Andras Kapus. Phosphorylation of N-Cadherin-associated Cortactin by Fer kinase regulates N-Cadherin mobility and intercellular adhesion strength. *Molecular biology of the cell*, 16(12):5514–5527, 2005. (Cited on page 121.)

[350] Vidya Chandrasekaran and Steven K Beckendorf. Tec29 controls actin remodeling and endoreplication during invagination of the *Drosophila* embryonic salivary glands. *Development*, 132(15):3515–3524, 2005. (Cited on page 122.)

[351] Mahaboobi Jaleel, R Jeremy Nichols, Maria Deak, David G Campbell, Frank Gillardon, Axel Knebel, and Dario R Alessi. LRRK2 phosphorylates Moesin at

threonine-558: characterization of how Parkinson's disease mutants affect kinase activity. *Biochemical Journal*, 405(2):307–317, 2007. (Cited on page 122.)

[352] Loukia Parisiadou, Chengsong Xie, Hyun Jin Cho, Xian Lin, Xing-Long Gu, Cai-Xia Long, Evy Lobbestael, Veerle Baekelandt, Jean-Marc Taymans, Lixin Sun, et al. Phosphorylation of Ezrin/Radixin/Moesin proteins by LRRK2 promotes the rearrangement of actin cytoskeleton in neuronal morphogenesis. *The Journal of Neuroscience*, 29(44):13971–13980, 2009. (Cited on page 122.)

[353] Mark W Dodson, Ting Zhang, Changan Jiang, Shengdi Chen, and Ming Guo. Roles of the *Drosophila* LRRK2 homolog in Rab7-dependent lysosomal positioning. *Human molecular genetics*, 21(6):1350–1363, 2012. (Cited on page 122.)

[354] Songhee Jeon, Jung-Keug Park, Chang-Dae Bae, and Joobae Park. NGF-induced Moesin phosphorylation is mediated by the PI3K, Rac1 and Akt and required for neurite formation in PC12 cells. *Neurochemistry international*, 56(6):810–818, 2010. (Cited on page 122.)

[355] Harn Shiue, Mark W Musch, Yingmin Wang, Eugene B Chang, and Jerrold R Turner. Akt2 phosphorylates Ezrin to trigger NHE3 translocation and activation. *Journal of Biological Chemistry*, 280(2):1688–1695, 2005. (Cited on page 122.)

[356] Javier Verdu, Michael A Buratovich, Elizabeth L Wilder, and Morris J Birnbaum. Cell-autonomous regulation of cell and organ growth in *Drosophila* by Akt/PKB. *Nature cell biology*, 1(8):500–506, 1999. (Cited on page 122.)

[357] Sung-Eun Kim, Jae-Young Cho, Kyung-Sup Kim, Su-Jae Lee, Ki-Hoo Lee, and Kang-Yell Choi. *Drosophila* PI3 kinase and Akt involved in insulin-stimulated proliferation and ERK pathway activation in Schneider cells. *Cellular signalling*, 16(11):1309–1317, 2004. (Cited on page 122.)

[358] Yu Lu and Jeffrey Settleman. The role of Rho family GTPases in development: lessons from *Drosophila* . *Molecular Cell Biology Research Communications*, 1(2):87–94, 1999. (Cited on page 122.)

[359] James E Johndrow, Craig R Magie, and Susan M Parkhurst. Rho GTPase function in flies: insights from a developmental and organismal perspective. *Biochemistry and cell biology*, 82(6):643–657, 2004. (Cited on page 122.)

[360] Alex H Hutagalung and Peter J Novick. Role of Rab GTPases in membrane traffic and cell physiology. *Physiological reviews*, 91(1):119–149, 2011. (Cited on page 123.)

[361] Tanmay Bhuin and Jagat Kumar Roy. Rab proteins: the key regulators of intracellular vesicle transport. *Experimental cell research*, 328(1):1–19, 2014. (Cited on page 123.)

[362] Elaine Del Nery, Stéphanie Miserey-Lenkei, Thomas Falguieres, Clément Nizak, Ludger Johannes, Franck Perez, and Bruno Goud. Rab6A and Rab6A′ GTPases play non-overlapping roles in membrane trafficking. *Traffic*, 7(4):394–407, 2006. (Cited on page 123.)

[363] Ilya Grigoriev, Daniel Splinter, Nanda Keijzer, Phebe S Wulf, Jeroen Demmers, Toshihisa Ohtsuka, Mauro Modesti, Ivan V Maly, Frank Grosveld, and Casper C Hoogenraad. Rab6 regulates transport and targeting of exocytotic carriers. *Developmental cell*, 13(2):305–314, 2007. (Cited on page 123.)

[364] Jean-Baptiste Coutelis and Anne Ephrussi. Rab6 mediates membrane organization and determinant localization during *Drosophila* oogenesis. *Development*, 134(7):1419–1430, 2007. (Cited on page 123.)

[365] Takunori Satoh, Yuri Nakamura, and Akiko K Satoh. Rab6 functions in polarized transport in *Drosophila* photoreceptors. *Fly*, pages 1–5, 2016. (Cited on page 123.)

[366] Nozomi Iwanami, Yuri Nakamura, Takunori Satoh, Ziguang Liu, and Akiko K Satoh. Rab6 is required for multiple apical transport pathways but not the basolateral transport pathway in *Drosophila* photoreceptors. *PLoS Genet*, 12(2):e1005828, 2016. (Cited on page 123.)

[367] Oliver Ullrich, Sigrid Reinsch, Sylvie Urbé, Marino Zerial, and Robert G Parton. Rab11 regulates recycling through the pericentriolar recycling endosome. *The Journal of cell biology*, 135(4):913–924, 1996. (Cited on page 123.)

[368] Akiko K Satoh, Joseph E O′Tousa, Koichi Ozaki, and Donald F Ready. Rab11 mediates post-Golgi trafficking of rhodopsin to the photosensitive apical membrane of *Drosophila* photoreceptors. *Development*, 132(7):1487–1497, 2005. (Cited on page 123.)

[369] Udo Häcker and Norbert Perrimon. DRhoGEF2 encodes a member of the Dbl family of oncogenes and controls cell shape changes during gastrulation in *Drosophila* . *Genes and Development*, 12(2):274–284, 1998. (Cited on page 123.)

[370] Sergei N Prokopenko, Anthony Brumby, Louise O′Keefe, Leanne Prior, Yuchun He, Robert Saint, and Hugo J Bellen. A putative exchange factor for Rho1 GTPase is required for initiation of cytokinesis in *Drosophila* . *Genes & development*, 13(17):2301–2314, 1999. (Cited on page 123.)

[371] Greg J Bashaw, Hailan Hu, Catherine D Nobes, and Corey S Goodman. A novel Dbl family RhoGEF promotes Rho-dependent axon attraction to the central nervous system midline in *Drosophila* and overcomes Robo repulsion. *The Journal of cell biology*, 155(7):1117–1122, 2001. (Cited on page 123.)

[372] Justina Sanny, Vincent Chui, Caillin Langmann, Carla Pereira, Baharak Zahedi, and Nicholas Harden. *Drosophila* RhoGAP68F is a putative GTPase activating protein for RhoA participating in gastrulation. *Development genes and evolution*, 216(9):543–550, 2006. (Cited on page 123.)

[373] (Cited on page 123.)

[374] Stephen L Rogers, Ursula Wiedemann, Udo Häcker, Chris Turck, and Ronald D Vale. *Drosophila* RhoGEF2 associates with microtubule plus ends in an EB1-dependent manner. *Current biology*, 14(20):1827–1833, 2004. (Cited on page 123.)

[375] G Hime and R Saint. Zygotic expression of the *pebble* locus is required for cytokinesis during the postblastoderm mitoses of *Drosophila*. *Development*, 114(1):165–171, 1992. (Cited on page 123.)

[376] W Gregory Somers and Robert Saint. A RhoGEF and Rho family GTPase-activating protein complex links the contractile ring to cortical microtubules at the onset of cytokinesis. *Developmental cell*, 4(1):29–39, 2003. (Cited on page 123.)

[377] Sabine Schumacher, Tanja Gryzik, Sylvia Tannebaum, and H-Arno J Müller. The Rhogef Pebble is required for cell shape changes during cell migration triggered by the *Drosophila* FGF receptor Heartless. *Development*, 131(11):2631–2640, 2004. (Cited on page 123.)

[378] Masha Smallhorn, Michael J Murray, and Robert Saint. The epithelial-mesenchymal transition of the *Drosophila* mesoderm requires the Rho GTP exchange factor Pebble. *Development*, 131(11):2641–2651, 2004. (Cited on page 123.)

[379] Andreas van Impel, Sabine Schumacher, Margarethe Draga, Hans-Martin Herz, Jörg Großhans, and H Arno J Müller. Regulation of the Rac GTPase pathway by the multifunctional Rho GEF Pebble is essential for mesoderm migration in the *Drosophila* gastrula. *Development*, 136(5):813–822, 2009. (Cited on page 123.)

[380] Michael J Murray, Michelle M Ng, Hamilton Fraval, Julie Tan, Wenjie Liu, Masha Smallhorn, Julie A Brill, Seth J Field, and Robert Saint. Regulation of

Drosophila mesoderm migration by phosphoinositides and the PH domain of the Rho GTP exchange factor Pebble. *Developmental biology*, 372(1):17–27, 2012. (Cited on page 123.)

[381] Jun Hee Lee, Kyoung Sang Cho, Jihyun Lee, Dohoon Kim, Sung-Bae Lee, Jungsik Yoo, Guang-Ho Cha, and Jongkyeong Chung. *Drosophila* PDZ-GEF, a guanine nucleotide exchange factor for Rap1 GTPase, reveals a novel upstream regulatory mechanism in the mitogen-activated protein kinase signaling pathway. *Molecular and cellular biology*, 22(21):7658–7666, 2002. (Cited on page 124.)

[382] JL Bos, K De Bruyn, J Enserink, B Kuiperij, S Rangarajan, H Rehmann, J Riedl, J De Rooij, F Van Mansfeld, and F Zwartkruis. The role of Rap1 in integrin-mediated cell adhesion. *Biochemical Society Transactions*, 31(1):83–86, 2003. (Cited on page 124.)

[383] Andrea L Knox and Nicholas H Brown. Rap1 GTPase regulation of adherens junction positioning and cell adhesion. *Science*, 295(5558):1285–1288, 2002. (Cited on page 124.)

[384] Leo S Price, Amra Hajdo-Milasinovic, Jun Zhao, Fried JT Zwartkruis, John G Collard, and Johannes L Bos. Rap1 regulates E-cadherin-mediated cell-cell adhesion. *Journal of Biological Chemistry*, 279(34):35127–35132, 2004. (Cited on page 124.)

[385] Hong Wang, Shree Ram Singh, Zhiyu Zheng, Su-Wan Oh, Xiu Chen, Kevin Edwards, and Steven X Hou. Rap-GEF signaling controls stem cell anchoring to their niche through regulating DE-Cadherin-mediated cell adhesion in the *Drosophila* testis. *Developmental cell*, 10(1):117–126, 2006. (Cited on page 124.)

[386] Jack Bateman, Huidy Shu, and David Van Vactor. The guanine nucleotide exchange factor Trio mediates axonal development in the *Drosophila* embryo. *Neuron*, 26(1):93–106, 2000. (Cited on pages 124 and 134.)

[387] Zhongzhen Nie, Dianne S Hirsch, and Paul A Randazzo. Arf and its many interactors. *Current opinion in cell biology*, 15(4):396–404, 2003. (Cited on page 124.)

[388] Thomas Hummel, Kristina Schimmelpfeng, and C Klambt. Commissure formation in the embryonic CNS of *Drosophila* . *Development*, 126(4):771–779, 1999. (Cited on page 124.)

[389] Susanne Önel, Liane Bolke, and Christian Klämbt. The *Drosophila* ARF6-GEF Schizo controls commissure formation by regulating Slit. *Development*, 131(11):2587–2594, 2004. (Cited on page 124.)

[390] Kenneth J Kemphues, James R Priess, Diane G Morton, and Niansheng Cheng. Identification of genes required for cytoplasmic localization in early *C. elegans* embryos. *Cell*, 52(3):311–320, 1988. (Cited on page 125.)

[391] Zita Balklava, Saumya Pant, Hanna Fares, and Barth D Grant. Genome-wide analysis identifies a general requirement for polarity proteins in endocytic traffic. *Nature cell biology*, 9(9):1066–1073, 2007. (Cited on page 125.)

[392] Takashi Nishimura and Kozo Kaibuchi. Numb controls integrin endocytosis for directional cell migration with aPKC and PAR-3. *Developmental cell*, 13(1):15–28, 2007. (Cited on page 125.)

[393] Alicia M Viloria-Petit, Laurent David, Jun Yong Jia, Tuba Erdemir, Anita L Bane, Dushanthi Pinnaduwage, Luba Roncari, Masahiro Narimatsu, Rohit Bose, Jason Moffat, et al. A role for the TGFβ-Par6 polarity pathway in breast cancer progression. *Proceedings of the National Academy of Sciences*, 106(33):14028–14033, 2009. (Cited on page 125.)

[394] Yabing Mu, Guangxiang Zang, Ulla Engström, Christer Busch, and M Landström. TGFβ-induced phosphorylation of Par6 promotes migration and invasion in prostate cancer cells. *British journal of cancer*, 112(7):1223–1231, 2015. (Cited on page 125.)

[395] Miriam Barrios-Rodiles, Kevin R Brown, Barish Ozdamar, Rohit Bose, Zhong Liu, Robert S Donovan, Fukiko Shinjo, Yongmei Liu, Joanna Dembowy, Ian W Taylor, et al. High-throughput mapping of a dynamic signaling network in mammalian cells. *Science*, 307(5715):1621–1625, 2005. (Cited on page 125.)

[396] Hong-Rui Wang, Yue Zhang, Barish Ozdamar, Abiodun A Ogunjimi, Evguenia Alexandrova, Gerald H Thomsen, and Jeffrey L Wrana. Regulation of cell polarity and protrusion formation by targeting RhoA for degradation. *Science*, 302(5651):1775–1779, 2003. (Cited on page 126.)

[397] Hilary F Clark, Doris Brentrup, Kay Schneitz, Allan Bieber, Corey Goodman, and Markus Noll. *dachsous* encodes a member of the cadherin superfamily that controls imaginal disc morphogenesis in *Drosophila*. *Genes & Development*, 9(12):1530–1542, 1995. (Cited on page 126.)

[398] Ulrich Tepass, Eileen Gruszynski-DeFeo, Thomas A Haag, Lili Omatyar, T Török, and Volker Hartenstein. *shotgun* encodes *Drosophila* E-cadherin and is preferentially required during cell rearrangement in the neurectoderm and other morphogenetically active epithelia. *Genes & development*, 10(6):672–685, 1996. (Cited on page 126.)

[399] José Casal, Peter A Lawrence, and Gary Struhl. Two separate molecular systems, Dachsous/Fat and Starry night/Frizzled, act independently to confer planar cell polarity. *Development*, 133(22):4561–4572, 2006. (Cited on page 126.)

[400] Peter A Lawrence, Gary Struhl, and José Casal. Planar cell polarity: one or two pathways? *Nature Reviews Genetics*, 8(7):555–563, 2007. (Cited on page 126.)

[401] Kynan T Lawlor, Daniel C Ly, and Stephen DiNardo. *Drosophila* Dachsous and Fat polarize actin-based protrusions over a restricted domain of the embryonic denticle field. *Developmental biology*, 383(2):285–294, 2013. (Cited on page 126.)

[402] Haeryun Lee and Paul N Adler. The function of the Frizzled pathway in the *Drosophila* wing is dependent on inturned and fuzzy. *Genetics*, 160(4):1535–1547, 2002. (Cited on page 126.)

[403] Paul N Adler. The Frizzled/Stan pathway and planar cell polarity in the *Drosophila* wing. *Current topics in developmental biology*, 101:1, 2012. (Cited on page 126.)

[404] Cristina Organisti, Irina Hein, Ilona C Grunwald Kadow, and Takashi Suzuki. Flamingo, a seven-pass transmembrane cadherin, cooperates with Netrin/Frazzled in *Drosophila* midline guidance. *Genes to Cells*, 20(1):50–67, 2015. (Cited on page 126.)

[405] Yasuhide Furuta, Satoshi Kanazawa, Naoki Takeda, Kenji Sobue, Norio Nakatsuji, Shintaro Nomura, Jiro Fujimoto, Masato Okada, Tadashi Yamamoto, and Shinichi Aizawa. Reduced cell motility and enhanced focal adhesion contact formation in cells from FAK-deficient mice. *Nature*, 377(6549):539–544, 1995. (Cited on page 126.)

[406] Simon W Moore, Xian Zhang, Christopher D Lynch, and Michael P Sheetz. Netrin-1 attracts axons through FAK-dependent mechanotransduction. *The Journal of Neuroscience*, 32(34):11574–11585, 2012. (Cited on page 127.)

[407] Elizabeth E Grevengoed, Donald T Fox, Julie Gates, and Mark Peifer. Balancing different types of actin polymerization at distinct sites roles for Abelson kinase and Enabled. *The Journal of cell biology*, 163(6):1267–1279, 2003. (Cited on page 127.)

[408] Roberta Hopmann, John A Cooper, and Kathryn G Miller. Actin organization, bristle morphology, and viability are affected by actin capping protein mutations in *Drosophila* . *The Journal of cell biology*, 133(6):1293–1305, 1996. (Cited on page 127.)

[409] Florence Janody and Jessica E Treisman. Actin capping protein α maintains vestigial-expressing cells within the *Drosophila* wing disc epithelium. *Development*, 133(17):3349–3357, 2006. (Cited on page 127.)

[410] Barbara Jezowska, Beatriz García Fernández, Ana Rita Amândio, Paulo Duarte, Cláudia Mendes, Catarina Brás-Pereira, and Florence Janody. A dual function of *Drosophila* Capping protein on DE-Cadherin maintains epithelial integrity and prevents JNK-mediated apoptosis. *Developmental biology*, 360(1):143–159, 2011. (Cited on page 127.)

[411] Jeong K Song, Ramakrishnan Kannan, Gunter Merdes, Jaskirat Singh, Marek Mlodzik, and Edward Giniger. Disabled is a *bona fide* component of the Abl signaling network. *Development*, 137(21):3719–3727, 2010. (Cited on page 127.)

[412] Fumiko Kawasaki, Janani Iyer, Lisa L Posey, Chichun E Sun, Samantha E Mammen, Huaru Yan, and Richard W Ordway. The disabled protein functions in Clathrin-mediated synaptic vesicle endocytosis and exoendocytic coupling at the active zone. *Proceedings of the National Academy of Sciences*, 108(25):E222–E229, 2011. (Cited on page 128.)

[413] Jessica L Lee and Charles H Streuli. Integrins and epithelial cell polarity. *J Cell Sci*, 127(15):3217–3225, 2014. (Cited on page 128.)

[414] Hsin-Ho Sung, Ivo A Telley, Piyi Papadaki, Anne Ephrussi, Thomas Surrey, and Pernille Rørth. *Drosophila* Ensconsin promotes productive recruitment of Kinesin-1 to microtubules. *Developmental cell*, 15(6):866–876, 2008. (Cited on page 128.)

[415] Kari Barlan, Wen Lu, and Vladimir I Gelfand. The microtubule-binding protein Ensconsin is an essential cofactor of Kinesin-1. *Current Biology*, 23(4):317–322, 2013. (Cited on page 128.)

[416] Jason E Duncan, Nikki K Lytle, Alfredo Zuniga, and Lawrence SB Goldstein. The microtubule regulatory protein Stathmin is required to maintain the integrity of axonal microtubules in *Drosophila* . *PloS one*, 8(6):e68324, 2013. (Cited on page 128.)

[417] Silvia Aldaz, Luis M Escudero, and Matthew Freeman. Dual role of myosin ii during *Drosophila* imaginal disc metamorphosis. *Nature communications*, 4:1761, 2013. (Cited on page 134.)

[418] Peytee Khoo, Kirsten Allan, Lee Willoughby, Anthony M Brumby, and Helena E Richardson. In *Drosophila* , RhoGEF2 cooperates with activated Ras in tumorigenesis through a pathway involving Rho1-Rok-Myosin-II and JNK signalling. *Disease Models and Mechanisms*, 6(3):661–678, 2013. (Cited on page 134.)

[419] Monique Arpin, Dafne Chirivino, Alexandra Naba, and Ingrid Zwaenepoel. Emerging role for ERM proteins in cell adhesion and migration. *Cell adhesion & migration*, 5(2):199–206, 2011. (Cited on page 140.)

[420] Emmanuel Caussinus, Oguz Kanca, and Markus Affolter. Fluorescent fusion protein knockout mediated by anti-GFP nanobody. *Nature structural & molecular biology*, 19(1):117–121, 2012. (Cited on page 141.)